Department of Chemical and Process Engineering

Hollow Fiber Poly(vinyl chloride) (PVC) Gas Separation Membranes Prepared by Dry/Wet Spinning Production Methods

Colin Alexander Jones

PhD Chemical and Process Engineering

2015

This thesis is the result of the author's original research. It has been composed by the author and has not been previously submitted for examination which has led to the award of a degree.

Signed:

Date:

Abstract

Hollow fiber gas separation membranes manufactured from Poly(vinyl chloride) (PVC) have been produced via a dry/wet spinning method for end use in ozone/oxygen gas separations.

Ambient temperature production mechanisms were initially targeted. A number of spin runs were undertaken changing aspects of the dope solution and the spinning conditions but produced only very low selectivity membranes. It was concluded that ambient condition spinning was unattainable for the solutions used.

In order to explain the low selectivity a rheological study was undertaken which considered flow, oscillatory and creep rheological conditions and modelling of the flow patterns observed across the spinneret annulus. This study showed large differences between the dope at 20°C and 60°C in terms of viscosity and viscoelastic nature. These differences were predicted to make spinning difficult through slippage on the spinneret walls and viscoelastic nature of the solution.

Spinning at elevated temperature was undertaken and used to produce membranes under different spinning conditions according to a Taguchi model and which would allow graphical comparisons also in order to assess the validity of the Taguchi analysis in these applications. The membranes produced an array of results all of which indicated solution diffusion through PVC as the controlling transport mechanism under the spinning conditions. Both graphical and Taguchi analysis concluded the same conditions to be optimal; low dope extrusion rate but high convective gas flow rate and residence time producing the best selectivity.

The membrane permeation results were used alongside scanning electron microscopy images to model the active layer thickness in the membranes. This concluded that the higher selectivity membranes exhibited lower active layer thicknesses and porosity resulting from the quick formation of a dense surface layer for nodule coalescence preventing further mass transport and hence halting penetration of the active layer.

Ozone/oxygen binary gas mixtures showed qualitative evidence of separation. Unfortunately due to equipment limitations it was not possible to provide quantitative data to support this. The membranes have displayed good resistance to oxidative environment and therefore they perhaps offer a viable solution for processes occurring in this type of environment which more common membrane materials may not be suitable for.

Acknowledgements

At the start of this thesis there is a declaration which asserts that the contents are the results of my own original research and that I have compiled and composed the work myself. This is true and yet this is only half the story as behind all this work is a supporting cast without whom the results would not be half of what they are. To all these people I owe a huge debt and I apologise that I don't specifically name you all here, you know who you are though and if you want to claim some return on services rendered then just let me know.

First the staff at the university, whether helping with administration, laboratory experimentation or simply being ready with some advice thank you for making my time at the university run that much smoother and more enjoyably than it otherwise would have.

To my advisor, Simon Shilton, thank you for the opportunity to conduct this work. The faith you have had in me throughout the process and the invaluable advice when things were not as expected is something I only hope to have repaid to some extent in the following pages.

To my friends both at university and outside of it, you just make life easier. Having a group of friends like you around to make me laugh and provide encouragement makes everything more enjoyable. The lunch time group though has to be given some special attention, I think lunch is always one of the highlights of any working day but our lunches were something I wish everyone got the chance to experience. Whether the chat was work based or one of any number of random contributions to the white board nothing could have made the time better.

To my family, I first offer an apology for bringing the grouchiness home with me. I know you have put up with a lot but I could not have done it without you. Whether the help is in the form of just knowing you are there from me or constant prodding to hurry up and finish you have all contributed something to my efforts and most definitely have my gratitude.

Finally, my most special thank you to Jaclyn Dunn. You make my life better and happier than I ever thought possible. You have had more to put up with over this time than anyone else yet manage to be nothing but helpful and supportive. I don't think it is possible to state how much it means to me or how amazing you are.

Thank you everyone.

Contents

List of Figures

Section 1: Introduction

Section 3: Equipment, Methods and Common Calculations

Section 5: Rheological Testing

Section 6: Elevated Temperature Spinning

Section 7: Membrane Characterisation

Section 8: Oxygen/Ozone Binary Gas Mixture Separations

List of Tables

Section 1: Introduction

Section 3: Equipment, Methods and Common Calculations

Section 4: Ambient Temperature Spinning

Section 5: Rheological Testing

Section 6: Elevated Temperature Spinning

Section 7: Membrane Characterisation

Abbreviations

PVC	Poly(vinyl chloride)
PTFE	Polytetrafluroethylene
PDMS	Polydimethylsiloxane
PSF	Polysulfone
DMac	N,N-dimethylacetamide
THF	Tetrahydrofuran
DC	Direct Current
SEM	Scanning Electron Microscopy

1. Introduction

1.1. Conventional Separation Processes

Separations processing is a huge part of the modern chemical and process industry. There are not many processes which can escape the fact that taking a mixture of two or more components, regularly on a large scale, and separating them into streams of greater purity is often a necessary, complicated and expensive activity. Take for example a simple mixture of water and ethanol, the first approach which might suggest itself is learned in school and consists of boiling off the ethanol component and collecting it. However, the distillation process of separating ethanol and water reaches an azeotrope; a point in the separation process where the vapour being produced is containing equal parts of water and ethanol.

This implies a limit on the capability of industry to perform the water/ethanol separation process. However, there has been a large amount of research done in this area which has looked at varying separation processes: pervaporation[1-3], pressure swing distillation[4] and pressure swing adsorption[5, 6]. Even after the selection of a process type to perform a separation there is a great deal of work involved in moving these processes from laboratory and pilot scales to process plant production units. Additionally and in some cases perhaps most importantly to businesses are the assessed costs and benefits which are associated with the process.

The example given above shows the complexity of separation processes for even a binary and supposedly simple system such as water and ethanol. However, separation processes are necessary in so many and such complicated processes that it has been estimated they may account for 40-70% of both capital and operating costs in industry[7]. This high cost makes them a prime target for savings and for the use of cutting edge technology which makes the processes more efficient in terms of both production and economics.

Apart from cost related issues there are other aspects of market, legal and social pressures which are driving improvements in separation processes. The emergence of competitor companies using the latest technologies forces large companies to continue developing better

processes so they do not fall behind. From a socio-political view point legislation such as the Climate Change Act 2008[8] in the United Kingdom means there is closer monitoring of effluent and energy usage of process plant than ever before and the public like to see companies that take responsibility for using greener processes as their knowledge on the subject increases. These things lead to reform in the way in which materials are processed and a number of conventional separation processes are being superseded or improved upon by more environmentally friendly and efficient alternatives.

Conventional separating processes such as distillation, evaporation and adsorption face challenges which are dependent upon the phases and type of separation which is undertaken. However, a common theme which runs through most of the problems is the amount of energy which has to be put into the process and this is most commonly the area of improvement for process plant.

A change in the type of separating process being used has become a more common feature of work in separation processes and one field which is often of interest and has been experiencing growth is that of membrane separation processes.

1.2. General Membrane Separation Processes

1.2.1. Advantages and Disadvantages of Membrane Processes in Comparison to Conventional Separation Methods

The growth which has been and is occurring in the membrane market is driven by the need to improve the processes already in place and there are a number of ways which this can be achieved and reasons why membranes should always enter the discussion:

- Membrane processes have applications for separating processes dealing with species from the molecular level up to particles large enough to see giving a large number of processes which are applicable.

- Generally membrane processes do not require a phase change which can lead to large savings on energy requirements.
- A membrane process does not normally require a lot of moving parts or complex control mechanisms and as such can offer a relatively simple solution to separation processing.
- Depending upon the process and materials used it is possible in certain circumstances to produce very high degrees of separation.
- The materials used for membrane production, often polymers or other inorganic materials, cover a wide range of operating conditions and requirements and often do not cost a lot.
- The materials used in membrane processes are usually less toxic or harmful to the environment than chemical procedures which are used in separations.
- Membrane processes are often able to recover minor but valuable components from a stream without substantial costs.
- Membrane processes are easy to scale up being modular processes which can scale by addition of further modules in either series or parallel depending on the required effect.

However, this is not to say that membranes are a wonderful achievement of engineering which do not have any drawbacks:

- Producing two pure product streams is usually very difficult or impossible in membrane systems with at least one of the exit streams from the system being contaminated.
- Some traditional separation processes such as distillation can be staged to draw off different concentration components at different positions in the process but this is not easily carried out with membrane systems.
- Since membranes are a method of physical separation the materials have to come into contact with the species to be separated and this can lead to incompatibility issues.
- In some processes where the conditions under which the separation must be carried out are extreme e.g. high temperature it may be difficult to find suitable membrane materials which will maintain their performance.

- Fouling can be a major issue to membrane separation. Since the membrane must be in contact with the species to be separated any fouling which blocks the surface of the membrane reduces its effectiveness.

Overall membranes can be a very effective separation technique if they are employed under the right set of conditions and in the right process. The suitability and availability of membranes for carrying out separations is something which industry should take seriously when planning they're processes because they have the potential to save money, reduce the process impact on the environment and possibly improve upon separation performance.

1.2.2. **Membrane Structures for Separation Processes**

Membrane processes are physical separation processes; they pose a barrier to the mass transfer of a feed stream, containing the components to be separated, which is designed to allow certain components to pass through the barrier more easily than others leading to concentration occurring. Membrane processes tend to split the feed stream in two parts: the permeate stream will be more highly concentrated in the species which travel fastest through the membrane while the retentate stream will contain a higher concentration of the slower species than was present in the feed stream. Therefore since concentration occurs in both of the streams the desired product could be in either exit flow from the process. Preferential transport of one species over another can be as the result of factors such as solubility and diffusion coefficients of the species in the membrane material and the driving force which is acting in the process.

The actual mechanism by which transport through the membrane occurs is dependent upon the process which is being carried out but two main structures were identified by *Mulder* in 1996: porous and non-porous membranes[9]. The porous structure was described by *Baker* in 2012 as a rigid, highly voided structure with randomly distributed interconnected pores[10]. In this structure the separation which occurs is dependent upon the ability of the species to be separated passing through the pores in the membrane and is therefore most highly dependent

upon the molecular size and the pore size distribution. This method of separation is similar to that of conventional filtration but on a smaller scale and is seen in membranes utilised for micro and ultrafiltration.

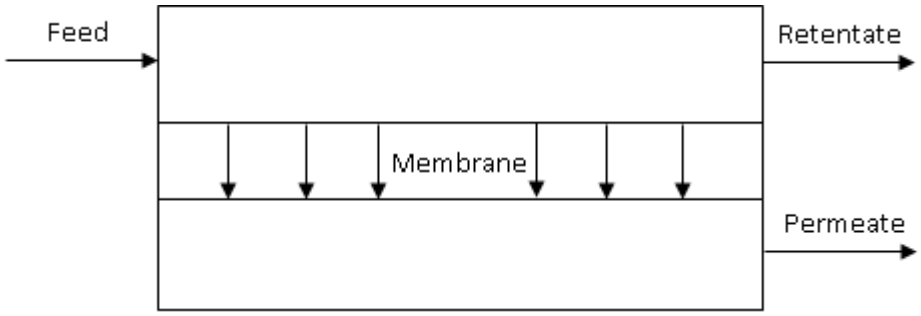

Figure 1.2.2-1: Membrane separation process flow diagram

On the other hand a non-porous membrane is dense with very low porosity. The dense nature of the membrane material is vital to how processes work which require this type of membrane. The rate of transport through these membranes is governed by the diffusivity and solubility of the species to be separated in the membrane and upon the driving force for the particular process which could be a potential, chemical or electrical gradient across the membrane, in the case of gas this driving force is provided by a pressure gradient. The other factors which affect the flux of gas through the membranes are surface area which is directly proportional, and the membrane thickness which shows an inversely proportional relationship to rate. Transfer of the species through the membranes under these conditions is referred to as solution diffusion. It is really important in these membranes that the porosity is really low and that any pores which do exist are too small for the mass transfer of the process species through them. The transport of material through pores is so preferential that it does not take a large degree of imperfection in the membrane for the desired separation to be compromised.

The size and number of pores is particularly important for gas separation processes as the density and diameter of gases is so low that passing through pores is particularly easy for species in that state. In order to encourage the predominance of solution diffusion as the primary mode of transport through the membrane the important factor is the ratio of the mean free path length to the radius of the pores. If this number (the Knudsen number) is

greater than 10 then Knudsen flow will occur through the pores, if the number is less than 0.01 then viscous flow will occur in the pores and between the extremes a mixed regime will exist[11]. Even with the presence of pores in the membrane it was first outlined by Henis and Tripodi[12, 13] that with the application of a layer of silicone to a porous membrane then it may become selective. Large pores make the Knudsen diffusion effect too strong to obtain the heightened separation through the membrane and only modest Knudsen separations will be achieved.

1.2.3. **Mass Transport Modelling**

The modelling of membrane processes has become an important aspect of the field of membrane science as it has grown. It has become a vital tool in the design and implementation of membrane systems that they are modelled and behave as the model predicts they will. A large degree of the work is directly related to the optimisation of a specific processes[14-17]. These works and many others like them look at how to produce models which can accurately predict the passage of species from one side of a membrane to another. Data in these models is often based on pure gas permeation properties and then go on to predict the binary separation processes by an array of methods like: utilising a set of relationships such as the Maxwell-Stefan equations[14, 18, 19] or by numerical methods[20-22].

The modelling which is required is dependent upon the sort of process which is to be carried out. The separation which is required of a solid from a liquid for example is very different from that which is required between two gases as is the case in this work. This is reflected in the processes which are used to carry out the different kinds of separation. The model used to describe the separation which is occurring is therefore closely related to the process which is being used, the species being separated and the characteristics of the separation medium as well as the process units which are to be used in the separation.

There are also different aspects of membrane separation which can be modelled together or separately. These aspects are the modelling of the transport through the membrane[14, 23-25] and

the modelling of the membrane module design[26-29]. The object in this work is the initial development of a membrane which is capable of gas separation using PVC so it is the first of these two different approaches which is considered. As with almost any modelling there are a large number of different ways in which to approach the problem and differing mathematical techniques to utilise. Just looking at the four references given above shows *Kangas et al. (2013)* using a Maxwell-Stefan model, *Shen and Lua (2012)* using both the Maxwell-Stefan model and free volume theory, *Golzar et al. (2014)* utilising molecular simulations and *Farno et al. (2011)* using neural network modelling.

The theory used here was first developed by Henis and Tripodi[12, 13] when they postulated about the possibility of using a silicone layer to block the pores in a porous membrane and thereby impart improved gas separation properties onto the membranes. However, the model that they developed was limited and Fouda *et al* (1991)[30] were able to improve upon what had been built by the use of a Wheatstone bridge model which looks at the problem in an manner similar to an electric circuit with resistances built in. The model has hence become known as a resistance model and has seen use by a number of authors[31-34].

In order to model gas separation membranes the factors which have an impact on the permeation rates of gases have to be considered. The factors about the species being separated which have to be considered are the solubility of the gases in the membrane, the partial pressure difference across the membrane, gas diffusion through the membrane material and the physical dimensions and characteristics of the membrane. The resistance modelling carried out here aimed to use the measured separating characteristics of the membranes in conjunction with equations describing the transfer mechanisms in order to calculate the physical characteristics of active layer thickness and surface pore fraction. The data obtained from the oxygen and nitrogen gas pair experiments were focused on due to the literature information available for the gas permeability in PVC.

1.2.3.1. Gas Transport Mechanisms - Knudsen and Viscous Flow

The different mass transfer mechanisms through various membrane structures need to be understood. There are three mechanisms for gas transport through a membrane structure which are solution diffusion, Knudsen flow and viscous flow. Of these three the two most important for transfer through a solid membrane are solution diffusion and Knudsen flow through pores although large pores can also lead to viscous (Poiseuille) flow.

Knudsen flow is a diffusive based flow regime which is expected to occur in narrow channels and pores. The pore sizes in which Knudsen flow is expected to occur are obtained by calculation of the Knudsen number. The Knudsen number, N_K, is found from the mean-free-path length, λ_i, for the particular molecule, i, and the pore radius, r_0:

$$\boldsymbol{N_K = \frac{\lambda_i}{r_0}} \qquad \textbf{Equation 1.2.3.1.1}$$

$$\boldsymbol{\lambda_i = \frac{R_0 T}{\sqrt{2}\pi p N_A d_M^2}} \qquad \textbf{Equation 1.2.3.1.2}$$

The mean-free-path length is calculated from kinetic theory where it is assumed that the velocities of the particles have a Maxwell distribution. The mean-free-path length as described by Equation 1.2.3.1.2 describes the average distance in metres which a particle has to travel between collisions with another molecule in the gaseous state. In this equation R_0 is the universal gas constant, T is the temperature in Kelvin, p is the pressure, N_A is the Avogadro constant and d_M is the molecular diameter.

There are two methods which are often used for the determination of the molecular diameter to be used in these equations. The first rule also stems from kinetic theory and requires determination of the viscosity of the gas so that it can be used in Equation 1.2.3.1.3. There are various means of determining gas viscosity which tend to rely on the flow dynamics of the gas under a certain situation with the most common being laminar capillary flow. In Equation 1.2.3.1.3 the viscosity, μ_i, at a particular temperature, T, is related to molecular diameter, d_M, by the species molecular weight, MW_i, and a number of common scientific constants:

$$\mu_i = \left(\frac{MW_i R_0 T}{\pi^3}\right)^{1/2} \frac{1}{N_A d_M^2}$$ **Equation 1.2.3.1.3**

The use of this formula results in the calculation of the molecular diameters shown in Table 1.2.3.1-1 where the viscosities of the gases are taken at 20°C from *Kaye and Laby, Tables of physical and chemical constants (1995)*[35].

Table 1.2.3.1-1: Molecular diameters of gases determined from the experimental gas viscosities

Gas	Molecular Weight (g/mol)	Viscosity (μPa.s)	Molecular Diameter (Å)
Oxygen	32	20.4	3.59
Nitrogen	28	17.6	3.74
Carbon Dioxide	44	11.0	4.58
Methane	16	14.7	4.11

The second method of determining the molecular diameter is to use the b constant from the Van der Waals equation of state, an adaptation of the ideal gas law to better describe the behaviour which is seen in real gas systems. The improvements on the ideal gas law come about as a result of incorporating molecular size and interaction forces into the calculation. The conventional derivation from the ideal gas law is described below but there is a second route to the final equation using statistical thermodynamics.

The ideal gas law relates the pressure produced by a number of moles of a gas, n, to the volume, V, which the gas will occupy at a stated temperature through the universal gas constant:

$$p_i = \frac{R_0 T}{V_M}$$ **Equation 1.2.3.1.4**

The volume is composed of two parts, space between particles and the particles themselves. If the particles are considered to be hard spheres which cannot overlap then the spaces they occupy can be subtracted from the total volume. This term is referred to as the excluded

volume, b, since it is not available for all the particles to occupy. The value of b differs for each molecule.

$$p_i = \frac{R_0 T}{V_M - b}$$ **Equation 1.2.3.1.5**

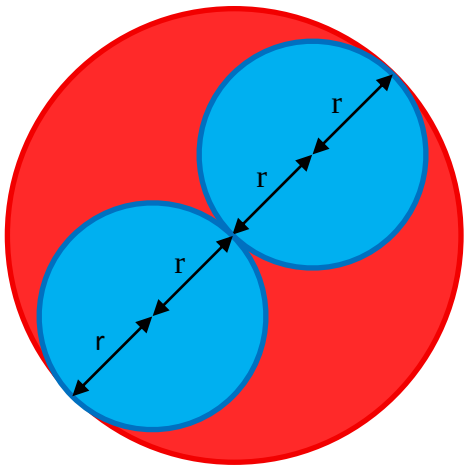

Figure 1.2.3.1-1: Representation of exclusion volume when two hard spheres interact

An important realisation is that the excluded volume is not as simple as being the volume occupied by a single hard sphere but rather is four hard sphere radii in diameter. When two hard sphere particles contact each other the smallest exclusion which can be drawn is the red circle as shown in Figure 1.2.3.1-1. Where the diameter of the red sphere is d_T the total exclusion volume, b', for the interaction of two particles is described by Equation 1.2.3.1.6 and simplifies by introduction of the radius and halving the result to get the volume for a single particle, b. The single actual value will normally be slightly less than that calculated as a molecule is not a hard sphere.

$$b' = \frac{4}{3}\pi d_T^3 = \frac{4}{3}\pi * 2^3 * r_T^3 = \frac{32}{3}\pi r_T^3$$ **Equation 1.2.3.1.6**

$$b = \frac{b'}{2} = \frac{32}{2*3}\pi r_T^3 = \frac{16}{3}\pi r_T^3$$ **Equation 1.2.3.1.7**

The second refinement is the introduction of a term which takes into account the attractive forces between molecules in the gas. Two molecules exhibit little force on each other over long range, however, as they come closer together the interaction is one of attraction up to a maximum where the interaction will move towards a repulsion of increasing magnitude until the molecules are contacted.

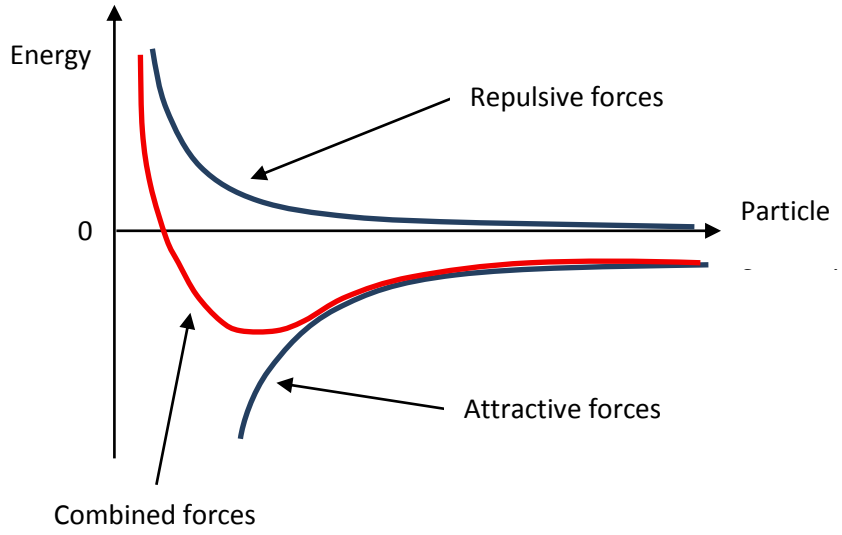

Figure 1.2.3.1-2: Energy of particle interactions varying with separation

In order to implement an interaction term Van der Waals made assumptions about the nature of the gas particles, first that the density of the fluid is homogeneous and second that the attractive force is small enough that the majority of molecules are unaffected by the walls of the container. With these assumptions the particles near the walls experience a net force acting towards the bulk of the container. The effect of this force is to reduce the pressure recorded as there will be less collisions occurring with the walls, to take this change into account the concept of an effective pressure, p_{eff}, is introduced. The attractive forces pulling the outer molecules inwards can be described by a factor proportional to the square of the number density, (N_{Ai}^2/V_i^2). So where a_i is the factor associated with a particular species and V_M is the molar volume the effective pressure is:

$$p_{eff} = \mathrm{p} + a_i \left(\frac{N_A}{V}\right)^2 = p + \frac{a_i}{V_M^2}$$ **Equation 1.2.3.1.8**

The two modifications to the ideal gas law by Van der Waals result in the final equation form:

$$\mathrm{p} = \frac{RT}{V_M - b} - \frac{a}{V_M^2}$$ **Equation 1.2.3.1.9**

Now where a/V_M^2 is the internal pressure of the system the relationship above can be fitted to experimental data. This allows the determination of both a and b parameters for the equation. Therefore the back calculation of the diameter is possible where the hard sphere approximation is applied to the molecules. The values of a and b for some common gases used in gas separation membranes are given in Table 1.2.3.1-2 along with the resultant Van der Waals diameter.

Table 1.2.3.1-2: Van der Waals parameters and resultant diameter

Gas	a (L^2/mol^2)	b (L/mol)[36]	Diameter (Å)[36]
Oxygen	1.382	0.0318	2.93
Nitrogen	1.370	0.0391	3.14
Carbon Dioxide	3.658	0.0427	3.24
Methane	2.303	0.0428	3.24

Comparing the tables containing the molecular diameters for the two different calculation methods, Van der Waals equation and gas flow dynamic experimentation, it can be seen that a slight variation in the value arrived at by the methods exists. The general trend is for the number calculated from the viscosity measurements to be higher than that obtained from the Van der Waals assumptions and the ideal gas equation. For the purpose of this work the values for molecular diameter obtained using the viscosity measurements will be used in the modelling and result in mean free path lengths and Knudsen numbers as shown in Table 1.2.3.1-3.

The pressure used in order to determine the mean free path length is the mean of the pressure difference across the membranes being used, for all the tests carried out in this work the

membrane units were pressurised to 5bar and the permeate side was at atmospheric pressure. This approach is justified by the pore flow model for porous membranes which assumes that the pressure gradient across the membrane reduces as a constant gradient, for Knudsen flow to dominate the transport method must be through pores and thus the same theory applies.

$$p_{mean} = \frac{500000Pa + 101325Pa}{2} = 300663Pa \qquad \text{Equation 1.2.3.1.10}$$

Table 1.2.3.1-3: Calculated mean free path and Knudsen number for tested gases by experimental determination

Gas	Molecular Diameter (Å)	Mean Free Path (Å), at p_{mean} and 20°C	Knudsen Number
Oxygen	3.59	235	65.5
Nitrogen	3.74	216	57.8
Carbon Dioxide	4.58	144	31.4
Methane	4.11	179	43.6

So far these calculations have based the values entirely on the properties of the free gas. This has allowed the calculation of the mean free path length which a molecule has before it hits another molecule in an unconstrained environment. However, in the pore flow being described the walls of the pore could have a bigger influence than the other molecules of gas so the pore diameter which corresponds to a Knudsen number of 10 should be found in order to determine the pore size for the onset of the transition and viscous flow regions. The Knudsen number for the pore flow is calculated from Equation 1.2.3.1.1 which essentially replaces the molecular diameter (used in the calculation in Table 1.2.3.1-3) with the pore radius.

Table 1.2.3.1-4: Pore radii which induce conditions associated with different flow conditions

Gas	Molecular Diameter (Å)	Pore Radius (Å), at p_{mean} and 20°C, for Knudsen Number 10	Pore Radius (Å), at p_{mean} and 20°C, for Knudsen Number 1	Pore Radius (Å), at p_{mean} and 20°C, for Knudsen Number 0.01
Oxygen	3.59	23	235	22966
Nitrogen	3.74	22	216	20007
Carbon Dioxide	4.58	11	108	10352
Methane	4.11	24	239	23366

The transport through a porous membrane has been shown by Barrer *(1941)*[37] and Treybal *(1980)*[38] to be related to the surface porosity (A_p), the pressure difference (Δp), pore radius (r), pore length (L) and the membrane surface area (A).

$$Q_K = \frac{8}{3}\left(\frac{1}{2\pi R_0 T MW_i}\right)^{1/2}\frac{r}{L}A_p A\Delta p \qquad \textbf{Equation 1.2.3.1.11}$$

In addition to this Barrer also provided an equation describing the transport through a porous membrane under the viscous flow regime (Q_V) where p_f and p_p are the feed and permeate side pressures:

$$Q_V = \frac{r^2}{8R_0 T}\left(\frac{p_f + p_p}{2}\right)\frac{A_p A\Delta p}{L\mu} \qquad \textbf{Equation 1.2.3.1.12}$$

These equations for the two different transport mechanisms can then be combined with Equation 1.2.3.1.3 for the viscosity in order to determine the ratio of these types of flow to each other for different pore radii:

$$\frac{Q_V}{Q_K} = \frac{3\sqrt{2}\pi^2 N_A d_M^2}{64R_0 T}\left(\frac{p_f + p_p}{2}\right) \qquad \textbf{Equation 1.2.3.1.13}$$

Figure 1.2.3.1-3 shows the linear trend between the two flow types as the pore radius increases. This produces the expected effect whereby the proportion of flow by viscous means increases with pore radius. Dushman[39] stated that even at pore sizes giving Knudsen numbers of 1 the flow would still be 85% Knudsen diffusion. If the flow is 85% Knudsen then the ratio of Q_V/Q_K = 0.15/0.85 = 0.176. Using this value for the ratio it is possible to back calculate the corresponding pore radius and Knudsen Number for each gas which corresponds to this. The pore radius for a Knudsen number of 1 was calculated for Table 1.2.3.1-4 and is also included in Table 1.2.3.1-5 for comparison to the prediction of Dushman.

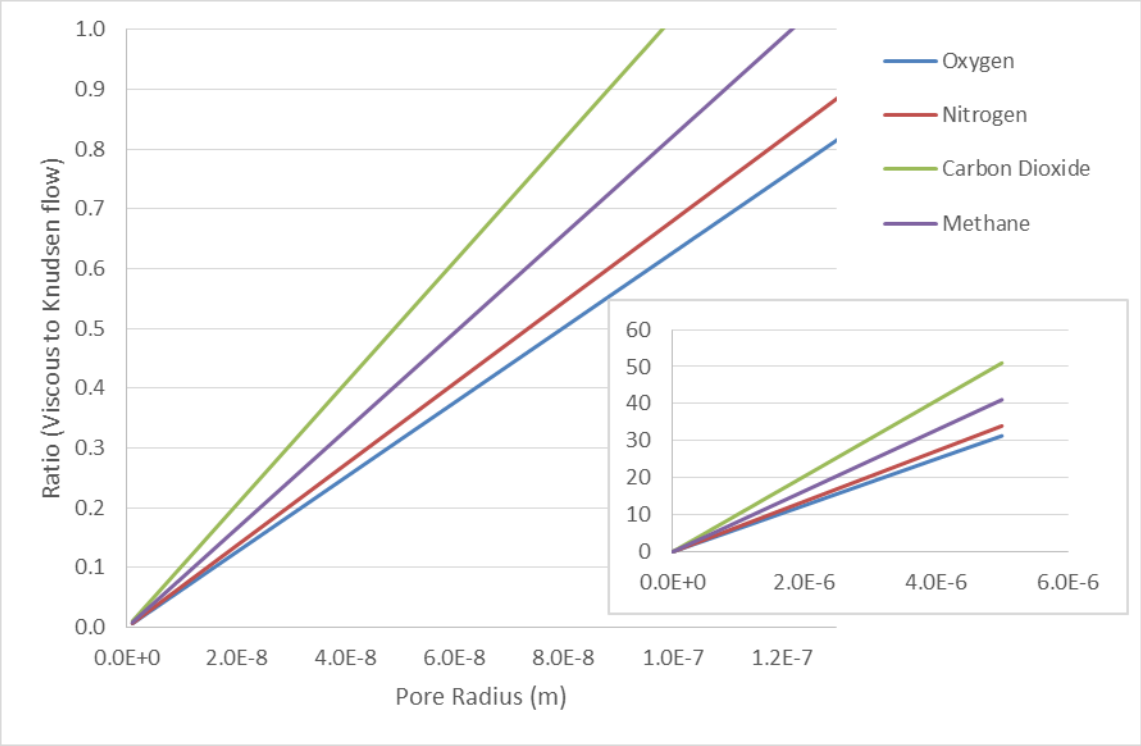

Figure 1.2.3.1-3: Ratios of viscous to Knudsen flow over a range of pore radii for the test gases used in this work

Table 1.2.3.1-5: Comparison of pore sizes and Knudsen numbers for 85% Knudsen diffusion

Gas	Pore Radius (Å), at p_{mean} and 20°C, for Knudsen Number 1	Pore Radius (Å), at p_{mean} and 20°C, for 85% Knudsen Flow	Knudsen Number, at p_{mean} and 20°C, for 85% Knudsen Flow
Oxygen	235	281	0.84
Nitrogen	216	259	0.84
Carbon Dioxide	108	173	0.63
Methane	239	214	1.12

The calculated values show that the point of 85% Knudsen flow and hence also for the pore radius regions where particular flow regimes occur are dependent upon the gas which is being transmitted through the pore. The values show a tendency for larger diameter gas molecules to be under the prediction of Dushman in terms of Knudsen number when the flow mechanism is 85% Knudsen flow while the opposite is true of lower diameter molecules. The figures are

reasonably close to the value of 1 and this would provide a reasonable estimate for most gas molecules.

It has been established that the Knudsen diffusion selectivity is governed by the square root of the ratio of the molecular weights of the gas species such that:

$$\sigma_{KO_2/N_2} = \sqrt{\frac{MW_{N_2}}{MW_{O_2}}} = 0.94$$ **Equation 1.2.3.1.14**

$$\sigma_{KCO_2/CH_4} = \sqrt{\frac{MW_{CH_4}}{MW_{CO_2}}} = 0.60$$ **Equation 1.2.3.1.15**

These relationships are used extensively to explain the results for uncoated and ambient coated membranes in this work. Selectivity values for the membrane similar to those above suggests that the primary transport mechanism through the membranes was Knudsen diffusion since its selectivity is dominant. Selectivity of approximately 1 could be either viscous flow or it could be the balance of solution diffusion to Knudsen flow giving that selectivity. Selectivity of greater than 1 is likely due to solution diffusion in the case of the gas pairs included above.

1.2.3.2. Gas Transport Mechanisms – Solution Diffusion

Two mechanisms were proposed during the 19th century for the transport of molecules through media being used for separation processes[40]. The first of these was the pore flow model in which permeant molecules are separated by pressure driven convective flow through small pores in a similar way to Knudsen diffusion although with the postulated pore flow module there was a large contribution through filtration where one of the species was excluded. This idea is certainly plausible although the pore definition required in order to produce a filtration effect when dealing with the small diameter differences between gas molecules in gas separation processes would be very difficult to control and design towards.

The second transport mechanism proposed was that of solution diffusion. In solution diffusion the species to be transferred through the membrane have to dissolve into the material and

then diffuse through it following a chemical potential gradient. The chemical potential gradient can take a number of forms including concentration, pressure, temperature or electromotive force but it is supposed in the mathematical development of a solution diffusion equation that these are all inter-related aspects which combine to produce an overall chemical potential[40].

Initially due to the ease of visualisation and relation to physical processes familiar in everyday life at the time the pore flow model of mass transport was more popular than solution diffusion as an explanation. However, the solution diffusion model met with great success in application to gas transport properties and eventually success moved into the field of reverse osmosis also.

The steps in the derivation are dependent upon the species which the process has to describe. As this work is interested in gas separations it is necessary to make some assumptions:

- The gas on either side of the membrane is in equilibrium with the membrane material at the interface i.e. no variation in chemical potential gradient from one side of the membrane to the other due to edge effects.
- The rate of absorption and desorption from the membrane interfaces is higher than the rate of diffusion through the material. In order for the first assumption to stand this must be the case or the rate determining step would occur at the interface and hence affect the chemical potential gradient.
- For solution diffusion to apply then the pressure through the membrane must remain constant. In the pore flow transport mechanisms discussed in section 1.2.3.1 this is not the case and it is the concentration which is assumed to be constant (hence the use of p_{mean} in the above section).

The solution diffusion model still includes a difference in pressure between the two sides of the membrane which provides a chemical potential driving force, however, in the case of gases this is manifest as a concentration gradient since the membrane is assumed to transmit a pressure difference in the same way as a liquid does i.e. from Pascal's law a pressure exerted anywhere in a confined incompressible fluid is transmitted equally in all directions throughout the fluid such that initial pressure variations remain the same.

The starting point for the derivation is with Fick's first law since the solution diffusion process is a diffusive mechanism. Fick's first law relates the flux, J, to the diffusion coefficient, D, and the rate of change of the concentration, c, through the membrane thickness, L.

$$\mathbf{J} = -\mathbf{D}\frac{\mathbf{dc}}{\mathbf{dL}} \qquad \textbf{Equation 1.2.3.2.1}$$

This law is applicable in the steady state situation which the assumptions above combine to give. Therefore it is possible to integrate Equation 7.1.3.1 to give a relationship for J in terms of the concentrations of the species on either side of the membrane, c_1 and c_2.

$$\mathbf{J} = \mathbf{D}\frac{\boldsymbol{c_1} - \boldsymbol{c_2}}{\mathbf{L}} \qquad \textbf{Equation 1.2.3.2.2}$$

In the case of gases Henry's law states that at a constant temperature the concentration of a gas which is dissolved at equilibrium conditions in a liquid (again the membrane is treated as a liquid for diffusion purposes) is proportional to the partial pressure of the gas. In this case the coefficient relating the concentration to the gas partial pressure, p, is the solubility coefficient, S. This relationship allows the replacement of the concentration term with gas partial pressure:

$$\mathbf{J} = \mathbf{DS}\frac{\boldsymbol{p_1} - \boldsymbol{p_2}}{\mathbf{L}} \qquad \textbf{Equation 1.2.3.2.3}$$

Conventionally the product of the solubility diffusivity coefficient is referred to as the permeability coefficient, P. Also, the flux is a measure of the permeation per unit area, in practice membranes do not commonly have an area of one unit so the flow through them due to solution diffusion is given by Equation 1.2.3.2.4.

$$\mathbf{Q} = \frac{\mathbf{PA}\boldsymbol{\Delta p}}{\mathbf{L}} \qquad \textbf{Equation 1.2.3.2.4}$$

The permeability coefficient is often quoted in units of Barrer for a particular penetrant dissolving in a particular material at standard temperature and pressure. The non-SI unit of

Barrer is named after Richard Barrer who was known for his work in gas permeability but in SI units the conversion becomes:

$$1\text{Barrer} = 10^{-10}\ \text{cm}^3(\text{STP})\ \text{cm}\ \text{cm}^{-2}\ \text{s}^{-1}\ \text{cmHg}^{-1}$$

The unit contains a number of length terms which could be cancelled out but each refers to a specific aspect of the membrane so they are normally all left in for clarity as to what is being described:

- cm^3 is related to the flow of the gas which is penetrating the membrane.
- cm is related to the thickness of the membrane.
- cm^2 is related to the area of the membrane.

1.2.4. **Membrane Materials**

Membranes can be produced from many different kinds of materials such as ceramics[41, 42] and even metals[43, 44] however these materials tend to be restricted to very specific processes and are far outweighed by the presence of polymeric membranes in the market. There has not been a great deal of work done on the comparison between polymeric and ceramic membranes within the same paper for a particular purpose[45] and it seems likely that these materials will both continue to be used for distinct applications for which they are suitable. In general no matter which materials membranes are produced from they have shown and continue to show promise in many applications.

Polymeric membranes continue to be the most common in part due to their low cost, flexibility in use and provision of a range of different properties which make them suitable in varying applications. The production of these membranes tends to start from a polymer solution. Although for some processes a melt extrusion technique can be used it is rare for this type of process to be applied in practice[46]. When polymers are melt extruded they tend not to solidify into a morphology which is conducive towards practical separation or reaction applications. Therefore a polymer solution, commonly known as a dope, is used as the extrusion media and

vitrifies as a result of mass and or heat balances into various different structural forms depending upon the conditions and process used, hence with careful study the performance of the membrane can be tuned to some extent.

The focus of this work is on polymer membranes and in particular poly(vinyl chloride) membranes, in the following discussion the term membranes generally refers to polymeric based membranes.

1.2.5. **Membrane Geometry and Resulting Processes Module Design**

1.2.5.1. Flat Sheet Membranes

There are two commonly recognised membrane conformations which have applications in industry. The first is to have the membrane in a flat sheet format and the second is to produce hollow fibers. Both types of unit have advantages and disadvantages associated with them and the selection of which type of membrane to use has to be based around the process which it is to be targeted for.

The flat sheet membrane has been developed for use in a number of different processes including; membrane bioreactors (MBR)[47, 48] and many filtration[49-51] or reverse osmosis[52-54] systems. Flat sheets provide some advantages to the user in ease of production and also in mechanical strength, however they also provide low surface areas per unit volume with some designs. The production of flat sheet membranes is usually undertaken by casting the membrane onto a support material. This makes the process itself simple to achieve if an even distribution of polymer can be achieved. The support material itself depends on whether or not it also has a role in the separation process. In the laboratory environment the support is often a glass plate which the cast membrane can be lifted from and used as a free form entity but in industry a film produced this way would be too thin to withstand the rigours of most processes. For industrial applications the most common method of support is to produce a co-polymer

membrane with a highly porous polymer acting as the support, polyester is commonly selected as the material to provide the strength.

As with all membranes flat sheets can be produced in two distinct symmetries across their width known as either symmetric or asymmetric membranes. A symmetric membrane is one which has approximately the same morphology all the way through and the full travel distance through the membrane plays an equal role in the separation which occurs. In an asymmetric membrane the morphology changes across the thickness of the membrane and this leads to the separation being dominated by the slowest mode of transport available. Normally this asymmetric nature is characterised by having a porous support layer with a dense separating layer sitting on top. The asymmetric membrane has the advantage of reducing the thickness of dense membrane required for mechanical strength and therefore aiding the production of higher flux membranes since the slow separation stage is usually the dense section. This is particularly the case for gas separation membranes.

The first producers of an asymmetric membrane which was suitable for use in desalination processes were Loeb and Sourirajan[55]. They developed a method whereby a thin film of cellulose acetate solution was cast and allowed a short evaporation time to form a dense layer followed by submersion in ice-water to form the supporting substructure[55]. The method which was developed gained favour with both Bouchilloux et al[56] and with Kimura[57] who were successful in producing the first gas separation membranes. The method was applied to polymer membranes later by Peinemann and Pinnau to produce membranes of both polyethersulfone[58] and polyetheramide[59].

Another method for the production of flat sheet membranes is to produce symmetrical membranes by casting onto a porous support which provides the same effect as if it was an asymmetrical membrane[60-63] from one material. This means that the membrane can be cast in an extremely thin layer onto the support and allowed to vitrify using a standard process of submerging the membrane on its support in a bath of non-solvent for the polymer (an explanation of how this works will be given below in the hollow fiber discussion since it is a similar process).

As with most things however, there is a trade off in the use of flat sheet membranes and in this case it comes in the form of the area of separating material which can be placed in a specified volume. Flat sheets can be difficult to pack into a unit in a manner which provides easy access to the membrane surface while not giving high pressure drops or making the membrane module prone to fouling. There has been some research done into how to produce units which can maximise the potential of different flat sheet arrangements and one which has gained popularity is the spiral wound module[64-66] indeed this arrangement has been successful enough that even some gas separation applications have been seen[67].

1.2.5.2. Hollow Fiber Membranes

The use of flat sheets for gas separation membrane processes is a surprise because flat sheet membranes tend to have a greater restriction on area than is seen for hollow fiber modules. What often swings the balance of favour towards the use of flat sheet membranes with the lower surface area is the use of liquids and other "heavy" species in the separation processes which would take a greater toll on the lifetime of thin hollow fiber membranes than they do on the flat sheets. In gas separation processing however there is less chance of the hollow fiber membranes being seriously compromised during processes and therefore the comparative vulnerability to damage is not such a big issue. This allows the possibility in gas separation processes to use modules of either vertically or horizontally strung hollow fibers which can be closely packed, for commercial modules packing density is often between 45-60%[68] which can give surface to volume ratios of 2000-4000ft^2/ft^3. This is the best illustration of why gas separations processes utilise the hollow fiber arrangement as the surface area available for plate and frame flat sheets is 100-150ft^2/ft^3 and for spiral wound modules is 200-250ft^2/ft^3, indeed this is the main reason behind the 80%[69] prevalence of hollow fiber modules for gas separation.

The production of hollow fiber modules can be accomplished in a large number of ways. The type of module used is generally process specific especially when dealing with processes such as ultrafiltration where damage to the membranes could be a problem. The modelling of modules and analysis of the flow patterns which are produced within them see a lot of interest

from the scientific community particularly on the shell side[70-74]. However, due to the low density and viscosity and the high diffusivities of the species involved in gas separation processes a number of the main effects seen in liquid separation processes are not considered relevant to the study and design modules for these purposes. One example of these differences in the processes is the flow maldistribution which has been a major topic of study for processes with liquids but does not significantly impact gas separation processes.

The flow on the lumen side of the membranes was studied by Park and Chang[75] who showed that there were a large number of influences on the flow experienced on this side of the membrane. These effects ranged from the manifold size and shape through expected influences like fiber inner diameter and tube length but also included some influences from the shell side flows such as shell diameter, packing fraction and Reynolds number. This shows that the design of hollow fiber modules has to be very carefully considered with regards to flow and mass transfer as the different sides of the separation can have an influence on each other. The relationship between different sides of the separation is unsurprising since the key to separations is a potential gradient between the two sides. Again these factors have much less influence on gas separation processes than it does on processes which involve liquids.

In the laboratory setting small numbers of hollow fibers are often used in comparison to industry where a module may contain thousands of strands. There are various reasons for this including the facilities available, ease of module production and. In this work the largest module used contained sixty individual membranes but the most common sizes were either single strands or three strands. The actual set up is described more thoroughly in the experimental section.

1.3. Hollow Fiber Gas Separation Membrane Preparation Methods

1.3.1. Preparation of Hollow Fibers for Gas Separation

The production of the hollow fiber membranes to go in modules is a highly specialised process. There are four general methods of production which are commonly referred to in the literature: melt spinning, dry spinning, wet spinning and dry wet spinning[76]. There is a great deal of secrecy around the industrial processes and equipment which are used and this is particularly true of the main piece of equipment; the spinneret, which is almost always patented whenever a new design is utilised. Research is also published on the best way to go about designing spinnerets[77, 78] and the focus of this research is often directed at the spinneret nozzle and the best design to obtain a spinning process which is stable and consistent in the quality of fibre which it produces[79].

The shape of the spinneret can have a significant influence on the production of the hollow fibers. It is often shape of spinneret which is responsible for fiber instabilities such as draw resonance, necking, capillary break-up, irregular cross-section and melt fracture or extrudate distortion[80-83]. The results of such instabilities are most commonly seen as fiber breakage or non-uniform cross sectional area during the spinning process and have mechanisms which are influenced by fluctuations in the polymer flow lines which are the result of drawing and capillary forces produced by the spinneret design[79].

The spinneret design is therefore an important part of the production of hollow fiber membranes however the processes which take place within the design are all very similar. In general the spinneret will allow the flow of a polymer medium (either melt or dope) through an outer annulus and introduce a bore fluid into the centre of this flow to hold the hollow nature of the membrane and stop the membrane wall collapsing. In order to do this the bore fluid encourages the formation of an inner wall which will provide structural stability to the hollow nature of the membrane. For melt extrusion processes this can be brought about by a temperature variation but in solution processes the solidification is usually accomplished via a combination phase inversion of the outer layer combined with phase inversion induced by the bore fluid being a non-solvent for the polymer material. The separation for the hollow fiber membranes is most usually conducted at the outer surface so for most applications, and

especially gas separation, the internal wall will form part of the porous section of an asymmetric membrane. The bore fluid properties should be selected so as to expedite the formation of this porous structure.

The formation methodology of the outer skin for the separation depends upon the production method which is being used. Of the four mentioned above the most common to be seen in the literature are wet spinning and dry wet spinning. These methods avoid some of the energy requirements which are associated with melt spinning production and the wet phase allows more control over the processes which are occurring than is generally achieved by a purely dry manufacturing process. The mechanisms behind the wet process were described J.A. van't Hof *et al* in 1992[84] where a dual bath coagulation method was presented while the dry/wet spinning method and theories behind it were discussed by I. Pinnau and W.J. Koros in 2003[85].

1.3.2. **Preparation of Hollow Fiber Gas Separation Membranes by the Wet Method**

1.3.2.1. Liquid-Liquid De-mixing

The wet method described by van't Hof *et al* utilises liquid-liquid de-mixing methods to produce layers in asymmetric gas separation membranes, they built on the work of Reuvers *et al* on the liquid-liquid de-mixing process[86, 87] who had shown that there were two methods by which the de-mixing could proceed: instantaneous and delayed. The type of de-mixing which occurs is related to how well the different solvents which make up the solution are able to interact with each other, it is thought that this is still the critical factor even when ternary solutions are used as they often are in membrane production[88].

Where the interaction between solvent in the dope and non-solvent in the casting medium is good the result will be an instantaneous de-mixing processes. If a membrane dope enters a non-solvent solution which interacts strongly with the solvent in the dope then the de-mixing process will begin as soon as the contact between the dope and non-solvent occurs. The de-mixing process happens instantaneously because the ratio of outflow of solvent to inflow of

non-solvent is lower than is seen in the delayed de-mixing process. The result of this is a dense top layer which tends to be imperfect due to the amount of non-solvent influx and is therefore unsuitable for gas separating. The sub-layer also de-mixes rapidly resulting in a local polymer concentration hardly changed from that which was present in the dope solution initially which means that the structure formed during the de-mixing is an open porous network.

Delayed de-mixing occurs where the interaction between the solvent in the dope and the non-solvent in the casting medium is poor. Here, as the name suggests, the onset of liquid-liquid de-mixing is delayed from the time of contact of the solvent and non-solvent by the necessity for non-solvent to penetrate completely through the film (or fiber) being formed. Only when this is complete can the local concentration of non-solvent rise high enough to allow liquid-liquid de-mixing to occur. The reason behind this delayed progression to de-mixing lies in the different diffusion rates which are occurring during the delay time as a result of thermodynamic interaction and the friction coefficients which are present in the system[86, 89]. These factors combine to give a large outflow of solvent but with only a low inflow of non-solvent therefore leading to an increased concentration of the polymer in the dope solution near the interface. The thickness of the concentrated layer grows with respect to the square root of the contact time between the two solutions but only up to a maximum concentration which is less than that required for de-mixing. When the concentration front reaches the other side of the membrane the concentration in the membrane can go above the threshold for de-mixing to occur. At the interface between the solutions solidification of the polymer can occur producing a dense top layer as would be desirable for gas separation membranes, however in the sub-layer the result is a closed cell structure network which has high resistance to gas transport which is undesirable. This structure is formed because the high polymer concentration hinders nuclei growth in the polymer lean phase and the amount of solvent/nonsolvent available will be limiting growth factors[84].

1.3.2.2. Utilising Liquid-Liquid De-mixing to Produce Gas Separation Membranes

From their understanding of the two de-mixing mechanisms outlined above van't Hof *et al* concluded that in order to obtain a good gas separation membrane it would be beneficial if a

method could combine the two different mechanisms: firstly a short period of the delayed de-mixing mechanism to produce the dense surface layer followed by instantaneous de-mixing to produce the sub layer with an open pore network. The method developed utilises two different non-solvent baths, the first of which displays poor interactions with the casting solution and the second displays good interaction. The time in the first bath can be optimised to produce a thin defect free active layer and normally has a lower submersion time than the time taken for the interface concentration to reach its maximum value i.e. submersion time is less than delay time. This can pose a problem as the submersion times required are so short in order to achieve a very thin dense layer that they lead to high casting or spinning speeds which can be detrimental to the structure (as it has no mechanical stability on leaving the first bath since only the concentration has been increased and no precipitation has occured) or difficult to achieve.

The difficulties are particularly true of hollow fibre membranes which have no casting support but have to be self-supporting. The result is that the method described by van't Hof often requires some clever manipulation of the solvent/non-solvent systems so that the delayed de-mixing process occurs in a less dense non-solvent layer sitting on top of the denser non-solvent in which the instantaneous de-mixing occurs in a single coagulation bath. This has other difficulties associated with it in terms of the non-solvent mixing which occurs as the fiber passes through the interface of the two non-solvents. Careful design of the mechanical means of transporting the hollow fibre between the two baths can also be utilised where miscible non-solvents are to be used whereby a small diameter hollow only fractionally bigger than the fiber itself may be used between the baths giving minimal mixing of the two.

1.3.2.3. Preparation of Hollow Fiber Gas Separation Membranes by the Dry/Wet Method

Due to the difficulties which have been described above, in this work the dry/wet method described by Pinnau and Koros was favoured as a spinning method since it could be set up to avoid not only these issues but also to avoid the use of larger amounts of solvents/non-solvent in the system. In the method developed by van't Hof *et al* and described above there is no

definitive time allowed in which evaporation of solvent or non-solvent from the casting/spinning solution can occur between the casting or extrusion of the membrane and it entering into the coagulation baths. However, it was found in the early seventies by Strathmann *et al*[90, 91] that the thickness of the active layer and the porosity of it can both be affected by an evaporation step, this result has since been backed up by a number of research groups. In the dry/wet methods phase separation brought about in the outer layer during the evaporation step produces the active layer then the sub-layer is formed by liquid-liquid phase separation by submersion in a non-solvent bath as before in the wet method.

1.3.2.4. Phase Diagram in Dry/Wet Method Gas Separation Membrane Preparation

The dope solutions which are used for dry/wet formation methods are generally at least three component solutions. These solutions will contain a solvent, non-solvent and polymer component, however the solutions can also have an additional high volatility solvent introduced to shift the position of the composition on a ternary diagram. The diagram in Figure 1.3.2.4-1 shows the progress of the solution during the dry step of the process. Here the extruded membrane is exposed to a set of forced convective conditions in the form of a gas stream which causes evaporation of the solvent from the outer regions of the membrane. The effect of the evaporation is to change the concentrations of the components in this region such that the volume fractions (Φ) traverse a path similar to that from point A to point D in Figure 1.3.2.4-1. The physical processes which occur at each of these point are controlled by the Gibbs free energy for mixing of the system[92]

The binodal curve is defined by the composition of polymer rich and polymer poor phases which the unstable solution inside the curve will split into as shown along the tie lines. Along this boundary each of the two phases which the solution separates into will have the same chemical potential which is the equilibrium value[92]. Phase separation can occur in this region and proceeds by a process of nucleation and growth. If the Gibbs free energy is plotted against the mole fraction of a component present in a phase then the minima present on this curve will reflect the binodal compositions at this point. For a binary system this results in a single

manner in which the solution will split however in a ternary system a much more complicated relationship is required and most commonly the Flory-Huggins theory is used.

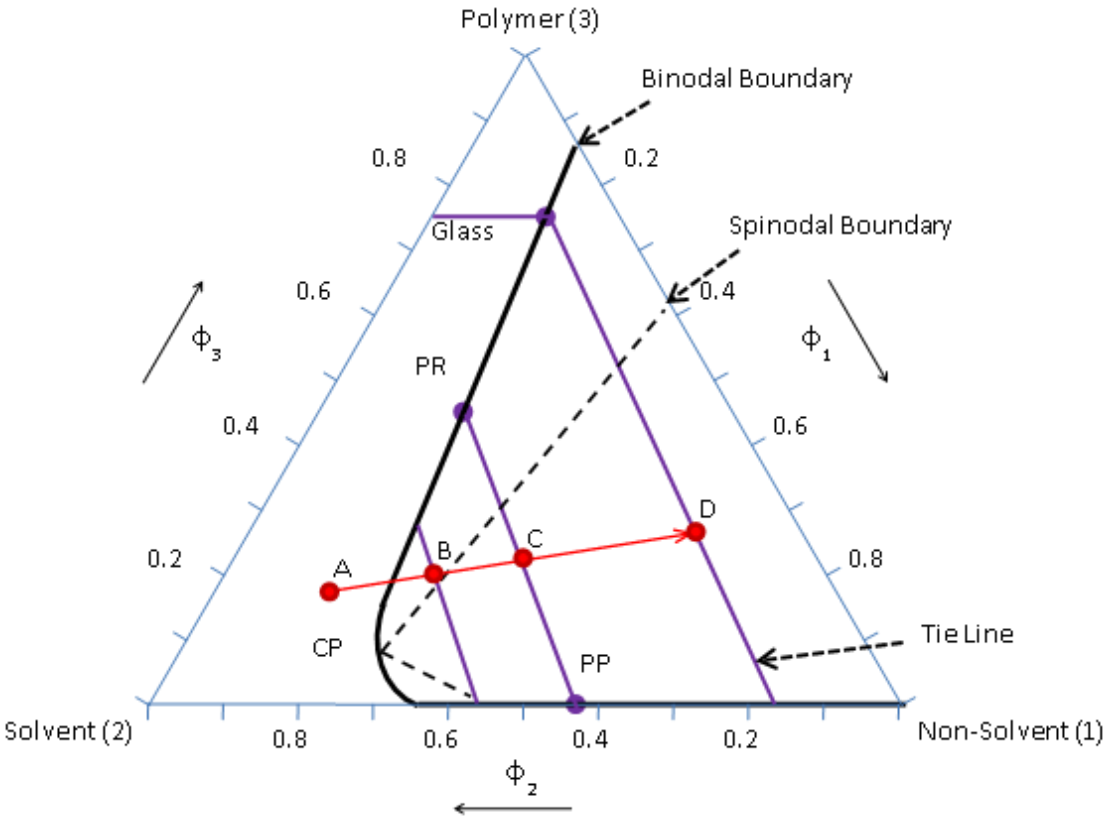

PR = Polymer Rich PP = Polymer Poor

CP = Critical Point Φ = Volume Fraction

Figure 1.3.2.4-1: Dope solution composition possible progression during dry step

The plot of the Gibbs free energy will also contain points of inflection between the maxima and minima present within it and these are the points which represent the spinodal boundary. This is a critical region in the systems behaviour as the only barrier present to phase separation in this region is diffusion and hence the system will phase separate spontaneously into two interpenetrating polymer rich and polymer poor phases given that the smaller phase has at least a volume of 15% of the overall volume[93]. Spinodal decomposition is related to time with

the initial structure remaining unchanged while the compositions of the two phases depart from the average composition and approach the binodal regions compositions and eventually the structure coarsens and interconnectivity is lost[92]. Again this simple discussion is best applied to a binary system and for the more relevant ternary systems Flory-Huggins theory is often applied.

1.3.2.5. Flory Huggins Theory

The Flory Huggins theory relates the Gibbs free energy of the system to the volume fractions of each component in the system, which is a direct replacement from the mole fractions in the binary system theory but also has to take into account interactions between each binary pair present in the system[94-96].

$$\frac{\Delta G_M}{RT} = n_1 \ln \phi_1 + n_2 \ln \phi_2 + n_3 \ln \phi_3 + \chi_{12} n_1 \phi_2 + \chi_{13} n_1 \phi_3 + \chi_{23} n_2 \phi_3 \qquad \textbf{Equation 1.3.2.5.1}$$

Where; ΔG_M is the Gibbs free energy of mixing, R is the universal gas constant, T is the temperature, n is the number of moles, Φ is the volume fraction and the subscripts refer to the components of the solution where non-solvent (1), solvent (2) and polymer (3). This situation is complicated by the addition of a more highly volatile solvent to the system but for simplicity the two solvents are considered as a single component in this discussion. In order to describe the situation completely in ternary solutions however ternary interaction parameters would be required in this equation also however a number of researchers have found success utilising binary interactions alone[97-100].

The interaction parameters are also concentration dependent and so obtaining accurate parameters over the full range is a time consuming process which has led researchers to keep some of the parameters constant while changing others. It is not clear which parameters this should be done with however as results have been found using either the non-solvent/solvent[97] interaction or the solvent/polymer[99] interaction as the dependent

parameter which have allowed replication of the experimentally found miscibility gaps by theoretical methods.

In a multiphase system the chemical potential of a component is split between the phases which are present and these chemical potentials must be in equilibrium with each other, as for the production of the binodal curve earlier, such that where $\Delta\mu$ is the chemical potential difference between the pure and solution state chemical potential and A and B represent the two phases the for each component i:

$$\boldsymbol{\Delta\mu_{i,A} = \Delta\mu_{i,B}}$$ **Equation 1.3.2.5.2[92, 101]**

Since the change in chemical potential is also equal to the derivative of the Gibbs free energy then by taking the partial derivative of Equation 1.3.2.5.1 with respect to the number of moles of the component and combining this with Equation 1.3.2.5.2 expressions can be obtained for the chemical of each component. Note that for these equations all interaction parameters have been assumed constant and υ is the molar volume of the component in the pure state.

$$\frac{\boldsymbol{\Delta\mu_1}}{\boldsymbol{RT}} = \boldsymbol{\ln\phi_1 + 1 - \phi_1 - \frac{\nu_1}{\nu_2}\phi_2 - \frac{\nu_1}{\nu_3}\phi_3 + (\chi_{12}\phi_2 + \chi_{13}\phi_3)(\phi_2 + \phi_3) + \chi_{23}\frac{\nu_1}{\nu_2}\phi_2\phi_3}$$ **Equation 1.3.2.5.3[92]**

$$\frac{\boldsymbol{\Delta\mu_2}}{\boldsymbol{RT}} = \boldsymbol{\ln\phi_2 + 1 - \phi_2 - \frac{\nu_2}{\nu_1}\phi_1 - \frac{\nu_2}{\nu_3}\phi_3 + \left(\chi_{12}\frac{\nu_2}{\nu_1}\phi_1 + \chi_{23}\phi_3\right)(\phi_1 + \phi_3) + \chi_{13}\frac{\nu_2}{\nu_1}\phi_1\phi_3}$$ **Equation 1.3.2.5.4[92]**

$$\frac{\boldsymbol{\Delta\mu_3}}{\boldsymbol{RT}} = \boldsymbol{\ln\phi_3 + 1 - \phi_3 - \frac{\nu_3}{\nu_1}\phi_1 - \frac{\nu_3}{\nu_2}\phi_2 + \left(\chi_{13}\frac{\nu_3}{\nu_1}\phi_1 + \chi_{23}\frac{\nu_3}{\nu_2}\phi_2\right)(\phi_1 + \phi_2) + \chi_{12}\frac{\nu_3}{\nu_1}\phi_1\phi_2}$$ **Equation 1.3.2.5.5[92]**

This system contains six unknowns, the volume fractions present in each of the phases for the three different components, which allow the location at the binodal boundary to be calculated. There are five equations which relate the six variables, three of these equations are obtained

by substituting Equations 1.3.2.5.3,4,5 into Equation 1.3.2.5.2 and the other two are the material balances which describe the volume fractions of each component in each phase given by Equation 1.3.2.5.6:

$$\sum \boldsymbol{\phi_{i,A}} = \sum \boldsymbol{\phi_{i,B}} = \mathbf{1} \qquad \textbf{Equation 1.3.2.5.6}$$

In order to define which point of the phase diagram is being looked at the volume fraction of one of these components in the phase has to be defined, doing this leaves five equations and five variables and the system of equations can therefore be solved although the methods employed to do so may be complicated.

The spinodal curve on the phase diagram is defined thermodynamically as the second partial derivative of Gibbs free energy with respect to the volume fraction of a component or two components:

$$\frac{\boldsymbol{\delta^2 \Delta G_M}}{\boldsymbol{\delta \phi^2}} = \mathbf{0} \qquad \textbf{Equation 1.3.2.5.7}^{[102]}$$

So where non-solvent (1) is taken as the reference component then the spinodal curve was shown to be obtainable by *Tompa*[96] and separately by *Kurata*[103] from:

$$\frac{\boldsymbol{\delta^2 \Delta G_M}}{\boldsymbol{\delta \phi_2^2}} \frac{\boldsymbol{\delta^2 \Delta G_M}}{\boldsymbol{\delta \phi_3^2}} = \left(\frac{\boldsymbol{\delta^2 \Delta G_M}}{\boldsymbol{\delta \phi_2 \phi_3}} \right)^{\mathbf{2}} \qquad \textbf{Equation 1.3.2.5.8}$$

So from the Gibbs free energy relationship shown in Equation 1.3.2.5.1 and carrying out these partial derivations it can be found that where u_1 and u_2 are the volume fractions of non-solvent and solvent respectively on a polymer free basis[92, 102]:

$$\boldsymbol{u_1} = \frac{\boldsymbol{\phi_1}}{\boldsymbol{\phi_1 + \phi_2}} \qquad \textbf{Equation 1.3.2.5.9}$$

$$\boldsymbol{u_2} = \frac{\boldsymbol{\phi_2}}{\boldsymbol{\phi_1 + \phi_2}} \qquad \textbf{Equation 1.3.2.5.10}$$

$$\frac{\delta^2 \Delta G_M}{\delta \phi_2^2} = \frac{1}{\phi_1} + \frac{\nu_1}{\nu_2 \phi_2} - 2\chi_{12} + 2(u_1 - u_2)\left(\frac{d\chi_{12}}{du_2}\right) + u_1 u_2 \left(\frac{d^2\chi_{12}}{du_2^2}\right) \quad \textbf{Equation 1.3.2.5.11}$$

$$\frac{\delta^2 \Delta G_M}{\delta \phi_2^2} = \frac{1}{\phi_1} - (\chi_{12} + \chi_{13}) + \frac{\nu_1}{\nu_2}\chi_{23} + u_2(u_1 - 2u_2)\left(\frac{d\chi_{12}}{du_2}\right) + u_1 u_2^2 \left(\frac{d^2\chi_{12}}{du_2^2}\right) \quad \textbf{Equation 1.3.2.5.12}$$

$$\frac{\delta^2 \Delta G_M}{\delta \phi_2^2} = \frac{1}{\phi_1} + \frac{\nu_1}{\nu_3 \phi_3} - 2\chi_{13} + 2u_2^2(1 - u_1)\left(\frac{d\chi_{12}}{du_2}\right) + u_1 u_2^3 \left(\frac{d^2\chi_{12}}{du_2^2}\right) \quad \textbf{Equation 1.3.2.5.13}$$

Back substitution of these equations into Equation 1.3.2.5.8 along with the material balance equation allows the solving of this system in a similar fashion to that used for the binodal curve. Again there is a requirement to fix one of the variables in order to determine the location of the data being sought and this will normally be one of the volume fractions.

1.3.2.6. Phase Separation as Depicted by the Phase Diagram

For any given position within the metastable or unstable region of the phase diagram the composition will split along a tie line to give the polymer rich and polymer poor phases. The ratio of one phase to the other can be determined from the lever rule. The lever rule states that the length of the line from the composition point to the split on the binodal boundary in the polymer rich phase multiplied by the amount of the polymer rich phase is equal to the same thing for the polymer poor phase i.e. for Figure 1.3.2.4-1 point C:

$$n_{PR}\overrightarrow{L_{CPR}} = n_{PP}\overrightarrow{L_{CPP}} \quad \textbf{Equation 1.3.2.6.1}$$

The start of this split effect occurs where the spinodal and binodal boundary come together at the critical point (CP). The critical point is most important for phase separation which proceeds by nucleation and growth. By comparing the polymer concentration at the critical point to that

of the composition of the solution in the metastable region the phase which will nucleate can be found where:

- polymer concentration lower than the critical point gives nucleation of the polymer rich phase.
- polymer concentration higher than the critical point gives nucleation of the polymer poor phase..

Point A shows the starting position of the dope solution composition. In this region of the ternary diagram the dope is stable and will not phase separate. However, as the solution is exposed to a forced convective gas stream the evaporation of the most volatile component in the solution will evaporate first, this is an important assumption as it means that the penetration through the phase diagram is partially controlled by the concentration of the highest volatility component. This is the reason why a second high volatility solvent often forms part of the dope solution to give the user more control over the process. The high volatility solvent forms a part of the solvent component on the ternary diagram and therefore the ratio of non-solvent to polymer in the solution remains the same through the process.

If the evaporation phase leads to a composition in the outer layer of the membrane at point B where it lies inside the binodal boundary but outside the spinodal boundary (the metastable region) the liquid-liquid phase separation can proceed by nucleation and growth. This type of mechanism results in a phase separation which gives a dispersion of polymer lean phase in a continuous polymer rich phase and as described above the position of the composition within the phase diagram will determine the result[92]:

- low polymer concentration nucleation of the polymer rich phase results in a powdery type structure forming which will not have the integrity to produce successful membranes.
- high polymer concentration nucleation of the polymer poor phase results in a closed cell micro-porous morphology suitable for the membrane substructure in gas separation but not the active layer formation which the evaporation step aims to produce.

Either longer exposure time in the dry step or a higher forced convective gas velocity can move the composition of the solution at the surface to position C. In this region the phase separation is spinodal in nature and the polymer rich phase produced by the separation will contain a higher concentration of polymer than the binodal separation from the same polymer concentration which results in the formation of a bicontinuous network of polymer rich and polymer poor phases[93]. This bicontinuous network results in the outer layer of the membrane having a nodular structure consisting of high concentration polymer spheres with interstitial spaces filled with polymer poor phase[104-106].

There are two suggested ways possible for why this nodular structure could benefit the separation. The first of these is by multiple layers of nodules stacking such that the interstitial space on one layer overlaps with a nodule on the lower layer thus filling and plugging the gap. The second mechanism is nodule coalescence. It seems likely that the final separation of the membrane is aided by both of these mechanisms. It is nodule coalescence which this thesis focuses on as a method for explanation of the separations which are seen from the membranes.

1.3.2.7. Nodule Coalescence

Kesting, (1973)[107] suggested that the coalescence of nodular structures was playing an important role in the formation of membranes which were produced by dry step phase inversion but, it was *Pinnau and Koros (1993)*[85] however who suggested the mechanism by which this is believed to occur. They proposed that capillary pressure acting at the interface between the membrane and the air could cause the surface nodules to coalesce producing a dense layer. This was an already existing phenomenon in drying of latex to produce films and could be promoted by the solvent and non-solvents present in the polymer solution exhibiting a plasticising effect on the polymer rich phase. A number of authors had studied the film formation of latex[108-113] but it was the work of *Brown (1956)*[114] which provided the impetus to produce the theory for membrane formation.

Brown (1956)[114] proposed that during the drying process the condition for film formation of water-based polymer (latex) emulsions must come from the force exerted by capillary pressure (F_C) being greater than the resistance of the polymer to deformation from its nodular shape (F_G):

$$F_C > F_G \qquad \textbf{Equation 1.3.2.7.2}$$

The capillary pressure in the latex system comes about as a result of the curvature of the water between the latex particles and this was seen to be analogous to the polymer lean phase between the polymer rich nodules. The capillary pressure exerted acts in a normal direction to the interface between the polymer and interstitial fluid as shown in

Figure 1.3.2.7-1 causing the deformation of the polymer nodule into the interstitial space assuming the nodule is "soft" enough.

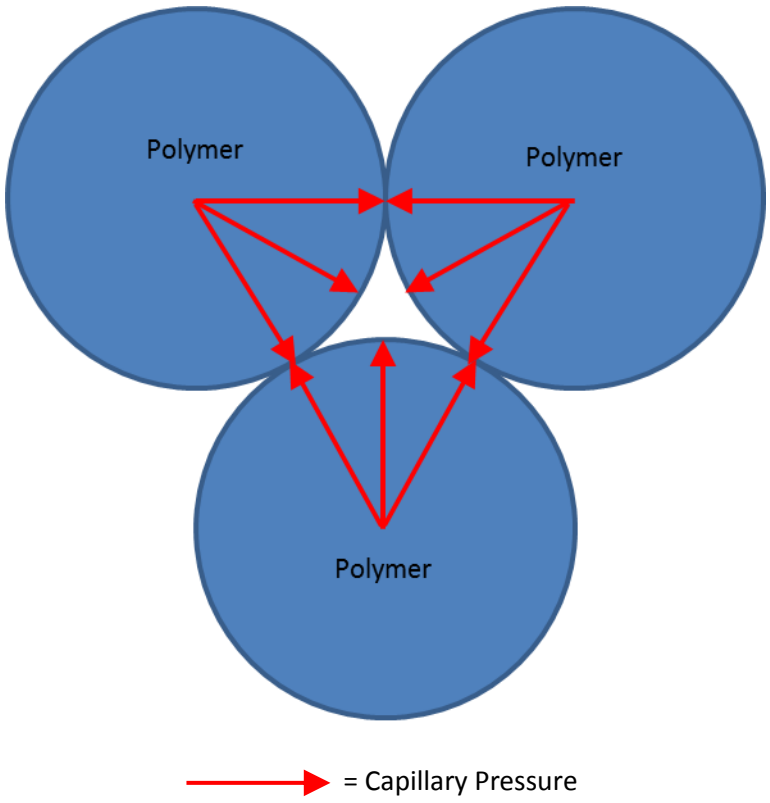

Figure 1.3.2.7-1: Polymer nodules showing capillary pressure

The pressure which is applied onto the polymer spheres is associated with the Young-Laplace equation for perfect wetting so long as the contact angle is zero and is related to the surface tension of the interstitial fluid (γ) and the radius of the interstitial space:

$$P_C = \frac{2\gamma}{r}$$ **Equation 1.3.2.7.3[114]**

This equation can be exchanged for one relating the radius of the polymer spheres (R) if they are considered to form an array of packed hexagons:

$$P_C = \frac{12.9\gamma}{R}$$ **Equation 1.3.2.7.4[114]**

Brown[114] also derived the relationship for when a film would be formed by an array of hexagonal closed-packed spheres related to the shear modulus, G:

$$G < \frac{35\gamma}{R}$$ **Equation 1.3.2.7.5[114]**

In reality it is highly unlikely that the spinodal phase separation produced bi-continuous network will result in as regular a structure of spheres as is supposed in this theory however studying the nature of polymers and putting in some values reveals why it is not a completely unreasonable condition to apply.

The ability of the polymer to form a film through capillary pressure effects being related to the modulus is important because the modulus of polymers can vary significantly under different conditions. This suggests that the range of polymers which could be used for gas separation membranes is larger than the range currently being studied intensely if the right conditions can be found for production. The relationship between modulus and temperature for amorphous polymers will typically show five regions of behaviour as shown in Figure 1.3.2.7-2 where for any polymer material near its glass transition temperature (T_g) the same five regions may be expected to be found. In the case of this work the PVC material being used has a glass transition temperature of around 85°C which is much lower than the more commonly used

polysulfone which shows a T_g nearer 180°C so it is expected to see these regions in the work. The limits on each of the regions depend on various factors but molecular weight and its distribution are major contributors[85].

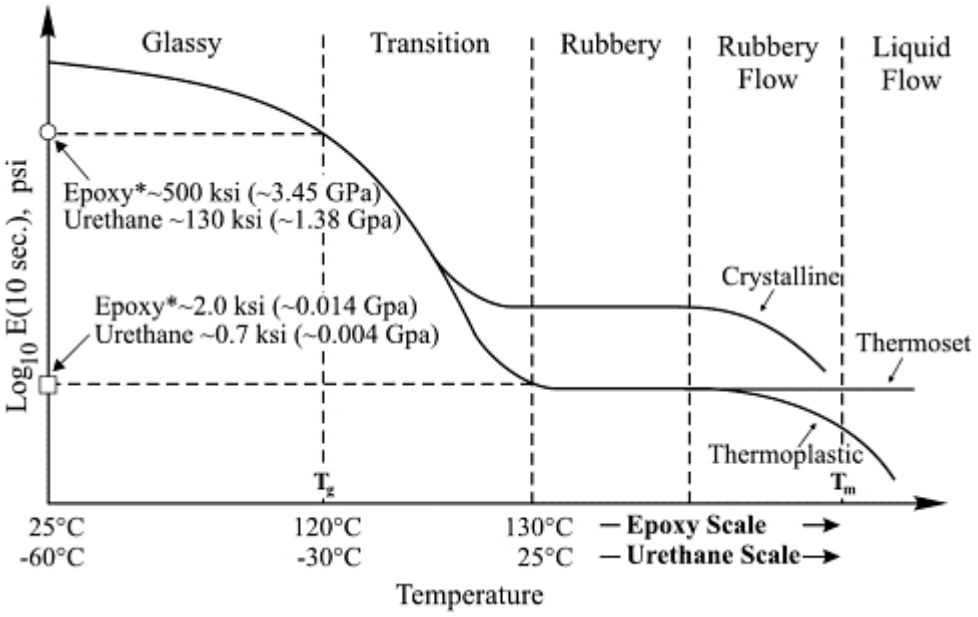

Figure 1.3.2.7-2[115]: Five regions of viscoelastic behaviour of polymers based on epoxy and urethane examples. The curves for polymers all contain the same regions but can present different values of modulus within them at different temperatures.

Membrane formation processes are generally carried out at constant temperature but the procession of the composition through the phase diagram will also produce the effect of giving the five regions of behaviour. Burghardt *et al* (1987)[116] and Gaides and McHugh (1989)[117] made predictions for the behaviour of polymer solutions and estimated that the glassy phase would correspond to polymer concentration greater than 70%. In the glassy state polymers are more brittle than at higher temperatures. The molecules in a glassy state experience a greater level of difficulty in rearrangement with realistically only vibrational and short range rotational motions being enabled. Transition to a glassy state quickly enough can lock the polymer molecules in a higher energy state as they are not free to move into a more thermodynamically favourable orientation. This could be a helpful factor for the production of gas separation

membranes as it has been shown that molecular orientation helps to improve the separating properties which can be achieved. The reduction in molecular mobility is caused by a reduction in the specific volume of the materials which shows a change in the slope and defines the location of the glass transition temperature at the point where the straight line relationships of the glassy and rubbery state intersect.

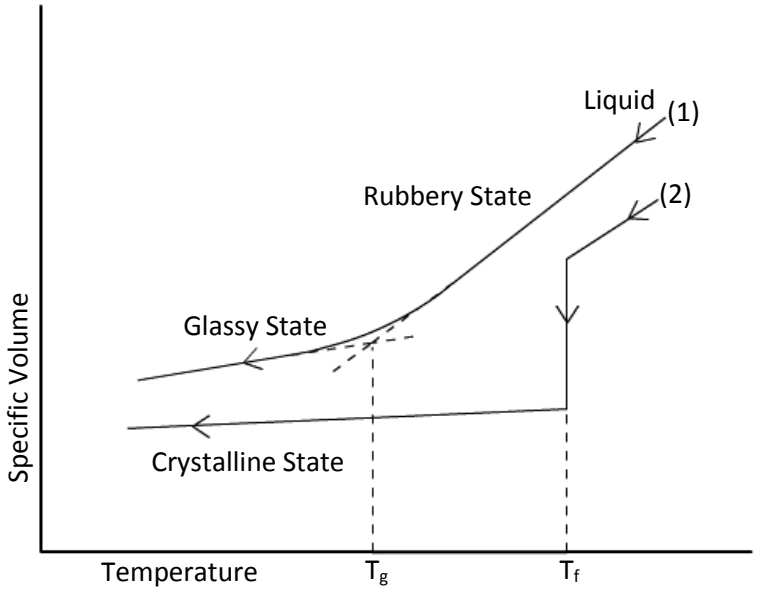

Figure 1.3.2.7-3: Relationship between specific volume and temperature for a crystalline (2) and an amorphous (1) material. T_g is defined as the point on the amorphous curve where if the lines for the glassy state and rubbery state were both extended straight they would cross.

The reduction in the specific volume of the polymer could also prove useful as if there is less space available between molecules then the material will exhibit lower porosity and this should be good for the skin of a gas separation membrane. However, at the high polymer concentration associated with the glassy state (70% V/V) the modulus of polymers is expected to fall into the range of 100-1000MPa[85]. The high modulus in the glassy state can result in the inability to coalesce the nodules in the skin formation process.

Pinnau and Koros (1993)[85] used the work of *McMaster (1975)*[105] who suggested that phase separation in polymer solvent systems occurs with particle sizes in the range of 150Å to 6000Å, in conjunction with their own experiences with SEM's of polymeric membranes showing an active layer between 200Å and 500Å to set a range of particle sizes which could exhibit coalescence. This range has since been corroborated by a number of authors and with different materials[118-121]. Using this data and Equation 1.3.2.7.5 along with a surface tension of 0.02N/m for organic solvents in casting solutions[122] the range of particle sizes which could coalesce to form an active layer was plotted and gave a range of pressures of 7-70MPa which suggests moduli would also have to fall into this range.

From the above work it can be concluded that entering into the glassy phase of the viscoelastic behaviour would prevent the polymer surface from coalescing effectively and means the tie line on Figure 1.3.2.4-1 which passes through point D and represents the glass transition composition would not coalesce. It has been suggested that polymer concentrations of between 50-70 volume% would give a modulus in the range of 2-40MPa[85] which does fall inside the theoretical range of pressures which are expected to be produced at the surface of the membrane. However, in practice it is expected that a lower capillary pressure than expected will exist due to the limits placed on it by the tensile strength of the fluid in the interstitial spaces. *Sheetz (1965)*[123] suggested that the maximum capillary pressure available in water-based emulsions is approximately 4.1MPa if this is used as a guide for the dope solutions then this value would only correspond with the lower end of the concentration band identified above.

Summing-up the conditions necessary to allow phase separation and nodule coalescence to occur based on the above discussions: Equation 1.3.2.7.5 must be satisfied and "particle size" of the nodules must be small enough to allow capillary pressures greater than the resistance to deformation of the nodule. This corresponds to approximately position C in Figure 1.3.2.4-1 which will allow spinodal phase separation to occur at the surface of the membrane. Under these conditions the nodules will coalesce and seal the outer extremities of the membranes with a dense homogeneous layer. Since when this layer forms there are no longer any interstitial spaces at the surface, then below the surface the polymer takes on a nodular

structure over the depth which spinodal decomposition has occurred however without capillary pressure the network will remain open.

1.3.2.8. Structure Formation in Dry/Wet Gas Separation Membrane Preparation

In order to form the structures which are described above the spinodal decomposition must take place within the dry step. If the membrane enters the wet quench step then the whole membrane will instantly de-mix, as this is what the wet step is designed to do, but if this occurs before the spinodal separation and nodule coalescence has progressed far enough then the whole membrane will be porous from this mechanism. The kinetics associated with the dry step of the process are exceptionally quick, in fact if they are related to the more easily quantifiable kinetics of thermal spinodal decomposition then for practical purposes the time frames involved in the creation of the dense top layer are instantaneous[85]. This can be seen in practice when the membranes pass through the spinneret and are exposed to the forced convective gas stream as the surface begins to haze very quickly as the phase separation occurs. The effect of the length of time the membrane is exposed to the dry step therefore has a greater effect on the thickness of the layer which undergoes spinodal decomposition before quenching than on the formation of the dense layer itself.

From the dry step convection chamber the membranes enter into the quench baths which form the wet step of the process. Entering into the wet step the surface layer of the membrane is a thin coalesced layer atop a partially spinodally phase separated layer with a final layer of composition which has hardly moved from its original state. The support layer of the membrane will not yet have had time to coalesce under the influence of the bore fluid as the liquid-liquid de-mixing by solvent exchange takes longer than the influence of the dry evaporation step. It is desirable to maintain as much of the structure as possible before pores in the spinodally phase separated region can collapse and hence it is important to attain instantaneous de-mixing in the quench baths.

By utilising a non-solvent which has good interaction with the solvents in the dope solution forming the membrane the phase separation occurs rapidly transforming the surface layer into

a non-porous, homogeneous layer. The top layer is so thin it allows diffusion of species through it from both sides and this exchange allows the vitrification of the sub layer to occur from both the surface and from the solvent exchange with the bore fluid. The wet step instantaneous de-mixing results in an open porous structure with the dense homogeneous surface layer representing the best profile for a gas separation membrane.

1.3.3. **Additional Stages in Membrane Preparation**

The membranes produced by either a wet method or a dry/wet method contain a large amount of non-solvent within the structure. The most common practice at this point is to allow the membranes to dry in air. However, often the non-solvent which is used in order to quench the membranes is not highly volatile e.g. water and this means that it can be difficult for the centre of the membrane structure to dry out in particular because it is porous. In order to work around this there is often a solvent exchange step introduced before the membranes are potted in modules.

During solvent exchange the membranes are soaked in a high volatility non-solvent for the membrane material. This displaces a large amount of the low volatility solvent from inside the membranes and then when the membranes are again allowed to air dry they are left in a much drier state since it is easier for the evaporation to occur.

Gas separation membranes require a high degree of perfection in order to be effective. Even with a consistent and developed process it can be difficult to achieve a surface layer which is completely homogeneous over the full area and even if this were accomplished they are very susceptible to damage by handling during processing including module production. *Henis and Tripodi* were the first to provide a solution to the problem of small pores in the membrane surface when they developed a process by which a silicone coating was applied to the membrane surface[12, 13]. This process does not have to be complicated with dip coating into a solvent containing the silicone solution being enough to accomplish the desired effect of

covering the pores. Indeed this work was successful enough that it led to a number of patents for both the inventors and the Monsanto company[124, 125].

1.4. Gas Separation Membranes Development Paths and Industrial Usage

1.4.1. Historical Overview

The use of gas separation membranes in industry began to take off with the patents gained by Henis and Tripodi and Monsanto. They spearheaded the development of the first industrial applications of gas separation membranes in the production of ammonia where they were used to recover hydrogen from nitrogen based purge streams. In the early 1980's this process was estimated to be accounting for $5*10^6 ft^3$/day of Hydrogen recovered, however by 1994 the rapid growth in membrane technology and understanding meant this number had elevated to $4*10^8 ft^3$/day[126]. The clear interest from industry in the use of membrane technology for gas separation provided impetus for research both industrially and within academia. A field of study which had been open since Sir Thomas Graham published "*On the absorption and dialytic separation of gases by colloidal septa*"[127] suddenly saw renewed interest with developments and progression following quickly[92].

Figure 1.4.1-1 shows some examples of industrial developments in polymeric gas separation membranes between 1980 and 2010. These highlights show the different areas of improvement which have contributed to the continued success of membranes; modules (which have been discussed already), preparation method (the switch to hollow fibers from flat sheets) and also in the materials which are being used to produce membranes.

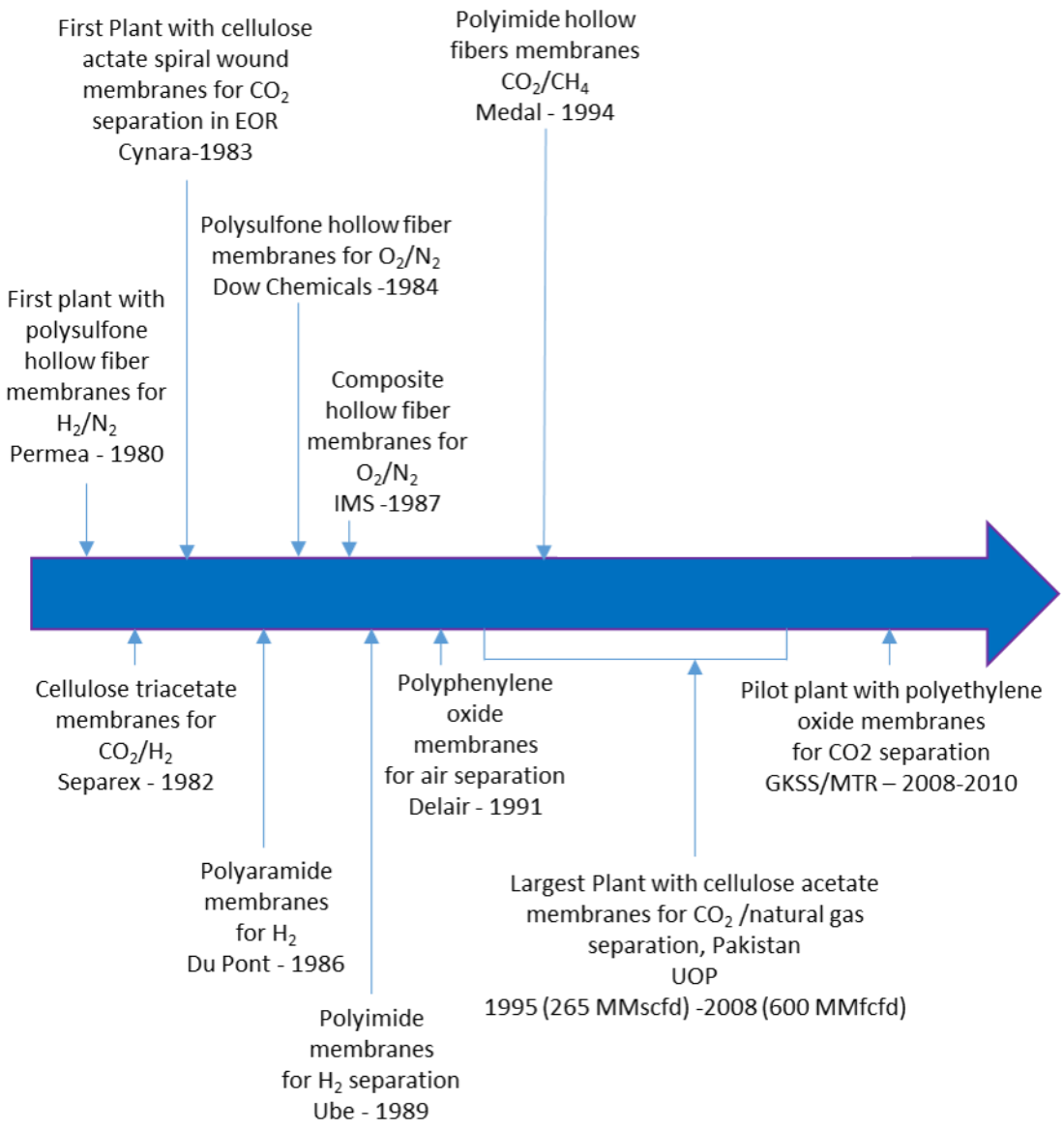

Figure 1.4.1-1: Timeline of important industrial gas separation membrane application advances[128]

A large amount of work has been put into the development, refining and characterisation of different materials for producing membranes. These materials can consist of pure polymers[129-133] similar to those of the initial polysulfone membranes produced for use by Monsanto or can have been modified by processes to crosslink[134-137] or chemically alter the base polymer structure[138-141]. One natural extension of the development of materials is to produce

membranes which contain multiple materials, these co-polymer membranes produce different combinations of properties than the pure polymers used to make them and this has become a popular method of attempting to improve the properties[142-145].

1.4.2. **Robeson Upper Bound**

Another method of combining the properties of different materials in order to achieve gas separation membrane performance is mixed matrix membranes. These membranes tend to incorporate non-polymeric materials into a standard polymeric membrane in an attempt to use the inclusions properties to boost the performance. The idea came about as a result of a paper published by *Robeson (1991)*[146], this is generally considered a landmark paper for polymeric membranes as it postulated an upper limit on the selectivity which could be achieved by using solely polymeric membranes.

Robeson conducted a thorough literature search and plotted the values of selectivity which polymeric membranes were achieving for different gas pairs. The selectivity values were plotted against the permeability of the fastest permeating gas in the membrane and it was found that almost no values existed above the upper bound of this line which had a slope related to the Lennard-Jones Kinetic diameter. This resulted in *Robeson* drawing the conclusion that the separating capabilities were governed by the diffusion coefficient of the membrane. In a more recent update of his work *Robeson (2008)* concluded that there had been only minor shifts in the positions of his upper bound for most gas pairs since he had first published[147].

Figure 1.4.2-1 shows a schematic of a Robeson diagram which may be produced on completion of a literature search for polymeric membranes for a particular separation. The key aspect of this however was that it referred to polymeric membranes. In order to produce membranes which could improve upon the upper bound and produce better separating properties at higher gas fluxes researchers began working with carbon membranes[148]. Carbon membranes proved themselves capable of beating the rules imposed on most polymeric membranes by Robeson's upper bound[149, 150]. However, in spite of the growing popularity of producing carbon

membranes by the pyrolysis of polymer precursor membranes they have flaws: production can be relatively expensive to obtain high quality membranes, therefore there is a tendency to display a fragility unpractical for industrial modules in some cases[151-155].

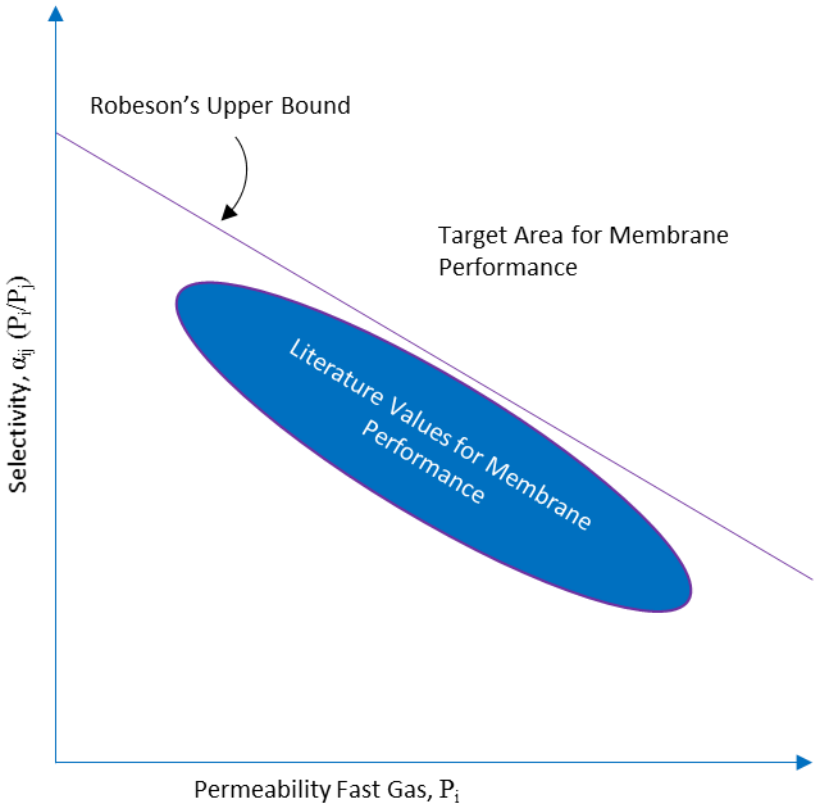

Figure 1.4.2-1: Robeson's upper bound diagram

1.4.3. Mixed Matrix Membranes

As a compromise to the flaws of both polymeric membranes and their carbon membrane counterparts the idea of mixed matrix membranes was developed. In these membranes solid inclusions are added to the polymer dope solutions and cast or spun along with the polymer. This produces a membrane which contains solid particles throughout its structure with the aim being that enough of the inclusions better separating qualities are imparted to the membrane

to improve its functionality while the polymer matrix provides the mechanical properties desirable in gas separation membranes. These strategies have met with success at times and the nature of the inclusions has progressed from the use of simple components like carbon black[156] and silica[157, 158] to more complex modern materials such as zeolites[159, 160], metal organic frameworks (MOFs)[161, 162] and carbon gels[163].

The mixed matrix membrane appears to give the best of both worlds, however, as with anything there are draw backs and issues associated with them. From solution preparation issues where the even dispersion of finely ground particles through what can be a highly viscous solution presents a challenge to the final characterisation of the more heterogeneous structure. Production issues also exist, particularly in the production of hollow fiber membranes where the particles have a much higher propensity for blocking the spinneret or causing uneven flow resulting in the fiber breaking during production. Perhaps the most troublesome issue however is with obtaining a strong adhesion between the particulate inclusion and the polymer matrix[164, 165]. If interfacial separation between the particles and the polymer is too large they act as a fast transport route for the gases to pass through reducing the effectiveness of the separation, it was shown by *Aroon et al 2010* that this was a bigger problem with rubbery polymers than glassy ones[166].

1.4.4. Gas Species Targeted for Gas Separation

A look at the industrial processes which are described in Figure 1.4.1-1 reveals that industrially gas separation membrane milestones are largely devoted to a small range of gases including oxygen, nitrogen, hydrogen and carbon dioxide. These gases represent a large proportion of the gases utilised in academic work also with the inclusion of methane to the list. The most commonly seen gas pairs studied are oxygen/nitrogen and carbon dioxide/methane (or hydrogen). There are a number of reasons for this:

- These gases are prolific throughout industry and so represent a large target demographic and possibility for funding opportunities

- They are simpler and safer to work with than most gases
- Other gases tend to have a much greater deleterious effect on the membrane materials (carbon dioxide does present issues associated with swelling whereby the free volume of the polymer is reduced and flux suffers without a great benefit in selectivity)
- Generally the research direction seems to have been towards understanding the mechanisms of gas separations and how different membrane materials and modifications can affect the properties of the final product.

These reasons are valid enough for the focus on a limited gas range. However, there are deviations from this route with a focus on gases such as more complicated organics[167]. The use of these gases often severely hampers the choices of materials which can be used to produce the membrane through damage which they will cause over time or reductions in flux which occur over time. This work is focused on producing a gas separation suitable for dealing with one such unusual mixture in the form of ozone/oxygen systems.

1.5. Gas Separation Membranes in this Thesis

1.5.1. **Ozone Gas**

1.5.1.1. Ozone Properties

Ozone, O_3, is the triatomic allotrope of oxygen. It is a widely known chemical mostly for its presence in the Earth's atmosphere and the effect its depletion is having on global warming. This is in spite of the fact that it only accounts for about 0.6ppm of the Earth's atmosphere. Natural ozone is produced by two mechanisms: from diatomic oxygen molecules under the influence of ultraviolet light (this is the mechanism which prevents some of the suns radiation reaching the Earth) and from natural electrical discharges in the atmosphere i.e. thunderstorms.

Ozone gas has a bale blue colour and a very strong odour being detectable to humans by this trait at concentrations down to about 0.1ppm[168]. Exposure to ozone should be limited and is regulated in the UK by the *Health and Safety Executive* which gives a recommended exposure concentration of no more than 0.1ppm as an 8hour time weighted average or a short term exposure limit of 0.3ppm as a 15min time weighted average concentration.

There are also safety concerns around the use of ozone due to its capability to react explosively. Ozone is highly reactive and can undergo a number of different reactions but the most important with respect to the explosive nature of the reaction is the conversion back to diatomic oxygen.

$$2O_3 \rightarrow 3O_2$$

At room temperature and pressure with ozone gas this decomposition is not so quick as to pose a threat of explosion, it has been found that the half-life time of ozone is highly dependent on temperature and humidity conditions and could vary between 39mins and 24hours over a range of conditions[169]. The slowest reactions occur at low temperature, humidity and pressure. Even although the gas does not pose a spontaneous explosion risk at atmospheric conditions at concentrations of more than 10% deflagration can be triggered by an ignition source[170].

1.5.1.2. Industrial use of Ozone

The safety implications of working with ozone make it less attractive than it might otherwise be for use in industry. However, the characteristics of ozone and the potential which it has for use across industry mean that it has gradually gained popularity. The widespread use of ozone and its varied use began in 1840 when German Scientist Christian Friedrich Schönbein officially discovered and named ozone from the Greek “ozein” meaning to smell. The first specialised ozone generator was patented by Nikola Tesla in 1896 followed by the commercial application in the water industry which began in 1903 in Niagra Falls but took off particularly in France where by 1916 there were 26 industrial plants utilising ozone. Progress was steady across

industry but the progression in the USA is best seen by the progression of the Food and Drug Administration (FDA) approvals:

- 1976 – approved as antimicrobial oxidiser
- 1982 – granted generally recognised as safe (GRAS) status for use in bottled water
- 1997 – an expert panel from the electric power research institute finds in favour of granting GRAS for ozone direct contact with food and the FDA agrees
- 1998 – US Environmental Protection Agency confirms ozone is effective in removing hazardous pathogens and chlorine resistant Cryptosporidium from water
- 2001 – FDA approves ozone as a secondary direct food additive as an antimicrobial agent.

Ozone now has applications across industry seeing use in pharmaceuticals, lubricants, cleaning, water, food and even medical industries.

1.5.1.3. Ozone Production

Having such a wide range of applications means that the production of ozone is itself quite a large industry. Provision of ozone to processes is not as simple as for many other species due to the half-life issues which have been mentioned above. The fall out of these handling difficulties is that ozone tends to be produced on-site, local to the application in order to avoid transportation losses. The production also tends to be on a continuous but on-demand basis.

The production methods for ozone involve four main methods: corona discharge, ultraviolet light, cold plasma and electrolytic. Each method has advantages associated with it which influence the choice of process for the production. Corona discharge is the most commonly used method and involves the production of an electrical discharge to spark the feed gas (air or pure oxygen) to produce ozone in concentrations which range from 3-15% dependant on feed and the generator. There are some modern models such as the SEMOZON® AX8407 which can do better than this achieving 18.5% ozone by weight. Where air is used in the feed harmful nitrates can also be produced by these production units.

Ultraviolet production methods utilise the same mechanisms as take place in the Earth's atmosphere in order to produce ozone without the production of the nitrates seen in corona discharge. However, ozone concentrations are often in the region of 0.5% and the time for production of ozone is slower due to the lower energies involved.

Cold plasma utilises pure oxygen and exposes it to plasma which splits the oxygen into single atoms which can then recombine as ozone. These generators produce ozone in maximum concentrations of approximately 5% and even although they are capable of doing this very quickly the systems are very expensive both in capital cost compared to other types and in operational costs.

Finally electrolytic production involves splitting of water molecules into H_2, O_2, and O_3. This produces ozone where some is lost in solution but still modern generators can achieve up to 30% concentration ozone. The production requires a large energy input and as such is costly.

It is important for the production of ozone that all these generators can be produced from materials which are compatible with ozone. This is a bigger limitation on the equipment than with most species due to the high reactivity of ozone. Metals will generally be oxidised by ozone to the extent that even stainless steel of grade 304 will gradually degrade under the influence of ozone and grade 316 is required for production units. On the side of polymers and rubbers most materials will be degraded by the presence of ozone with the most resistance being offered by carbon chains which are completely saturated and contain few functional groups.

1.5.1.4. Ozone Reactivity and Half-life

The restriction on unit construction materials may seem like a property which would further restrict the use of ozone but it is the high reactivity and oxidation potential which in fact makes it such a valuable tool in essentially all of the applications with which it is associated. The oxidation potential of ozone is huge in comparison to other commonly used oxidisers as Table 1.5.1.4-1 shows it has over 1.5 times the electrochemical potential as chlorine which is perhaps the best known oxidising agent in general use. This large potential means that ozone will drive

reactions to occur, and is able to break down compounds and species which other oxidising agents cannot and therefore it is particularly useful where the extent of reaction is crucial such as in the water industry. The additional benefit which comes from ozone is the bi-products of the reactions which it undertakes, where with other oxidisers the bi-products tend to also be dangerous e.g. halogenated organics, these do not exist with ozone which in fact will attack them and break them down.

Table 1.5.1.4-1: Electorchemical potential of various common oxidising agents

Oxidising Reagent	Electrochemical Potential (V)
Ozone	2.07
hydrogen peroxide	1.77
chlorine dioxide	1.57
Chlorine	1.36
Oxygen	1.23
Bromine	1.09
hypochlorite	0.94
Chlorite	0.76
Iodine	0.54

Ozone does have challenges and limitations on the uses with which it can be put. Some of the handling issues have been touched on but it is the concentration limitation and production of these higher concentrations requiring a large investment which is stunting what has otherwise been a rapid growth in ozone use in a number of markets. Looking at the review of the production methods above the highest concentration which can be produced of ozone is the electrolytic method at 30%. This is a much higher concentration than the other methods and opens up other potential uses and a higher efficiency in established processes. However, it is more expensive. Likewise improvements can be made in the production methods which utilise gas stream inputs by switching from air input to pure oxygen input. This has benefits on processes in multiple ways giving not only a higher concentration of ozone but also avoiding the production of side products like nitrous oxides which can be particularly problematic in

corona discharge production. The down side of making this switch is the cost associated with supplying pure oxygen feed to the process and that the oxygen which is unconverted often goes to waste.

The research to find an answer to the concentration tends to focus on the efficiency of and improvements to the ozone generator[171-174] in order to reduce costs. However, this is not the only route available. A large amount of the cost involved in the use of pure oxygen gas is incurred in the oxygen which goes to waste having not been converted but being unable to be recycled. If a separation process was developed which allowed the recycling of this oxygen then this could be a valuable contribution in allowing the use of pure oxygen feeds which results in a double method of ozone concentration improvement i.e. use of pure oxygen feed improves concentration and the separation process again improves concentration.

The high reactivity of ozone has benefits for the processes which ozone is useful in, however clearly makes handling an issue. This is also a problem which applies to the separation processes which could be applicable because chemical methods result in the ozone reacting. Membrane gas separation avoids some of these issues but since gas separation membranes are most commonly made out of polymer materials a polymer which is ozone resistant must be used as the base case for the membranes. This base case could then be changed to improve membrane performance by addition of particulates to form a mixed matrix membrane or by modification of the polymer chains. However, modification of the polymer material presents problems as the addition of functional groups into the structure makes it more likely that the ozone will have a group which it can react with.

The membrane also should be produced from a material having properties which lend it to the production of hollow fibers. This means that a glassy state (at room temperature) polymer which is saturated and does not contain functional groups which are subject to attack has the best properties. Traditional membrane materials such as polysulfone are generally unsuitable for use with ozone so the possibility of using poly(vinylchloride) was identified.

1.5.2. **Poly(vinyl chloride) (PVC)**

1.5.2.1. Industrial Usage of PVC

Poly(vinyl chloride) is one of the most commonly used polymers in the world with production falling behind only that of polyethylene and polypropylene as far as plastics are concerned[175]. The development of poly(vinyl chloride) to this state of popularity was not altogether smooth. The polymerised form of vinyl chloride is believed to have been discovered accidently at least twice during the 19th century, first in 1835 by French chemist Henri Victor Regnault and then in 1972 by German chemist Eugen Baumann. However, it was not until 20th century that serious attempts were made to utilise the material in commercial products. Unfortunately these early attempts were stymied due to the rigid and sometimes brittle nature of the polymer they were attempting to use. Most modern PVC products are produced with the addition of plasticiser into the pure PVC compound. These plasticisers have the effect of producing a material which is easier to work with. Inclusion of plasticisers is not desirable in this work as these may be subject to the chemical attack of ozone, especially since the most common plasticisers are species of the phthalate family which introduces an aromatic nature into the compound which is very susceptible to ozone.

1.5.2.2. Beneficial Polymer Structures for Gas Separation Membranes

The review of polymer materials and the potential for their use conducted by *S.A. Stern (1994)*[176] gives a thorough overview of the important polymers in the gas separation membrane field and the polymer properties which are considered to have an important effect on the production of a high selectivity gas separation membrane. Structurally the best polymers have a stiff backbone, low inter-segmental packing of the polymer and low energy inter-chain interactions.

A polymer with a stiff backbone is beneficial because it allows better discrimination between different gas species. The selectivity of the membrane is linked to the amount of free volume which is present in the polymer matrix and the size of the spaces between the molecules. A rigid backbone generally will allow the molecules of the polymer to pack better with less chain

folding and this helps to better define the interchange spacing resulting in a more uniform molecular pore size. If the size of the inter-chain spaces is then in the region of the size required to separate gases then this can have a profound effect on the separation qualities of the membranes.

Low inter-segmental packing follows a similar reasoning as that of the stiff backbone where with low chain folding the structure is more regular. The regular structure in turn allows better molecular packing and from this a better selectivity can be achieved.

Finally if the inter-chain interactions between the molecules are large then they can increase the energy of certain conformations of the polymer molecules. This can result in the chains not packing particularly well as they find lower energy states to arrange themselves in when coming out of the solution. The shear forces involved in the production of membranes, particularly hollow fibers, can help to relieve this issue somewhat by the shear forces stretching the polymer chains out to provide a greater degree of molecular orientation and then this conformation being frozen in place during the formation of the active layers.

These factors all help to improve the selectivity of the membrane but they also help explain the inverse relationship between the selectivity and the permeability since they all involve the closer packing of chains and hence a reduction in free volume. Reduction in free volume decreases the permeability because the gas permeation mechanisms allow for faster mass transport through a more porous structure. These properties are also all physical in nature and therefore ignore effects which could be induced by interactions between the gases being separated or interaction between the gases and the polymer being used.

1.5.2.3. PVC Structure

PVC is a glassy amorphous polymer. This means that before the application of shear forces the polymer chains are not stacked in a structured manner and therefore the free volume could be expected to be larger than for a closely packed polymer matrix. However, with the application of a shear force the amorphous nature of the polymer makes it easier for the chains to rearrange themselves along the flow lines and if this molecular orientation can be frozen into

the structure then it could lead to a highly aligned structure in that area of the membrane with a low free volume. In the case of unmodified PVC there are no large side groups to disturb this orientation process which could lead to very tight packing.

The limited use of PVC for gas separation membranes which does exist in the literature tends towards the use of modified PVC. The work which has been done shows that the unmodified version exhibits good selectivity but low permeability in the production of cast sheet membranes[177-180]. This low permeability has been seen as prohibitive to the use of pure PVC membranes and so modifications made have been targeted at opening the structure slightly to improve the transmittance of the gas[177-180]. Unfortunately due to the reactivity of ozone the modification of PVC is not seen as viable for a starting material and instead the pure PVC membranes are preferred as a starting point.

1.5.2.4. Influence of Molecular Weight

Another aspect of the polymer utilised which can have an impact on the separation which is achieved is the molecular weight. There are a few methods of calculating the molecular weights of polymers but there are two which are more common than the others: number average and mass average. The number average molecular weight (M_n) is the mean of the molecular masses (M_i) of the number of molecules (N_i) which make up the total mass:

$$\boldsymbol{M_n = \frac{\sum N_i M_i}{\sum N_i}} \qquad \textbf{Equation 1.5.2.4.1}$$

The mass average molecular weight of a polymer is the molecular weight which a randomly selected molecule will have on average and is found by:

$$\boldsymbol{M_W = \frac{\sum N_i M_i^2}{\sum N_i M_i}} \qquad \textbf{Equation 1.5.2.4.2}$$

The effect of the molecular weight is reflected in the membrane by the relationship which it displays with the specific free volume (SFV) of the polymer matrix:

$$\boldsymbol{SFV = \frac{(V_T - V_0)}{M_W}} \qquad \textbf{Equation 1.5.2.4.3}^{[181]}$$

Where V_T is the specific volume of the polymer at temperature T, and V_0 is the hypothetical specific volume of the material at 0K. This free volume is further affected by the processes which produce the membranes i.e. shear forces. These shear forces and their affects on the material also vary with molecular weight adding a further layer of complexity to the situation. It has already been described how the shear effects seen in the spinneret during hollow fiber production can cause the polymer to experience rubbery behaviour even at temperatures below the glass transition temperature. This is especially true since a larger molecular weight polymer is likely to produce a dope solution which has a higher viscosity which can have implications on the spinning processes of hollow fiber production. Since the free volume changes significantly with the changing nature of the material it is difficult to predict the effects of initial free volume on the final structure but it is expected that the general relationship (Equation 1.5.2.4.3) should have an impact.

The relationship between the free volume and molecular weight is therefore inversely proportional so following this equation one way to increase selectivity is to use a lower molecular weight polymer starting material which will also give reduced permeability of the membrane. The most commonly used gas separation membrane polymer is polysulfone which is available from *Aldritch* with number average molecular weights of 16000g/mol and 22000g/mol. With respect to PVC *Aldritch* offer three different number averaged molecular weights at 22000g/mol, 35000g/mol and 47000g/mol. Since the densities of PVC (1400kg/m^3) and polysulfone (1240kg/m^3) are similar at 25°C and the specific volume is the inverse of density it was concluded that the use of the 22000g/mol PVC would give a free volume which was most similar to that which is seen in polysulfone membranes.

Another impact which may be seen through the molecular weight of the material being used is the consistency between membranes which are produced. The requirement for molecular weight to be expressed as an average comes from the range of different molecular weight polymer molecules which exist for a particular product. The distribution of this molecular weight range depends on the processes and the materials used to form the final product. It could be expected that a narrow molecular weight distribution would provide a greater degree of consistency in final membrane products than might be seen from much wider distributions.

The effects of this however are likely to be very small and hence are unlikely to be able to be isolated through variations contributing from other factors.

1.5.2.5. PVC Reactivity

The use of PVC in this application comes around partly as a result of its relatively low reactivity being a saturated organic molecule with the only group place susceptible to chemical attack really being the site of the chlorine bond. While this helps provide a stable membrane under the target process conditions PVC is not the best choice of polymer when it comes to producing a solution. The range of suitable solvents is slim and for the dry/wet process the desired dope solution composition utilises both a high volatility solvent and a low volatility solvent. One relationship which is well known for being used with polysulfone membranes is to use dimethylacetamide (DMA) as the low volatility solvent and tetrahydrofuran (THF) as the high volatility solvent. THF is a good solvent for PVC and is used as a solvent for the polymer in a number of industrial processes including resin production. DMA is not as good a solvent for the PVC but does have a much lower volatility than alternatives such as toluene which is a good solvent. The most likely alternative to DMA would be dimethylformamide (DMF) but both offer similar properties and hazards so DMA was used as there was experience in working with it.

The final two components are the non-solvent for the dope solution for which ethanol was used and the non-solvent for the coagulation baths. One advantage of the use of these solvents is that they allow the use of water in the coagulation baths which reduces the cost of the hollow fiber production process significantly.

Finally, it is worth noting that although this thesis focuses on the ozone and oxygen relationship PVC exhibits good resistance to a number of oxidising materials. This property means that there are also opportunities for the use of PVC membranes in applications which involve an oxidative environment unsuitable for other membrane materials.

1.6. Bibliography

1. Chen, S-H, Liou, R-M, Hsu, C-S, Chang, D-J, Yu, K-C, and Chang, C-Y, *Pervaporation separation water/ethanol mixture through lithiated polysulfone membrane.* Journal of Membrane Science, 2001. **193**(1): p. 59-67.
2. Ohya, H, Matsumoto, K, Negishi, Y, Hino, T, and Choi, HS, *The separation of water and ethanol by pervaporation with PVA-PAN composite membranes.* Journal of Membrane Science, 1992. **68**(1–2): p. 141-148.
3. Yanagishita, H, Maejima, C, Kitamoto, D, and Nakane, T, *Preparation of asymmetric polyimide membrane for water/ethanol separation in pervaporation by the phase inversion process.* Journal of Membrane Science, 1994. **86**(3): p. 231-240.
4. Mulia-Soto, JF and Flores-Tlacuahuac, A, *Modeling, simulation and control of an internally heat integrated pressure-swing distillation process for bioethanol separation.* Computers & Chemical Engineering, 2011. **35**(8): p. 1532-1546.
5. Simo, M, Brown, CJ, and Hlavacek, V, *Simulation of pressure swing adsorption in fuel ethanol production process.* Computers & Chemical Engineering, 2008. **32**(7): p. 1635-1649.
6. Guan, J and Hu, X, *Simulation and analysis of pressure swing adsorption: ethanol drying process by the electrical analogue.* Separation and Purification Technology, 2003. **31**(1): p. 31-35.
7. Humphrey, JL and Keller, GE, *Separation process technology*1997, New York: McGraw-Hill. xv, 408 p.
8. *Climate Change Act 2008*, 2008, The Stationary Office Limited: UK.
9. Mulder, M, *Basic principles of membrane technology*. 2nd ed1996, Dordrecht ; Boston: Kluwer Academic. 564 p.
10. Baker, RW, *Membrane technology and applications*. 3rd ed2012, Chichester, West Sussex ; Hoboken: John Wiley & Sons. xiv, 575 p.
11. Kirk, AD, *The range of validity of Graham's Laws.* Journal of Chemical Education, 1967. **44**(12): p. 745.

12. Henis, JMS and Tripodi, MK, *Composite hollow fiber membranes for gas separation: the resistance model approach.* Journal of Membrane Science, 1981. **8**(3): p. 233-246.
13. Henis, JMS and Tripodi, MK, *A Novel Approach to Gas Separations Using Composite Hollow Fiber Membranes.* Separation Science and Technology, 1980. **15**(4): p. 1059-1068.
14. Kangas, J, Sandström, L, Malinen, I, Hedlund, J, and Tanskanen, J, *Maxwell–Stefan modeling of the separation of H2 and CO2 at high pressure in an MFI membrane.* Journal of Membrane Science, 2013. **435**(0): p. 186-206.
15. Ji, G, Wang, G, Hooman, K, Bhatia, S, and Diniz da Costa, JC, *Simulation of binary gas separation through multi-tube molecular sieving membranes at high temperatures.* Chemical Engineering Journal, 2013. **218**(0): p. 394-404.
16. Ahmad, F, Lau, KK, Shariff, AM, and Murshid, G, *Process simulation and optimal design of membrane separation system for CO2 capture from natural gas.* Computers & Chemical Engineering, 2012. **36**(0): p. 119-128.
17. Mirzaee, H and Mirzaee, F, *Modeling and simulation gas separation by membrane of poly dimethyl siloxane.* Journal of King Saud University - Engineering Sciences, 2012. **24**(1): p. 35-43.
18. Krishna, R and van Baten, JM, *Maxwell–Stefan modeling of slowing-down effects in mixed gas permeation across porous membranes.* Journal of Membrane Science, 2011. **383**(1–2): p. 289-300.
19. Yu, M, Falconer, JL, Noble, RD, and Krishna, R, *Modeling transient permeation of polar organic mixtures through a MFI zeolite membrane using the Maxwell–Stefan equations.* Journal of Membrane Science, 2007. **293**(1–2): p. 167-173.
20. Moradi Shehni, P, Amooghin, AE, Ghadimi, A, Sadrzadeh, M, and Mohammadi, T, *Modeling of unsteady-state permeation of gas mixture through a self-synthesized PDMS membranes.* Separation and Purification Technology, 2011. **76**(3): p. 385-399.
21. Makaruk, A and Harasek, M, *Numerical algorithm for modelling multicomponent multipermeator systems.* Journal of Membrane Science, 2009. **344**(1–2): p. 258-265.
22. Ciavarella, P, Moueddeb, H, Miachon, S, Fiaty, K, and Dalmon, J-A, *Experimental study and numerical simulation of hydrogen/isobutane permeation and separation using MFI-zeolite membrane reactor.* Catalysis Today, 2000. **56**(1–3): p. 253-264.

23. Shen, Y and Lua, AC, *Structural and transport properties of BTDA-TDI/MDI co-polyimide (P84)–silica nanocomposite membranes for gas separation.* Chemical Engineering Journal, 2012. **188**(0): p. 199-209.
24. Golzar, K, Amjad-Iranagh, S, Amani, M, and Modarress, H, *Molecular simulation study of penetrant gas transport properties into the pure and nanosized silica particles filled polysulfone membranes.* Journal of Membrane Science, 2014. **451**(0): p. 117-134.
25. Farno, E, Ghadimi, A, Kasiri, N, and Mohammadi, T, *Separation of heavy gases from light gases using synthesized PDMS nano-composite membranes: Experimental and neural network modeling.* Separation and Purification Technology, 2011. **81**(3): p. 400-410.
26. Thundyil, MJ and Koros, WJ, *Mathematical modeling of gas separation permeators — for radial crossflow, countercurrent, and cocurrent hollow fiber membrane modules.* Journal of Membrane Science, 1997. **125**(2): p. 275-291.
27. Coroneo, M, Montante, G, Giacinti Baschetti, M, and Paglianti, A, *CFD modelling of inorganic membrane modules for gas mixture separation.* Chemical Engineering Science, 2009. **64**(5): p. 1085-1094.
28. Ismail, AF and Yaacob, N, *Performance of treated and untreated asymmetric polysulfone hollow fiber membrane in series and cascade module configurations for CO2/CH4 gas separation system.* Journal of Membrane Science, 2006. **275**(1–2): p. 151-165.
29. Gottschlich, DE, Roberts, DL, and Way, JD, *A theoretical comparison of facilitated transport and solution-diffusion membrane modules for gas separation.* Gas Separation & Purification, 1988. **2**(2): p. 65-71.
30. Fouda, A, Chen, Y, Bai, J, and Matsuura, T, *Wheatstone bridge model for the laminated polydimethylsiloxane/polyethersulfone membrane for gas separation.* Journal of Membrane Science, 1991. **64**(3): p. 263-271.
31. Hashemifard, SA, Ismail, AF, and Matsuura, T, *A new theoretical gas permeability model using resistance modeling for mixed matrix membrane systems.* Journal of Membrane Science, 2010. **350**(1–2): p. 259-268.

32. Peng, F, Liu, J, and Li, J, *Analysis of the gas transport performance through PDMS/PS composite membranes using the resistances-in-series model.* Journal of Membrane Science, 2003. **222**(1–2): p. 225-234.
33. Huang, RYM and Feng, X, *Resistance model approach to asymmetric polyetherimide membranes for pervaporation of isopropanol/water mixtures.* Journal of Membrane Science, 1993. **84**(1-2): p. 15-27.
34. Shilton, SJ, Bell, G, and Ferguson, J, *The deduction of fine structural details of gas separation hollow fibre membranes using resistance modelling of gas permeation.* Polymer, 1996. **37**(3): p. 485-492.
35. Kaye, GWC and Laby, TH, *Tables of physical and chemical constants*1995: Longman.
36. Haken, H and Wolf, HC, *Molecular Physics and Elements of Quantum Chemistry: Introduction to Experiments and Theory*2004: Springer.
37. Barrer, RM, *Diffusion in and through solids*1941: The University Press.
38. Treybal, RE, *Mass-transfer operations*1980: McGraw-Hill.
39. Dushman, S, *Scientific foundations of vacuum technique*1962: Wiley.
40. Wijmans, JG and Baker, RW, *The solution-diffusion model: a review.* Journal of Membrane Science, 1995. **107**(1–2): p. 1-21.
41. Finley, J, *Ceramic membranes: a robust filtration alternative.* Filtration & Separation, 2005. **42**(9): p. 34-37.
42. Krishnan, ER, Muhammad, N, Haught, RC, Sinha, R, and Patterson, CL, *Evaluation of Ceramic Filtration for Drinking Water Treatment in Small Systems*, in *World Environmental and Water Resource Congress 2006*. p. 1-11.
43. Jayaraman, V, Lin, YS, Pakala, M, and Lin, RY, *Fabrication of ultrathin metallic membranes on ceramic supports by sputter deposition.* Journal of Membrane Science, 1995. **99**(1): p. 89-100.
44. Dobrev, D, Neumann, R, Angert, N, and Vetter, J, *Formation of metal membranes by direct duplication of etched ion-track templates.* Applied Physics A, 2003. **76**(5): p. 787-790.
45. Hofs, B, Ogier, J, Vries, D, Beerendonk, EF, and Cornelissen, ER, *Comparison of ceramic and polymeric membrane permeability and fouling using surface water.* Separation and Purification Technology, 2011. **79**(3): p. 365-374.

46. McKelvey, SA, Clausi, DT, and Koros, WJ, *A guide to establishing hollow fiber macroscopic properties for membrane applications.* Journal of Membrane Science, 1997. **124**(2): p. 223-232.

47. Le-Clech, P, Chen, V, and Fane, TAG, *Fouling in membrane bioreactors used in wastewater treatment.* Journal of Membrane Science, 2006. **284**(1–2): p. 17-53.

48. Yamanoi, I and Kageyama, K, *Evaluation of bubble flow properties between flat sheet membranes in membrane bioreactor.* Journal of Membrane Science, 2010. **360**(1–2): p. 102-108.

49. Cobry, KD, Yuan, Z, Gilron, J, Bright, VM, Krantz, WB, and Greenberg, AR, *Comprehensive experimental studies of early-stage membrane scaling during nanofiltration.* Desalination, 2011. **283**(0): p. 40-51.

50. Van der Bruggen, B, Hawrijk, I, Cornelissen, E, and Vandecasteele, C, *Direct nanofiltration of surface water using capillary membranes: comparison with flat sheet membranes.* Separation and Purification Technology, 2003. **31**(2): p. 193-201.

51. Libralato, G, Volpi Ghirardini, A, and Avezzù, F, *Toxicity removal efficiency of decentralised sequencing batch reactor and ultra-filtration membrane bioreactors.* Water Research, 2010. **44**(15): p. 4437-4450.

52. Liu, M, Wu, D, Yu, S, and Gao, C, *Influence of the polyacyl chloride structure on the reverse osmosis performance, surface properties and chlorine stability of the thin-film composite polyamide membranes.* Journal of Membrane Science, 2009. **326**(1): p. 205-214.

53. B. McCray, S, Vilker, VL, and Nobe, K, *Reverse osmosis cellulose acetate membranes II. Dependence of transport properties on acetyl content.* Journal of Membrane Science, 1991. **59**(3): p. 317-330.

54. Yu, S, Lü, Z, Chen, Z, Liu, X, Liu, M, and Gao, C, *Surface modification of thin-film composite polyamide reverse osmosis membranes by coating N-isopropylacrylamide-co-acrylic acid copolymers for improved membrane properties.* Journal of Membrane Science, 2011. **371**(1–2): p. 293-306.

55. Loeb, S and Sourirajan, S, *Sea Water Demineralization by Means of an Osmotic Membrane*, in *Saline Water Conversion?II*1963, AMERICAN CHEMICAL SOCIETY. p. 117-132.

56. J. Bouchilloux, AF, A. Faure, *Anisotropic organosilicon polymer membrane.* United States Patent, 1973. **3754375**.

57. Kimura, SG, *Preparation of asymmetric polymer membranes.* United States Patent, 1973. **3709774**.

58. K.V. Peinemann, IP, *Method for producing an integral asymmetric gas separating membrane and the resultant membrane.* United States Patent, 1988. **4746333 A**.

59. Peinemann, KV, *Method for producing and integral, asymmetric membrane and the resultant membrane.* United States Patent, 1987. **US 4673418 A**.

60. Bottino, A, Capannelli, G, and Comite, A, *Novel porous poly (vinylidene fluoride) membranes for membrane distillation.* Desalination, 2005. **183**(1–3): p. 375-382.

61. Jiang, JS, Greenberg, DB, and Fried, JR, *Preparation of a Nafion composite membrane using a porous teflon support.* Journal of Membrane Science, 1997. **132**(2): p. 273-276.

62. Bissett, H, Zah, J, and Krieg, HM, *Manufacture and optimization of tubular ceramic membrane supports.* Powder Technology, 2008. **181**(1): p. 57-66.

63. Peyravi, M, Rahimpour, A, and Jahanshahi, M, *Thin film composite membranes with modified polysulfone supports for organic solvent nanofiltration.* Journal of Membrane Science, 2012. **423–424**(0): p. 225-237.

64. Li, Y-L and Tung, K-L, *The effect of curvature of a spacer-filled channel on fluid flow in spiral-wound membrane modules.* Journal of Membrane Science, 2008. **319**(1–2): p. 286-297.

65. Winter, D, Koschikowski, J, and Ripperger, S, *Desalination using membrane distillation: Flux enhancement by feed water deaeration on spiral-wound modules.* Journal of Membrane Science, 2012. **423–424**(0): p. 215-224.

66. Singh, V, Jain, PK, and Das, C, *Performance of spiral wound ultrafiltration membrane module for with and without permeate recycle: Experimental and theoretical consideration.* Desalination, 2013. **322**(0): p. 94-103.

67. Lin, D, Ding, Z, Liu, L, and Ma, R, *Modeling spiral-wound membrane modules with applications for gas/vapor permeation.* Computers & Chemical Engineering, 2012. **44**(0): p. 20-33.

68. Li, D, Wang, R, and Chung, T-S, *Fabrication of lab-scale hollow fiber membrane modules with high packing density.* Separation and Purification Technology, 2004. **40**(1): p. 15-30.

69. Baker, RW, *Future Directions of Membrane Gas Separation Technology.* Industrial & Engineering Chemistry Research, 2002. **41**(6): p. 1393-1411.

70. Zhongwei, D, Liying, L, and Runyu, M, *Study on the effect of flow maldistribution on the performance of the hollow fiber modules used in membrane distillation.* Journal of Membrane Science, 2003. **215**(1–2): p. 11-23.

71. Noda, I, Brown-West, DG, and Gryte, CC, *Effect of flow maldistribution on hollow fiber dialysis — experimental studies.* Journal of Membrane Science, 1979. **5**(0): p. 209-225.

72. Tompkins, CJ, Michaels, AS, and Peretti, SW, *Removal of p-nitrophenol from aqueous solution by membrane-supported solvent extraction.* Journal of Membrane Science, 1992. **75**(3): p. 277-292.

73. Lemanski, J and Lipscomb, GG, *Effect of shell-side flows on hollow-fiber membrane device performance.* Aiche Journal, 1995. **41**(10): p. 2322-2326.

74. Günther, J, Schmitz, P, Albasi, C, and Lafforgue, C, *A numerical approach to study the impact of packing density on fluid flow distribution in hollow fiber module.* Journal of Membrane Science, 2010. **348**(1–2): p. 277-286.

75. Park, JK and Chang, HN, *Flow distribution in the fiber lumen side of a hollow-fiber module.* Aiche Journal, 1986. **32**(12): p. 1937-1947.

76. Thakur, BK and De, S, *A novel method for spinning hollow fiber membrane and its application for treatment of turbid water.* Separation and Purification Technology, 2012. **93**(0): p. 67-74.

77. Cabasso, I, Klein, E, and Smith, JK, *Polysulfone hollow fibers. I. Spinning and properties.* Journal of Applied Polymer Science, 1976. **20**(9): p. 2377-2394.

78. Aptel, P, Abidine, N, Ivaldi, F, and Lafaille, JP, *Polysulfone hollow fibers — effect of spinning conditions on ultrafiltration properties.* Journal of Membrane Science, 1985. **22**(2–3): p. 199-215.

79. Widjojo, N, Chung, T-S, Arifin, DY, Weber, M, and Warzelhan, V, *Elimination of die swell and instability in hollow fiber spinning process of hyperbranched polyethersulfone*

(HPES) via novel spinneret designs and precise spinning conditions. Chemical Engineering Journal, 2010. **163**(1–2): p. 143-153.

80. Lipscomb, GG, *The melt hollow fiber spinning process: steady-state behavior, sensitivity and stability.* Polymers for Advanced Technologies, 1994. **5**(11): p. 745-758.
81. Larson, RG, *Instabilities in viscoelastic flows.* Rheologica Acta, 1992. **31**(3): p. 213-263.
82. Petrie, CJS and Denn, MM, *Instabilities in polymer processing.* Aiche Journal, 1976. **22**(2): p. 209-236.
83. Piau, JM, El Kissi, N, and Tremblay, B, *Influence of upstream instabilities and wall slip on melt fracture and sharkskin phenomena during silicones extrusion through orifice dies.* Journal of Non-Newtonian Fluid Mechanics, 1990. **34**(2): p. 145-180.
84. van't Hof, JA, Reuvers, AJ, Boom, RM, Rolevink, HHM, and Smolders, CA, *Preparation of asymmetric gas separation membranes with high selectivity by a dual-bath coagulation method.* Journal of Membrane Science, 1992. **70**(1): p. 17-30.
85. Pinnau, I and Koros, WJ, *A qualitative skin layer formation mechanism for membranes made by dry/wet phase inversion.* Journal of Polymer Science Part B: Polymer Physics, 1993. **31**(4): p. 419-427.
86. Reuvers, AJ, van den Berg, JWA, and Smolders, CA, *Formation of membranes by means of immersion precipitation : Part I. A model to describe mass transfer during immersion precipitation.* Journal of Membrane Science, 1987. **34**(1): p. 45-65.
87. Reuvers, AJ and Smolders, CA, *Formation of membranes by means of immersion precipitation : Part II. the mechanism of formation of membranes prepared from the system cellulose acetate-acetone-water.* Journal of Membrane Science, 1987. **34**(1): p. 67-86.
88. Reuvers, AJ, *Membrane formation : diffusion induced demixing processes in ternary polymeric systems*, 1987: Enschede. p. 185.
89. Dunlop, PJ, *Frictional Coefficients for Binary and Ternary Isothermal Diffusion.* The Journal of Physical Chemistry, 1964. **68**(1): p. 26-30.
90. Strathmann, H, Scheible, P, and Baker, RW, *A rationale for the preparation of Loeb-Sourirajan-type cellulose acetate membranes.* Journal of Applied Polymer Science, 1971. **15**(4): p. 811-828.

91. Seymour, RB, Stahl, GA, and American Chemical Society., *Macromolecular solutions : solvent-property relationships in polymers*1982, New York: Pergamon Press. ix, 233 p.
92. Paul, DR and Yampol'skii, YP, *Polymeric gas separation membranes*1994, Boca Raton: CRC Press. x, 623 p.
93. Cahn, JW, *Phase Separation by Spinodal Decomposition in Isotropic Systems.* The Journal of Chemical Physics, 1965. **42**(1): p. 93-99.
94. Flory, PJ, *Thermodynamics of High Polymer Solutions.* The Journal of Chemical Physics, 1942. **10**(1): p. 51-61.
95. Huggins, ML, *Solutions of Long Chain Compounds.* The Journal of Chemical Physics, 1941. **9**(5): p. 440-440.
96. Tompa, H, *Phase relationships in polymer solutions.* Transactions of the Faraday Society, 1949. **45**(0): p. 1142-1152.
97. Altena, FW and Smolders, CA, *Calculation of liquid-liquid phase separation in a ternary system of a polymer in a mixture of a solvent and a nonsolvent.* Macromolecules, 1982. **15**(6): p. 1491-1497.
98. Wijmans, JG, Kant, J, Mulder, MHV, and Smolders, CA, *Phase separation phenomena in solutions of polysulfone in mixtures of a solvent and a nonsolvent: relationship with membrane formation.* Polymer, 1985. **26**(10): p. 1539-1545.
99. Yilmaz, L and McHugh, AJ, *Analysis of nonsolvent–solvent–polymer phase diagrams and their relevance to membrane formation modeling.* Journal of Applied Polymer Science, 1986. **31**(4): p. 997-1018.
100. Zeman, L and Tkacik, G, *Thermodynamic analysis of a membrane-forming system water/N-methyl-2-pyrrolidone/polyethersulfone.* Journal of Membrane Science, 1988. **36**(0): p. 119-140.
101. Prausnitz, JM, Lichtenthaler, RN, and de Azevedo, EG, *Molecular Thermodynamics of Fluid-Phase Equilibria*1998: Pearson Education.
102. Barzin, J and Sadatnia, B, *Theoretical phase diagram calculation and membrane morphology evaluation for water/solvent/polyethersulfone systems.* Polymer, 2007. **48**(6): p. 1620-1631.
103. Kurata, M, *Thermodynamics of Polymer Solutions*1982: Harwood Academic Publishers.

104. Cahn, JWC, R. J., *The Initial Stages of Phase Separation in Glasses.* Physics and Chemistry of Glasses, 1965. **6**: p. 181-191.

105. Mc, MLP, *Aspects of Liquid-Liquid Phase Transition Phenomena in Multicomponent Polymeric Systems*, in *Copolymers, Polyblends, and Composites*1975, AMERICAN CHEMICAL SOCIETY. p. 43-65.

106. Kesting, RE, *The four tiers of structure in integrally skinned phase inversion membranes and their relevance to the various separation regimes.* Journal of Applied Polymer Science, 1990. **41**(11-12): p. 2739-2752.

107. Kesting, RE, *Concerning the microstructure of dry-RO membranes.* Journal of Applied Polymer Science, 1973. **17**(6): p. 1771-1785.

108. Mason, G, *Formation of films from latices a theoretical treatment.* British Polymer Journal, 1973. **5**(2): p. 101-108.

109. Brodnyan, JG and Konen, T, *Experimental study of the mechanism of film formation.* Journal of Applied Polymer Science, 1964. **8**(2): p. 687-697.

110. Imoto, T, *The mechanism of film formation of emulsions.* Progress in Organic Coatings, 1974. **2**(3): p. 193-205.

111. Lamprecht, J, *Ein neues Filmbildungskriterium für wäßrige Polymerdispersionen.* Colloid and Polymer Science, 1980. **258**(8): p. 960-967.

112. Kast, H, *Aspects of film formation with emulsion copolymers.* Die Makromolekulare Chemie, 1985. **10**(S19851): p. 447-461.

113. Eckersley, STR, A., *Mechanism of Film Formation From Polymer Latexes.* Journal of Coatings Technology, 1990. **62**: p. 89-100.

114. Brown, GL, *Formation of films from polymer dispersions.* Journal of Polymer Science, 1956. **22**(102): p. 423-434.

115. Brinson, HF and Brinson, LC, *Polymer Engineering Science and Viscoelasticity: An Introduction*2007: Springer.

116. Burghardt, W, Yilmaz, L, and McHugh, A, *Glass transition, crystallization and thermoreversible gelation in ternary PPO solutions; relationship to asymmetric membrane formation.* Polymer, 1987. **28**(12): p. 2085-2092.

117. Gaides, G and McHugh, A, *Gelation in an amorphous polymer: a discussion of its relation to membrane formation.* Polymer, 1989. **30**(11): p. 2118-2123.

118. Sharpe, ID, Ismail, AF, and Shilton, SJ, *A study of extrusion shear and forced convection residence time in the spinning of polysulfone hollow fiber membranes for gas separation.* Separation and Purification Technology, 1999. **17**(2): p. 101-109.

119. Peter, J and Peinemann, KV, *Multilayer composite membranes for gas separation based on crosslinked PTMSP gutter layer and partially crosslinked Matrimid® 5218 selective layer.* Journal of Membrane Science, 2009. **340**(1–2): p. 62-72.

120. Jansen, JC, Buonomenna, MG, Figoli, A, and Drioli, E, *Asymmetric membranes of modified poly(ether ether ketone) with an ultra-thin skin for gas and vapour separations.* Journal of Membrane Science, 2006. **272**(1–2): p. 188-197.

121. Kazama, S and Sakashita, M, *Gas separation properties and morphology of asymmetric hollow fiber membranes made from cardo polyamide.* Journal of Membrane Science, 2004. **243**(1–2): p. 59-68.

122. Pinnau, I, *Skin formation of integral-asymmetric gas separation membranes made by dry/wet phase inversion*, 1991, University of Texas: Austin.

123. Sheetz, DP, *Formation of films by drying of latex.* Journal of Applied Polymer Science, 1965. **9**(11): p. 3759-3773.

124. Co., M, *Methods for preparing anisotropic hollow fiber membranes comprising polymer of acrylonitrile and styrene and hollow fiber membranes produced therefrom*, 1982.

125. Co., M, *Multicomponent Membranes for Gas Separation*, 1980.

126. Puri, PS, *Gas Separation Membranes.* La Chimica e l'Industria, 1996. **78**: p. 815.

127. Graham, T, *On the absorption and dialytic separation of gases by colloidal septa.* Philosophical transactions of the Royal Society, 1866. **156**: p. 399-439.

128. Bernardo, PC, G., *30 years of membrane technology for gas separation.* Chemical Engineering Transactions, 2013. **32**: p. 1999-2004.

129. Ettouney, HM, El-Dessouky, HT, and Abou Waar, W, *Separation characteristics of air by polysulfone hollow fiber membranes in series.* Journal of Membrane Science, 1998. **148**(1): p. 105-117.

130. Kawakami, H, Mikawa, M, and Nagaoka, S, *Formation of surface skin layer of asymmetric polyimide membranes and their gas transport properties.* Journal of Membrane Science, 1997. **137**(1–2): p. 241-250.

131. White, LS, Blinka, TA, Kloczewski, HA, and Wang, If, *Properties of a polyimide gas separation membrane in natural gas streams.* Journal of Membrane Science, 1995. **103**(1–2): p. 73-82.

132. Chua, ML, Xiao, YC, and Chung, T-S, *Effects of thermally labile saccharide units on the gas separation performance of highly permeable polyimide membranes.* Journal of Membrane Science, 2012. **415–416**(0): p. 375-382.

133. Aroon, MA, Ismail, AF, Montazer-Rahmati, MM, and Matsuura, T, *Morphology and permeation properties of polysulfone membranes for gas separation: Effects of non-solvent additives and co-solvent.* Separation and Purification Technology, 2010. **72**(2): p. 194-202.

134. Staudt-Bickel, C and J. Koros, W, *Improvement of CO2/CH4 separation characteristics of polyimides by chemical crosslinking.* Journal of Membrane Science, 1999. **155**(1): p. 145-154.

135. Askari, M and Chung, T-S, *Natural gas purification and olefin/paraffin separation using thermal cross-linkable co-polyimide/ZIF-8 mixed matrix membranes.* Journal of Membrane Science, 2013. **444**(0): p. 173-183.

136. Ma, C and Koros, WJ, *High-performance ester-crosslinked hollow fiber membranes for natural gas separations.* Journal of Membrane Science, 2013. **428**(0): p. 251-259.

137. Wright, CT and Paul, DR, *Feasibility of thermal crosslinking of polyarylate gas-separation membranes using benzocyclobutene-based monomers.* Journal of Membrane Science, 1997. **129**(1): p. 47-53.

138. Barbari, TA and Datwani, SS, *Gas separation properties of polysulfone membranes treated with molecular bromine.* Journal of Membrane Science, 1995. **107**(3): p. 263-266.

139. Kim, SR, Lee, KH, and Jhon, MS, *The effect of ZnCl2 on the formation of polysulfone membrane.* Journal of Membrane Science, 1996. **119**(1): p. 59-64.

140. Jansen, JC, Buonomenna, MG, Figoli, A, and Drioli, E, *Ultra-thin asymmetric gas separation membranes of modified PEEK prepared by the dry–wet phase inversion technique.* Desalination, 2006. **193**(1–3): p. 58-65.

141. Kumbharkar, SC and Li, K, *Structurally modified polybenzimidazole hollow fibre membranes with enhanced gas permeation properties.* Journal of Membrane Science, 2012. **415–416**(0): p. 793-800.

142. Sanaeepur, H, Amooghin, AE, Moghadassi, A, and Kargari, A, *Preparation and characterization of acrylonitrile–butadiene–styrene/poly(vinyl acetate) membrane for CO2 removal.* Separation and Purification Technology, 2011. **80**(3): p. 499-508.

143. Mousavi, SA, Sadeghi, M, Motamed-Hashemi, MMY, Pourafshari Chenar, M, Roosta-Azad, R, and Sadeghi, M, *Study of gas separation properties of ethylene vinyl acetate (EVA) copolymer membranes prepared via phase inversion method.* Separation and Purification Technology, 2008. **62**(3): p. 642-647.

144. Camacho-Zuñiga, C, Ruiz-Treviño, FA, Hernández-López, S, Zolotukhin, MG, Maurer, FHJ, and González-Montiel, A, *Aromatic polysulfone copolymers for gas separation membrane applications.* Journal of Membrane Science, 2009. **340**(1–2): p. 221-226.

145. Reijerkerk, SR, Wessling, M, and Nijmeijer, K, *Pushing the limits of block copolymer membranes for CO2 separation.* Journal of Membrane Science, 2011. **378**(1–2): p. 479-484.

146. Robeson, LM, *Correlation of separation factor versus permeability for polymeric membranes.* Journal of Membrane Science, 1991. **62**(2): p. 165-185.

147. Robeson, LM, *The upper bound revisited.* Journal of Membrane Science, 2008. **320**(1-2): p. 390-400.

148. Pabby, AK, Rizvi, SSH, and Requena, AMS, *Handbook of Membrane Separations: Chemical, Pharmaceutical, Food, and Biotechnological Applications*2008: Taylor & Francis.

149. Jones, CW and Koros, WJ, *Carbon molecular sieve gas separation membranes-I. Preparation and characterization based on polyimide precursors.* Carbon, 1994. **32**(8): p. 1419-1425.

150. Kusuki, Y, Shimazaki, H, Tanihara, N, Nakanishi, S, and Yoshinaga, T, *Gas permeation properties and characterization of asymmetric carbon membranes prepared by pyrolyzing asymmetric polyimide hollow fiber membrane.* Journal of Membrane Science, 1997. **134**(2): p. 245-253.

151. Jones, CW and Koros, WJ, *Characterization of Ultramicroporous Carbon Membranes with Humidified Feeds.* Industrial & Engineering Chemistry Research, 1995. **34**(1): p. 158-163.

152. Jones, CW and Koros, WJ, *Carbon molecular sieve gas separation membranes-II. Regeneration following organic exposure.* Carbon, 1994. **32**(8): p. 1427-1432.

153. Koresh, JE and Soffer, A, *The Carbon Molecular Sieve Membranes. General Properties and the Permeability of CH4/H2 Mixture.* Separation Science and Technology, 1987. **22**(2-3): p. 973-982.

154. Liang, C, Sha, G, and Guo, S, *Carbon membrane for gas separation derived from coal tar pitch.* Carbon, 1999. **37**(9): p. 1391-1397.

155. Koros, WJ and Mahajan, R, *Pushing the limits on possibilities for large scale gas separation: Which strategies?* Journal of Membrane Science, 2000. **175**(2): p. 181-196.

156. Bhardwaj, V, Macintosh, A, Sharpe, ID, Gordeyev, SA, and Shilton, SJ, N. Y. Acad. Sci., 2003. **984**: p. 1.

157. Sadeghi, M, Semsarzadeh, MA, and Moadel, H, *Enhancement of the gas separation properties of polybenzimidazole (PBI) membrane by incorporation of silica nano particles.* Journal of Membrane Science, 2009. **331**(1-2): p. 21-30.

158. Wahab, MFA, Ismail, AF, and Shilton, SJ, *Studies on gas permeation performance of asymmetric polysulfone hollow fiber mixed matrix membranes using nanosized fumed silica as fillers.* Separation and Purification Technology, 2012. **86**(0): p. 41-48.

159. Bastani, D, Esmaeili, N, and Asadollahi, M, *Polymeric mixed matrix membranes containing zeolites as a filler for gas separation applications: A review.* Journal of Industrial and Engineering Chemistry, 2013. **19**(2): p. 375-393.

160. Casado-Coterillo, C, Soto, J, T. Jimaré, M, Valencia, S, Corma, A, Téllez, C, and Coronas, J, *Preparation and characterization of ITQ-29/polysulfone mixed-matrix membranes for gas separation: Effect of zeolite composition and crystal size.* Chemical Engineering Science, 2012. **73**(0): p. 116-122.

161. Arjmandi, M and Pakizeh, M, *Mixed matrix membranes incorporated with cubic-MOF-5 for improved polyetherimide gas separation membranes: Theory and experiment.* Journal of Industrial and Engineering Chemistry, (0).

162. Valero, M, Zornoza, B, Téllez, C, and Coronas, J, *Mixed matrix membranes for gas separation by combination of silica MCM-41 and MOF NH2-MIL-53(Al) in glassy polymers.* Microporous and Mesoporous Materials, (0).

163. Magueijo, VM, Anderson, LG, Fletcher, AJ, and Shilton, SJ, *Polysulfone mixed matrix gas separation hollow fibre membranes filled with polymer and carbon xerogels.* Chemical Engineering Science, 2013. **92**(0): p. 13-20.

164. Mahajan, R and Koros, WJ, *Factors Controlling Successful Formation of Mixed-Matrix Gas Separation Materials.* Industrial & Engineering Chemistry Research, 2000. **39**(8): p. 2692-2696.

165. Zimmerman, CM, Singh, A, and Koros, WJ, *Tailoring mixed matrix composite membranes for gas separations.* Journal of Membrane Science, 1997. **137**(1–2): p. 145-154.

166. Aroon, MA, Ismail, AF, Matsuura, T, and Montazer-Rahmati, MM, *Performance studies of mixed matrix membranes for gas separation: A review.* Separation and Purification Technology, 2010. **75**(3): p. 229-242.

167. Lahiere, RJ, Hellums, MW, Wijmans, JG, and Kaschemekat, J, *Membrane vapor separation. Recovery of vinyl chloride monomer from PVC reactor vents.* Industrial & Engineering Chemistry Research, 1993. **32**(10): p. 2236-2241.

168. Streng, AG, *Tables of Ozone Properties.* Journal of Chemical & Engineering Data, 1961. **6**(3): p. 431-436.

169. McClurkin, JD, Maier, DE, and Ileleji, KE, *Half-life time of ozone as a function of air movement and conditions in a sealed container.* Journal of Stored Products Research, 2013. **55**(0): p. 41-47.

170. Koike, K, Nifuku, M, Izumi, K, Nakamura, S, Fujiwara, S, and Horiguchi, S, *Explosion properties of highly concentrated ozone gas.* Journal of Loss Prevention in the Process Industries, 2005. **18**(4–6): p. 465-468.

171. Park, S-L, Moon, J-D, Lee, S-H, and Shin, S-Y, *Effective ozone generation utilizing a meshed-plate electrode in a dielectric-barrier discharge type ozone generator.* Journal of Electrostatics, 2006. **64**(5): p. 275-282.

172. Manojlovic, D, Ostojic, DR, Obradovic, BM, Kuraica, MM, Krsmanovic, VD, and Puric, J, *Removal of phenol and chlorophenols from water by new ozone generator.* Desalination, 2007. **213**(1–3): p. 116-122.
173. Bartlett, GFH, *Improvement in ozone-generators*, 1878, Google Patents.
174. Uys, R, *Ozone generator*, 1994, Google Patents.
175. Allsopp, MW and Vianello, G, *Poly(Vinyl Chloride)*, in *Ullmann's Encyclopedia of Industrial Chemistry*2000, Wiley-VCH Verlag GmbH & Co. KGaA.
176. Alexander Stern, S, *Polymers for gas separations: the next decade.* Journal of Membrane Science, 1994. **94**(1): p. 1-65.
177. Bierbrauer, K, López-González, M, Riande, E, and Mijangos, C, *Gas transport in fluorothiophenyl modified PVC membranes.* Journal of Membrane Science, 2010. **362**(1–2): p. 164-171.
178. Tiemblo, P, Guzman, J, Riande, E, Mijangos, C, and Reinecke, H, *Erratum: Effect of physical aging on the gas transport properties of PVC and PVC modified with pyridine groups (Polymer (2001) 42 (4817-4823) PII: S0032386101003391).* Polymer, 2001. **42**(19): p. 8321.
179. Tiemblo, P, Guzmán, J, Riande, E, Mijangos, C, and Reinecke, H, *The gas transport properties of PVC functionalized with mercapto pyridine groups.* Macromolecules, 2002. **35**(2): p. 420-424.
180. Tiemblo, P, Guzmán, J, Riande, E, Mijangos, C, Herrero, M, Espeso, J, and Reinecke, H, *Diffusion of small molecules through modified poly(vinyl chloride) membranes.* Journal of Polymer Science Part B: Polymer Physics, 2002. **40**(10): p. 964-971.
181. Lee, WM, *Selection of barrier materials from molecular structure.* Polymer Engineering & Science, 1980. **20**(1): p. 65-69.

2. Objectives

The primary objective of this work was the production, characterisation and structural modelling of a hollow fibre gas separation membrane which displayed properties making it suitable for the separation of binary mixtures of ozone and oxygen. In order to achieve this membranes were to be produced and tested for their separation properties utilising common test gases of oxygen, nitrogen, carbon dioxide and methane. The use of these gases allows for comparison of the membranes to those in the literature as these gases are commonly represented among the wide array of papers on gas separation membranes unlike the niche gas of ozone. Once separating properties have been achieved the next target was to set up a system involving ozone/oxygen separation.

The first step in producing membranes was to identify a suitable material for the membrane production as ozone is a highly reactive oxidising agent which attacks most common polymeric membrane materials. The selection of material had to consider a number of factors including the permeation properties of the material, solution properties for spinning, chemical resilience and strength. The polymer selected as a result of this study was PVC, the reasons for this have been set out in the introduction section of this report, and as such the rest of the objectives for the work were set around the use of PVC.

In order to produce membranes suitable for gas separation it was decided to base the production around the successful dope compositions and spinning parameters associated with the use of polysulfone. Polysulfone has been successfully applied in a number of gas separation applications and the production of these membranes has been shown to be economically viable. Hence, if membranes could be produced under similar conditions with PVC then, since PVC is considerably cheaper as a raw material, the economic value of such membranes would hopefully represent viable output.

During the initial stages it was desired to produce a membrane batch which demonstrated a level of gas separation which would be in line with solution diffusion transport mechanisms.

The membranes were produced under ambient conditions and the stability of the production over the course of a full run was assessed to determine if comparisons of membranes produced at the start of a spinning run compared to membranes produced later in a spinning run are justified.

The spinning conditions used for the initial experiments were chosen such that they represented spinning parameters which are commonly employed for a variety of membrane production applications. Due to the use of spinning conditions which could be reasonably expected to produce separating membranes, although perhaps not optimally, the next aim was to use the results obtained from the first production runs in order to make changes to the dope solution as required in order to tune it. Following, the tuning of the dope under the generalised spinning conditions the aim was to move to optimising the spinning conditions being used. In order to determine the best dope composition and spinning conditions for the membrane both the pressure normalised flux through the membrane and the selectivity had to be considered in order to obtain a balance between them.

In addition to the investigation into the membrane production the dope solution itself was rheologically investigated under a variety of conditions in an attempt to reconcile the rheological properties of the dope solution with those observed in the membranes separations. The rheological investigation aimed to use flow, oscillatory and creep rheological methods to produce data on the solution nature over a range of different stress and shear conditions. These studies were conducted with a focus on considering different possibilities for producing membranes at ambient and raised temperature and also consider the implications of the delay in the time which the dope was used after preparation.

It was then aimed to use the data collected from the rheological studies in combination with a software package to model the flow of the dope solution as it passes through the spinneret. This combination was utilised in order to determine what spinning conditions might best benefit the dope solution and whether or not spinning at an increased ambient temperature may help in producing better flow characteristics through the spinneret for the production of gas separation membranes. This information was to be implemented into the production process in further attempts to produce higher quality membranes.

Post spinning processes such as coating were also known to have an influence on the performance of membranes and a further aim of the work was to consider the application of an additional coating layer to the membranes. The literature on membranes commonly refers to the coating of membranes for use in gas separation properties as it is known to improve the membrane properties. This investigation aimed to study the effect of an additional coating layer to obtain information on whether the dip coating process employed for the work was effective in a single coating rotation or whether a double coating could further increase the results obtained.

Once conditions under which membranes could be produced showing potential for achieving the ozone/oxygen separation required had been established they were to be characterised through a number of methods. It was an objective of the characterisation process to produce a model based on the principles of resistance modelling which could predict the active layer thicknesses and surface porosity of the membranes which were manufactured.

In order to help with some of the input factors required for the modelling and to study the structure of the membranes scanning electron microscopy (SEM) was identified as a technique which could be used to provide visual images of the membranes and their characteristics. It was also hoped that SEM could be used to provide confirmation on the influence of the coating process and assess if it contributed anything significant to the membrane characteristics.

The strength of membranes was also investigated through tensile testing conducted on the membranes themselves. Tensile strength gives an indication of how long industrial membrane modules might last under operating conditions before the influence of broken membranes has too large a negative impact on the module performance. This investigation aimed to compare the properties of the PVC membranes with the mechanical strength of literature sourced values for membranes produced from other materials.

Finally it was aimed to conduct experimental work to assess whether the membranes exhibited any ozone/oxygen separating capabilities. The first aspect of this involved the creation of an experimental set-up which allowed the connection of a generation system to a membrane test chamber taking into account the issues surrounding the handling of ozone. Secondly, it was hoped to conduct experiments with ozone/oxygen binary mixtures to prove that the concept of

a PVC membrane could influence the output concentrations of the retentate and permeate streams.

A number of these sections of work resulted in conclusions being drawn which mean that further work would be required in order to refine the membranes presented here or improve the processes through which they are tested. It was also an aim of this work to take these conclusions and suggest possible future lines of investigation which could help resolve some of the issues faced.

3. Equipment, Methods and Common Calculations

All of the equipment used in this work was designed at the University of Strathclyde. Some of this was undertaken by Dr S. J. Shilton and L. Allan for past work but everything has been redesigned, refitted and re-commissioned by the author and L. Allan. The exception to this is the spinneret which was loaned to the University for research purposes by Air Products and Chemicals Inc.

3.1. Dope Preparation

Preparation of polymer dope solutions took place in a fume cupboard. The round bottom vessel and other glassware equipment shown in Figure 3.1-1 were Quickfit® products. Equipment which was used but is not shown in the diagram for simplicity includes retort stands with clamps and rings for supporting the set-up, hosing for supply of cold water to the condenser and various beakers, measuring cylinders and watch glasses for the measuring out and addition of solution components to the round bottom flask.

First, the stirrer was placed in the bottom half of the round bottom flask before the top half was lowered over it threading the stirrer shaft through the central port in which it was sealed with a Polytetrafluroethylene (PTFE) stopper designed to allow the stirrer to rotate. The flanged vessel was sealed using a clamp which fit tightly all the way round the flange and was designed for the purpose. The flask was then placed in a retort stand ring and lowered into the water bath to a level slightly below the flange, the level was important to establish a good heat transfer area between the water in the bath and the vessel but also to minimise the chances of water gaining access to the system. Retort stand clamps were used to provide extra stability to the flask.

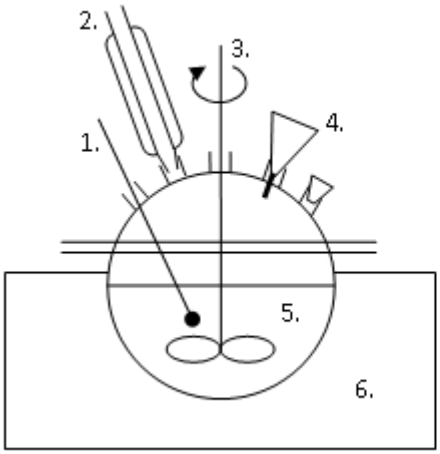

1. Digital Thermometer
2. Condenser
3. Stirrer
4. Solids Funnel
5. Polymer Solution in Flanged Round Bottom Flask
6. Water Bath

Figure 3.1-1: Apparatus set-up for dope preparation

The stirrer motor was moved into position over the flask, directly above the stirrer shaft. The motor used was a 50W thyristor speed controlled DC shunt wound motor geared to a maximum speed of 780rpm. The motor set up was selected because it is capable of maintaining its speeds with the viscous solutions which occur when dealing with polymers. With the motor in position the stirrer was attached to it and the motor turned on to check for excessive vibrations produced by the alignment of the stirrer shaft through the port in the flask. Once the motor was correctly aligned to minimise the vibration the other pieces of equipment to be placed in the ports were added and, where appropriate, sealed in place.

The digital thermometer was placed into the flask through another PTFE stopper and reached into the flask to a point just above the stirrer to obtain the most accurate reading possible of the solution temperature. Controlling the solution temperature is important so as not to completely evaporate the volatile solvent which was present in the solution. The condenser and funnel were Quickfit® apparatus and therefore fit snugly into the flask themselves with plastic clips used to secure them in place. The

extra port in the flask had a stopper placed in it. The condenser was then hooked up to the cold water supply and a clamp retort stand used to provide it with some support.

When all the equipment was set up the water bath was turned on and set to 50°C. The bath was then left for a couple of hours to reach this temperature.

Dry solvents and non-solvent were used to produce dope solution. The liquids were added to the vessel through a long stem funnel, placed temporarily in the stoppered port, which allowed the fluids to be added to the bottom of the flask and thus preventing it seeping into the flange. For this work the low volatility solvent was dimethylacetamide (DMA), the high volatility solvent was tetrahydrofuran (THF) and the non-solvent was ethanol.

The appropriate mass of polymer, poly(vinyl chloride) (PVC) in this case, was then weighed and added to the vessel via the solid funnel. The PVC addition was carried out slowly in order to prevent agglomeration of the solid particles. The stirrer speed was adjusted over the course of the addition to cope with the change in the nature of the solution; although the effect of viscosity was reduced by the temperature of the bath some of the solutions prepared were still highly viscous. Generally the required change was an increase in the stirrer speed. Once the addition of the required mass of solid was complete the funnel was removed and a stopper inserted into the port instead; if the funnel was left in place it would have provided an easy route for solvent evaporation from the system. The condenser retained the volatile components within the system which was sealed with the exception of the condenser. The solid particles generally took in the region of 2-3hrs to completely dissolve.

When the solid was completely dissolved the solution was homogeneous or contained bubbles of gas. It was hoped these bubbles were air introduced by the mixing process, although it is likely there was a component of high volatility solvent as well. Dependant on the polymer concentration, and hence viscosity of the dope produced, the bubbles

present would rise through the solution and pop at the surface given a couple minutes rest time; this process was aided by the elevated temperature of the water bath. However, for some thicker solutions it was necessary to degas the solution. This was carried out on the system shown in Figure 3.1-2.

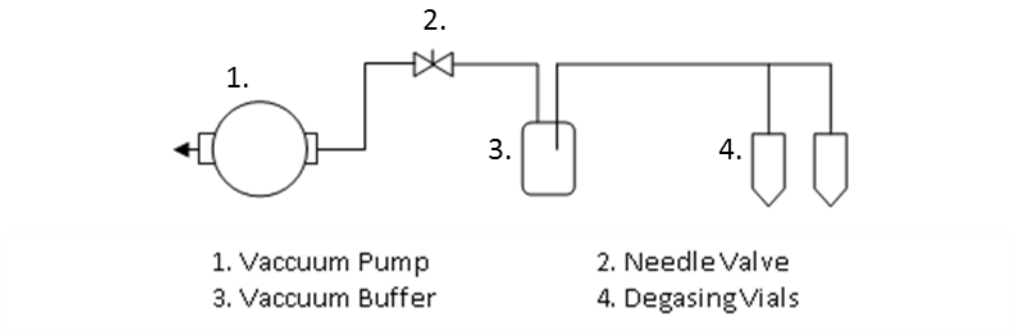

Figure 3.1-2: Degasing set-up

The vacuum pump used was an Edwards E2M2 BS 2208, two stage pump. The vials for the solution were 200ml centrifuge tubes. The needle valve allows control of the vacuum which was being exerted on the polymer solution. The pressure is controlled to degas the bubbles in the solution slowly, as it was feared the high volatility solvent, THF, would come out of solution rapidly at low pressure. The vacuum buffer was put in place to help prevent fluid coming through the tubing from reaching the vacuum pump. The buffer was a glass container which could withstand low pressure at low temperature so it could be kept in an ice/water bath. The lower temperatures in the buffer aid the condensation process of gaseous components. The process is described in more detail in section 3.3.

3.2. Membrane Production

The membrane spinning process was carried out using the set-up shown in Figure 3.2-1. The dope solution was placed in the dope pot (a pressure vessel with two ports in the top). A pressure head of 20psig was applied to the dope pot from the gas cylinder

(Nitrogen). The application of the pressure head achieved two goals: any bubbles which were present in the solution would be reduced or collapsed by the increase in the pressure head and it also provided the driving force to push the solution through the piping. The application of the pressure head to provide the driving force for the solution means that the gear pump was acting as a metering device although, since it is a positive displacement type pump it should have no bother with the high viscosity of the solution. The gear pump used was Slack and Parr – SPLA 0.3ml/rev driven by a 50W thyristor speed controlled DC shunt wound motor geared to a maximum speed of 40rpm. The motor also utilised a double gear reduction to give steady rotation even at slow speeds. From the gear pump the polymer line goes to the spinneret where the fibres are produced.

The section of the spinning rig described so far was used for both elevated and ambient temperature spinning. In order to convert from the ambient temperature method to the elevated temperature method heat tape was wrapped around the piping between the dope pot and spinneret, this included wrapping the gear pump and spinneret mount, while the dope pot was placed in a water bath. Both the heat tape and water bath were set to 50°C and controlled at this temperature for the duration of the experiment. This was the only section of the spinning process which changes for spinning at elevated temperature.

Also leading to the spinneret was a supply of bore fluid. The bore fluid was introduced to the centre of the fibre by the design of the spinneret; the resulting appearance of the spinneret base was of concentric circles as shown in Figure 3.2-2. The bore fluid was a non-solvent for the polymer, in this case a 20% w/w potassium acetate solution, and was contained in a reservoir. The flow of bore fluid was controlled using a Waters 510 HPLC (high performance liquid chromatography) Pump 115/230V 50/60Hz selected for its ability to provide a continuous flow rate under the low flow operating conditions required.

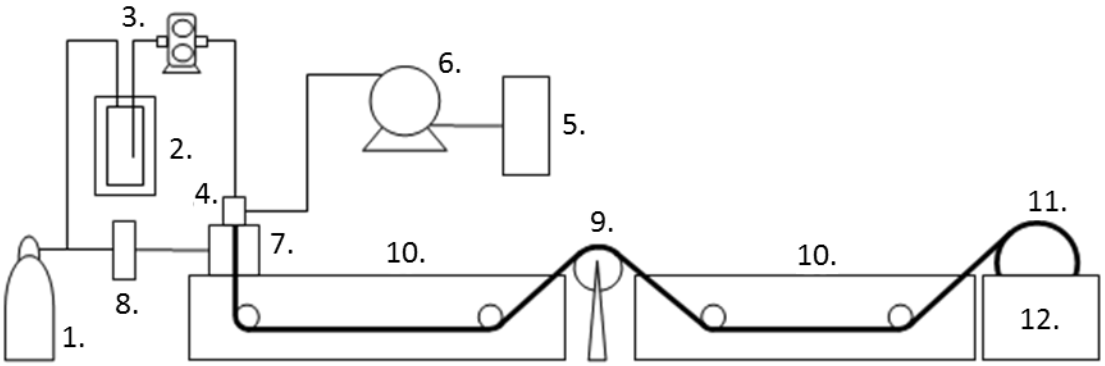

1. Gas Cylinder
2. Jacketed Dope Pot
3. Gear Pump
4. Spinneret and Support
5. Bore Fluid Reservoir
6. Centrifugal Pump
7. Forced Convection Chamber
8. Rotameter
9. Intermediate Roller
10. Coagulation Baths 1 and 2
11. Wind-up Drum
12. Wind-up Bath

Circle in the baths represent rollers to guide the membrane and the bold line gives a graphical representation of the membrane route through the system from the spinneret to the wind up drum

Figure 3.2-1: Membrane Spinning Apparatus

The spinneret was held within a specifically designed mount made of stainless steel. The bore fluid feed is attached directly to the spinneret however the dope feed is attached to the holding unit. Inside the holding unit the dope solution passes into the spinneret through a set of holes placed in a circle, equidistant from the centre, in the top surface of the spinneret. The outer diameter of the extrusion area for the dope was $6.35*10^{-4}$m and the inner diameter was $2.29*10^{-4}$m. More detailed data on the inner workings of the spinneret is not available as it was provided for research purposes by Air Products and Chemicals Inc. and these dimensions were all the data which were provided with it.

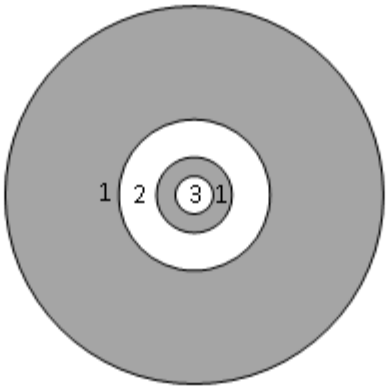

1. Stainless Steel
2. Dope Extrusion Ring
3. Bore Fluid Outlet

Figure 3.2-2: Schematic of spinneret outlet

Fixed below the spinneret was the forced convection chamber. The chamber was a tube of Perspex with 3 holes bored into the side wall at the same height on the tube and 120° apart. These holes were where the gas lines from the Nitrogen cylinder were attached to the column. The gas cylinder fed Nitrogen gas to the convection chamber at a rate determined by the rotameter flow controller. The convection chamber was clamped in place between two rings at the top and bottom of the chamber. The bottom ring of the support was held in place level with the top of coagulation bath 1 so as to maintain the same distance between the bottom of the chamber and the surface of the coagulant in the bath. The height of the top ring of the support above the bottom ring however was freely and easily adjusted. The adjustments could be carried out mid spin run in order to change the conditions under which the membranes were being produced without stopping the flows of any of the feeds. The ability to make changes mid process was important as restarting the membrane production successfully could pose difficulties if it was stopped mid run.

The coagulation baths were made out of stainless steel and contained PTFE rollers which directed the membrane through the baths without damaging it. The first coagulation bath which the membrane entered was deep to begin with, allowing the first guide to be placed 40cm below the surface of the water bath. This arrangement meant that the membrane was kept vertical after extrusion and hence the surface would not be damaged by being flexed around a corner until it was strong enough to do so. After this initial deep section the membrane was guided back to a depth of 5cm by the rollers so that the bath would not be so large that if coagulation fluids other than water were to be used then the cost of filling them would not be prohibitive. For this work the coagulant in both baths was water from the mains supply. In the second coagulation bath the membrane was always at a depth of 5cm under the surface. The first bath was 1.60m in length while the second was 1.40m. These lengths were adequate to produce a strong enough fibre to withstand being wound up on a drum without suffering damage as a result. The wind-up bath plays a lesser role in the membrane formation but serves to keep them wet while they are collected which helps the sub structure of the membrane continue to form.

The wind-up drum itself was 16.5cm diameter and therefore gave membrane sections approximately 52cm in length when they were cut free. The length of each membrane does however depend on how long the membrane on the drum is allowed to build up between removing the membranes as a build up of material on the drum contributes to a steady increase in apparent diameter. The standard practice for when to cut the membranes off the drum was to do so before they started to build a second layer which kept the membranes a consistent length and also prevented the possibility of the first membranes onto the drum being crushed by additional layers. Once the membranes had been cut free of the drum they were transferred to a separate water bath for 24hours to ensure complete formation of the membrane.

The wind-up drum was connected to a motor which allowed control of its rotational speed. This meant that the wind-up drum could be used to set the jet-stretch ratio of fibres being produced where this is the ratio of extrusion rate to wind-up rate. There was also the possibility of connecting the roller guide between the coagulation baths to a motor which would allow two different fibre stretch methods to be investigated, initial stretch between the spinneret and the roller and secondary stretch between the roller and the wind-up drum: by altering the speeds of the motors on both the roller and wind-up drum.

The final step in the production of the membranes was a solvent exchange process followed by drying. The solvent exchange takes place for 48hours and was carried out by placing the membranes in a methanol bath for this period. This step occurs after the membranes have spent the 24hour period in a water bath. Methanol was used because it is a non-solvent for PVC and has higher mobility and vapour pressure than water. Solvent exchange has two functions the first is to further ensure the complete formation of the membranes as the high mobility of the methanol means that it can ensure penetration to the centre of the membrane and fully forming the substructure, where water might have had problems penetrating this deeply into the membrane. By replacing the water which is contained within the membranes it also makes the drying process much simpler as the methanol has a higher volatility. This means that after 48hours the membranes can be removed from the methanol and allowed to air dry at room temperature for another 48hours. The solvent exchange and drying process were carried out in a fume cupboard as it was likely there would be loss of methanol vapour.

3.3. Potting-up

Potting-up is the process of building a unit which could be placed in the permeation test rig. The final potted up membrane consists of the membrane held in a tube at one end and in an end cap at the other. All work associated with potting up was carried out in a well-ventilated area.

The membranes were held in place using a two component polyurethane resin. The production of this resin and the degasing of it were part of the potting-up process where the equipment used in the degasing was as shown in Figure 3.1-2. The two parts of the polyurethane resin were mixed together in a disposable beaker. This was done slowly to minimise the amount of air which was incorporated into the resin and hence speed up the degassing process.

After mixing the resin was transferred to two 50ml centrifuge vials which were designed to be used at low pressure. The vials containing the polyurethane were then connected to a vacuum pump via a solvent trap and a needle valve. The solvent trap was kept in an ice water bath and meant any vapours which were given off by the polyurethane would hopefully condense in the solvent trap and not reach either the needle valve or the vacuum pump. The needle valve allowed control of the extent of vacuum which was applied to the vials. The vacuum pump used was an Edwards E2M2 BS 2208, two stage pump.

It was important that the extent of vacuum was controlled carefully during the degassing process. The resin vials were only filled with 20cm^3 of polyurethane solution at a time, in spite of having a capacity of 50cm^3. This was done so as to allow head space for the bubbles which form during the degassing process, however even with this headspace if the full vacuum were applied to the vials straight off the mark then the bubbles would be drawn up through the system towards the solvent trap.

To begin the degassing process the needle valve was kept fully open when the pump was turned on. The height of the bubbles inside the vials was monitored and if they came close to getting sucked back through the system then the pump was turned off, the bubbles would relax and then the process could be tried again. If the height of the bubbles did not reach the top of the vial then the needle valve would be closed slightly. This monitoring and closing of the needle valve continued until the needle valve was closed as far as it would allow. Needle valves are not designed to be able to completely shut off so when it was fully closed the needle valve bleed line would be fitted with a blank to enable the full extent of the vacuum to be applied to the vials. The degassing process had to be carried out as efficiently as possible as the polyurethane resin would only be suitable for handling for a limited time.

After degassing the polyurethane was transferred from the resin vials to a disposable syringe for use in the production of the modules. The first stage in module production was the preparation of the tube sheets in a manner which allowed the resin to be injected to them without damaging the fibre. The modules were prepared for the introduction of resin before the resin preparation outlined above was carried out.

A tube sheet consisted of a length of ¼inch diameter stainless steel pipe with fittings at either end appropriate to connecting to the permeation test rig. These fittings were provided by Swagelok®. Each of these tube sheets had a piece of flexible tubing placed over one end and was then placed in the lower level of the potting rack.

The lower level of the potting rack consisted of a series of holes in a line which were large enough for the flexible tubing to pass through but not so large that the whole tube sheet could pass through it. On the other side of the lower level another matching series of impressions are cut, these do not go all the way through so that when the end caps are potted up they can sit in these holes.

A small screw clamp was then put over the flexible tubing but not completely closed so that it would still be possible for resin to flow through the constriction in the tubing.

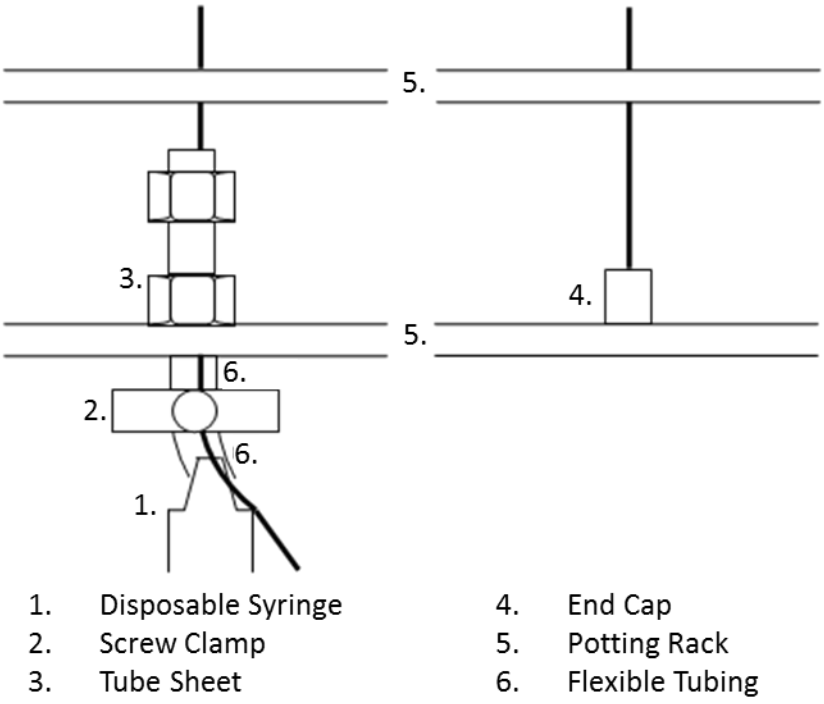

Figure 3.3-1: Potting apparatus

A suitable fibre had to be selected for gas permeation testing and be placed in the tube sheet. A fibre was selected from the bundle of dry membranes and a magnifying glass used to examine it for defects and suitability. A suitable fibre was one which had; a near circular cross section, a centrally positioned bore when viewing the cross section, no obvious imperfections such as pin holes or bubbles on the surface and no areas where the hollow fibre had collapsed. It was noted that under the inspection lamp a suitable fibre tended to have a slight sheen to the surface.

The selected fibre was threaded through the upper level of the potting rack, the tube sheet and flexible tubing as shown in Figure 3.3-1 where the fibre is represented by the bold line. The upper level of the potting rack consisted of a series of holes in a line

which acted as guides for the fibre when potting the tube sheet. On the far side was another series of holes which acted as guides for the potting of the end caps through which the fibre was threaded and inserted into the end cap. The guide holes meant that the fibre went into either the tube sheet or the end cap vertically and thus minimised stress on the fibre at the point where it meets the Polyurethane when hanging in a test chamber as it would not have a kink at this point. The rack was also suitably sized so that the membranes could be cut to a length of 28cm between the tube sheet and end cap without damaging the membranes by making them curve too sharply.

With the module now constructed it was ready to be filled with Polyurethane, which would be prepared at this point as described previously. The syringe containing the Polyurethane was then placed into the open end of the flexible tubing. The tubing was held tight to the syringe nozzle while the Polyurethane was slowly injected. This resulted in the tube sheet slowly filling with resin from the bottom up. It was important this process was carried out slowly so as to allow the Polyurethane to fill all the available space in the module and not get air bubbles trapped inside. Doing the process slowly also means that it is easier to control when to stop injecting the Polyurethane; it should not coat any of the fibre above the tube sheet, this would reduce the effective operating area of the membrane since the Polyurethane is impermeable.

The injection of Polyurethane was halted when it was a short distance away from the top of the tube sheet. This meant that as the screw clamp was tightened, which it now was, the reduction in volume of the flexible tubing caused the Polyurethane to fill the rest of the tube sheet volume. When the screw clamp was fully tightened the syringe was removed from the tubing and after checking the fibre was entering the centre of the tube sheet this section of the module could be left to cure.

The end cap was then potted up by removing the fibre from it and filling the cap with Polyurethane. This was done by inserting the syringe to the bottom of the end cap and

then slowly filling it from the bottom up to make sure no air bubbles were introduced to it. When the end cap was full the fibre was then reinserted to and centred within it.

The curing process took 24hours to reach full completion and relied upon a heat catalysed exothermic reaction. If the heat provided to the reaction was not great enough then the curing process would not go to completion within the time and would have to be left for an extended period to finish curing or the module would not be strong. When large enough volumes of the Polyurethane resin are being used this is not a problem because the heat produced by the reaction itself is enough to catalyse to completion at room temperature. However, in the case of potting up the volumes being used are small and are also enclosed in metal which will very efficiently transfer the heat produced away from the Polyurethane resulting in a poor cure. To counter this effect a heat gun was used to warm the tube sheet and end cap to around 35°C for the first part of the curing process (around half an hour) and this proved to be effective in allowing the curing process to go to completion in the expected 24hours.

3.4. Sylgard 184 Coating

The hollow fibre membranes are coated to improve separation performance as explained in the introduction. The coating process used was a simple dip coating and was based on a patent passed by the United States patent office for Ward *et al* in 1980[1].

The coating material used for the PVC membranes was Sylgard 184. This is a two component system consisting of a silicone elastomer and a curing agent which combine

to produce Polydimethylsiloxane (PDMS). Both the elastomer and the curing agent are soluble in Hexane however the final PDMS is not.

To coat the membranes a solution of the two components in the ratio of 10 parts elastomer to 1 part curing agent dissolved in Hexane is produced, mixed well and transferred to a measuring cylinder. The standard coating procedure used a 5% w/w solution of Sylgard 184.

The membrane to be coated was suspended in the measuring cylinder of Sylgard solution so that the full area of separating membrane was covered. The membrane module was suspended such that the end cap was at the bottom of the cylinder and as small a portion of tube sheet as possible was under the surface as coating the tube sheet could have resulted in a poor seal between it and the permeation test rig. The support to the tube sheet for holding it steady was provided by a retort stand which held a pipe and fitting which attached to the tube sheet. The dip coating procedure lasted for 15mins in the standard coating procedure after which time the membranes were left to dry. The membranes were usually hung vertically for the drying process although it would be better if they could be set out horizontally to prevent a thicker coating being formed at the bottom of the membrane than at the top.

A number of membranes were usually coated at the same time and it was necessary to make sure that the Hexane/Sylgard solution was well stirred between each one to maintain an equal concentration throughout the measuring cylinder. Also After coating 10-15 membranes the Hexane/Sylgard solution was changed to prevent Sylgard concentration varying too much between samples.

All work relating to the coating processes was carried out in a fume cupboard and a diagram of the apparatus is shown in Figure 3.4-1.

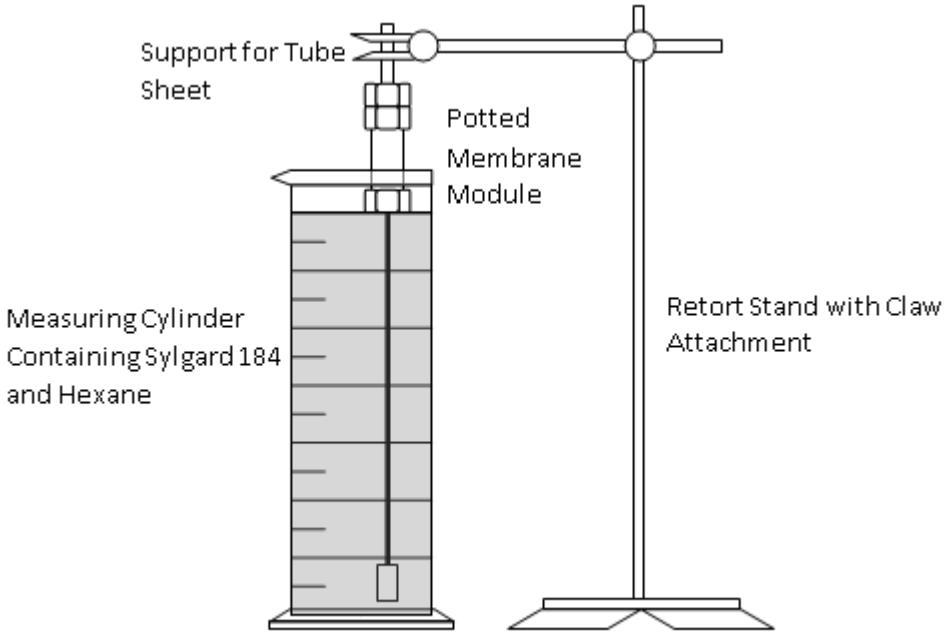

Figure 3.4-1: Sylgard 184 coating apparatus

3.5. Permeation Testing

Testing of the membranes was carried out on the permeation rig. The rig had five chambers capable of testing modules, so they could be tested in batches, the diagram of the permeation system shown in Figure 3.5-1 shows two modules for simplicity.

The permeation rig set up allows for testing with a single gas at a time and the gases used here were Oxygen, Nitrogen, Carbon Dioxide and Methane. If attached to a gas chromatograph instead of bubble flow meters and by using the valves labelled V104 and V110 to recycle a portion of the gas flow it would also be possible to do testing of gas mixtures with the design shown in Figure 3.5-1. V114 was also in place for multiple gas testing and was used to send the shell side gas to the gas chromatograph for analysis. However, in this work all the testing

carried out was with single gases and so the valves for multiple gas testing were permanently closed.

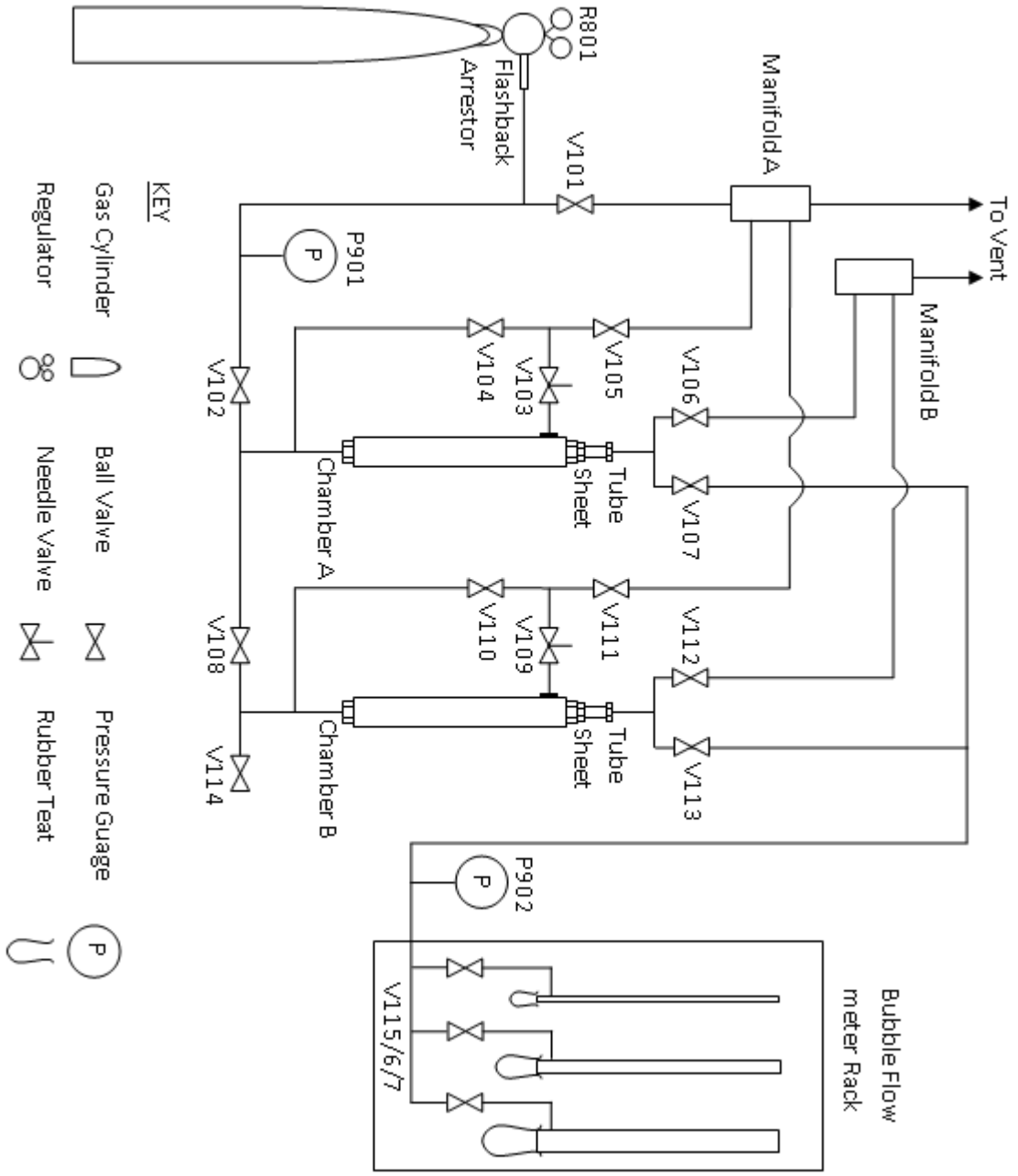

Figure 3.5-1: Permeation rig pipe and instrumentation diagram

Potted up membranes were placed into the test chambers so they hung vertically. For start-up V102/108/106/112 were open and the other valves were shut. The first gas to be tested was connected to the system and the system was pressurised to 5bar using P901 to measure the pressure so that the same gauge was used for each gas. With the system pressurised V101/103/105/109/111 were opened for a short time purging gases other than the test gases, then those valves were closed again.

The membranes were left in the test gas for a period of at least an hour before any permeation tests were carried out, this time period was intended to allow for any immediate swelling of the membranes resulting from exposure to the test gas occurred and that the consecutive pressure normalised flux measurements did not trend due to this swelling. Towards the end of this time the bubble flow meters were prepared for use by using a syringe to pass bubble solution (washing up liquid in water) through the column thus wetting the inner surface. The rubber teat on the bottom of the flow meter was then half filled with bubble solution

To test the first membrane module V106 was closed and V107 was opened. A suitable bubble flow meter was selected using V115/116/117 for measuring the gas flow being directed towards it by the valve system and five measurements of the flow of gas through the membrane were recorded using the bubble flow meter. To check if the membrane properties were consistent over short time periods after 15mins a second set of times were taken and if they were consistent with the first times then it was expected the membranes from that test batch could be tested with that gas.

Once the times had been recorded for the module in Chamber A V106 and V107 were opened and closed respectively to reset the flows. This allows V112 to be closed and V113 opened to test the membrane in Chamber B. Only one set of times was recorded for the second module and the rest of the modules in that batch.

P902 was used to monitor the pressure which was being fed to the bubble flow meters because they were constructed from glass. If the pressure exceeded 0.5bar then the flow was diverted to vent.

3.6. Chemicals and Materials

- Poly(vinyl chloride), number average molecular weight M_n: 22000g/mol, weight average molecular weight M_W: 43000g/mol, CAS number: 9002-86-2, Formula: C_2H_3Cl, manufacturer: Aldritch
- N,N-dimethylacetamide, grade: CHROMA SOLV® Plus for HPLC, assay: >=99.9%, manufacturer: Aldritch
- Tetrahydrofuran, grade: CHROMA SOLV® Plus for HPLC, assay: >=99.9%, manufacturer: Aldritch
- Ethanol, grade: CHROMA SOLV® absolut for HPLC, assay: >=99.8%, manufacturer: Aldritch
- Methanol, grade: CHROMA SOLV® for HPLC, assay: >=99.9%, manufacturer: Aldritch
- Hexane, grade: CHROMA SOLV® for HPLC, assay: >=95.0%, manufacturer: Aldritch
- Polyurethane, grade: PU 3410, manufacturer: Alchemie
- Polydimethylsiloxane, grade: Sylgard® 184, manufacturer: Dow Corning
- Carbon dioxide, grade: CP, purity: 99.995%, manufacturer: BOC
- Methane, grade: research, purity: 99.995%, manufacturer: BOC
- Nitrogen, grade: CP, purity: 99.9992%, manufacturer: BOC
- Oxygen, grade: CP, purity: 99.999%, manufacturer: BOC
- Ozone, produced from university generator and destroyed via catalyst before exhaust release

3.7. Calculations

3.7.1. Calculating Pressure Normalised Flux

The methodology for collection of results from the permeation rig was discussed in the experimental section but a fuller analysis of how to use the data acquired is necessary. As was mentioned, five times were recorded for the amount of time, t, it took a set volume, V, of gas

to permeate through the membrane. After the membranes had been tested in the permeation rig the modules were removed and the length of exposed membrane surface, L, and membrane diameter, d, measured in order to obtain the membrane surface area, A.

$$\boldsymbol{A = Ld} \qquad \textbf{Equation 3.7.1.1}$$

Using the permeation measurements, area and pressure across the membrane in the permeation rig during testing, P, a pressure normalised flux, PNF, could then be calculated for each membrane according to Equation 3.7.1.2.

$$\boldsymbol{PNF = \frac{V}{AtP}} \qquad \textbf{Equation 3.7.1.2}$$

The mean, $\bar{x}$, pressure normalised flux was then calculated for each different category of membranes. The mean pressure normalised flux for a category is given by Equation 3.7.1.3 where; i, is the category, j, is the different samples within the category and n, is the number of samples with category i.

$$\boldsymbol{\bar{x}_{PNF_i} = \frac{\sum_{j=1}^{n} PNF_j}{n}} \qquad \textbf{Equation 3.7.1.3}$$

The mean pressure normalised flux was calculated for each gas which the membranes were tested with.

The units of pressure normalised flux are consistent with the equation used to calculate it where volume is measured in cm^3, membrane area in cm^2, time in s, and pressure in cmHg. However, since this calculation results in a very small number with complicated units in order to make the measurements more readily presentable and understandable they are often abbreviated to gas permeability unit (GPU) where 1 GPU=$1*10^{-6}$ $cm^3cm^{-2}s^{-1}cmHg^{-1}$. GPU will be used as the unit of pressure normalised flux from this point on.

3.7.2. Calculating Selectivity between Gas Pairs

The selectivity of the membranes was calculated for each gas pair which was tested. In this work the gas pairs used were:

- Oxygen and nitrogen
- Carbon dioxide and methane

A large amount of the research involving gas separation membranes uses these pairs[1-4], although there are other options such as helium and hydrogen. For reasons of both safety and expense the pairs above are used in this work preferentially. Since the final aim for the PVC membranes is in the separation of ozone and oxygen using light gases such as these rather than hydrocarbons are more suitable representations of the final procedure. Although ozone was to be used in order to generate the oxidative environment to show the PVC membranes could survive such conditions additional safety precautions are required when dealing with ozone. Due to these considerations it was elected to prove the membranes first in a non-oxidising environment using benign gases.

The selectivity for the membranes between gas pairs can be determined in a couple of different ways which lead to different values. It is not normally commented upon in the literature as to which method is used to obtain the selectivity which can lead to confusion in the interpretation of the results presented. One method for the calculation is taking the ratio of the mean pressure normalised fluxes for each gas pair giving Equation 3.7.2.1 where a and b represent the two different gases.

$$\boldsymbol{\Omega_{i.a,b}} = \frac{\overline{\boldsymbol{x}}_{\boldsymbol{PNF_{i.a}}}}{\overline{\boldsymbol{x}}_{\boldsymbol{PNF_{i.b}}}} \qquad \textbf{Equation 3.7.2.1}$$

The second method which can be used is to calculate the selectivity of each membrane within the category and take the mean value of those selectivities.

$$\overline{\boldsymbol{x}}_{\boldsymbol{\Omega_{i.a,b}}} = \frac{\sum_{j=1}^{n} \boldsymbol{\Omega_{j.a,b}}}{\boldsymbol{n}} = \frac{\sum_{j=1}^{n} \frac{\boldsymbol{PNF_{j.a}}}{\boldsymbol{PNF_{j.b}}}}{\boldsymbol{n}} \qquad \textbf{Equation 3.7.2.2}$$

In this work the method shown in Equation 3.7.2.2 will be used due to the difference which this makes in the standard deviation calculation for selectivity (see section 3.7.3).

3.7.3. Standard Deviation in PNF and Selectivity

For statistical analysis and to obtain an impression of the variation in membrane samples the standard deviation, σ, and standard deviation of the mean, σ_{mean}, were calculated where appropriate. The sample standard deviation was calculated separately for each gas, a, the membranes were tested with and represents the spread of results from the mean value. For the pressure normalised flux, where, j, represents the different membrane samples the standard deviation is given by Equation 3.7.3.1.

$$\boldsymbol{\sigma_{PNF_{i.a}}} = \sqrt{\frac{\mathbf{1}}{\boldsymbol{n-1}}\sum_{\boldsymbol{j=1}}^{\boldsymbol{n}}\left(\boldsymbol{PNF_{j.a}} - \boldsymbol{\overline{x}_{PNF_{i.a}}}\right)} \qquad \textbf{Equation 3.7.3.1}$$

The standard deviation of the mean or standard error is used to obtain information about the precision of the mean value which has been calculated for the sample.

$$\boldsymbol{\sigma_{meanPNF_{i.a}}} = \frac{\boldsymbol{\sigma_{PNF_{i.a}}}}{\sqrt{\boldsymbol{n}}} \qquad \textbf{Equation 3.7.3.2}$$

The standard deviation in the selectivity can be found by two different methods dependent upon which of the two methods for calculating selectivity has been used. Equation 3.7.3.3 shows the equation for the selectivity as a ratio of the means of the PNF for the gas pair through that membrane category, when this form is used the standard deviation of the value is found by a sum the squares method as shown in Equation 3.7.3.3.

$$\frac{\boldsymbol{\sigma_{\Omega_{i.a,b}}}}{\boldsymbol{\Omega_{\mathrm{i.a,b}}}} = \sqrt{\left(\frac{\boldsymbol{\sigma_{PNF_{i.a}}}}{\boldsymbol{\overline{x}_{PNF_{i.a}}}}\right)^{\mathbf{2}} + \left(\frac{\boldsymbol{\sigma_{PNF_{i.b}}}}{\boldsymbol{\overline{x}_{PNF_{i.b}}}}\right)^{\mathbf{2}}} \qquad \textbf{Equation 3.7.3.3}$$

When Equation 3.7.3.4 is used the equation for selectivity standard deviation becomes similar to that as for pressure normalized flux standard deviation.

$$\sigma_{\Omega_{i.a,b}} = \sqrt{\frac{1}{n-1}\sum_{j=1}^{n}\left(\Omega_{j.a,b} - \overline{x}_{\Omega_{i.a,b}}\right)} \qquad \textbf{Equation 3.7.3.4}$$

The difference in the calculated standard deviations between these two equations is the reason for choosing to use Equation 3.7.2.2 to calculate the selectivity. Like the value of selectivity the standard deviation differs dependent upon which equation is used, having carried out the calculations with both equations it seems that the smallest error is incurred in the value of selectivity when using Equation 3.7.3.4 which means the appropriate selectivity calculation has to be used. This is demonstrated in Table 3.7.3-1 using a set of results which will be discussed later.

The table shows results for 5 membranes which were all produced under the same conditions so the results are from the same category. For each membrane a pressure normalized flux for oxygen and nitrogen was calculated and the selectivity between this gas pair was also calculated. For pressure normalized flux the mean value of the 5 membranes and the standard deviation is given calculated as outlined above. For selectivity the two different methods for calculating the values are given according to the equation number used in the calculations.

From the mean value of selectivity calculated using Equation 3.7.2.2 and the value calculated using Equation 3.7.2.1 it can be seen that there is not a large difference in the result. Although Equation 3.7.2.2 is a slightly better selectivity the percentage increase from Equation 3.7.2.1 is only 2.9%. On the other hand, the standard deviation in the two methods shows a massive comparative difference with a 96.2% increase going from Equation 3.7.2.2 to Equation 3.7.2.1. The standard deviation in Equation 3.7.2.1 predicts a range and spread of results in the value of selectivity which would be so large as to render the calculated value almost meaningless and looking at the selectivity of the individual membranes clearly is not representative of the spread. It therefore is Equation 3.7.2.2 which is the better, more accurate method of calculating selectivity and will be used throughout.

Table 3.7.3-1: Membrane results to demonstrate calculation method differences

Membrane Identity	PNF (GPU)			Selectivity Method O_2/N_2	
	O_2	N_2		3.7.2.1	3.7.2.2
1	2.276	0.494		4.612	
2	2.667	0.689		3.870	
3	2.478	0.537		4.613	
4	2.912	0.910		3.200	
5	2.086	0.555		3.761	
Mean	2.484	0.637		4.011	3.899
σ	0.323	0.169		0.605	1.187

The final advantage of using Equation 3.7.2.2 is that it also allows for the calculation of the standard deviation of the mean for selectivity as it is carried out for pressure normalized flux.

$$\boldsymbol{\sigma_{mean\Omega_{i.a}} = \frac{\sigma_{\Omega_{i.a}}}{\sqrt{n}}} \qquad \textbf{Equation 3.7.3.2}$$

3.8. Plotting Graphs and Error Bars

In the sections of this thesis which contain results and discussion of the experiments the results are sometimes shown in graphical form and some of these charts contain error bars. Where there are error bars displayed it is the standard error which has been used.

3.9. Bibliography

1. R. R. Ward, R. C. Chang, J. C. Danos, J. A. Carden Jr.; *Processes for coating bundles of hollow fiber membranes*; United States Patent; **1980**.
2. Tin, PS, Chung, TS, Liu, Y, Wang, R, Liu, SL, and Pramoda, KP, *Effects of cross-linking modification on gas separation performance of Matrimid membranes.* Journal of Membrane Science, 2003. **225**(1–2): p. 77-90.
3. Hasbullah, H, Kumbharkar, S, Ismail, AF, and Li, K, *Preparation of polyaniline asymmetric hollow fiber membranes and investigation towards gas separation performance.* Journal of Membrane Science, 2011. **366**(1–2): p. 116-124.
4. Barbari, TA and Datwani, SS, *Gas separation properties of polysulfone membranes treated with molecular bromine.* Journal of Membrane Science, 1995. **107**(3): p. 263-266.
5. Li, Y, Cao, C, Chung, T-S, and Pramoda, KP, *Fabrication of dual-layer polyethersulfone (PES) hollow fiber membranes with an ultrathin dense-selective layer for gas separation.* Journal of Membrane Science, 2004. **245**(1–2): p. 53-60.

4. Ambient Temperature Spinning

4.1. Initial Dope Design

The polymer concentration used in the dope for producing gas separation membranes is a key component in the properties of the membranes. In this case this means that the concentration of poly(vinyl chloride) (PVC) to be used in the dope has to be selected. Literature values for PVC hollow fiber membranes are commonly in the 10-15% range[1-3]. In this case however there are a couple of issues with direct comparison to other PVC hollow fibers: the literature search has not revealed any other PVC hollow fiber membranes being targeted at gas separation purposes (ultrafiltration being the most common application), for other membranes the PVC is often part of a blend of polymers being used to create the material where the total dope solids content is nearer 20% by weight[2-4]. With membranes being produced for ultrafiltration it is desirable to have a porous structure all the way through the membrane whereas for gas separation a higher polymer concentration may be used in the hope of achieving a higher linear density. A higher linear density in the dope was considered to make it easier to produce the dense active layer characteristic of the gas separation membrane and also make the production of a higher strength membrane more likely[5]. It was concluded that these reasons justified the use of a relatively high concentration of PVC in the dope.

The group at Strathclyde has extensive experience working to produce polysulfone gas separation membranes over a wide range of concentrations[6-8]. In an analogous situation it was determined to base the initial concentration of PVC on the range of concentrations commonly observed in polysulfone membranes and hence a concentration of 24% was selected.

The use of a high volatility solvent for the polymer is important in the production of the active layer, when using dry/wet spinning methods, since it is expected to evaporate rapidly from the surface of the membrane during forced convection driving the surface composition of the membrane into the two phase region of the phase diagram. In this case tetrahydrofuran (THF) was selected as the solvent due to the volatility and solvating properties it provides and also due to THF being a common choice for the high volatility solvent in dope solutions. The concentration

of THF can therefore have a large influence on the thickness of the active layer produced[5]. With hollow fiber gas separation membranes produced from other polymers the concentration of the high volatility solvent (THF) is often high and in some cases is equal to that of the low volatility solvent, for instance Ismail, (1999)[8] produced polysulfone membranes using THF at a concentration of 31.8% which was in balance with the N,N-dimethylacetamide concentration.

However, it was determined in the case of PVC to initially use a low concentration of the high volatility solvent due to the capabilities of PVC in terms of gas permeation. As outlined in the introduction PVC is a glassy, low permeability polymer. This means that the production of a thick active layer could be prohibitive to the transmittance of gas through the membrane at a rate which would allow the membrane to be practically useful. So the low concentration of THF at the surface should mean that rapid evaporation of it does not lead to a thick skin forming during the dry step of the spinning process. For the initial dope solution a value of 7% set for the concentration of THF.

Another common component of the dopes used for hollow fiber production is the non-solvent. This non-solvent is included in the dope to push the composition closer towards the phase separation boundary. The closer the solution is to the binodal phase separation boundary at the start of the spinning process the better the easier it is to control penetration into the phase diagram during the dry step as the composition has to change less in order to begin the phase separation processes.

Commonly ethanol is used as the non-solvent in gas separation membrane dope solutions. However, there was an issue with the supply lines of ethanol to the laboratory at this point in time so it was determined to select another non-solvent and attempt to use this. In order to choose a non-solvent to be used in the system the important factors which contribute to the choice of non-solvent had to be identified while bearing in mind that using a solvent similar to ethanol would be good as it has an existing basis in the field. The factors which make a good non-solvent have been outlined in the introduction and it was concluded from them that another similar alcohol would make a reasonable choice to give similar properties. Methanol was thought best avoided as it would increase the health hazard presented by the experiments and after propanol in the homologous series the water miscibility reduces quickly. Water miscibility is

important during the quench step for substructure formation, therefore propanol was deemed a reasonable replacement. When the properties of the two propanol isomers are considered (propan-1-ol and propan-2-ol) it is found that of the boiling points of the two (97°C and 82.5°C respectively) the propan-2-ol boils nearer the temperature of ethanol (78.5°C) and it was selected for this reason. The concentration of propan-2-ol was set at 16% by weight to begin with as it was felt this value provided scope to increase or decrease the concentration as required and is not outside commonly seen non-solvent concentrations in dope solutions.

The final part of the dope solution is N,N-dimethylacetamide (DMac) which is a good solvent for PVC and makes up the majority of the composition. DMac acts as the carrier solvent and therefore was expected to have less of an impact on the spinning processes than other components. The DMac made up the balance of the weight of the initial dope solution giving it a concentration of 53% by weight.

The resulting polymer solution for the first batch of membranes contained 24% PVC, 53% DMac, 7% THF and 16% ethanol.

4.2. Propan-2-ol Non-solvent Dope Component Membranes (MB1)

The compositions of the streams used to produce MB1 are shown in Table 4.2-1. The set-up of the spinning rig used to produce the first batch of membranes (MB1) with propan-2-ol as the non-solvent in the system are shown in Table 4.2-2. The processes involved in producing and testing the membranes were carried out as described in the experimental section of this thesis.

MB1 was the first set of membranes to be produced on the spin rig, after it was recommissioned, following a number of years of dormancy so apart from the results themselves it acted as a test batch of membranes to check all the equipment was working as expected. Since this was the first batch and a test it was not felt necessary to try and change the conditions being used to produce the membranes while the spin run was in progress but rather to target producing hollow fibers that were consistent over the full spin run.

Table 4.2-1: Compositions of the input streams to the spinning process for MB1

Dope Composition	
Chemical	**Concentration (weight %)**
Poly(vinyl chloride)	24%
Dimethylacetamide	53%
Tetrahydrofuran	7%
Propanol	16%
Bore Fluid Composition	
Chemical	**Concentration (weight %)**
Water	80%
Potassium Acetate	20%
Coagulation Bath Composition	
Chemical	**Concentration (weight %)**
Water	100%

Table 4.2-2: Spinning conditions for MB1

Spinning Conditions	
Extrusion rate (cm^3/min)	2.5
Dope temperature (°C)	19
Jet stretch ratio	1
Bore fluid flow rate (cm^3/s)	0.8
Bore fluid temperature (°C)	18
Convective gas	Nitrogen
Convective gas flow rate (L/min)	4
Convective gas temperature (°C)	18
Convection chamber height (cm)	6
Distance to gas jets (cm)	3
Bath temperature (°C)	14
Air temperature (°C)	20

Fibers for this section should all provide equal results since they are all spun under the same set of conditions. A selection of five fiber samples were taken from the spin run and potted up for testing. The fibers were selected at equal intervals over the course of the production process to check for variations which could occur during the run. The samples were numbered 1 through 5

and the time into the spin run which each sample was taken at was recorded in Table 4.2-3, the dope solution ran out after 43mins so the fifth sample was taken very close to the end of the run.

The results for the uncoated samples are shown in Table 4.2-4 and the results for the coated samples are shown in Table 4.2-5.

Table 4.2-3: MB1 membrane sample definitions

Membrane Identity	Spinning Time Elapsed (mins)
1	0
2	10
3	20
4	30
5	40

Table 4.2-4: MB1 uncoated results and calculations

Membrane Identity	PNF (GPU)				Selectivity	
	O_2	N_2	CO_2	CH_4	O_2/N_2	CO_2/CH_4
1	3228	2560	2940	4596	1.261	0.640
2	2574	1833	2272	3619	1.404	0.628
3	2974	2688	2766	4301	1.106	0.644
4	2007	1831	1865	2920	1.096	0.640
5	2060	1886	1894	3022	1.092	0.626
$\overline{x}$	2568	2159	2347	3692	1.192	0.636
σ	541	427	492	748	0.138	0.008
σ_{mean}	242	191	220	334	0.062	0.003

The uncoated results show high fluxes combined with low selectivity. The results of uncoated membranes are often not published in academic papers as it is well known that the uncoated performance of membranes for gas separation is heavily hampered by defects in the surface. However, when some of the results in the literature are studied the pressure normalised fluxes tend to be in the order of hundreds GPU[9-13], although this is influenced by the material and conditions present during the spinning process. MB1 gave particularly high values of uncoated flux with the mean values for all gases being at least an order of magnitude higher than is commonly seen. The standard deviations in the flux and the mean flux were also fairly large showing the membranes have some inconsistency present over the course of the spin run

although none of the deviations suggest that the PNF could be low enough to fit in with other uncoated results.

The uncoated selectivity of MB1 for oxygen/nitrogen and carbon dioxide/methane gas pairs show values of 1.192 and 0.636 respectively. The oxygen/nitrogen results show very low levels of selectivity which suggest either a highly compromised active layer or very low levels of selectivity from solution diffusion. As PVC selectivity is known to be around 4.5 for oxygen/nitrogen this suggests that the surface is highly flawed. Since the values are so close to 1.0 for this selectivity in a number of cases and the gas flux is so high it is likely that the major mass transport method is viscous flow. The carbon dioxide/methane figures are very close to the theoretical Knudsen diffusion separation which would be achieved of 0.6 and since the standard deviations are small it seems likely that the mass transport across the membrane is primarily by a Knudsen diffusion mechanism. The difference between the transport mechanisms for the two different gas pairs suggests that the pore size is very close to being at the transition region between Knudsen and viscous flow.

Table 4.2-5: MB1 coated results and calculations

Membrane Identity	PNF (GPU)				Selectivity	
	O_2	N_2	CO_2	CH_4	O_2/N_2	CO_2/CH_4
1	115	132	262	243	0.870	1.08
2	81.9	87.7	206	89.6	0.933	2.30
3	28.2	27.5	35.0	30.3	1.02	1.16
4	68.4	65.7	68.9	86.7	1.04	0.795
5	20.7	23.0	33.2	32.1	0.898	1.04
$\bar{x}$	62.8	67.3	121	96.4	0.953	1.27
σ	39.1	45.3	106	86.9	0.076	0.589
σ_{mean}	17.5	20.2	47.3	38.9	0.034	0.264

The high flux obtained suggests three possibilities:

- Under the spinning conditions used to produce MB1 no active layer is formed.
- The active layer formed during the spinning of MB1 was similar to other gas separation membranes but was subsequently damaged prior to testing.

- The active layer formed in MB1 is much more highly porous than would be expected in gas separation membranes.

The possibility that no active layer was formed during the production process is not easy to disprove, however the spinning conditions used to produce MB1 are similar to conditions used to produce other membranes which have been successful in separating gases[5, 14-16] and so it was expected that while the conditions may not be optimal they would give a working membrane. Additionally the substructure which was expected to form in the membranes would be highly porous; the nature of this substructure means it would be likely that the selectivity would move away from the Knudsen value as more of the mass transport would occur by viscous flow mechanisms depending upon the size of the pores present.

The influence of damage to the membrane surface was minimised throughout the experimental procedure including handling damage and where handling of the membranes was required the section of membrane which would be carrying out the separation was avoided. A great deal of effort is put into the preparation of the membrane modules to ensure the integrity of the membranes so this option is discounted.

Of these three options it was deemed most likely that the third was occurring. If the membrane active layer had many areas which were highly porous then it would bring the selectivity down to Knudsen values so long as the pores are not so large as to allow viscous flow. When this is the case it is expected that applying the coating layer to the membranes plugs these pores and allows the true selectivity of the membrane to come through accompanied by a reduction in the flux.

Looking at the PNF results for MB1 coated they do indeed show a large reduction in the mass transport attained. However, while these results are much lower than the uncoated values when compared to the PNF attained for other polymers through hollow fibers such as polysulfone[5, 7, 12, 13] they show higher values. This was an unexpected result since as mentioned in the introduction the permeability of PVC is so low in comparison to polymers such as polysulfone. This means that either the active layer present in MB1 is exceptionally thin, even for a gas separation membrane, or even after coating the membranes still contain defects.

The statistical analysis of PNF also shows that the membranes are highly variable across the production process since the standard deviation is so high in comparison to the mean and the accuracy of the mean is poor. This lack of consistency in the membranes suggested that some may be suffering from larger defects or more concentrated smaller defects which the coating solution was unable to plug effectively. The possibility of larger defects which the coating solution could not plug is also backed up by the nearer viscous selectivity shown by the oxygen/nitrogen pair.

The selectivity for oxygen/nitrogen shows a shift towards oxygen for the coated membranes and is a part of the coated results where the standard deviation and error in the mean are low enough to say it is a property of the membrane which is consistent.

The selectivity of carbon dioxide/methane returns to having a large standard deviation which renders the result meaningless as far as consistency is concerned but the fact that all the membranes show improved selectivity from the uncoated membranes means the same discussion as for oxygen/nitrogen can still be applied.

Since the uncoated results show either Knudsen or viscous flow types it was proposed that the size of pores must be too large for the coating procedure to effectively coat everything in a manner which forces the gases through the polymer. Instead due to the amount of the surface which is now governed by the coating it is mostly the low selectivity of the coating which is having an effect and even this is limited by how well the coating material is filling the pores.

Another possibility is that the active layer is so thick as well as being a highly porous active layer that even with a coating which is not blocking pores as it would be expected to, for instance due to poor binding with the PVC, there is still a slight improvement in selectivity being observed.

The possible reasons for the membrane having such a porous and possibly thick structure are mostly found in the conditions used to spin in the air gap. However, as mentioned above the conditions used are not abnormal ones for gas separation membranes produced by the dry/wet spinning method. For instance a high forced convective gas flow rate could lead to both thick skins and a highly permeable structure by causing solvent to be driven off deep into the

membrane during the dry step but moving the phase diagram into the glassy region and producing nodules too hard to coalesce.

When analysing the results for MB1 there was always a question mark of having used propan-2-ol rather than ethanol in the dope solution, in spite of the justification provided for its selection as a replacement non-solvent. It was a concern that its use had resulted in a reduction in the mobility of the solvents in the system due to its large molecular weight or that it had different interactions in the system than ethanol does changing the phase diagram in some way. The conclusion arrived at was that it would be sensible to repeat the above membrane production but to the use of ethanol rather than propan-2-ol in the system.

4.3. Ethanol Non-Solvent Dope Component Membranes (MB2)

The spinning of MB2 took place under the conditions outlined in Table 4.3-1 and Table 4.3-2 following the directions given in the experimental section for production and testing of membrane units.

MB2 was carried out in the same manner as MB1 as far as sample selection goes so that the results would be directly comparable to the propan-2-ol non-solvent membranes and the sampling is outlined in Table 4.2-3. For this spinning session the dope solution ran out after 42mins and so again the final sample was taken close to the end of the run.

The permeation testing results for the membranes are shown in Table 4.3-3 and Table 4.3-4.

Table 4.3-1: Compositions of input streams to the spinning process of MB2

Dope Composition	
Chemical	**Concentration (weight %)**
Poly(vinyl chloride)	24%
Dimethylacetamide	53%
Tetrahydrofuran	7%
Ethanol	16%

Bore Fluid Composition	
Chemical	**Concentration (weight %)**
Water	80%
Potassium Acetate	20%
Coagulation Bath Composition	
Chemical	**Concentration (weight %)**
Water	100%

Table 4.3-2: Spinning conditions for MB2

Spinning Conditions	
Extrusion rate (cm^3/min)	2.5
Dope temperature (°C)	20
Jet stretch ratio	1
Bore fluid flow rate (cm^3/s)	0.8
Bore fluid temperature (°C)	18
Convective gas	Nitrogen
Convective gas flow rate (L/min)	4
Convective gas temperature (°C)	18
Convection chamber height (cm)	6
Distance to gas jets (cm)	3
Bath temperature (°C)	14
Air temperature (°C)	21

The uncoated PNFs for MB2 show similarities to those for MB1. They continue to give higher than expected mean values for uncoated membranes and have high variation indicated by the standard deviation. The samples do appear to show a generally increasing PNF as the spinning time goes on in the case of the MB2 membranes where each of the gases displayed the same trend. However, since only a single fiber was tested for each time split it is impossible to say if this is a real trend or an artefact of the sampling method. Had the coated membranes proved to be effective at separating gases then further modules would have been potted up to further probe this trend, unfortunately the coated membranes did not show good separation

characteristics so further experimentation on this batch of membranes was deemed unnecessary.

Table 4.3-3: MB2 uncoated results and calculations

Membrane Identity	PNF (GPU)				Selectivity	
	O_2	N_2	CO_2	CH_4	O_2/N_2	CO_2/CH_4
1	2096	2322	2023	3196	0.903	0.633
2	2150	2375	2101	3293	0.905	0.638
3	3107	3397	3118	5162	0.915	0.607
4	3051	3352	3159	4859	0.912	0.651
5	3540	3713	3247	4990	0.957	0.651
$\overline{x}$	2789	3032	2730	4300	0.918	0.636
σ	637	640	612	970	0.022	0.018
σ_{mean}	285	286	274	434	0.010	0.008

Table 4.3-4: MB2 coated results and calculations

Membrane Identity	PNF (GPU)				Selectivity	
	O_2	N_2	CO_2	CH_4	O_2/N_2	CO_2/CH_4
1	53.6	33.4	143	64.6	1.77	2.29
2	59.9	38.9	148	64.3	1.55	2.31
3	242	214	405	321	1.15	1.31
4	286	279	419	408	1.03	1.03
5	230	194	317	347	1.54	0.92
$\overline{x}$	174	152	286	241	1.41	1.57
σ	109	110	135	164	0.308	0.679
σ_{mean}	48.9	49.3	60.2	73.4	0.138	0.304

The selectivity of the MB2 uncoated membranes continued to show Knudsen diffusion in a similar fashion to the propan-2-ol membranes. The Knudsen selectivity is very consistent across the spin run even with the high variation of PNF seen across the different membranes.

The uncoated results suggest that the membrane surface is highly porous due to the elevated PNF and that the pores which are contributing to the flow are small, falling into the diameter range which results in Knudsen controlled flow.

The coated membranes show PNFs which are split into two different groups: a couple of lower values for membranes 1 and 2 then three higher ones for membranes 3, 4 and 5. This leads to high standard deviations being present for the PNF calculations and a mean value which is difficult to ascribe meaning to. This split to the large PNF values, which are all much higher than anything seen in the propan-2-ol membranes, leads to a higher mean value than seen for the comparable production time elapsed membrane identity in MB1. The mean values in MB1 were approximately the mean for MB2 minus its standard deviation.

The selectivity of the coated membranes also shows some variability in the data which was seen in MB1 for carbon dioxide/methane but not for oxygen/nitrogen. However, the variability that is introduced still gives a mean value which according to the mean standard deviation is a reasonable depiction of the value. In comparison to MB1 the selectivity of MB2 is slightly higher for both gas pairs even taking the higher standard deviation into account. This is an interesting result because normally when dealing with gas separation membranes there is a trade-off which occurs between selectivity and pressure normalised flux. While this pattern does seem to hold true for carbon dioxide/methane one of the high selectivity values for oxygen/nitrogen is one of the higher flux membranes (membrane identity 5).

From the MB2 results it can be concluded that when the surface is not highly porous i.e. lower PNF, the membranes produced in MB2 show better separating properties than in MB1. This gives the conclusion that ethanol is a better selection for use as the non-solvent than propan-2-ol and hence ethanol was used as the non-solvent in the dope solution from this point onwards.

However, the progress in the membranes was not substantial enough to produce effective gas separating membranes so further improvements were required. The results do show that comparisons across a single spin run may not be valid due to the patterns observed in the coated results which exhibit a downward trend in selectivity for both gas pairs.

4.4. Investigation into the Influence of Dope Polymer Concentration (MB3 and MB4)

When producing gas separation membranes the concentration of polymer material is an important factor. It was put forward by Chung *et al.* in 1997[17] that based on their work on 6FDA-durene asymmetric hollow fibers[18] that there may be a critical concentration associated with the polymer in dope solutions for gas separation membranes. This critical concentration has also been found to exist in other systems[19, 20] and corresponds to a rapid change in slope of the viscosity vs. concentration curve at a particular temperature. It has been postulated in the works of Chung *et al.*[17, 18] that this change in the slope is related to chain entanglement of the polymer which could be an important factor. However, they then go onto suggest this might not exist in the same papers. What is clear is that when low polymer concentrations are used it can be difficult to form an active layer due to lower linear density[5].

Table 4.4-1: Compositions of input streams to the spinning process for MB3 and MB4

MB3 Dope Composition	
Chemical	**Concentration (weight %)**
Poly(vinyl chloride)	26%
Dimethylacetamide	52%
Tetrahydrofuran	6%
Ethanol	16%
MB4 Dope Composition	
Chemical	**Concentration (weight %)**
Poly(vinyl chloride)	28%
Dimethylacetamide	50%
Tetrahydrofuran	6%
Ethanol	16%
Bore Fluid Composition	
Chemical	**Concentration (weight %)**
Water	80%
Potassium Acetate	20%
Coagulation Bath Composition	
Chemical	**Concentration (weight %)**
Water	100%

In this work it was a concern that by using the polymer concentration of 24% for the first two spin runs the initial dope composition had moved into a region of the phase diagram which made production of an active layer difficult. It was concluded that two further membrane batches should be produced; one at 26% (MB3) and another at 28% (MB4) polymer concentration by weight. These two concentrations were chosen so as to increase the concentration being used without increasing the concentration to such an extent that the solution produced became un-spinnable. It was hoped that this would move the membranes towards giving higher selectivity at the expense of lower pressure normalised flux and would also act to refine the best concentration to use in the membrane production.

The other components of the dope were kept as close to that of the work already described as possible. This meant that, for the liquids in the solution, only the concentration of DMac was changed for the 26% PVC dope. The compositions of the dopes are shown in Table 4.4-1.

Both dopes were spun under the same conditions as had been used for both previous sets of membranes. The spinning conditions are shown in Table 4.4-2.

Table 4.4-2: Spinning conditions for MB3 and MB4

Spinning Conditions	
Extrusion rate (cm^3/min)	2.5
Dope temperature (°C)	20
Jet stretch ratio	1
Bore fluid flow rate (cm^3/s)	0.8
Bore fluid temperature (°C)	14
Convective gas	Nitrogen
Convective gas flow rate (L/min)	4
Convective gas temperature (°C)	18
Convection chamber height (cm)	6
Distance to gas jets (cm)	3
Bath temperature (°C)	13
Air temperature (°C)	18

The testing which was carried out on these membranes was also changed. In order to save on time and unnecessary testing of membranes which were not working these membranes were only tested with oxygen and nitrogen. The oxygen/nitrogen gas pairing was selected as the results which it gave in MB1 and MB2 showed less variation than the carbon dioxide/methane pairing. Using oxygen and nitrogen also avoids any issues associated with plasticisation effects which carbon dioxide is well known for causing in gas separation polymer membranes[21]. The samples for these batches were again taken across the full range in an attempt to back up the evidence from MB2 that the conditions during the run were changing.

Table 4.4-3: **Uncoated MB3 results**

Membrane Identity	PNF (GPU)		Selectivity
	O_2	N_2	O_2/N_2
1	145	154	0.944
2	826	879	0.940
3	827	881	0.939
4	781	786	0.994
5	212	228	0.930
x	558	586	0.949
σ	348	363	0.026
σ_{mean}	156	162	0.011

Table 4.4-4: **Uncoated MB4 results**

Membrane Identity	PNF (GPU)		Selectivity
	O_2	N_2	O_2/N_2
1	208	229	0.910
2	304	322	0.944
3	343	366	0.940
4	333	354	0.939
5	324	326	0.994
x	303	319	0.945
σ	54.5	53.8	0.030
σ_{mean}	24.4	24.0	0.014

Table 4.4-5: **Coated MB3 results**

Membrane Identity	PNF (GPU)		Selectivity
	O_2	N_2	O_2/N_2
1	106	95	1.11
2	122	113	1.08
3	106	94	1.13
4	118	114	1.03
5	90.5	80.4	1.13
x	108	99.2	1.10
σ	12.3	14.3	0.040
σ_{mean}	5.51	6.37	0.018

Table 4.4-6: **Coated MB4 results**

Membrane Identity	PNF (GPU)		Selectivity
	O_2	N_2	O_2/N_2
1	57.7	44.5	1.30
2	55.7	37.3	1.50
3	64.4	53.5	1.20
4	66.2	52.8	1.25
5	66.4	50.2	1.32
x	62.1	47.6	1.31
σ	5.02	6.81	0.111
σ_{mean}	2.24	3.05	0.049

The uncoated results for MB3 and MB4 offer some immediate improvement over the previous membranes with a 24% PVC dope solution. All the PNFs are under 1000GPU and much more in

keeping with values which are expected from uncoated gas separation membranes. The fluxes associated with MB3 do show a clear split into a high and low level which suggests the membranes are inconsistent during the spin run and this is reflected in the high standard deviations and low level of accuracy in the mean value. The fluxes for MB4 show a much more consistent level of mass transport through the membranes giving the lowest uncoated standard deviation and highest accuracy in the mean in the results to this point.

The selectivity for both sets of membranes continued to show very little variation over the course of the spin run when uncoated membranes were used and to provide a selectivity which is consistent with Knudsen diffusion being the primary transport mechanism.

From the uncoated membrane results it seems that while the membranes still contain pores on the scale of Knudsen diffusion they are now fewer in number since they have a lower PNF. This was the expected and desired result of increasing the polymer concentration and hence the linear density of the membranes.

The coated membrane results unfortunately do not reflect the improvements which the uncoated membranes promised after they were tested. The flux in MB3 does not fall lower than values which have been seen before, however, the values are more consistent as shown by the reduced standard deviations. This suggests that there are fewer major flaws in the membranes which the coating procedure could not properly plug. Even with this being the case though there are still too many pores present for an improved selectivity to be achieved.

The selectivity for oxygen/nitrogen of MB3 is barely above 1 which is not as high as has been seen before in the membranes produced for this work. Again the deviation in selectivity values has reduced so the membranes being produced are more consistent in morphology than those that had been produced prior to MB3.

The coated results for MB4 show more promise than any other results which have been discussed thus far. The mean PNF of the membranes is the lowest of the membranes which had been produced for both oxygen and nitrogen. Although there were individual membranes in previous batches which displayed lower PNF these were accompanied by membranes of poorer quality which would increase the mean value. The MB4 spin run produced not only lower PNF

but did so on a consistent basis across the membranes tested resulting in a low standard deviation and very good accuracy of the mean.

The PNF results suggest that the surface morphology of MB4 is improved towards gas separation applications as the lower flux being produced is indicative of a less defective surface. It would be expected that with this improvement there would be a similar improvement in selectivity but this is not really the case as far as comparisons to the intrinsic selectivity of literature values for flat sheet membranes goes.

What the selectivity results for MB4 do show is a selectivity consistently around 1.3 which is not the highest produced so far but is the highest selectivity produced with a smaller standard deviation. MB2 has a higher selectivity at 1.406 mean but could be down to a minimal of 1.098 taking the standard deviation into account, in comparison MB4 has a 1.315 mean but the lowest value using the standard deviation would be 1.204. MB4 also has a much more accurate mean value with a mean deviation of 0.049 as opposed to 0.138 from MB2. Looking at these values it is thought that MB4 is likely the best batch of membranes produced so far but it is still not viable as a gas separation membrane.

Additionally it was found that there was a noticeable difference in the viscosity of the dope as polymer concentration was increased from 24% to 28%. This resulted in the dope solution being difficult to handle and transfer between vessels at the higher concentration. The rapid change in viscosity over this region suggests that the critical concentration for the PVC, as discussed by Chung[17], for these solvent concentrations lies in this region and the 28% dope could be hoped to provide better possibilities for the formation of an active layer if the correct production conditions could be found.

Since the dope solution used in MB4 failed to produce the results which were hoped for while seemingly marking an improvement on the parameters observed during testing it was concluded that there may be something about the conditions being used to spin which were not suitable to producing a good active layer for gas separation. As discussed in the introduction section of this thesis the active layer is thought to be produced during the dry step of the spinning process by spinodal decomposition followed by nodule coalescence of the outer surface of the membrane. It is possible however that during the dry step process the composition of the dope at the outer

surface could rapidly penetrate too deeply into the unstable region of the phase diagram crossing over the solidus tie line and preventing coalescence from occurring. The result of this would be a highly porous surface which would allow Knudsen diffusion between the spaces in the polymer matrix formed by spinodal decomposition. This type of structure could be responsible for the results which have been found so far and it was therefore felt that the next step in producing suitable membranes was to reduce the penetration into the unstable region of the phase diagram.

4.5. Restricting Phase Diagram Penetration During the Dry Step (MB5)

When attempting to control the evaporation from the surface of the membranes in the spinning process there are a number of changeable factors which are applicable:

- concentration of the high volatility solvent
- concentration of the non-solvent
- driving force during forced convection

It was decided that altering all of these factors would give the best opportunity to produce "softer" nodules and hence improved results.

The concentration of the high volatility solvent, in this case THF, has an important effect because we assume that during the dry phase it is the rapid evaporation of this solvent from the surface which causes the movement through the phase diagram. Therefore if the concentration of THF is lowered then the penetration into the phase diagram which occurs during the dry step would be lower and this was expected to result in "softer" nodules which would more readily coalesce. Therefore for MB5 the concentration of THF was reduced from 6% in MB4 to 4% by weight.

The concentration of the non-solvent, ethanol, is another factor which has to be considered because the addition of ethanol into the system increases the instability of the solution. The ethanol is included with the specific purpose of making it easier for the spinodal decomposition

to occur as the initial solution composition is nearer to the unstable region, however, by lowering the concentration present in the starting dope solution the effect would be that the evaporation of THF does not lead to such deep penetration into the unstable region. In MB5 the concentration of ethanol was decreased from 16% in MB4 to 12% by weight.

The two reductions in concentration of THF and ethanol were made up in the solution by increasing the concentration of DMac from 50% in MB4 to 56% by weight. The change in solution mass was made up with DMac since the solution was already highly viscous and difficult to handle at 28% PVC and it was felt increasing this any further would make both solution production and handling of the solution difficult. As discussed above it was also felt that this concentration may correspond approximately to the critical concentration for these solutions where the dope becomes rapidly thicker. This left DMac as the only component which could have its concentration increased, serving as the carrier solvent in the dope solution it also makes sense to increase its concentration because changing the concentration of the highest concentration component has the smallest percentage impact to composition i.e. going from 50% to 56% concentration is only a percentage increase in DMac concentration of 12%. Whereas increasing polymer concentration by 6% by weight from 28% to 34% would reflect a 21% change in the concentration of the PVC component.

Finally the driving force of the evaporation has to be considered. The driving force for the evaporation is related to how long the nascent membrane is exposed to the dry gap and also to the flow rate of the forced convective gas. It was desirable to quickly move the composition of the dope solution into the spinodal decomposition section of the phase diagram however with too high a flow rate it would be expected that the active layer produced would be too thick as evaporation occurs too fast and deeply into the forming membrane[5]. In order to attempt to tune this value convective gas flow rates of 2, 4 and 6L/min were used over the course of a single spin run to produce three different categories of membrane.

MB5 was the first batch of membranes to be produced where the spinning conditions were changed over the course of the spin run. Of the results produced so far only a couple show indications of a pattern over the length of the spin run and it seems most likely that these are random occurrences due to the sampling. Nonetheless the membranes produced within 2mins

of start-up of the spinning rig or of any change made to the spinning conditions were sent to waste rather than sampled to avoid infringing on any time required to establish equilibrium in production.

Another change in the procedure for MB5 was in the procedure for when spinning was carried out in relation to dope preparation. Previously the dope solution had been prepared in an afternoon to be spun the next morning and while it was contained within a sealed vessel during this time it was feared that loss of THF could be occurring resulting in the poor performance of the membranes. For MB5 the dope solution was spun as soon as it appeared homogeneous in nature.

The system inputs are shown in Table 4.5-1 and spin conditions are shown in Table 4.5-2 and the results are shown in Table 4.5-3 and Table 4.5-4.

Table 4.5-1: Compositions of input streams to the spinning process for MB5

Dope Composition	
Chemical	**Concentration (weight %)**
Poly(vinyl chloride)	28%
Dimethylacetamide	56%
Tetrahydrofuran	4%
Ethanol	12%
Bore Fluid Composition	
Chemical	**Concentration (weight %)**
Water	80%
Potassium Acetate	20%
Coagulation Bath Composition	
Chemical	**Concentration (weight %)**
Water	100%

The results tables show the mean values and statistics for each of the three categories: low, medium and high convective gas flow rates. These values were arrived at by taking 5 samples for each condition. The spin run lasted 45mins with 15mins of the run being devoted to each category beginning with the low (2L/min) forced convection flow rate and culminating in the high (6L/min) forced convection flow rate.

Table 4.5-2: Spinning conditions for MB5

Spinning Conditions	
Extrusion rate (cm^3/min)	2.5
Dope temperature (°C)	20
Jet stretch ratio	1
Bore fluid flow rate (cm^3/s)	0.8
Bore fluid temperature (°C)	14
Convective gas	Nitrogen
Convective gas flow rate (L/min)	2-4-6
Convective gas temperature (°C)	17
Convection chamber height (cm)	6
Distance to gas jets (cm)	3
Bath temperature (°C)	14
Air temperature (°C)	20

Table 4.5-3: Uncoated results for MB5

Membrane Identity	Statistic	PNF (GPU)		Selectivity
		O_2	N_2	O_2/N_2
Low: 2 L/min	**x**	114	123	0.926
	σ	2.16	2.87	0.009
	σ_{mean}	1.25	1.65	0.005
Med: 4 L/min	**x**	116	121	0.954
	σ	2.57	2.84	0.003
	σ_{mean}	1.48	1.64	0.002
High: 6 L/min	**x**	105	113	0.933
	σ	2.07	1.72	0.004
	σ_{mean}	1.19	0.99	0.002

The uncoated results for MB5 were interesting because in all three categories of membrane produced the PNF was lower than any that had been seen before. This suggested that once again the morphology of the surface of the membrane was moving in the desired direction of having less pores for the gas to travel through by Knudsen diffusion. The results also suggest that the PNF for the 6 L/min flow rate is slightly lower than for the other two. This might be expected as

the higher driving force leads to a thicker active layer due to THF leaving the system from deeper within the structure than in the lower flow rates.

However, none of the uncoated results show anything other than Knudsen diffusion occurring as far as selectivity is concerned. This suggests that while the membrane porosity has been reduced there are still defects for pore flow to be the main mode of transport through the membrane.

The standard deviation of the samples and of the mean for both pressure normalised flux and selectivity are all low for the uncoated results suggesting that they are an accurate representation of what is occurring during the spin run.

Table 4.5-4: Coated results for MB5

Membrane Identity	Statistic	PNF (GPU)		Selectivity
		O_2	N_2	O_2/N_2
Low: 2 L/min	x	26.6	27.2	0.977
	σ	0.766	1.02	0.009
	σ_{mean}	0.442	0.588	0.005
Med: 4 L/min	x	26.9	28.2	0.958
	σ	4.52	5.23	0.023
	σ_{mean}	2.61	3.02	0.013
High: 6 L/min	x	19.6	19.5	1.006
	σ	1.14	1.09	0.003
	σ_{mean}	0.66	0.63	0.002

The coated results serve mostly to confirm what was seen in the uncoated results. All the categories produce a lower PNF than any that have been seen previously adding weight to the idea that the surface is less porous and they do so with a high degree of repeatability of the sampled membranes since the standard deviation and standard deviation in the mean are both low for all the categories. Even with these improvements the PNF is still at least an order of magnitude higher than the transport rates which would be expected from a gas separation membrane produced from PVC suggesting that there are likely still issues related to the presence of pores in the membranes and this appears to be borne out in the selectivity values.

It is a recognised occurrence in the membrane field that there tends to be a trade-off between selectivity and pressure normalised flux so that as one decreases the other increases. The results for MB5 show a reduction in flux from the previous membranes produced during this work but do not show the trade-off which is supposed to exist with selectivity. This expected pattern does seem to be shown to some extent between categories for MB5. Once again in the coated membranes the PNF associated with the high convective gas flow rate of 6 L/min are lower than those associated with the other two convective gas flow rates and this also converts to these membranes having a higher selectivity. Although this selectivity is only marginally higher the standard deviations of the data would not lead to a crossing of the error bars associated with the point.

This is an indication that the improvement in selectivity which is shown here and in other membrane batches in this thesis is not being majorly contributed to by the coating which is being used because the pattern in flux is one which is being preserved from the uncoated membranes and not introduced on the addition of coating. This suggests that the coating is acting as desired to force the gases through the membrane material by providing a minimal resistance to transport through the pores.

Unfortunately even with these improvements the selectivity being produced in the coated membranes is still being completely dominated by Knudsen diffusion mechanisms and this is why in spite of the reduced flux there is virtually no improvement in selectivity. Once again the statistical values for selectivity indicate a high degree of accuracy and repeatability in the data obtained for each category of membrane.

The results from MB5 showed improvement on what had been achieved before in this work. The changes that had been made to the dope solution being used seem to have had the expected impact on the formation of the outer layer by allowing a greater degree of coalescence to occur or at least reducing the porosity of the membrane as shown by the decreased value of PNF. The changes did not however have an effect on selectivity and without showing a selectivity improvement the membranes are not useful for gas separation applications.

It appeared at this point in the work like the changes being made to the solution and spinning conditions could have an effect on the membranes and they seemed to shift the results in the

manner predicted theoretically. Practically useful membranes were still out of reach though so it was felt that some aspect of the behaviour was being missed in the production of the membranes which was preventing them reaching the potential they had.

4.6. Overall Conclusion from Ambient Temperature Membrane Production

On reviewing the processes which were being carried out it was decided that there were two factors which should be investigated more thoroughly. The first of these was the time between preparation of the dope and its use in the spin rig, this procedure had been revised coming into MB5 as mentioned above but it was thought that it could be more thoroughly investigated. The second factor was the temperature at which the dope was being spun. These factors were not easily or finely controllable within a spin run or even between spin runs with the set-up which was currently in use on the spin rig and so it was decided that rheological methods of investigation would be more useful.

The decision to investigate these factors in particular was contributed to by some preliminary work carried out while spinning solutions at elevated temperature. This work was carried out by S.A. Gordeyev and was published alongside some of the ambient temperature spinning results in a communication in Polymer[22]. The dope composition by weight used for the elevated temperature spinning solution was 28% PVC, 6% THF, 16% ethanol and 50% DMac and when tested in a similar manner to the membranes produced at ambient conditions they gave the results shown in Table 4.6-1. These results are far superior to what was achieved at ambient temperature and it was hoped that the rheological analysis could reveal the reason for this.

Table 4.6-1: Preliminary Membranes

PNF (GPU)		Selectivity	PNF (GPU)		Selectivity
O_2	N_2	O_2/N_2	CO_2	CH_4	CO_2/CH_4
1.71	0.41	4.17	6.64	0.74	8.97

4.7. Bibliography

1. Khayet, M, Garcia-Payo, MC, Qusay, FA, and Zubaidy, MA, *Structural and performance studies of poly(vinyl chloride) hollow fiber membranes prepared at different air gap lengths.* Journal of Membrane Science, 2009. **330**(1-2): p. 30-39.
2. Xu, JA and Xu, ZL, *Poly(vinyl chloride) (PVC) hollow fiber ultrafiltration membranes prepared from PVC/additives/solvent.* Journal of Membrane Science, 2002. **208**(1-2): p. 203-212.
3. Alsalhy, QF, *Hollow fiber ultrafiltration membranes prepared from blends of poly (vinyl chloride) and polystyrene.* Desalination, 2012. **294**: p. 44-52.
4. Mei, S, Xiao, CF, Hu, XY, and Shu, W, *Hydrolysis modification of PVC/PAN/SiO2 composite hollow fiber membrane.* Desalination, 2011. **280**(1-3): p. 378-383.
5. Gordeyev, SA and Shilton, SJ, *Forced convection spinning of gas separation hollow fibre membranes: some underlying factors, mechanisms and effects.* Journal of Membrane Science, 2004. **229**(1-2): p. 225-233.
6. Shilton, SJ, Bell, G, and Ferguson, J, *The deduction of fine structural details of gas separation hollow fibre membranes using resistance modelling of gas permeation.* Polymer, 1996. **37**(3): p. 485-492.
7. Sharpe, ID, Ismail, AF, and Shilton, SJ, *A study of extrusion shear and forced convection residence time in the spinning of polysulfone hollow fiber membranes for gas separation.* Separation and Purification Technology, 1999. **17**(2): p. 101-109.
8. Ismail, AF, Dunkin, IR, Gallivan, SL, and Shilton, SJ, *Production of super selective polysulfone hollow fiber membranes for gas separation.* Polymer, 1999. **40**(23): p. 6499-6506.
9. Chung, T-S, Lin, W-H, and Vora, RH, *The effect of shear rates on gas separation performance of 6FDA-durene polyimide hollow fibers.* Journal of Membrane Science, 2000. **167**(1): p. 55-66.
10. Mohammadi, AT, Matsuura, T, and Sourirajan, S, *Gas separation by silicone-coated dry asymmetric aromatic polyamide membranes.* Gas Separation & Purification, 1995. **9**(3): p. 181-187.

11. Pagliero, C, Marchese, J, and Ochoa, N, *Effect of coating procedure on composite gas separation membrane performance.* Gas Separation & Purification, 1993. **7**(3): p. 147-149.
12. Ismail, AF and Shilton, SJ, *Polysulfone gas separation hollow fiber membranes with enhanced selectivity.* Journal of Membrane Science, 1998. **139**(2): p. 285-286.
13. Ismail, AF, Shilton, SJ, Dunkin, IR, and Gallivan, SL, *Direct measurement of rheologically induced molecular orientation in gas separation hollow fibre membranes and effects on selectivity.* Journal of Membrane Science, 1997. **126**(1): p. 133-137.
14. Hosseini, SS, Peng, N, and Chung, TS, *Gas separation membranes developed through integration of polymer blending and dual-layer hollow fiber spinning process for hydrogen and natural gas enrichments.* Journal of Membrane Science, 2010. **349**(1–2): p. 156-166.
15. Qin, J-J, Gu, J, and Chung, T-S, *Effect of wet and dry-jet wet spinning on the shear-induced orientation during the formation of ultrafiltration hollow fiber membranes.* Journal of Membrane Science, 2001. **182**(1–2): p. 57-75.
16. Santoso, YE, Chung, TS, Wang, KY, and Weber, M, *The investigation of irregular inner skin morphology of hollow fiber membranes at high-speed spinning and the solutions to overcome it.* Journal of Membrane Science, 2006. **282**(1–2): p. 383-392.
17. Chung, TS, Teoh, SK, and Hu, XD, *Formation of ultrathin high-performance polyethersulfone hollow-fiber membranes.* Journal of Membrane Science, 1997. **133**(2): p. 161-175.
18. Chung, TS, Kafchinski, ER, and Vora, R, *Development of a Defect-Free 6fda-Durene Asymmetric Hollow-Fiber and Its Composite Hollow Fibers.* Journal of Membrane Science, 1994. **88**(1): p. 21-36.
19. Shamsabadi, AA, Kargari, A, Babaheidari, MB, Laki, S, and Ajami, H, *Role of critical concentration of PEI in NMP solutions on gas permeation characteristics of PEI gas separation membranes.* Journal of Industrial and Engineering Chemistry, 2013. **19**(2): p. 677-685.
20. Jansen, JC, Macchione, M, Oliviero, C, Mendichi, R, Ranieri, GA, and Drioli, E, *Rheological evaluation of the influence of polymer concentration and molar mass distribution on the*

formation and performance of asymmetric gas separation membranes prepared by dry phase inversion. Polymer, 2005. **46**(25): p. 11366-11379.

21. Ismail, AF and Lorna, W, *Penetrant-induced plasticization phenomenon in glassy polymers for gas separation membrane.* Separation and Purification Technology, 2002. **27**(3): p. 173-194.
22. Jones, CA, Gordeyev, SA, and Shilton, SJ, *Poly(vinyl chloride) (PVC) hollow fibre membranes for gas separation.* Polymer, 2011. **52**(4): p. 901-903.

5. Rheological Testing

5.1. Set-up for Rheological Experiments

All rheological testing was carried out on a Carrimed CLS 500 rheometer (TA Instruments). A 2cm diameter parallel plate with solvent trap attachment was used on the rheometer for making measurements. The 2cm diameter plate was selected over a smaller plate in order to reach high shear rate values but not substantially increase the risk of inertia throwing the sample out of the geometry (the test cell) as can be an issue with high viscosity polymer solutions. The solvent trap was filled with THF before each test was carried out in order to minimize the evaporation of THF which would occur from the solution once it was open to the atmosphere.

The gap height between the stationary and moving plate on the rheometer was 200µm. This gap was selected as it was big enough to allow movement of the solution but not so big as to create relatively large differences in the shear rates being experienced across the height of the sample.

The composition of the dope solution to be tested rheologically had to be selected and it was decided to test with the dope solution which had produced good results in the preliminary work mentioned at the conclusion of the previous chapter:

- PVC: 28%
- DMac: 50%
- THF: 6%
- Ethanol: 16%

The use of this composition meant that the solution being used could definitely produce gas separation membranes which worked albeit under conditions which were not yet known. This was felt to be important because if there were differences which showed themselves in the rheology results it would be useful to help identify the condition which had previously been used and identify why the membranes produced so far for this thesis had not proven effective.

5.2. Flow Rheology

The starting point for the rheological investigation was to conduct a series of experiments using flow rheology. The most relevant type of rheological study to hollow fiber membrane spinning is capillary rheometry since it is also an extrusion process and allows the study of variables such as extensional viscosity. Unfortunately there was no capillary rheometer accessible to carry out experimentation on the dope solutions in this work. In the absence of capillary techniques flow rheology is a good starting point as it is possible to cover a wide range of shear rates including the high shears which are experienced by the dope solution within a spinneret.

The aim of the flow rheology experiments was to investigate if there were any differences in the nature or behaviour of the PVC dope solution at different temperatures and over different periods of sitting at rest.

In order to do this after dope preparation the solution was split into two sealed reservoirs. One of these reservoirs was maintained at 60°C, using a water bath, while the other was allowed to cool naturally to ambient temperature before the start of experimentation and for the duration of it. A fresh sample was taken from the relevant dope reservoir to carry out each test run.

The main effect which the rheology tests were designed to look at was the influence of temperature. The impact of temperature on a polymer solution can be large with the possibility for solutions to become unstable at either low or high temperature depending upon whether the solution exhibits lower or upper critical solution temperature. The temperature will also have a direct effect on the rheology of the solution, exactly what these effects are depends upon what rheological behavior the solution is exhibiting i.e. Newtonian or non-Newtonian region. Changes in the rheology of the solution will also have an influence upon the phase diagram for the system and thus the phase separation process.

A secondary investigation carried out in parallel to the temperature was into what the effect of the polymer solution being stored was on the rheology. This section was to investigate if the procedural improvement of producing and spinning the dope in a single day was necessary or not or if doing so was detrimental to the ideal rheological characteristics for spinning.

The effect of temperature on the rheology of the solution was investigated at two temperatures, 20°C and 60°C. The relevant dope reservoir was used to obtain the sample for each temperature and the testing was carried out at the same temperature the dope was stored at. The time effect was tested by carrying out four analyses on each sample: two on the day the dope was produced and two the following morning to match what the early spinning procedure had been for MB1 through MB4. A third series of tests was also carried out in an attempt to show which of the influences was having a bigger effect on rheology by using the dope stored in the 20°C reservoir but heating it in the rheometer to 60°C for testing. This set up gives the series of tests shown in Table 5.2-1 where the letters "a" to "d" represent the four runs of the time investigation with "a" being the earliest, "d" the latest and "i" in the test label representing one of these four letters.

Table 5.2-1: Label definitions for each rheological test for flow rheology

Storage Temperature (°C)	Testing Temperature (°C)	Time Series	Test Labels
20	20	a,b,c,d	2020i
20	60	a,b,c,d	2060i
60	60	a,b,c,d	6060i

When using the 2cm parallel plate with a 200µm gap between the plates for the flow rheology the maximum shear rate which could be analysed was 5000s^{-1}. The flow curves were produced over a period of 5-5000s^{-1} however, the rheometer produced erratic data immediately on start up. This is a common occurrence with the rheometer used and is not related to the use of the PVC dope, so the data displayed ranges from 7-5000s^{-1} after it is trimmed. The maximum shear rate of 5000s^{-1} was seen as beneficial from the 200µm gap because from previous experience the shear rate experienced in the spinneret would fall into this region and therefore the data could be used to obtain data on the dope behavior within the spinneret. The gap distance set-up is a balancing act between obtaining the shear rates required and avoiding particle or inertia effects contributing to the rheology results and 200µm was seen as a suitable compromise. The tests were carried out as shear rate controlled ramp experiments with 300 data points for each run where a run lasted for 30mins (15mins up ramp, 15mins down ramp).

First the effect of time on the polymer solution was considered. In order to do this the four flow curves for each of the three testing conditions were plotted on the same chart.

When considering the 6060i rheological tests in isolation it is difficult to ascribe any particular patterns to what is observed. It does appear that the two tests carried out on the afternoon of dope production (a and b) are less viscous than the later runs (c and d) but for both the early and later runs the order of the two tests within those groupings are the opposite of what would be expected were it a trend with b being less viscous than a and d less viscous than c. It might be expected that if there was loss of the high volatility solvent, THF, or even the ethanol from the system that there would be an increase in viscosity for the later results so it is possible evidence of this and that the change is not enough between the two runs on each day for the trend to be observed and the switch is cause by experimental error such as cell loading.

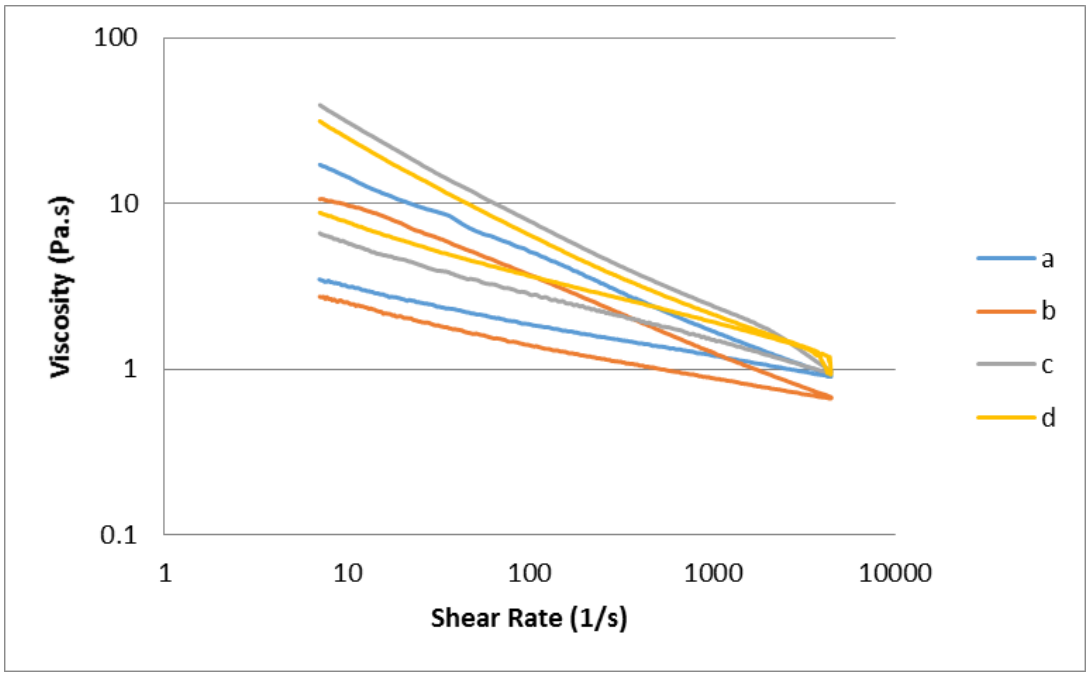

Figure 5.2-1: Up and down flow curves for dope stored at 60°C and tested at 60°C

There are two things which should be commented on now and that will be returned to at a later stage: time dependent behavior and slippage. There is a difference between the up curve, the top curve for any particular test run which was produced as the shear rate was ramped up, and the down curve, the bottom curve for any particular test run which was

produced as the shear rate ramps down. The difference in the curves is indicative of time dependent behavior in the fluid. Time dependent behavior is not a surprising occurrence for a polymer solution which displays shear thinning as it is a viscoelastic fluid and according to *Barnes, 1997*[1] a viscoelastic system shows time dependency because the microstructures involved in viscoelastic fluids, in polymer solutions these are likely to be to do with chain entanglement, take time to respond to flow/stress. Since the decrease in chain entanglement is always going to take time for a polymer solution, unless the molecular weight of the polymer is not above the critical value for chain entanglement to occur, it might be expected that all shear thinning polymer solutions would display some form of thixotropic (time dependent) behavior. Since we are looking to impart orientation through shear mechanisms the thixotropy would only be a problem if it was so slow as to prevent the microstructure from adapting to the shear but since responses are immediate in the solution to increasing shear this should not pose a problem. In fact the thixotropic nature of the fluid can help to seal in the orientated structure during the dry step as it takes time to relax to its former structure.

At the high shear rates produced during the up curve it can be seen that for the later test runs there is a sudden drop in the value of viscosity. This sudden change is a sign that the sample is slipping. When this occurs the fluid in the cell is not contacting properly with the parallel plates making the rotating plate slip across its surface rather than rotating the sample and this produces an artificially low viscosity. One of the major assumptions made when dealing with flow is that the no slip condition applies i.e. the “layer” of fluid closest to the boundary of the fluid is stationary but where this slip appears in the rheology it would be no longer possible to consider this assumption completely accurate for the flow in the spinneret which could be an important point which shall be returned to.

It should be noted that when the slippage does occur it seems to bring the up curves of the later experiments down to the viscosity of the early experiments however, even with this as a starting point for the down curves they diverge again to higher viscosity values as the shear rate decreases. This divergence suggests that the rheometer slowly recovers from the slippage effect as the shear rate drops.

When the 2060i curves are considered it appears there are very few differences between the test runs. There is no discernable pattern to the curves as time progresses from a to d. The

curves are all similar enough that loading error and other sources of experimental error cannot be discounted from causing the differences which are seen.

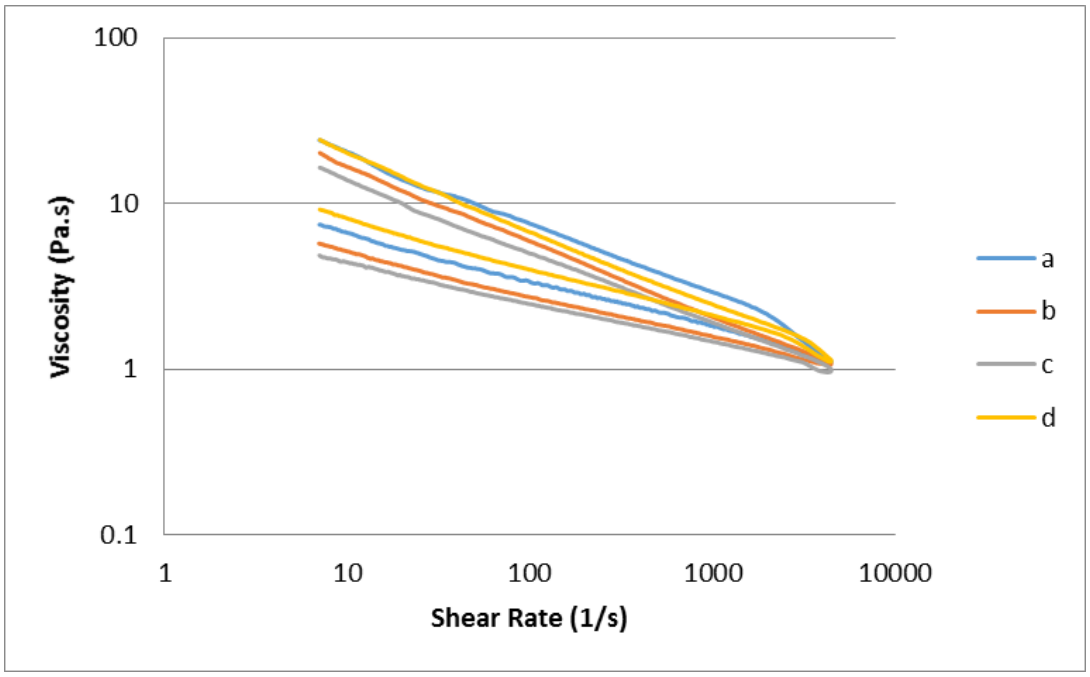

Figure 5.2-2: Up and down flow curves for dope stored at 20°C and tested at 60°C

The two trends which are clear to see once again are the thixotropic nature of the dope solutions which are being used and the slippage. The thixotropic effect does not appear to have changed any between the 6060i and 2060i tests although this can be better examined later. The same can be said for the slippage which occurs where there does not appear to be a big difference from what was seen previously.

The 2020i flow curves however do look different than those which have been looked at so far. There is no evidence that the early tests are any better than the later tests exhibited in the charts.

The thixotropy which is encountered also appears to be much larger however than in the previous two charts and this can again be shown better on the next series of figures.

What has very obviously increased dramatically is the slippage which occurs and with the 2020i tests this affect appears to be much longer lasting into the down curve with both test runs a and d not displaying recovery till below $300s^{-1}$. All the curves generally look a little less

smooth than they do for the other two sets of test conditions. This suggests that the rheometer is having a more difficult time gathering accurate data on the fluid.

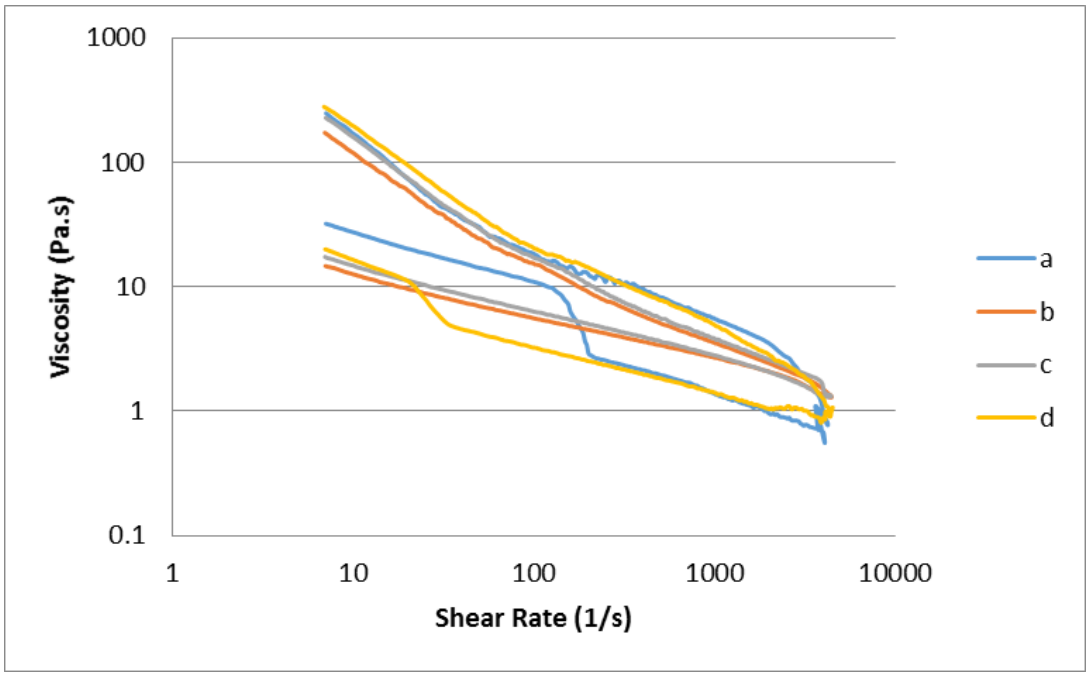

Figure 5.2-3: Up and down flow curves for dope stored at 20°C and tested at 20°C

The next series of graphs make it easier to compare trends between the different temperature conditions which the dopes were exposed to. This time each chart shows a single test run for each set of temperature conditions and the curves for each set correspond to the same testing time i.e. all the c test run curves on the same graph.

The first thing to notice when comparing the charts is the trends in viscosity between the categories. For both the 6060i and 2060i membranes the viscosities are at similar levels for all the curves produced throughout the time of the analysis. In the a and b tests the 6060i curves exhibit a lower viscosity but without the back-up of the c and d tests which almost lie on top of each other it is difficult to conclude that there is a difference. There is a possibility that the THF escapes the 6060i dope overnight while not escaping the dope stored at 20°C but it would be very coincidental that this would bring the curves into almost perfect agreement. More likely is that experimental error contributed a little to the disparate in runs a and b while not in c and d.

The viscosity of the dope which is stored at 20°C and tested at 20°C is higher than for the other two categories. This is obviously an expected difference to be observed as viscosity is temperature dependent however the difference is large over all the curves and over most of the range. The log scales on the graphs tend to make the differences look smaller but the curves which are closest together are likely for run c where at $1000s^{-1}$ the 6060c curve has a viscosity of approximately 2.4Pa.s while the 2020c curve has viscosity of approximately 3.8Pa.s at the same point. Even the curves which are closest are still more than 1.5 times as viscous. The only regions of the 2020°C curves which have the same or lower viscosity than the other categories are when slipping occurs.

The thixotropy of the 2020i curves appears to be larger than what is observed for the membranes which were tested at 60°C. Although, on the charts, the differences between the up and down curves are very similar distance wise between the categories since the viscosity is plotted on a log axis the same distance on the chart represents a much bigger jump. To illustrate this consider the curves for run a, at the lowest shear rate which measurements were recorded for the difference in viscosity between the up and down curves are:

- 6060a, 13.66Pa.s
- 2060a, 16.67Pa.s
- 2020a, 215.82Pa.s

The greater thixotropic nature means that if the solution was used at 20°C but underwent a preconditioning shear process then its viscosity may be more similar to that of the dope tested at 60°C and if these were more similar then perhaps the 20°C dope could be used to produce gas separation membranes.

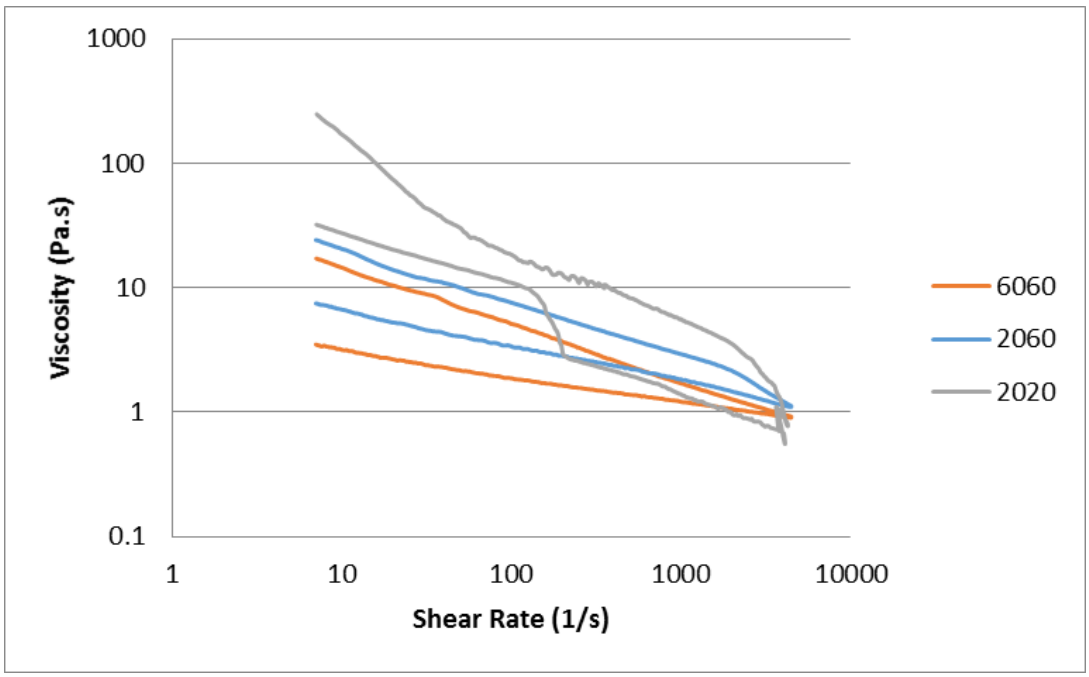

Figure 5.2-4: Up and down flow curves for test run a under each set of temperature conditions

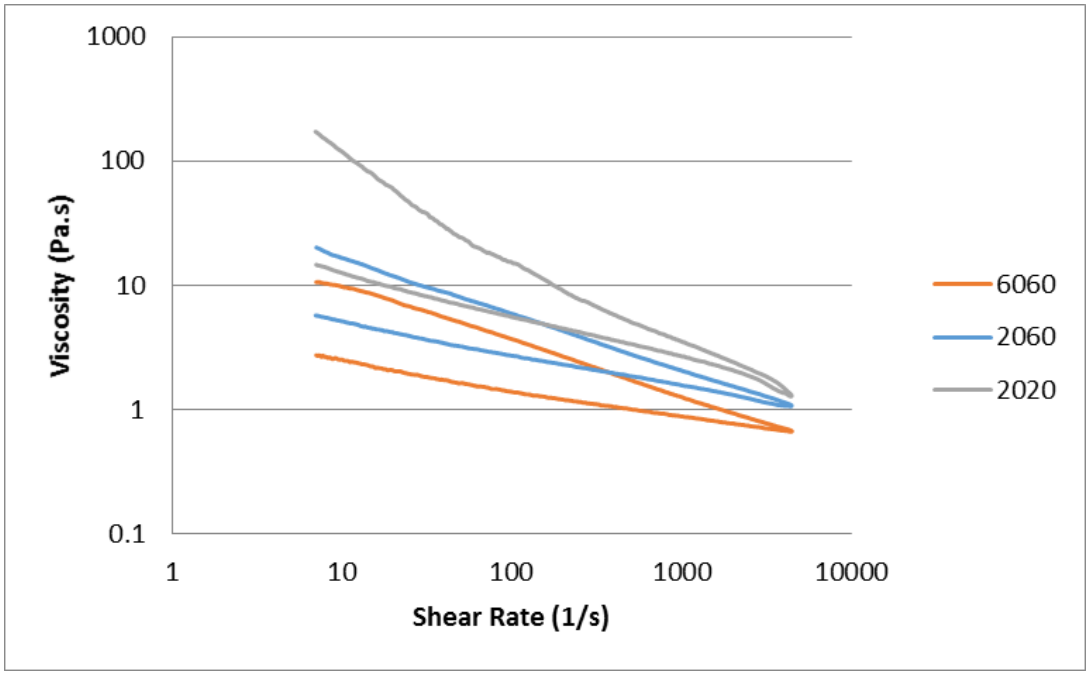

Figure 5.2-5: Up and down flow curves for test run b under each set of temperature conditions

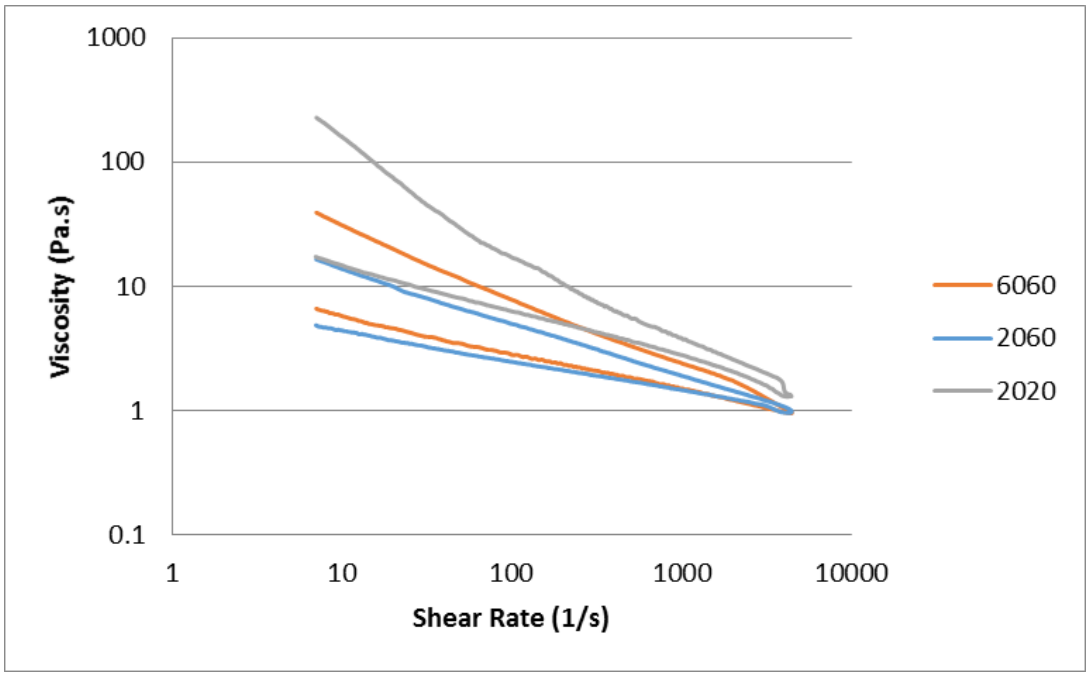

Figure 5.2-6: Up and down flow curves for test run c under each set of temperature conditions

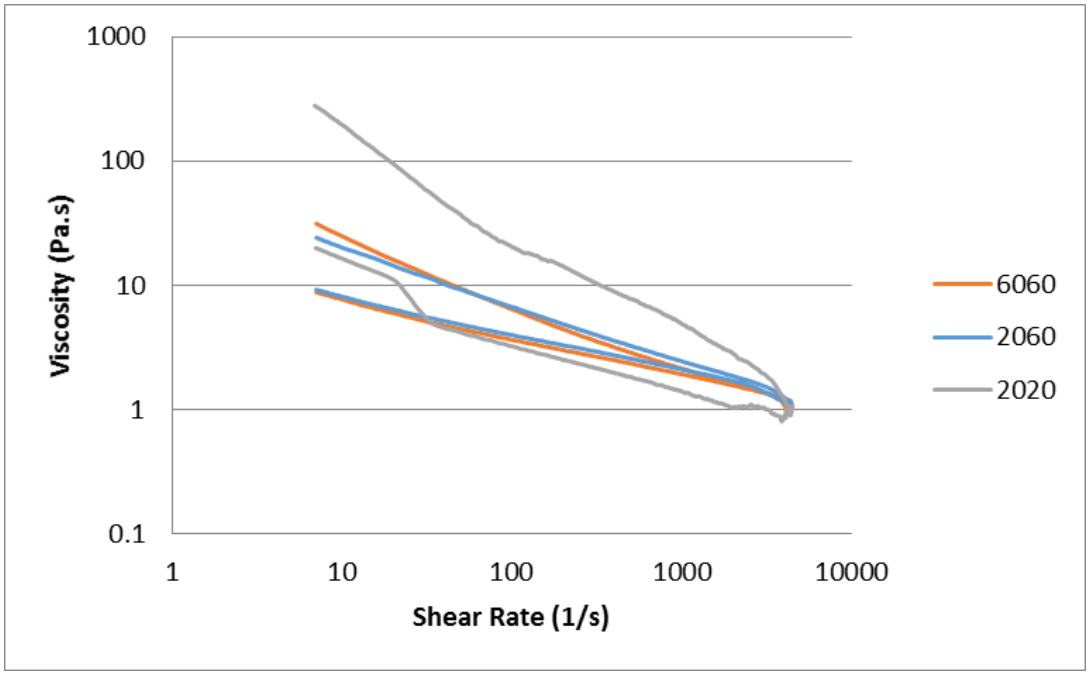

Figure 5.2-7: Up and down flow curves for test run d under each set of temperature conditions

The curves shown here contain only the power law region for the dope solutions. The first Newtonian region would have appeared as a flat plateau before the start of the power law region[2]. The transition point from one region to the other is recognized as being the point where chain uncoiling and molecular orientation begin to occur and is called the critical point.

Further tests were carried out at lower shear rates down to $0.01s^{-1}$ for the 20°C dope and there were signs that the curve was beginning to level off at this point, these shear rates are so low that the shear rates experienced in the spinneret are always going to be high enough to bring about molecular orientation. The reciprocal of this critical shear rate is defined as the time scale of deformation which in this case for the 20°C solution is 100s and is a value often used to estimate the relaxation time for molecular orientation.

Further tests carried out on the dope at 60°C found that the critical point was around $15s^{-1}$ and hence the molecular orientation relaxation time is 0.067s for the dope at the higher temperature. The reason these extra tests found the relaxation time at shear rates which were present in the other tests for the 60°C dope when they did not reveal it is the type of control which the rheometer was used under and its sensitivity in that set up. For the up and down flow curves the rheometer was used with shear rate control however for the single sweep to identify the relaxation time a higher sensitivity more gradual shear stress sweep was conducted. These are large relaxation times in comparison to those that are seen in polysulfone gas separation membranes where the relaxation times are down as low 0.0025s[3]. In fact according to the prediction methods employed by Tripathy and Das[4], the molecular orientation relaxation time for the polysulfone membranes used in the above paper would be between 0.00018s at $9000s^{-1}$ 0.004s at $400s^{-1}$.

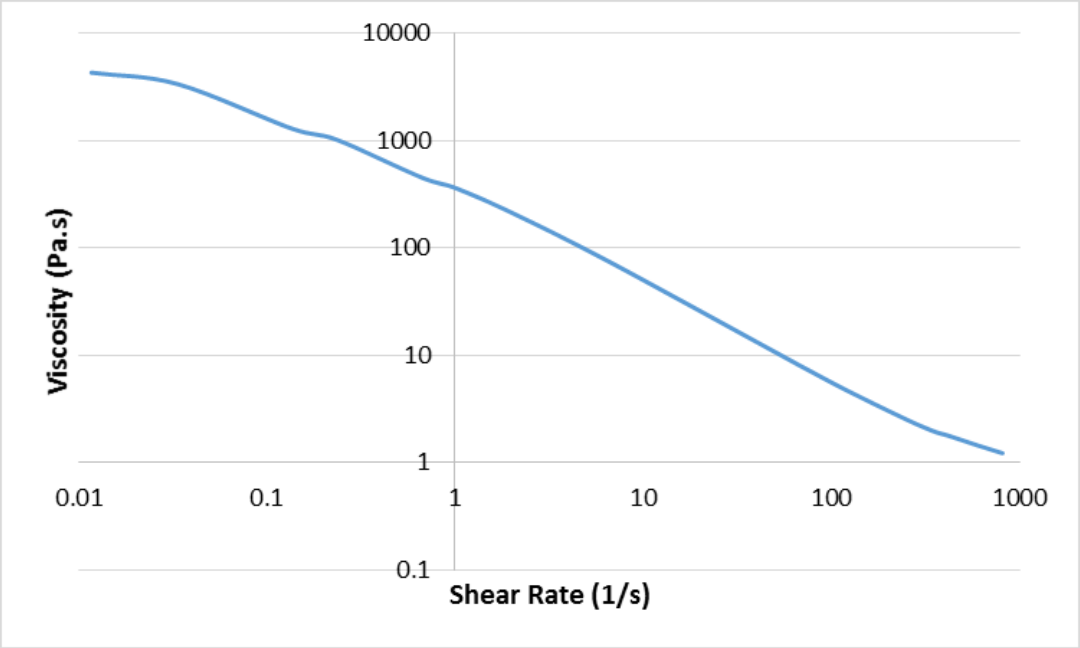

Figure 5.2-8: Flow curve for dope at 20°C showing critical point

These high molecular orientation relaxation times are good for the production of an orientated skin in the gas separation membranes. Since the relaxation times are high then the orientation is able to be frozen in place during the extrusion process by rapid formation of the external active layer. Within the relaxation time the THF near the surface of the membrane will evaporate causing phase inversion of the dope solution and resulting in the orientated active layer. Due to the length of the relaxation time it is likely that the depth of orientated layer will be larger than those seen in the paper by *Shilton et al*[3] where they used a mass transfer model and the amount of THF which could evaporate within the relaxation time to predict the thickness of orientated layer which was produced in therirmembranes. With the relaxation times seen with the PVC dopes being so long in comparison to the polysulfone dopes these calculations would have less meaning since the depth of orientation is likely to be limited by the mass transfer of the THF through the solution rather than the time for orientation to relax.

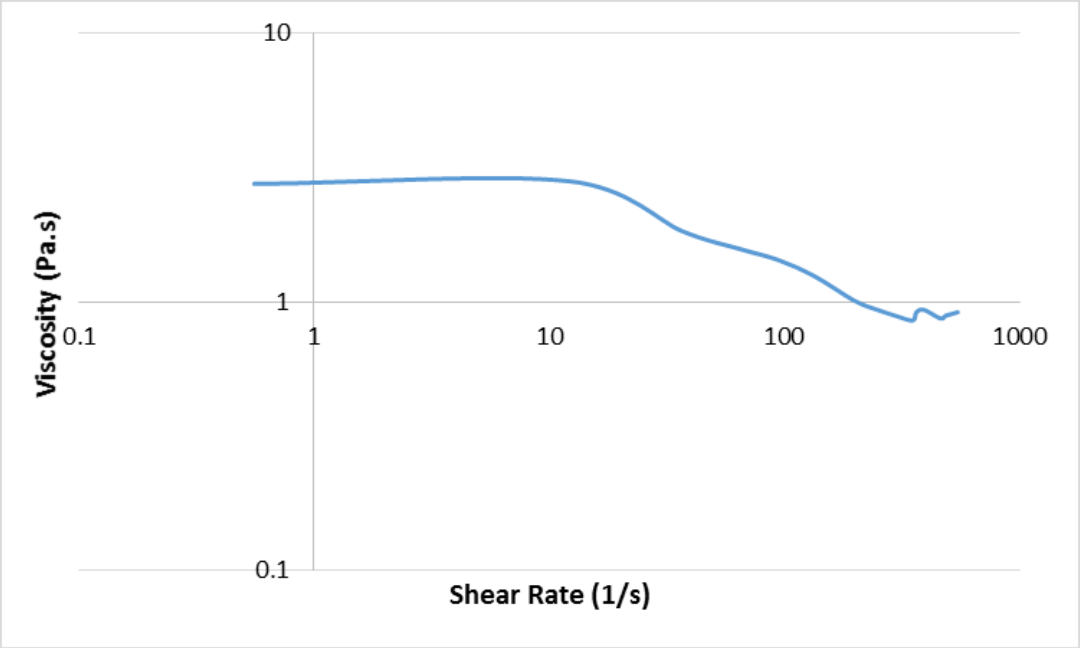

Figure 5.2-9: Flow curve for dope at 60°C showing critical point

As far as detecting an effect which is to do with the time the dope is stored for before use there is very little evidence to support any theory which could be put forward. This suggests that the vessels being used in the experimentation are well sealed and preventing the loss of the more volatile components such as THF, and even the ethanol, which would evaporate from these solutions if they were not properly sealed leading to an increased viscosity over time in the tests.

The temperature does have an effect on the viscosity of the solutions for certain and this pattern does not seem to be affected by reheating the solution. However, viscosity alone is not a good reason for why the PVC dopes used at 20°C failed to produce a good active layer in the gas separation membranes. The factor which may be of interest as far as explaining the poor performance of the membranes is the slippage within the rheometer. If there are shear rates present in the spinneret which are in the same regions as slippage was being seen here then it is possible that on extrusion through the spinneret the no slip condition does not apply. This would lead to the molecules at the surface of the fiber being un-orientated and therefore not producing a good active layer. This would also explain why some of the results show selectivity which is not Knudsen but also not that produced by the early membranes since the active layer is un-orientated and flawed.

In order to investigate this it is necessary to model the flow of the solutions in the spinneret.

5.3. Modeling Flow of Dope Solutions in the Spinneret

The model used to describe flow in the spinneret was developed by S.J. Shilton and is described fully in the paper: "Flow profile induced in spinneret during hollow fiber membrane spinning"[5]. While the work of Shilton is used in this thesis there are a number of different contributors to the study of flow in concentric piping, but most of the work concentrates on turbulent flow directed towards heat exchangers and other large scale uses[6-11].

The first thing to note about the model is the assumption that laminar flow is occurring within the spinneret. Since the velocity of the of the dope within the spinneret is low, an average velocity of 18.15cm/s at an extrusion rate of 3cm^3/min, and the solution is highly viscous then a low Reynolds number is likely to result. For example using a viscosity of 2Pa.s, density of 1100kg/m^3 and flow area diameter of 0.0406cm (the width of the polymer channel in the spinneret) then the Reynolds number can be calculated:

$$\boldsymbol{Re} = \frac{\boldsymbol{\rho v d}}{\boldsymbol{\mu}}$$

$$\boldsymbol{Re} = \frac{\mathbf{1100}\frac{\boldsymbol{kg}}{\boldsymbol{m^3}} * \mathbf{18.15}\frac{\boldsymbol{cm}}{\boldsymbol{s}} * \mathbf{0.0406}\boldsymbol{cm}}{\mathbf{2}\frac{\boldsymbol{kg}}{\boldsymbol{ms}}} * \left(\frac{\mathbf{1}\boldsymbol{m}}{\mathbf{100}\boldsymbol{cm}}\right)^{\mathbf{2}} \qquad \textbf{Equation 5.3.1}$$

$$\boldsymbol{Re} = 0.041$$

From this rough calculation using reasonable values and assumptions it can be seen that the assumption of laminar flow in the spinneret is justifiable. The question mark over this would be due to entrance and exit effects in the spinneret channel but it is hoped that these are small enough that the model holds.

Shilton's approach to producing a model takes a force balance over an element in a circular conduit giving:

$$\boldsymbol{\sigma = \frac{r}{2}\left(\frac{dP}{dZ} - \rho g\right) + \frac{k}{r}} \qquad \textbf{Equation 5.3.2}$$

Where; σ is shear stress, r is radius, P is pressure, Z is length of the element, ρ is density, g is acceleration due to gravity and k is a constant. Boundary conditions are then applied to Equation 5.3.2 for a concentric annulus. When dealing with this flow conformation the boundary conditions are more complex than they would be for circular pipe; the radius at which σ=0 is not clear and K≠0 this leaves us with two boundary conditions. When we assume the no slip rule is applicable then the velocity, v, will be zero at both walls so that where R_1 and R_2 are the radii at the inner and outer walls of the annulus respectively:

$$v=0 \text{ at } r=R_1$$

$$v=0 \text{ at } r=R_2$$

When these boundary conditions are applied it is found that the equations can only be solved numerically for a Newtonian fluid and an iterative process is required to solve for power law fluids such as the PVC dopes used in this work. Shilton sets up a series of equations which allows his program to determine the velocity, shear stress and shear rate profiles within the spinneret along with values of flow rate and pressure drop.

Utilisation of the flow program requires determination of the power law equation which represents the linear (power law relationship becomes linear on log-log scale) portion of the dope flow curves described in the last section. Knowing this equation gives knowledge of the power law index, n, and power law constant, K, which can be used in addition to the spinning parameters from the equipment set up to provide the data output from the software utility.

To obtain the power law index and constant parameters from the flow curve each of them was plotted individually. Once the curve had been plotted the data at the beginning and end of each curve where the trend was not a straight line was removed. A power law trendline was then fitted to the up curve, the up curve was chosen because there is only limited pre-shearing involved in the spinning process; although the mixing of the dope solution will impose a shear effect on the fluid the solution then has time to relax in the dope pot and the

process of passing through the gear pump is expected to break up order which has been imposed. Following the gear pump the flow is slow through a ¼" pipe and since the solution is viscous the shear is low. When the trendline was fitted to the curve the coefficient of determination, R^2, was also calculated and it was found that for the tests run at 60°C the value never dropped below 0.993 while for those at 20° it was never above 0.990. This illustrates again how the rheological behavior of the dope tested at 20°C was more difficult for the rheometer to pin down than for the dope being tested at 60°C. Figure 5.3-1 shows an example of one of these graphs using the 6060a test data.

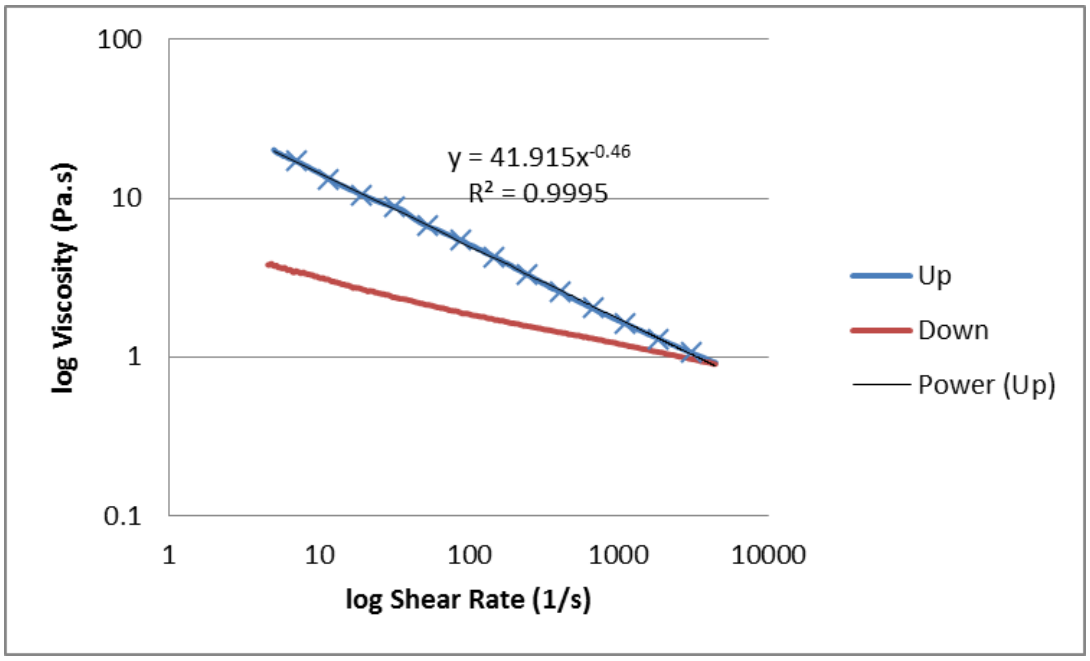

Figure 5.3-1: Sample individual rheological test with fitted trendline

When the trendline is fitted the form of the curve given is:

$$\mu_{eff} = K\gamma^{n-1} = K\left(\frac{dv}{dy}\right)^{n-1} \qquad \textbf{Equation 5.3.3}$$

So the value of K is given but the power given by the curve fitting is n-1 which has to be taken into account before entering values into the software. For the sample curve given in Figure 5.3-1 the inputs from the curve and the experimental would be as follows:

- annulus inner radius, R_1=0.229mm

- annulus outer radius, R_2=0.635mm
- spinneret length, L=0.2842mm
- dope density, ρ_{dope}=1.025g/cm^3 (found by weighing a set volume of dope)
- dope extrusion rate, DER=3cm^3/min
- power law index, n=0.54
- power law constant, K=41.915

Some of these factors i.e. the radii and length associated with the spinneret are the same for all curves produced. However, the other factors change for the different conditions being utilized and the different temperatures. The dope extrusion rates modelled were 2 and 3cm^3/min. The models were also produced at 20°C and 60°C, as per the rheology tests, using the appropriate density which was found by weighing a set volume of dope to be 1.059g/cm^3 and 1.025g/cm^3 at these temperatures respectively. The power law constant and index for each condition are contained in Table 5.3-1 below.

Table 5.3-1: Modeling Parameters from Rheological Testing

Rheology Test Label	Power Law Constant	Power Law Index
6060A	41.915	0.54
6060B	27.286	0.56
6060C	103.82	0.45
6060D	70.709	0.50
2060A	51.879	0.58
2060B	47.036	0.55
2060C	36.029	0.58
2060D	56.223	0.55
6060A	540.29	0.32
6060B	487.50	0.28
6060C	706.87	0.24
6060D	978.54	0.22

The data produced can then be plotted to show the profiles of velocity, shear stress and shear rate within the spinneret. A profile was produced for each set of test conditions which were used in the rheometer and at extrusion rates of 2 and 3cm^3/min. The naming method for each of the tests follows the same pattern as for the flow rheology with the addition of a 2 or 3 following the letter showing which run is occurring to indicate the flow rate the model is using.

The graphs for the different runs “a” through “d” for each category all produced very similar curves. The tests carried out at 60°C were consistent between runs, the 20°C tests varied a more but still showed consistency in the profiles being produced over the runs after the artifact filled parts of the flow curves had been removed. This consistency is caused by the equations of the fitted curves not changing greatly and since they were accurate with the R^2 value this is further proof there is very little time effect acting on the dope solution. For this reason and to save on space only the model curves for the first test run with each set of temperature conditions is displayed here i.e. run a.

The first factor which is considered is the velocity within the spinneret and the flow profiles are shown in Figure 5.3-2. The most obvious thing to note is the difference which is brought about between the step change in extrusion rate. On a drop from 3 to 2cm^3/min the model predicts that the maximum velocity will fall from around 6cm/s to around 4cm/s although it appears there is a bigger decrease in the maximum velocity when the temperature being used is 60°C than 20°C. This gap is expected and the change in maximum velocity difference is because the decrease comes from the ratio of the change in extrusion rate i.e. 2cm^3/min is two thirds of 3cm^3/min and therefore with all other factors remaining equal and no power term in the velocity extrusion rate relationship the velocity also decreases by two thirds, since the 20°C dope is at a lower starting value the decrease in going from 3cm^3/min to 2cm^3/min is smaller.

The velocity profiles also appear to be shifted slightly to the left from what might be expected to be witnessed in pipe flow. With pipe flow the profile would be expected to be perfectly symmetric assuming the walls of the pipe are perfect. However the flow in the spinneret is through an annulus so the profile presented describes the flow from the inner wall of the annulus to the outer wall of the annulus hence the radius where the profile begins is equivalent to R_1 and where the profile ends is R_2. Turbulent flow is most often studied and the shift in the position of maximum velocity is put down to the effects of combining two different boundary layers[6]. The nature of the turbulence at the outer wall is similar to that which would be expected in a pipe however the turbulence experienced at the inner wall is different due to the transverse nature of the curve and the result is that the position of maximum velocity moves toward the inner wall[6]. While the flow under consideration in this work is laminar there will still be different Reynolds numbers at the inner and outer walls resulting in a combination of the two flow regimes and an off center maximum velocity.

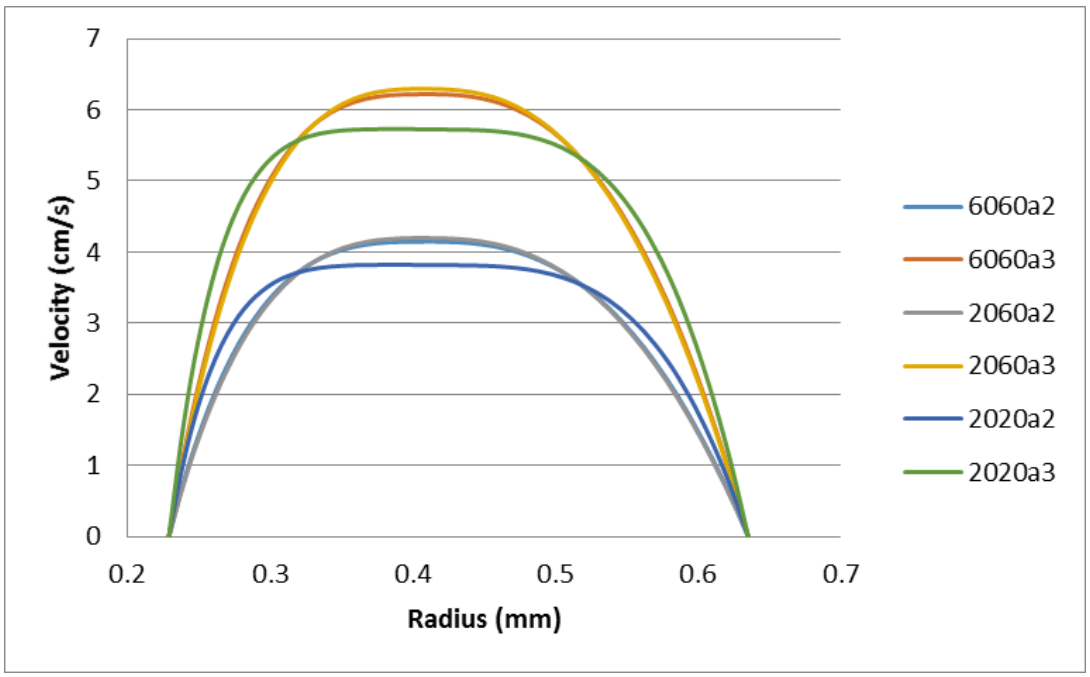

Figure 5.3-2: Velocity profiles within the spinneret for test run a of each set of temperature conditions

The final trend of interest is to note how flat the curves become in the centre of the annulus. This suggests that the dope solution is so thick in the centre of the pipe that it is flowing almost as plug. The model predictions for the low temperature conditions show a larger range of radii where the velocity is almost constant, creating a situation which results in a higher fluid velocity nearer the walls of the pipe.

The relationship between shear stress and radius is shown in Figure 5.3-3. The shear stress shows a greater variation than was observed with the velocity profiles. The stress rises towards the walls of the annulus as they are the source of frictional resistance. The lowest shear stresses are associated with the 6060i dope tests followed by 2060i and finally 2020i. The difference in the shear stress predicted for the two tests at 60°C is however much smaller, at less than 1000N/m^2, than when comparisons with the tests at 20°C are made, differences are over 2000N/m^2. This shows that there is a much larger stress being imposed on the 20°C dope during the spinning process.

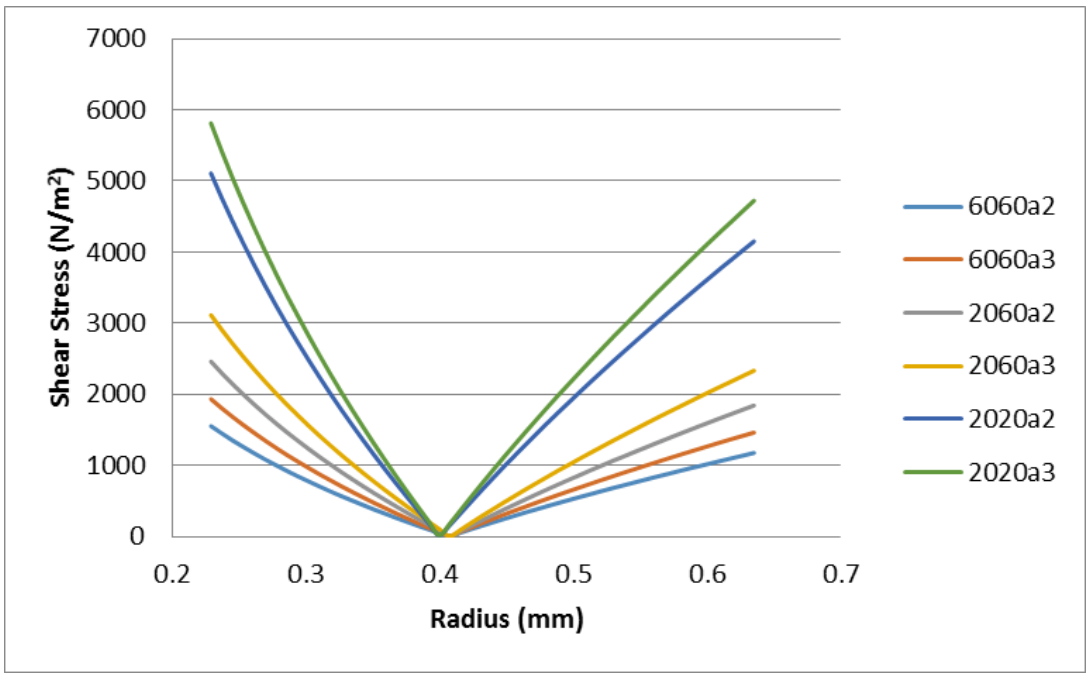

Figure 5.3-3: Shear stress profiles within the spinneret for test run a of each set of temperature conditions

The shear stress experienced by the dope is larger towards the inner wall of the annulus than it is towards the outer wall. This is the effect which is produced in the shear stress by the concentric annulus nature of the spinneret. The shear stress is related to the inner velocity and as such the same effects which cause the maximum velocity to shift off the center of the annulus also cause the region of zero shear to shift, this was one of the main study areas among early work on concentric annulus flow and indeed Knudsen and Katz *(1950)*[12], Brighton and Jones *(1964)*[13] and Quarmby *(1967)*[14] all found that the zero shear stress and maximum velocity positions coincided. However, Rehme *(1974)*[15] found experimentally that they were not coincidental and found that the zero shear stress was actually nearer to the inner wall than the maximum velocity.

So it is not surprising to see a shift in the shear stress in the same way as for velocity, on the other hand there does appear to be a bigger shift for the 20°C dope than for the 60°C dope which is difficult to find an explanation for in the literature. It is suggested that due to the more highly viscous nature of the dope at 20°C it is possibly more susceptible to differences in the Reynolds number, this would make sense as the slopes on the 20°C tested flow curves shown in Figure 5.2-4,5,6,7 are steeper than for those tested at 60°C, hence smaller changes in shear stress have a larger influence on dope rheological behavior and these would be

reflected in Reynolds number. A larger difference then in Reynolds number between the inner and outer walls of the annulus may then be expected to contribute to a larger shift in position of zero shear stress.

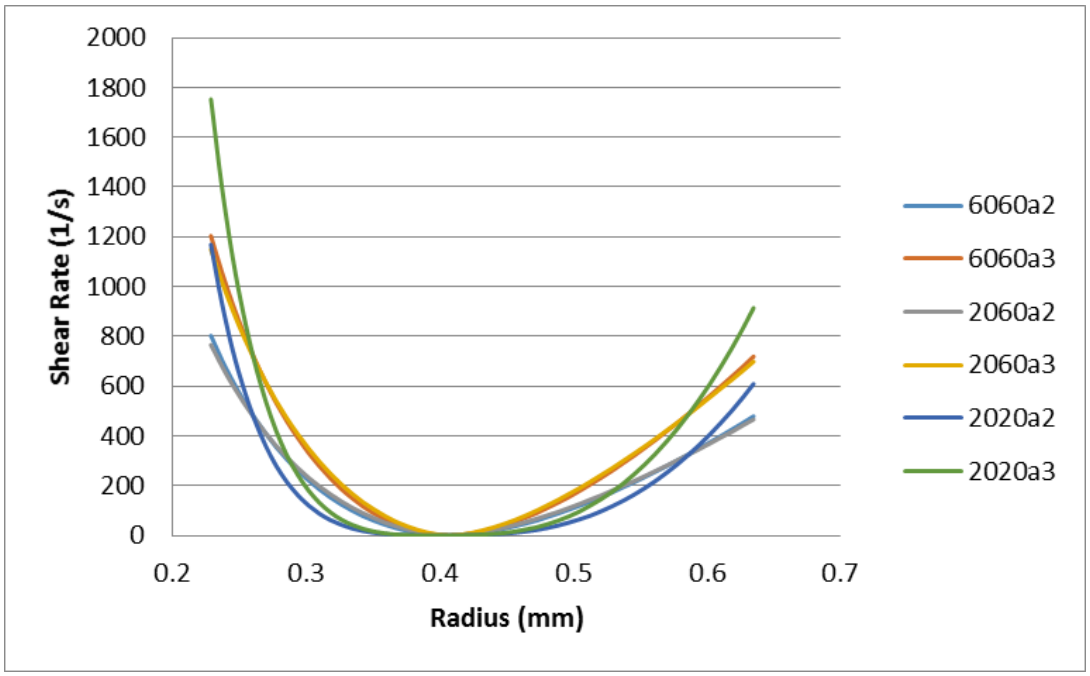

Figure 5.3-4: Shear rate profiles within the spinneret for test run a of each set of temperature conditions

The profiles associated with shear rate are related directly to the shear stress through the viscosity of the solution so it is not surprising that some of the trends which were seen in Figure 5.3-3 are also reflected in Figure 5.3-4. For example the shear rates predicted at 20°C are higher than those associated with 60°C for the same extrusion rate at the walls, however it is interesting that the shear rate toward the zero shear point for the system is actually lower for the 20°C solution. This is in line with the larger region for the 20°C solution where the velocity remains at a more constant and lower level in the middle of the annulus than for the 60°C dope.

The most important area of consideration as far as shear rate goes is the region of the curve closest to the outer wall of the annulus. This is the most important area because this is the shear rate which is being exerted on the dope solution which is to form the active layer and hence provides the molecular orientation to the active layer. The shear rates experienced by the dope solutions in this region are between approximately $500s^{-1}$ and $900s^{-1}$, when these

shear rates are looked at on the flow curves which were produced the conditions in the spinneret are taking place in a region of the curve which is approaching that of instability for the 20°C dope.

The high extrusion rate set up in particular (shear rate $900s^{-1}$) is pushing towards the beginnings of instability of the 20°C curve and for at least two of the down flow curves the dope solution has not recovered from the slipping effect until far below this value. The outcome of this is that there is a possibility that the 20°C dope is encountering slippage within the spinneret itself due to its highly viscous nature. If slippage were occurring then the boundary conditions now associated with the flow model no longer apply since the no slip condition is the basis for these. Under slippage conditions it would be expected that the shear experienced at the wall would be particularly low and therefore the molecular alignment induced in the outer layers of the dope solution would be minimal. The result of this would be the formation of a randomly assorted active layer in the membranes which would not provide a high degree of selectivity and without orientation the surface layer would be more susceptible to imperfections.

The results of low temperature spinning could possibly be explained by this as a completely un-orientated active layer might provide better selectivity than Knudsen diffusion but without the molecular orientation the structure is not ideal for solution diffusion. Imperfect packing of the molecules creates a larger free volume in the surface layers than would work for a gas separation membrane. This produces the selectivity seen in some of the better membranes from the ambient temperature spin runs where it is elevated above that of Knudsen diffusion but not by a lot.

5.4. Oscillatory and Creep Rheology tests

5.4.1. Creep Rheology Tests

The tendency for slippage could be exacerbated in the spinneret if the solution exhibits more gel like or solid properties. These properties would make it easier for the solution to be

extruded like a solid bar by slipping through the spinneret rather than flow through it especially under laminar flow conditions. In order to investigate these properties both oscillatory and creep rheological tests were carried out on the dope.

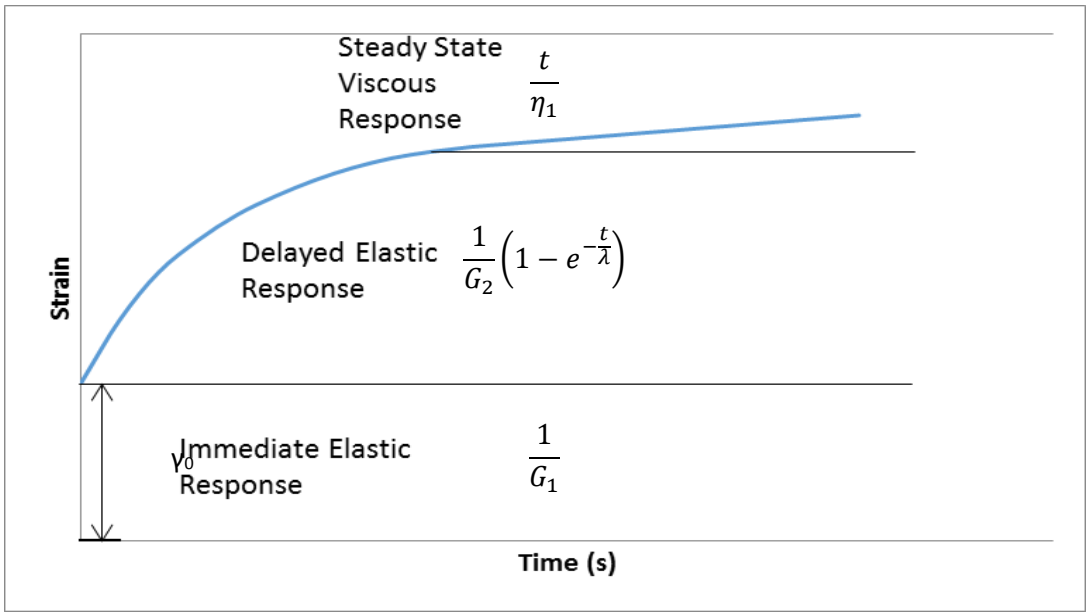

Figure 5.4.1-1: Typical creep test result with equations for each part of the response

As is hinted at by the name a viscoelastic fluid has both a viscous component and an elastic component. These two components can be separated and quantified in a creep test. A general creep test response and the sections which go along with it are shown in Figure 5.4.1-1. The test involves imposing a constant stress on the sample and monitoring the deviation (strain) caused. Initially there will be an immediate elastic response which is independent of time; this is followed by a delayed elastic response which is time dependent and finally a steady state viscous response which is often identified with the zero shear viscosity. Each of these three sections of the curve can be described by a different relationship which is indicated in Figure 5.4.1-1 and brought together in Equation 5.4.1.1.

The various parameters in the creep equation are defined as: G_1 is the immediate elastic response modulus, G_2 is the delayed elastic response modulus, t is the time and λ is the retardation time given by η_2/G_2.

$$\frac{\gamma(t)}{\sigma} = \frac{1}{G_1} + \frac{1}{G_2}\left(1 - e^{-\frac{t}{\lambda}}\right) + \frac{t}{\eta_1}$$ **Equation 5.4.1.1**

This equation comes about as a result of the combination of two well-known rheology mechanical models: the Maxwell liquid and the Kelvin solid, which combine to produce the model of the Burgers fluid. These models can be represented graphically as in Figure 5.4.1-2 using springs and dashpots. In these diagrams the springs represent a linear elastic element to the material such that it represents the behaviour of the material which is given by Hooke's law:

$$\sigma = G\gamma$$ **Equation 5.4.1.2**

Where; σ, is the strain, γ, is the angle of deformation the strain produces in the solid behaviour and G, is the elastic shear modulus. So the spring represents the solid like behaviour of the material.

The dashpot on the other hand represents the Newtonian liquid behaviour of the material and is given by a viscous response, where; η, is the viscosity and $\dot{\gamma}$, is the shear rate:

$$\sigma = \eta\dot{\gamma}$$ **Equation 5.4.1.3**

The Maxwell model combines these different behavioural aspects in series while the Kelvin model combines them in parallel. The Burgers fluid model then combines these two models to provide the relationship seen in Equation 5.4.1.1.

The responses of the Burgers model fluid to the strain applied during a creep test is caused by the immediate initial response of the spring from the Maxwell model, so G_1 is associated with the initial elastic response. The delayed elastic response is then as a result of the parallel spring and dashpot in the Kelvin model and hence G_2 and η_2 are associated with this section of the curve. However, the situation is complicated by the viscous response caused by the Maxwell model dashpot and the contribution of η_1 since it also responds immediately and contributes to all parts of the curve but its effect can be isolated in the viscous response section of the curve.

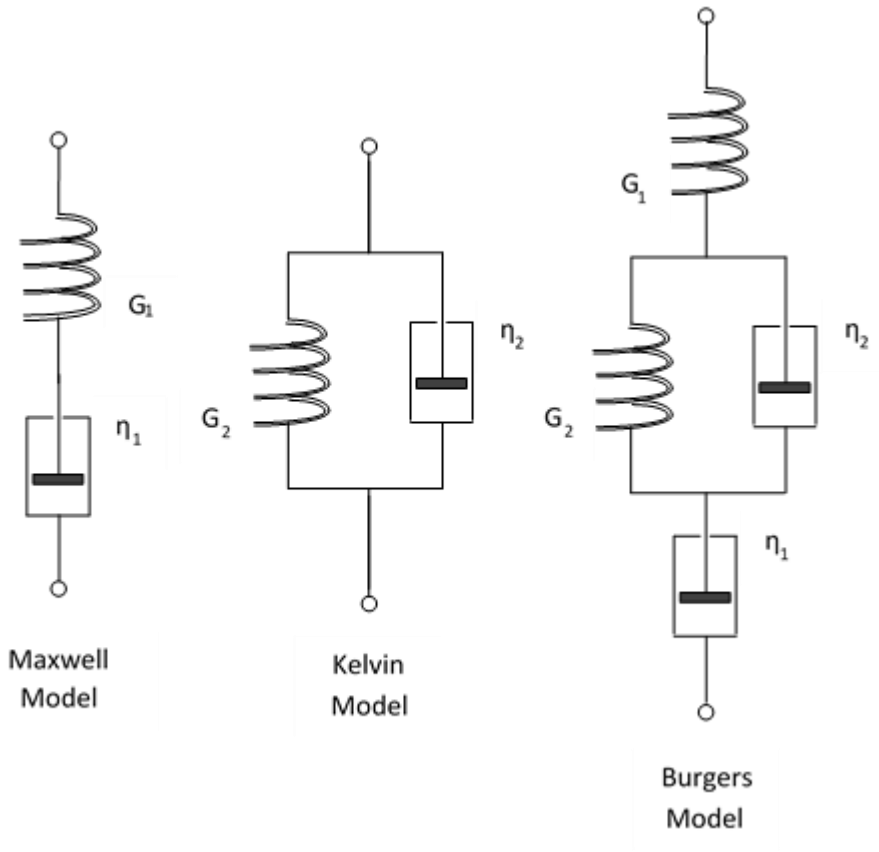

Figure 5.4.1-2: Fluid models using springs and dashpots

So far the creep test process which has been discussed has consisted entirely of applying strain to the material being tested, the second part of the test involves the release of this strain and the recovery of the energy used in the elastic deformations. The recovery will never return fully to zero because viscous flow has occurred during the course of the creep test, η_1. This means that the equation describing the behaviour of the fluid on relaxation becomes:

$$\frac{\boldsymbol{\gamma(t)}}{\boldsymbol{\sigma}} = \frac{\mathbf{1}}{\boldsymbol{G_1}} + \frac{\mathbf{1}}{\boldsymbol{G_2}}\left(\mathbf{1} - \boldsymbol{e}^{-\frac{\boldsymbol{t}}{\boldsymbol{\lambda}}}\right) \qquad \textbf{Equation 5.4.1.4}$$

The λ term now becomes known as the relaxation time and is a measure of the time taken for the stress to relax. This parameter is interesting for membrane hollow fibre spinning since it could provide some indication of the time it takes for the molecular orientation to relax in

the active layer of the extruded membrane once the shear of the spinneret walls is released. The recovery which is observed is an indication of how much solid/liquid character there is in the fluid with a greater recovery showing more solid like behaviour.

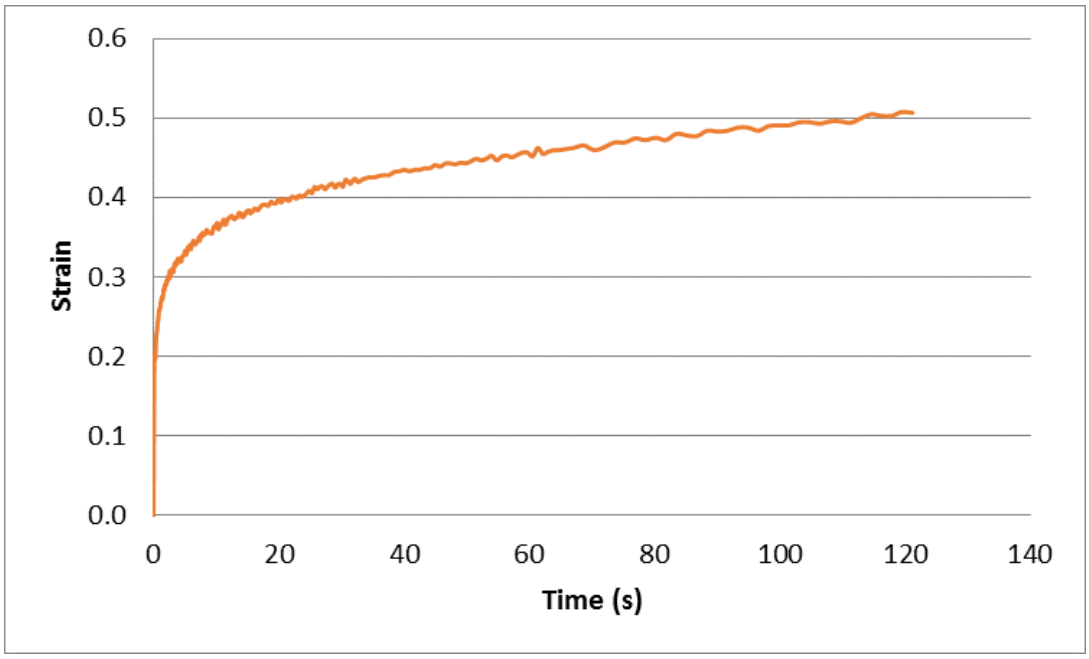

Figure 5.4.1-3: Response of dope at 20°C to a sudden applied stress of 10Pa

A number of creep tests were carried out in the rheometer to identify differences in the behaviour of the dope at 20°C as opposed to 60°C. In order to carry out these tests the value of imposed stress has to be set, for the 20°C dope stresses of 10, 20, 30 and 100Pa were used whereas for the 60°C only stresses of 1 and 10Pa were used due to the different behaviours observed. An example of the calculations carried out to identify each of the parameters involved is shown below for the 20°C, 10Pa imposed stress test following which the results are given for all the tests which were run.

Figure 5.4.1-3 shows the strain versus time relationship in the sample measured by the rheometer for the 20°C, 10Pa imposed stress test. The sections of the curve outlined above are clearly visible in the shape produced so it is expected that the fluid is a Burgers fluid displaying G_1, G_2, η_1, η_2 and λ.

Firstly the initial elastic response can be read straight from the graph, in this case the initial strain is 0.2. This allows the use of Equation 5.4.1.5 to obtain the value of G_1 where: γ, is the strain and σ, is the applied stress.

$$\gamma_0 = \frac{\sigma}{G_1}$$

Equation 5.4.1.5

$$G_1 = \frac{10}{0.2} = 50Pa$$

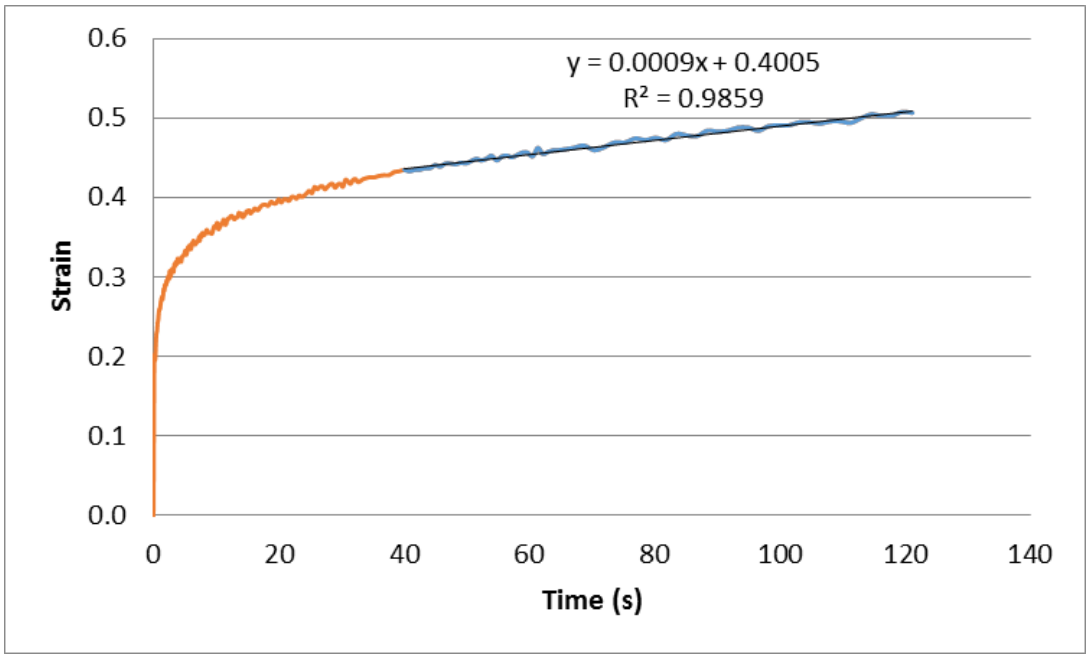

Figure 5.4.1-4: Trend line for the viscous section of the creep response curve with equation and fit for 20°C dope

The steady state viscous response at large values of time can then be considered. This section of the curve shows a straight line relationship between strain and time the gradient of which is associated with the steady shear rate, $\dot{\gamma}$. The shear rate and stress are related through η_1 as in Equation 5.4.1.6.

$$\dot{\gamma} = \frac{\sigma}{\eta_1}$$

Equation 5.4.1.6

$$\eta_1 = \frac{10}{0.0009} = 11111 Pa.s$$

With this information the first and third parts of the overall creep response are now known. This means that if the values of γ_0 and $\dot{\gamma}t$ are subtracted from all points of the original curve then the response which is left will be that of the delayed elastic response. The curve which this procedure results in is shown in Figure 5.4.1-5.

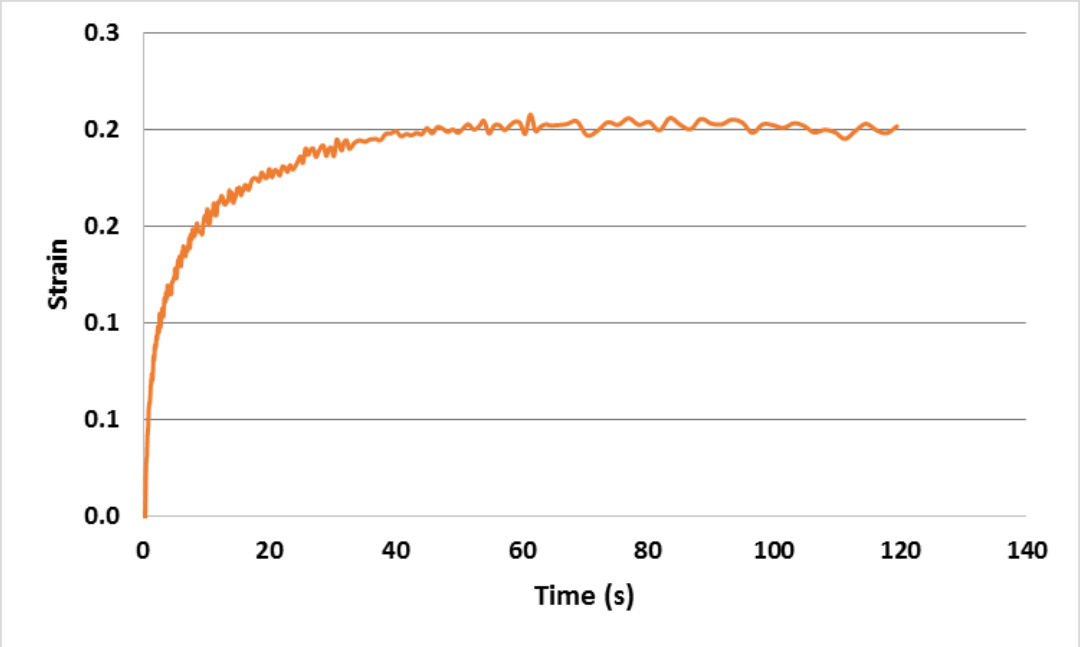

Figure 5.4.1-5: Delayed elastic response of 20°C dope on application of 10Pa stress

The plateau on this plot is equal to the ratio σ/G_2. In this case the ratio is equal to 0.2 and therefore G_2=50. With this knowledge it is possible to rearrange the equation for the delayed elastic response such that:

$$\ln\left(\frac{-\gamma(t) * G2}{\sigma} + 1\right) = -\frac{t}{\lambda} \qquad \text{Equation 5.4.1.7}$$

The resulting plot is shown in Figure 5.4.1-6. It should be a straight line through the origin of gradient -1/λ, as can be seen this is not quite the case due to experimental error. However, the line of best fit is not far off as shown by the R^2 value over 0.9 and should serve as a good estimate in this case.

The chart gives λ a value of 9.07s. This value can then be used to calculate η_2:

$$\eta_2 = \frac{G_2}{\lambda} = 5.51 Pa.s \qquad \text{Equation 5.4.1.8}$$

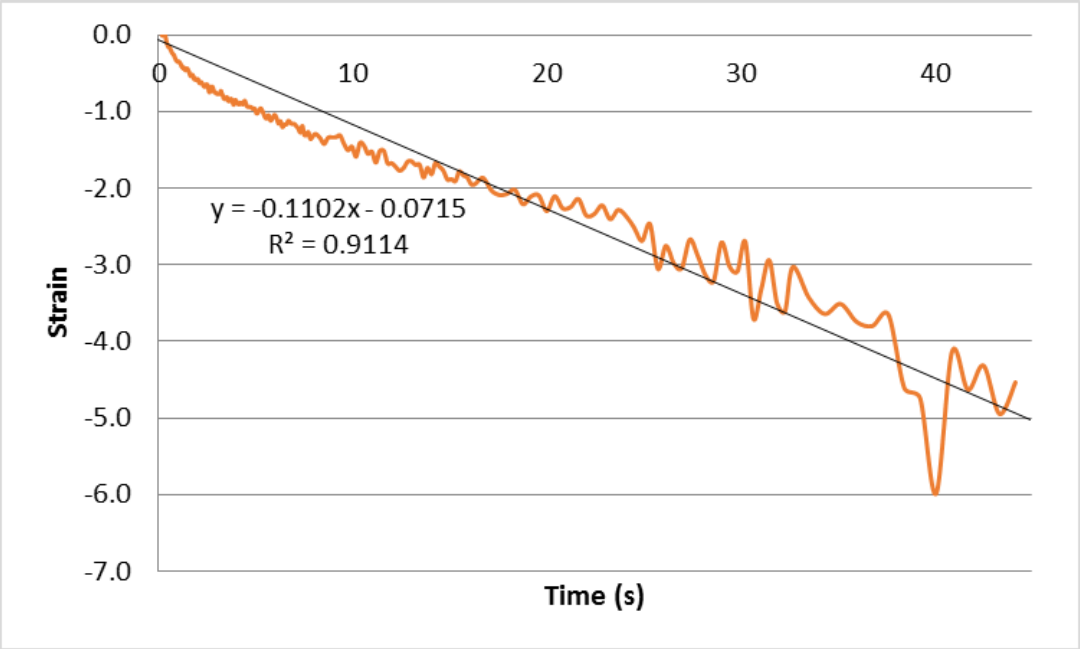

Figure 5.4.1-6: Graphical representation of Equation 5.4.7 allowing determination of λ

All the parameters calculated with the exception of retardation time show slight downward trend as the imposed stress increases, only the G_1 parameter in the 100Pa test contradicts this pattern. Creep analysis of polymer solutions is best suited to low imposed stresses as the rheometer can best assess the small deviations occurring if they are not with respect to a large applied force. For this reason the results for the applied stress of 10Pa are likely the most accurate. One of the most important parameters measured is η_1 because it can be associated with the zero shear viscosity. This is another reason for why the lower the stresses are better because the lower these are while providing sensible results the closer the system is to providing a true zero shear viscosity.

Table 5.4.1-1: Calculated parameters from creep analysis

Parameter	Imposed Stress (Pa)			
	10	**20**	**30**	**100**
G_1 (Pa)	50	48.78	42.856	52.63
G_2 (Pa)	50	47.96	44.11	31.45
η_1 (Pa.s)	11111	8889	9332	6573
η_2 (Pa.s)	5.51	4.724	3.984	0.717
λ (s)	9.07	10.15	11.07	43.86

After the increase in applied stress has been monitored for a period of time it is normal practice to remove this strain and allow the solution to relax. Since the energy loss process is a viscous response then it is expected that the more solid like the solution is in its behaviour then the more of the energy will be recovered.

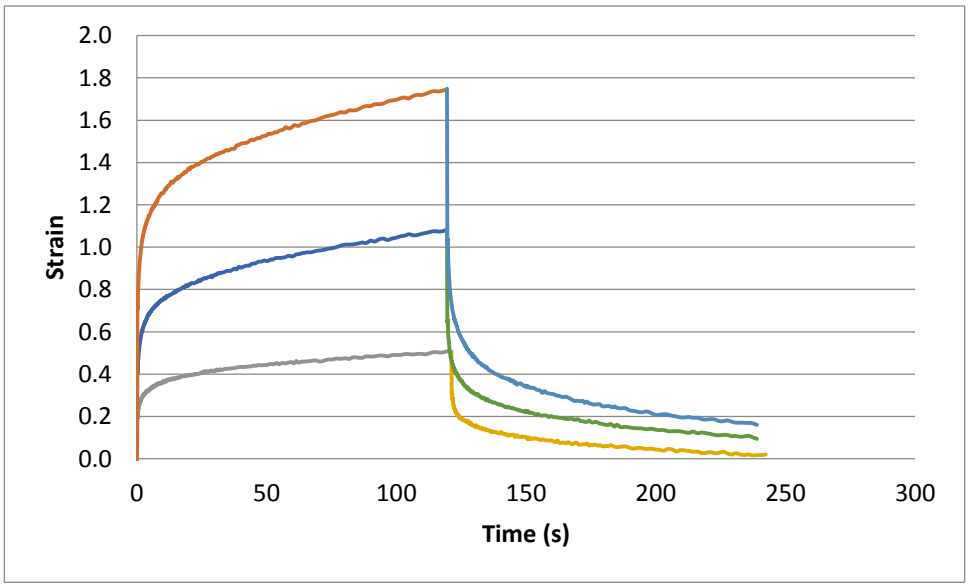

Figure 5.4.1-7: Creep analysis full strain and recovery curves for 10, 20 and 30Pa of imposed stress at 20°C

Figure 5.4.1-7 shows the 10, 20 and 30Pa imposed stress curves for both the strain applied step followed by the relaxation step. As would be expected the increase in stress applied results in an increase in the strain which occurs in the fluid. The interesting aspect of this is that the recovery step shows that the energy is recovered to a very similar level for all the curves and that this is close to full recovery suggesting very little viscous flow has occurred.

As described above this means that the 20°C dope is expressing a large amount of ordered or solid like behaviour.

Associated with the creep recovery curve is a relaxation time. The recovery behaviour should contain no viscous sections i.e. linearly decreasing sections, because the energy associated with the viscous flow in the retardation curves is lost through friction. This should mean that the recovery curves do not fully recover until infinity. The relaxation time is generally taken as the time taken for the elastic strain to be recovered to 1/e of its original value. The total elastic contribution in this case is estimated as being the difference between the point where the elastic response appears to be levelling off and the stress which was applied for the retardation curve. The rheometer used had a tendency to continue to exert a small strain and thus there was a slight viscosity contribution to the recovery curves which could not be taken into account by a purely mathematical method which has led to the relaxation time requiring a small degree of estimation.

Table 5.4.1-2: Creep statistics for recovery curve

Imposed Stress (Pa)	Maximum Strain	Linear Strain Onset	Recovered Strain	1/eth	Relaxation time λ_R (s)
10	0.505	0.086	0.419	0.241	1.06
20	1.076	0.218	0.858	0.535	0.86
30	1.729	0.309	1.42	0.834	0.96

The relaxation of the elastic behaviour component from the creep analysis occurs over a much shorter time frame than the relaxation of the molecular orientation as predicted by the critical point from the flow rheology for the 20°C dope, this means that the relaxation of the elastic strain imparted on the dope solution will relax before the molecular orientation of the dope relaxes. Relaxation times of a second should still mean that the conformation which is imparted to the dope solution by the spinneret will be frozen in place since much lower relaxation times than this are usually recorded for orientation and it still gets frozen into active layer of the membrane.

Creep tests were also carried out on the dope at 60°C for comparison between the temperatures. The same analysis and calculations of associated parameters was not possible

for this dope however. The graphs for the full creep tests for both retardation and relaxation are shown in Figure 5.4.1-8. They show completely different behaviour from that of the dope at 20°C. This shape of graph and especially the relaxation steps are indicative of an entirely viscous fluid i.e. the dope at 60°C shows virtually no solid like behaviour at the tested stresses. In order to check these results the rheometer was pushed to the limits of the set up being used and the applied stresses in the two graphs are 10 and 0.1Pa but no elastic solid behaviour could be detected.

The observed trends from the creep analysis support the possibility that the lack of good separation ability for the membranes at low temperature could be caused by the rheological nature of the solution. The curves produced show highly elastic characteristics in the dope at 20°C which, under the conditions tested, completely disappear at 60°C although will be present at high enough frequencies or low enough time frames.

The dope solution at rest is viewed classically as containing long molecules of PVC with solvent between the molecules which makes it easier for the solution to flow than it would be in a melt situation. The polymer chains are subject to Brownian motion and are therefore capable of taking up many transient forms and arrangements. Common to these arrangements will be areas where polymer chains intertwine and these are called entanglement junctions. These entanglements put a strain on the realignment of the polymer molecules under flow conditions and are the source of the viscoelastic properties. With an increase in temperature the Brownian motion also increases, this means that the entanglements are more easily broken and formed faster. Since it is these entanglements which are providing the strain which shows up as elastic behaviour if they are more easily broken at higher temperature then the 60°C dope will show less elasticity because the entanglements are not providing the same resistance to strain.

In order to attempt to further elucidate on these results oscillatory rheological tests were also carried out on the dope at 20 and 60°C. Creep analysis can have problems revealing the nature of solutions at rest due to instrument sensitivity and the ease with which some test materials, i.e. the dope at 60°C, can enter the non-linear region and beyond of their behaviour under stress. When this happens the behaviour can depart from that predicted due to shear thinning in a number of viscoelastic fluids and the dope solutions used in the membrane work are known to exhibit such behaviour from the flow rheology tests.

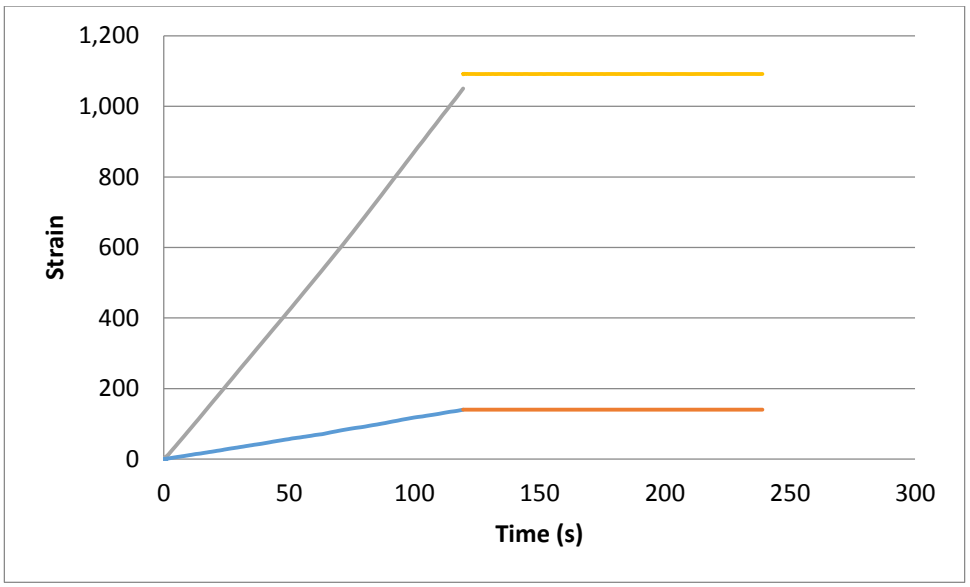

Figure 5.4.1-8: Creep analysis full strain and recovery curves for 0.1 and 10PA of imposed stress at 60°C

5.4.2. Oscillatory Rheology Tests

In an oscillatory test the rheometer plate puts a sinusoidal stress on the fluid which is of a very small magnitude and measures the strain which this creates. Due to this small amplitude of stress it is expected that even fluids which very easily move into the shear thinning section of their rheological behaviour can be examined for rest behaviour using oscillatory measurements. As with the creep testing materials such as polymer solutions are expected to exhibit a mixture of elastic and viscous response to the testing. For a completely elastic material the sinusoidal response of the polymer to the stress will be completely in phase with the stress applied since elastic response is instantaneous. For a completely viscous material the measured response will be exactly 90° out of phase with the input signal. Therefore by analysing the curves produced an example of which is shown in Figure 5.4.2-1 it is possible to determine the amounts of each physical component present in the material.

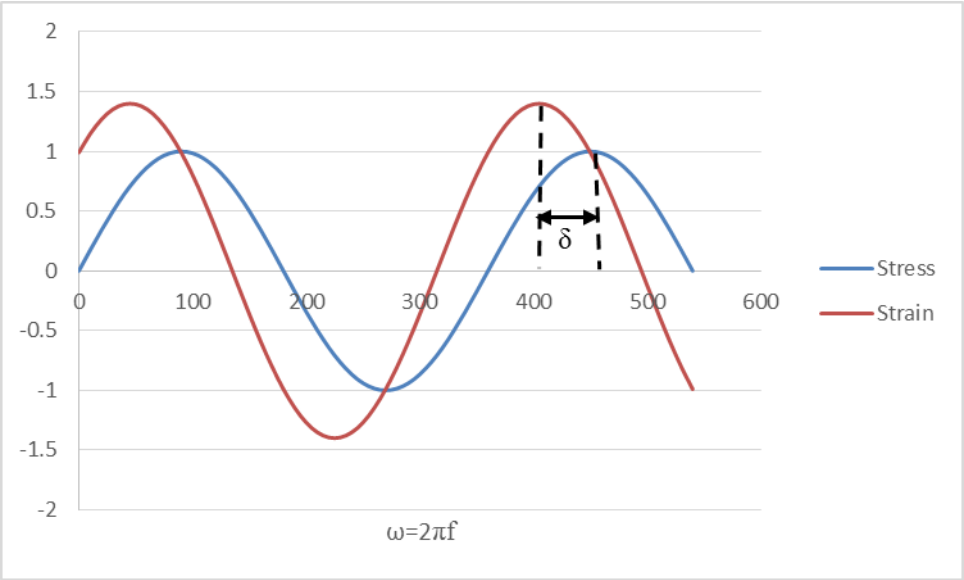

Figure 5.4.2-1: Example stress and strain signals from oscillatory testing

When carrying out oscillation rheometry it is possible to use either stress or strain controlled methods but both methods lead to the same information. For the case of a stress, σ, applied at frequency, ω, and amplitude, σ_0, the magnitude of the stress at time, t, is given by Equation 5.4.2.9 and the response of the strain, γ, is given by Equation 5.4.2.10.

$$\boldsymbol{\sigma = \sigma_0 \cos(\omega t)} \qquad \textbf{Equation 5.4.2.9}$$

$$\boldsymbol{\gamma = \gamma_0 \cos(\omega t - \delta)} \qquad \textbf{Equation 5.4.2.10}$$

$$\boldsymbol{\gamma = \gamma_0 \cos(\omega t)\cos(\delta) + \gamma_0 \sin(\omega t)\sin(\delta)} \qquad \textbf{Equation 5.4.2.11}$$

In the oscillatory relationships the amplitude of the strain component in phase with the stress is represented by $\gamma_0 \cos(\delta)$ and is related to the elastic response of the fluid. This allows the definition of the elastic modulus which is also known as the storage modulus as:

$$\boldsymbol{G' = \frac{\sigma_0 \cos(\delta)}{\gamma_0}} \qquad \textbf{Equation 5.4.2.12}$$

The component of the strain which is 90° out of phase is therefore related to the viscous response of the fluid and represented by $\gamma_0 \sin(\delta)$. The viscous or loss modulus can now also be defined:

$$G'' = \frac{\sigma_0 \sin(\delta)}{\gamma_0} \qquad \textbf{Equation 5.4.2.13}$$

The two moduli are the two major parameters used in defining oscillatory flow. There are also two viscosity parameters associated with the moduli which are related through the angular frequency such that, $\eta' = G''/\omega$ and $\eta'' = G'/\omega$, where η' is the dynamic viscosity. However the important viscosity from and oscillatory point of view is the complex viscosity which is given by:

$$|\eta^*| = \sqrt{(\eta') + \left(\frac{G'}{\omega^2}\right)} \qquad \textbf{Equation 5.4.2.14}$$

The oscillatory experiments were carried out at a constant stress for the dope kept at 60°C and 20°C. It was hoped to identify the crossover points between G' and G'' for both as this allows the calculation of the relaxation time for the test material. The maximum relaxation time is simply the inverse of the numerical value of the angular frequency measured in radians per second. The tests were carried out at various stress values to attempt to locate the crossover. For the 20°C dope the crossover was located when the applied stress was 20Pa (Figure 5.4.2-3), unfortunately at these stress values the 60°C dope was strongly affected by shear thinning so a lower stress had to be used but over the range from 50Pa to 5Pa the crossover could not be found. The 5Pa results are displayed here which were the smoothest (Figure 5.4.2-2).

As can be seen the dope at 60°C shows G'' has a larger magnitude throughout the experiment than G'. This is not surprising since G'' is associated with the viscous behavior of the material and the creep test showed there was a large degree of viscous behavior in the dope when it was kept at 60°C. This section of the oscillatory response is known as the viscous or terminal region and comes before the crossover so either higher frequency or stress would be

required to obtain the locations of the crossover. Neither of these could be achieved on the rheometer available.

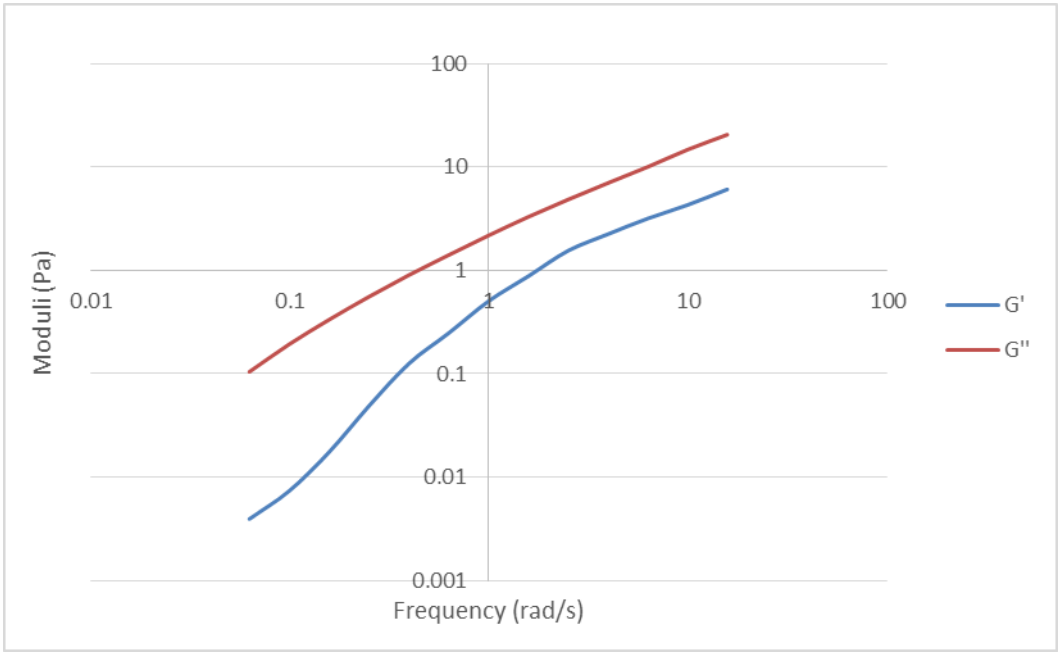

Figure 5.4.2-2: Oscillatory data for dope at 60°C, constant stress of 5Pa

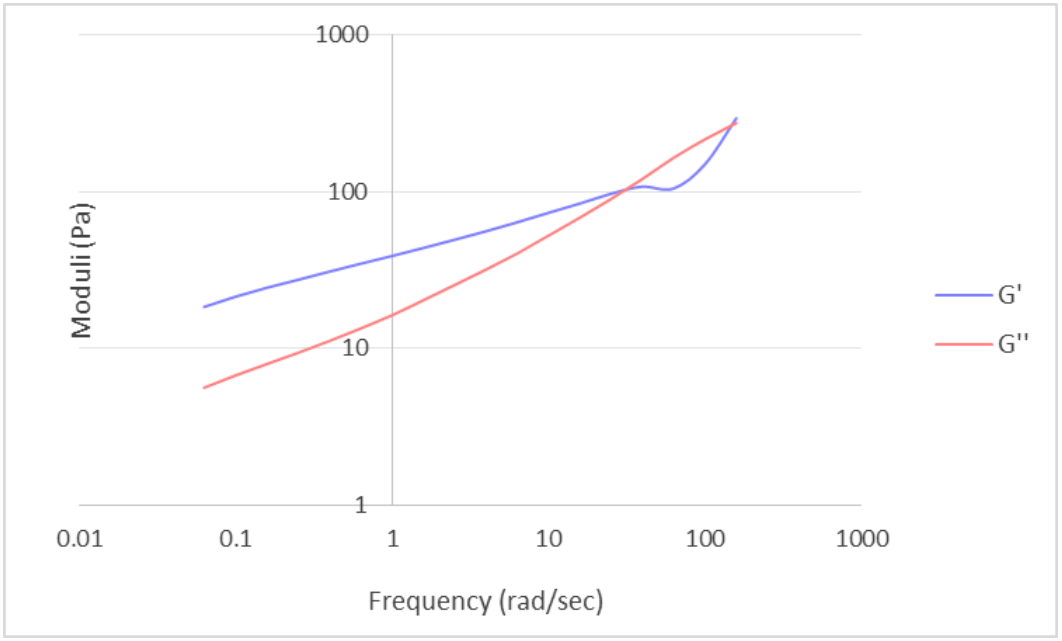

Figure 5.4.2-3: Oscillatory data for dope at 20°C, constant stress of 20Pa

When the dope was tested at 20°C and at a constant stress of 20Pa both the upper and lower crossover points were located on the graph. The lower crossover point is located at around 25rad/sec and is the crossover associated with relaxation time. The reciprocal of this time gives a relaxation time of 0.04s from the oscillatory motion.

The shape of the PVC curve is a little unusual for a polymer solution as it would be more expected that the curves associated with G' and G'' would be the opposite way around. However there are examples, such as low molecular weight polystyrene solution, where G' and G'' are also similar to the above curves[16]. The PVC used in this case is also a fairly low average molecular weight material at M_W=43000, the effect of this low molecular weight is that the dip in the G'' curve seen at the crossover is not highly pronounced. If a higher average molecular weight was used then it would be expected that the G'' valley would deepen and this would lead to less of an overlap in the case of PVC. Although this would also increase the contribution of G'' in general as the solid like behavior of the solution would be expected to have increased[17].

When comparing the oscillatory rheology results of the 20°C and 60°C tests the first thing to be noticed is that the moduli which represent both liquid and solid states are both lower for the 60°C results. This would be expected since the Moduli are related to the viscosities of the solution and the 20°C solution has a much greater viscosity. What is also clear is that where G'' dominates in the 60°C dope it is G' which dominates most of this region in the 20°C dope. This again highlights the difference in nature which is induced by the change in temperature. Where the viscous behavior is shown by the value of G' it is clear that the dope shifts towards having a greater proportion of viscous behavior as the temperature is increased. Indeed the range of frequency is surprisingly short for which G' is higher than G''[17]. It is most common to only see one or two of the five regions associated with polymer solutions being analysed by the oscillatory analyses. In this case as both crossover points are visible for the 20°C dope then it is on the edge of all five behavior regions be identifiable. This reflects what a small section of the behavior of the 20°C dope is viscous.

5.5. Summary of Rheological Analysis

All the rheological analysis carried out agree that the main difference which is brought about by increasing the temperature which the dope is processed at is a shift from predominantly solid elastic like behaviour at 20°C to predominantly liquid viscous like behaviour at 60°C.

Flow rheology highlighted that under low temperature conditions there were a couple of differences between the low and high temperature. Rheologicially the low temperature dope exhibited greater thixotropy which meant that the spinning process would be much more susceptible to the conditions the dope was exposed to prior to membrane fabrication. This might include residual differences in behaviour brought about as a result of slight differences in the conditions used to produce the dope if it is not allowed rest time between production and use. Slippage of the sample within the rheometer was also a much larger factor in the low temperature dope and it sometimes took an extended period of time within the test before the observed slippage was recovered from. The more solid or gel like behaviour of the dope under low temperature conditions was the factor which these phenomena were attributed to. In order to show this change in behaviour both creep and oscillatory rheometry measurements were carried out.

The creep analysis showed a stark difference between the tests carried out at the two temperatures with the 20°C exhibiting the expected curve with initial and delayed elastic responses followed by a viscous response while the 60°C curve only showed unrecoverable viscous flow. This was corroborated by the oscillatory results which showed that for the 20°C dope the storage modulus G' dominated over a wide range of frequencies and the crossover points where the loss modulus G'' dominates the behaviour were unusually close together. These results combined to show that the dope at 60°C has a very different nature to the dope at 20°C.

When polymer solutions are under strain they can relax by a number of different mechanisms which can be either mechanical or electrical[18, 19]. Each of these relaxation mechanisms has a different characteristic time associated with it and results in a spectrum of discrete relaxation times which are dependent on either the segmental mobility[20] of the polymer chains or the reciprocal of it[21], the molecular weight[18, 19] of the polymer and the polydispersity within the solution[20].

The critical point for polymer solutions obtained from flow rheology is often associated with the molecular orientation relaxation times[3] which for the 20°C was found to be 100s and for the 60°C dope was found to be 0.067s. These flow relaxation times present the only opportunity to compare the 60°C and 20°C relaxation times because for both the oscillatory and creep tests the nature of the 60°C solution was such that the relaxation times for these relaxation modes could not be identified. There is a large difference in the relaxation times which are described for the molecular orientation by the flow rheology.

From the list in the paragraph above of the factors which affect the relaxation times of the solutions there is only the segmental mobility of the molecule which can have an impact since the solutions are produced from the same PVC and therefore the molecular weight is the same and it is assumed that the solution is well mixed before the different samples are taken. The mobility of the molecules within the solution can be affected by the packing of the molecules within the solution and any structure which is contributed to by intermolecular forces. In the case of PVC it was shown by Cantera[22] that the mean squared dipole moment was related to the temperature by a negative coefficient such that there will be more attraction between the molecules at a lower temperature[22]. It was also shown by Lutskii[23] that the viscosity of a solution is affected by the dipole moment which is observed. Taking these two works and the effect that temperature has on the solution it is likely that the dope at 20°C has a greater amount of intermolecular forces present when it is sheared and the molecules line up than the 60°C dope does.

Before being sheared the molecules are classically considered to be wound up into polymer spheres which does not allow for optimisation of the possible intermolecular forces produced by the dipole moment. When the molecules are sheared the increase in the intermolecular forces available make it easy to provide the molecular orientation resulting in only low shear rates being required however, this also means the sheared structure is less inclined to relax to the equilibrium state and therefore provides long relation times. These long relaxation times should be good for the production of membranes unfortunately the PVC solution at 20°C appears so thick in nature and displays strong gel like characteristics so that at the spinning shear rate the solution simply slides through the spinneret and the beneficial characteristics of the solution for producing membranes cannot be taken advantage of as the orientation is never induced in the first place.

This means that although the relaxation time for the solution at 60°C is shorter it is not prohibitively shorter and the rheological results suggest that the use of high temperature spinning could provide a possible solution to producing membranes capable of providing gas separation.

5.6. Rheological Testing Bibliography

1. Barnes, HA, *Thixotropy - A review.* Journal of Non-Newtonian Fluid Mechanics, 1997. **70**(1-2): p. 1-33.
2. Kosvintsev, SR, Riande, E, Velarde, MG, and Guzmán, J, *Rheological behaviour of solutions of poly(2-hydroxyethyl methacrylamide) in glycerine.* Polymer, 2001. **42**(17): p. 7395-7401.
3. Gordeyev, SA and Shilton, SJ, *Forced convection spinning of gas separation hollow fibre membranes: some underlying factors, mechanisms and effects.* Journal of Membrane Science, 2004. **229**(1-2): p. 225-233.
4. Tripathy, AR and Das, CK, *Interchain crosslinking between NBR and polyacrylic rubber and effect on (i) processibility and blend-morphology.* Journal of Applied Polymer Science, 1994. **51**(2): p. 245-251.
5. Shilton, SJ, *Flow profile induced in spinneret during hollow fiber membrane spinning.* Journal of Applied Polymer Science, 1997. **65**(7): p. 1359-1362.
6. Chung, SY, Rhee, GH, and Sung, HJ, *Direct numerical simulation of turbulent concentric annular pipe flow: Part 1: Flow field.* International Journal of Heat and Fluid Flow, 2002. **23**(4): p. 426-440.
7. Chung, SY and Sung, HJ, *Direct numerical simulation of turbulent concentric annular pipe flow: Part 2: Heat transfer.* International Journal of Heat and Fluid Flow, 2003. **24**(3): p. 399-411.
8. Kaneda, M, Yu, B, Ozoe, H, and Churchill, SW, *The characteristics of turbulent flow and convection in concentric circular annuli. Part I: flow.* International Journal of Heat and Mass Transfer, 2003. **46**(26): p. 5045-5057.
9. Nouri, JM, Umur, H, and Whitelaw, JH, *Flow of Newtonian and Non-Newtonian Fluids in Concentric and Eccentric Annuli.* Journal of Fluid Mechanics, 1993. **253**: p. 617-641.
10. Nouri, JM and Whitelaw, JH, *Flow of Newtonian and Non-Newtonian Fluids in a Concentric Annulus with Rotation of the Inner Cylinder.* Journal of Fluids Engineering-Transactions of the Asme, 1994. **116**(4): p. 821-827.
11. Nouri, JM and Whitelaw, JH, *Flow of Newtonian and non-Newtonian fluids in an eccentric annulus with rotation of the inner cylinder.* International Journal of Heat and Fluid Flow, 1997. **18**(2): p. 236-246.
12. Knudsen, J, Katz, DL,, *Velocity profiles in annuli.* Proceedings of Midwestern Conference on Fluid Dynamics, 1950: p. 175-203.

13. Brighton, J, Jones, JB,, *Fully developed turbulent flow in annuli.* Journal of Basic Engineering, 1964. **86**: p. 835-844.
14. Quarmby, A, *An experimental study of turbulent flow through concentric annuli.* International Journal of Mechanical Science, 1967. **9**: p. 205-221.
15. Rehme, K, *Turbulent flow in smooth concentric annuli with small radius ratios.* Journal of Fluid Mechanics, 1974. **64**: p. 263-287.
16. Cassagnau, P, Montfort, JP, Marin, G, and Monge, P, *Rheology of polydisperse polymers: relationship between intermolecular interactions and molecular weight distribution.* Rheologica Acta, 1993. **32**(2): p. 156-167.
17. Barnes, HA, *A handbook of elementary rheology*2000: University of Wales, Institute of Non-Newtonian Fluid Mechanics.
18. Williams, ML, Landel, RF, and Ferry, JD, *The Temperature Dependence of Relaxation Mechanisms in Amorphous Polymers and Other Glass-forming Liquids.* Journal of the American Chemical Society, 1955. **77**(14): p. 3701-3707.
19. Ferry, JD, Williams, ML, and Stern, DM, *Slow Relaxation Mechanisms in Concentrated Polymer Solutions.* The Journal of Physical Chemistry, 1954. **58**(11): p. 987-992.
20. Rouse, JPE, *A Theory of the Linear Viscoelastic Properties of Dilute Solutions of Coiling Polymers.* The Journal of Chemical Physics, 1953. **21**(7): p. 1272-1280.
21. Bueche, F, *Influence of Rate of Shear on the Apparent Viscosity of A---Dilute Polymer Solutions, and B---Bulk Polymers.* The Journal of Chemical Physics, 1954. **22**(9): p. 1570-1576.
22. Blasco Cantera, F, Riande, E, Almendro, JP, and Saiz, E, *Configurational properties of vinyl chains. Dipole moments of poly(vinyl chloride).* Macromolecules, 1981. **14**(1): p. 138-142.
23. Lutskii, A, Zh. Obshch. Khim, 1955. **25**: p. 1086.

6. Elevated Temperature Spinning

6.1. Experimental Set-up

While rheological testing had been carried out on the solution at 60°C due to the difficulty of controlling temperature and the inevitable variations involved it was felt that 60°C was too close to the boiling point of THF at 66°C. Therefore, elevated temperature spinning was carried out at 50°C. In order to spin at an elevated temperature of 50 °C some changes had to be made to the spinning protocol. Some of these are mentioned in the equipment section of this report i.e. lagging lines with heat tape and using the water bath containing the dope pot at the elevated temperature. All heating of the equipment to be carried out was started as the dope solution approached a homogeneous state in its preparation i.e. during mixing, this meant the spinning equipment was pre-heated and up to the control temperature when the production process started. When the solution preparation was complete it was transferred immediately to the spin rig dope pot which had also been preheated to 50°C and the dope pot was attached to the rig. This immediate transfer and start to spinning meant that any time delay effects incurred in membrane properties due to the solution resting after production were as negated as possible.

The heat tape used to wrap the lines between the dope pot and spinneret was also wrapped around the spinneret holder which was made of stainless steel and therefore raised its temperature also. The bore fluid feed temperature was approximately 15°C from the HPLC pump, the low flow of bore fluid resulted in a raised temperature through the spinneret.

The dope solution to use at elevated temperature had to be selected. It was decided that the best plan was attempting to replicate the preliminary results from the information available on them. This meant using the same solution as described in section 4.6 and shown in Table 6.2-1.

It was also decided to switch back to testing with carbon dioxide and methane as well as oxygen and nitrogen for the high temperature spinning as it was hoped that spinning at high temperature would resolve the problems being experienced in producing an effective active layer at lower temperature.

6.2. Elevated Temperature Spinning – Initial Test Run (MB6)

Table 6.2-1: Compositions of input streams to the spinning process for MB6

Dope Composition	
Chemical	**Concentration (weight %)**
Poly(vinyl chloride)	28%
Dimethylacetamide	50%
Tetrahydrofuran	6%
Ethanol	16%
Bore Fluid Composition	
Chemical	**Concentration (weight %)**
Water	80%
Potassium Acetate	20%
Coagulation Bath Composition	
Chemical	**Concentration (weight %)**
Water	100%

Table 6.2-2: Spinning conditions for MB6

Spinning Conditions	
Extrusion rate (cm^3/min)	2.5
Dope temperature (°C)	50
Jet stretch ratio	1
Bore fluid flow rate (cm^3/s)	0.8
Bore fluid temperature (°C)	15
Convective gas	Nitrogen
Convective gas flow rate (L/min)	4
Convective gas temperature (°C)	17
Convection chamber height (cm)	6
Distance to gas jets (cm)	3
Bath temperature (°C)	15
Air temperature (°C)	21

The aim of MB6 was to produce results which replicate the preliminary result set shown in Table 4.6-1. In combination with this an analysis of variations over the course of the spin run similar to that in MB1 was considered advantageous. An additional aim post spinning was to investigate

the effect of doing more than one coating on the polymer with the same coating process, it was hoped this would achieve better coverage of the pores in the surface and hence drive up selectivity by encouraging solution diffusion.

The testing of spinning variations was carried out differently for MB6 than in previous runs. This time the 45min spin run was categorised into 15min sections with five samples being taken from the membranes collected during each time block. The mean values for each category and the statistics associated with these values are shown in Table 6.2-3, Table 6.2-4 and Table 6.2-5. The input compositions and spinning conditions are shown in Table 6.2-1 and Table 6.2-2.

Table 6.2-3: Uncoated Results for MB6

Membrane Identity	Statistic	PNF (GPU)				Selectivity	
		O_2	N_2	CO_2	CH_4	O_2/N_2	CO_2/CH_4
0-15mins	x	246.1	265.9	242.9	381.6	0.925	0.637
	σ	13.0	14.1	12.7	20.3	0.003	0.001
	σ_{mean}	5.8	6.3	5.7	9.1	0.001	0.001
15-30mins	x	245.5	268.3	233.3	374.7	0.915	0.623
	σ	15.7	16.2	14.4	23.4	0.004	0.005
	σ_{mean}	7.0	7.3	6.4	10.5	0.002	0.002
30-45mins	x	261.0	278.3	246.6	419.5	0.938	0.588
	σ	8.8	9.1	8.5	14.8	0.003	0.002
	σ_{mean}	4.0	4.1	3.8	6.6	0.001	0.001

The uncoated results show PNF values which are consistent across the full spin run. They are a little higher than had been seen in MB5 suggesting that these higher temperature membranes might be more porous than the ones created in MB5 but they are low enough that they display reasonable numbers for an uncoated membrane. The standard deviation and mean accuracy both suggest that the membranes show little change in behaviour between samples.

The selectivities of the uncoated membranes are, as would be expected from uncoated membranes, suggestive of a Knudsen diffusion controlled transport method and show the smallest deviation in this characteristic of the membranes produced in all batches.

After testing uncoated the membranes were all coated using the standard procedure as described in the Equipment and Methods section. They were then tested again after this single coating had been allowed to properly cure.

Looking at the results obtained for the each individual once coated membrane it was noted that the fifth membrane in each category presented pressure normalised flux values which were reduced and selectivity values which were higher than the rest of the membranes by a larger than statistically relevant amount. It was concluded that there may be a problem with the fifth test chamber and the results collected from this chamber have not been included in calculating the mean or statistical values for the membranes, note that five membranes were still tested the tests were simply not undertaken in this chamber.

Table 6.2-4: Once coated results for MB6

Membrane Identity	Statistic	PNF (GPU)				Selectivity	
		O_2	N_2	CO_2	CH_4	O_2/N_2	CO_2/CH_4
0-15mins	x	3.29	1.53	11.7	2.65	2.23	4.57
	σ	0.48	0.48	1.39	0.70	0.377	0.755
	σ_{mean}	0.24	0.24	0.70	0.35	0.189	0.378
15-30mins	x	3.15	1.16	11.6	2.66	2.75	4.47
	σ	0.20	0.21	0.93	0.46	0.323	0.763
	σ_{mean}	0.10	0.10	0.46	0.23	0.161	0.381
30-45mins	x	3.12	1.35	11.0	2.73	2.52	4.19
	σ	0.62	0.55	1.34	0.74	0.662	0.744
	σ_{mean}	0.31	0.28	0.67	0.37	0.331	0.372

After a single coating the results for the pressure normalised flux have reduced dramatically. For the first time the membranes produced in this work are comparable with the preliminary membranes as far as pressure normalised flux goes. There are some comparatively large discrepancies in the values of flux within in each membrane category and these are reflected in the standard deviations which range from a ninth of the mean for carbon dioxide up to a third of the mean for nitrogen. This large standard deviation and comparatively low mean accuracy for nitrogen in comparison to the carbon dioxide is likely due to the extremely low flow rate present for nitrogen permeation being affected more severely by external factors such as pressure fluctuations in the laboratory. This pattern appears to be borne out across all the gases in all the

categories as the ratio of standard deviation to the mean value decreases with permeation rate with the exception of oxygen and carbon dioxide in category 2 where the order is reversed. However the means are deemed accurate enough to still be valid.

When the PNF results are plotted over time to look for time of spinning effects over the course of the production process, Figure 6.2-1 and Figure 6.2-2, there appears to be a general trend for oxygen, nitrogen and carbon dioxide that the flux decreased over the length of the production time. However, the decrease is not a large amount and any observed trend is called into question by the error bars which overlap across the full spin run and for each gas. The methane trend through the spin run is for the membranes to show a consistent PNF. Again this may or not be accurate due to the error bars which are associated with the trend. Although the graph of the gas pair makes the error bars look smaller than for the other curves this is due to the larger y-axis scale in order to include the carbon dioxide results in the same figure.

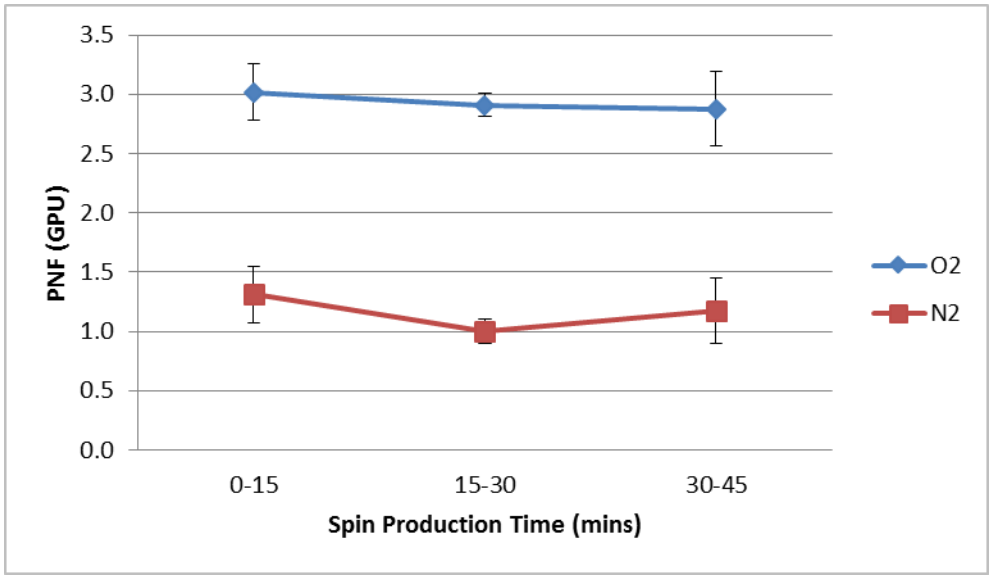

Figure 6.2-1: PNF of oxygen and nitrogen for MB6 over the duration of membrane production after single coating

The selectivities associated with the membranes after they have been coated once are the first values of selectivity to be high enough that it is considered Knudsen diffusion is not having a significant impact on the transport mechanism. The selectivity which is achieved is not as high as that of the preliminary measurements and is likely a combination of solution diffusion through

both the coating polydimethylsiloxane (PDMS) and the PVC as a result of the PDMS blocking pores. The results show that producing PVC membranes which are capable of separating gases is definitely possible on the current spinning rig set up as long as elevated temperatures are utilised. The standard deviations and standard error associated with the selectivities do indicate that there is some variation within the categories as to how well they separate the gas pairs but the variation is not outside reasonable limits and none indicate that the mean value could fall as low as it would have to in order to indicate Knudsen controlled flow.

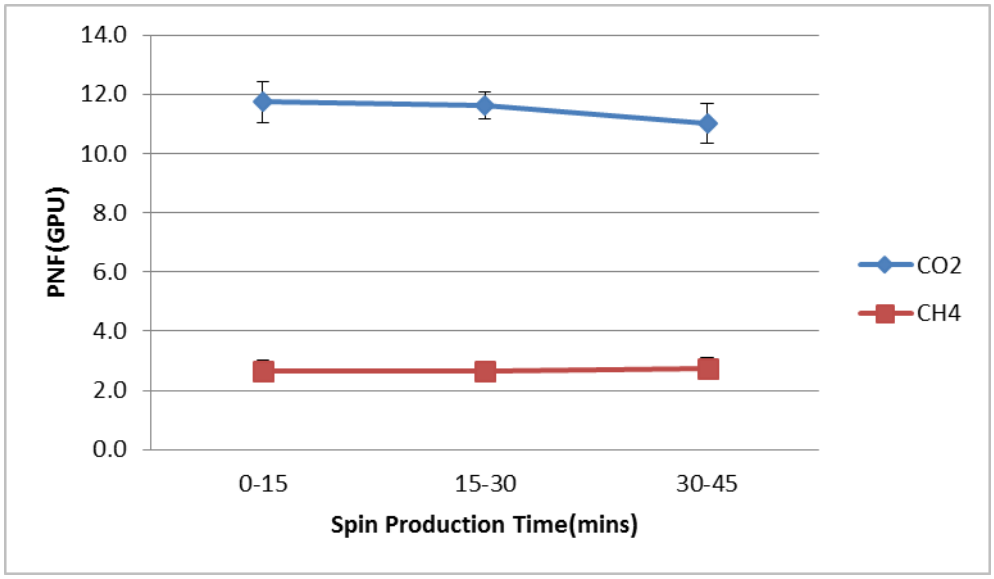

Figure 6.2-2: PNF of carbon dioxide and methane for MB6 over the duration of membrane production after single coating

When the selectivity changes over the period of the spin run are plotted, Figure 6.2-3, the curves indicate a decrease in carbon dioxide/methane selectivity but an increase in oxygen/nitrogen selectivity. This difference in the trends can be associated with the difference in the behaviours of the slow gases in each gas pair: nitrogen and methane. For both pairs the fast gases, oxygen and carbon dioxide, display similar decreasing trends in PNF of 5% and 6% respectively over the spin run. On the other hand for the slow gases nitrogen displays a 10% reduction in PNF and methane shows a 3% increase in PNF. These differences in the behaviour of each of the gas pairs result in opposite trends. It has already been pointed out that these PNF results are difficult to ascribe trends to across the spin run due to the errors associated with them overlapping so this

analysis of the differences in the slow gases while can be considered reflective of the data available is questionable on the basis of the error. The error bars associated with the selectivity also reflect that the values are all closely grouped even between categories since they also have error bars which overlap and again make it difficult to say anything conclusive about the trends over the spin run.

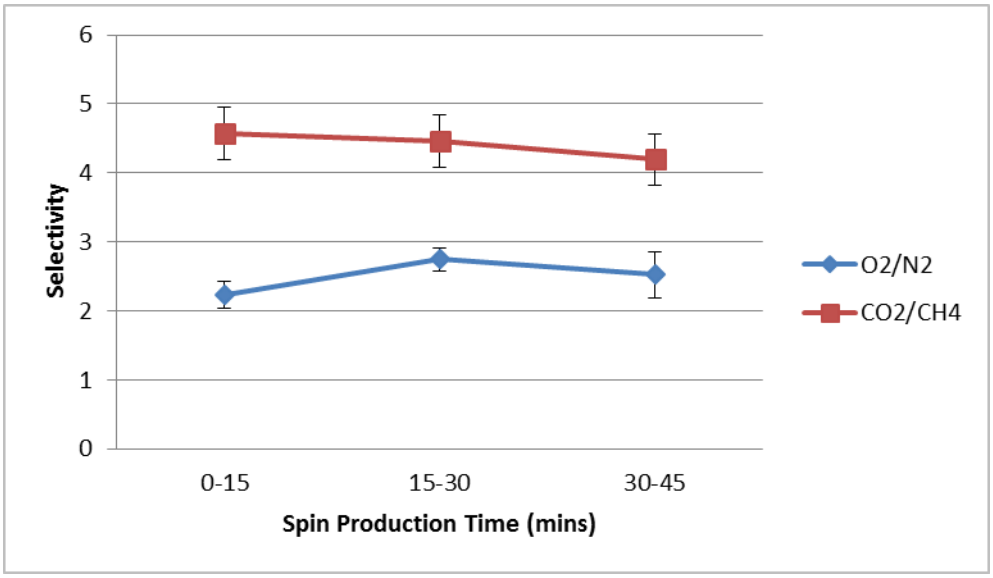

Figure 6.2-3: Selectivity of gas pairs for MB6 over the duration of membrane production after single coating

Overall after a single coating procedure the results suggest that the changes which occur over the course of a spin run are too small to be commented upon with a great deal of certainty. If further details were required carrying out more membrane production with the same set up in order to obtain more data points could improve the accuracy of the results. Trends could be better established by having more definition in the measurements i.e. use of smaller time periods and also by using a bigger dope reservoir to extend the period of spinning and hence allow more time for the patterns to form. However, in this work the fact that the changes were small was viewed as being a good sign moving forward since any changes made to the set up during the

course of a spin run should be comparable without needing any kind of factor applied to them to take into account the point in the spin run when the membranes being tested were produced.

Since the single coated membranes have selectivity values between those predicted by Knudsen diffusion and the intrinsic selectivity for PVC found from thin film experiments in the literature it can be concluded that the coating has sufficiently blocked the imperfections in the membrane surface for the mass transport to occur as a function of both the Knudsen and solution diffusion mechanisms. Although these results are not yet reflective of an industrially suitable gas separation membrane the first evidence of the membranes working to separate gases is an indication that the research was moving on the right track. The results also suggest that the membranes produced in the provisional work were prepared in an elevated temperature environment similar to what was being conducted here.

The membranes were then coated for a second time using the standard coating procedure as described in the methods section of this thesis. Once this coating cured fully the membranes were tested and the mean values and statistical results are shown in Table 6.2-5.

Similar to the membranes which had been single coated the statistical values presented in the table are calculated without using the membranes from test chamber 5.

Table 6.2-5: Twice coated results for MB6

Membrane Identity	Statistic	PNF (GPU)				Selectivity	
		O_2	N_2	CO_2	CH_4	O_2/N_2	CO_2/CH_4
0-15mins	**x**	2.58	0.657	11.2	1.89	4.07	6.03
	σ	0.271	0.188	1.23	0.411	0.680	0.767
	σ_{mean}	0.136	0.094	0.614	0.206	0.340	0.383
15-30mins	**x**	2.39	0.645	9.37	1.68	3.71	5.38
	σ	0.424	0.113	3.60	0.427	0.258	1.03
	σ_{mean}	0.212	0.057	1.80	0.214	0.129	0.516
30-45mins	**x**	2.37	0.684	10.3	1.96	3.46	5.25
	σ	0.387	0.100	1.63	0.316	0.163	0.176
	σ_{mean}	0.194	0.050	0.814	0.158	0.0813	0.088

The pressure normalised fluxes associated with the membranes after a second coating are reduced from what was achieved with a single coating. Although the values are still not as low

as those seen in the preliminary work they are very close and suggest that the preliminary membranes may have either been coated twice or could have been coated with a more concentrated solution perhaps as this may be expected to achieve lower fluxes also[1, 2]. The fluxes again show increasing deviation as a percentage when they are lower with nitrogen and methane exhibiting the biggest deviations as a percentage of the mean value, this having been said the standard error for the means suggest that they are a reasonably good fit overall.

The selectivity values are improved by the second coating also. The oxygen/nitrogen selectivity of around 4 is close to that observed in the preliminary work but the carbon dioxide methane selectivity is not as good at around 5.5 compared to 9 in the preliminary work. As could be expected there is a degree of deviation from the mean in the selectivity values being produced by the elevated temperature membranes which was not seen in the ambient temperature membranes. This can be explained by the mechanisms of mass transfer which are causing the selectivity to be produced. Whereby when more highly selective membranes are being produced the imperfections in individual membranes have a bigger impact on performance than when all the membranes are performing poorly.

The ambient temperature membranes are so porous that almost all of the transport through the membrane is coming from Knudsen diffusion through these pores as it is a much faster mode of mass transfer than solution diffusion. This means that the selectivity could be found directly from a single equation which governs Knudsen diffusion and as such is unlikely to produce large degrees of divergence. The situation for the elevated temperature membranes is more complicated because it is likely they have a combination of both Knudsen diffusion and solution diffusion contributing to the selectivity which is observed. Since Knudsen diffusion is so much faster as a transport method through the membranes it does not take a large increase in the paths available for Knudsen diffusion in order for it to have an impact on the results. Therefore small changes in surface morphology of the elevated temperature membranes produce bigger deviations in behaviour than are observed with the ambient temperature membranes.

Once more in comparison the means are indicated to be reasonably accurate as even the bigger deviations do not results in a large error being incorporated into the membranes.

When the data are plotted to look at trends across the membrane categories the curves produced are shown in Figure 6.2-4, Figure 6.2-5 and Figure 6.2-6. The trends in PNF show a split between the fast and slow gases. The fast gases PNF decrease slightly as the spin run progresses while the PNF of the slow gases holds fairly steady. The trends are masked slightly by the errors which are associated with the mean values which overlap and thus mean that statistically there might be no trend at all. However, only the ends of the error bars overlap so it seems reasonable to think there could be a trend and more weight is added to this when the selectivity results are considered. The trend in the selectivity shown for the membranes, in both gas pairs, is clearly for a reduction in selectivity over the course of the spin run and this time the error bars do not overlap so they are statistically relevant trend.

In order to attempt to explain the reasons for the observed trends the mechanisms of the gas transport through the membranes have to be considered. It is known that pores exist in the membranes from the previous results with them and thus there is a possibility for Knudsen diffusion to play a part in the trends observed, however, if there were to be an increase in surface porosity allowing Knudsen diffusion then it would be expected that the permeation of all gases would increase. If a reduction in Knudsen diffusive pores available was the cause then it may be expected the single coated membranes would also have shown this result more strongly. Additionally it would be expected that the change would occur in the slow gases rather than the fast gases as they are more favoured by Knudsen diffusion due to possessing a lower molecular weight.

The reason for the trends must therefore be coming about from the solution diffusion contribution to mass transfer. It has been shown that the free volume of the polymer matrix has a strong influence on the transport of gases through polymer membranes[3-6]. It has also been postulated by *Chen et al*[7] that high selectivity in membranes can be related to the cavity size of the free volume which was an idea which received backing from *Ismail et al*[8]. Both these works discussed an increase in selectivity when the mean free volume cavity diameter was in the same length scale as the kinetic diameter of the gas molecules whereby the cavity was the correct diameter to allow the small kinetic diameter fast gas through but the lower kinetic diameter slow gas was held up producing highly selective membranes.

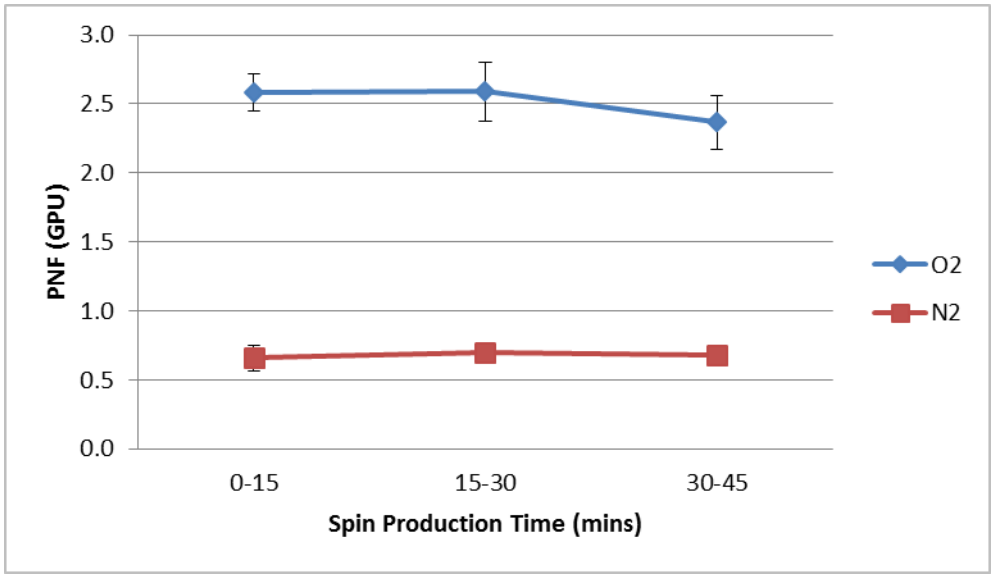

Figure 6.2-4: PNF of oxygen and nitrogen for MB6 over the duration of membrane production after double coating

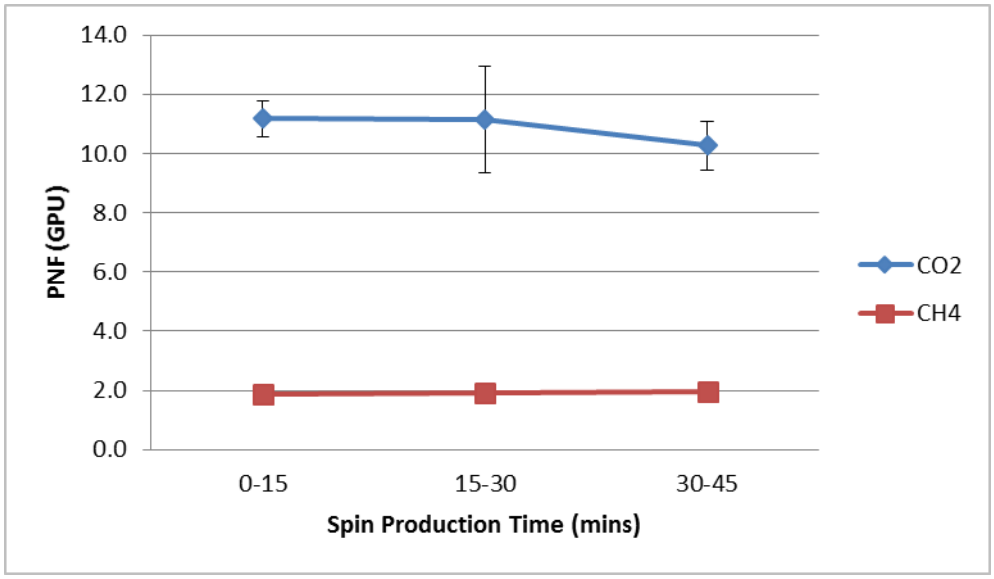

Figure 6.2-5: PNF of carbon dioxide and methane for MB6 over the duration of membrane production after double coating

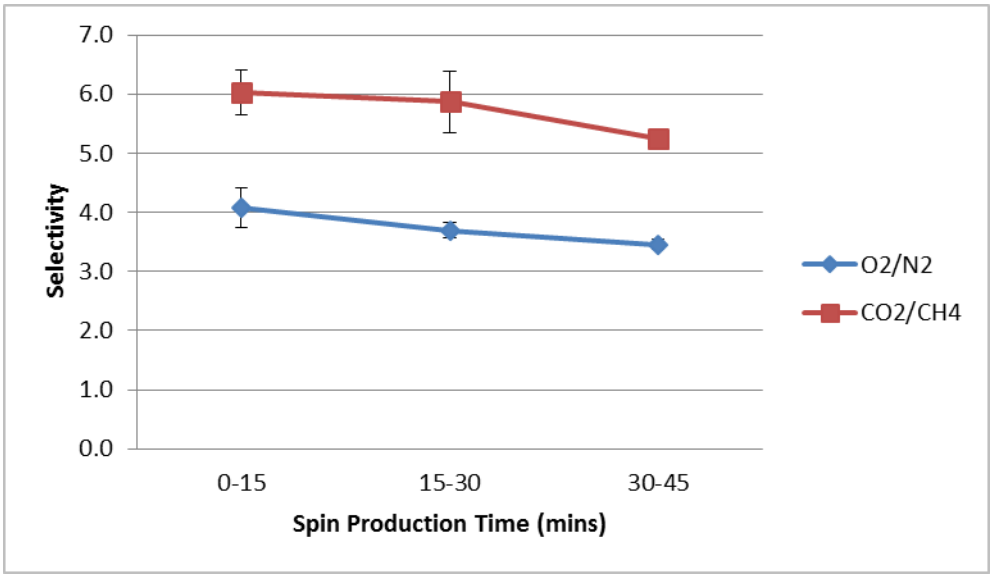

Figure 6.2-6: Selectivity of gas pairs for MB6 over the duration of membrane production after double coating

The idea of the mean cavity diameter can be extended to explain the trends seen for the PVC membranes. If the cavity diameter was initially in the region of preferentially allowing the passage of the smaller kinetic diameter gases but over the course of the spinning process there was a shift in the distribution of cavity sizes towards smaller cavities then it is conceivable that they could reach the point where some of the cavities are not acting as gates in the same way as they were when they were larger. This could cause the concentration of cavities providing higher fluxes to the oxygen and carbon dioxide than the larger methane and nitrogen molecules to decrease and hence selectivity to fall. While the reduction in these cavities would lead to lower flux for the fast gases since they were already presenting more barrier like properties to nitrogen and methane it might be expected that the fluxes of these gases could be less affected and hence the selectivity falls as seen in the results for MB6.

This is a possible mechanism but in order to test to see if it is reflected in the membrane structure it would be necessary to carry out positron annihilation lifetime spectroscopy (PALS). PALS has been used by a number of authors in order to study the structure of polymer membranes[9-13] and can give details about the total free volume available and the size of the pores[8, 14, 15]. This work has not been carried out at this point due to the availability of a PALS instrument.

The factors which could be affecting the free volume are varied because it is related to molecular orientation which is present in the polymer, the orientation of molecules in the outer layers of the membrane allows closer packing of the molecules and hence reduces free volume[16, 17]. The strongest influence on molecular orientation of molecules while being spun for hollow fibers has been suggested to be shear rate[17] and there are a number of studies reporting increased selectivity with higher shear rates which cite molecular orientation as the cause[8, 18-20]. So if the shear rate in the spinneret is taken as the key factor then this implies the rheological conditions of the dope have a big effect on the nature of the free volume which is produced and it could be that as the spin run progresses the nature of the solution being spun is changing.

The rheological examination in the last chapter suggested that there was no large time effect on the dope solution over a longer period than 45min so it is unlikely that the change in membrane properties is due to any sort of crystallisation or phase inversion before the dope reaches the spinneret. If this had been the case it is likely the trends observed over the spin run would have been the opposite to what is observed as the outer layers would already have partly formed by nucleation and growth, for either of these mechanisms, and therefore would not have coalesced from a spinodal decomposition process to produce the active layer.

The rheological examination did identify that there is a temperature effect on the dope where it displays much more solid like behaviour at 20°C and more liquid like behaviour at 60°C. The elevated temperature membranes are being spun at a temperature of 50° to try and encourage the dope solution to display liquid like characteristics but it is possible the temperature controls which have been put in place are allowing temperature fluctuations to occur over the course of the spin run. Every effort has been put into maintaining a steady temperature of the dope solution all the way through the process and the temperature is being monitored in as many places as possible but there could still be a net loss or gain of heat over the course of the run.

A reduction in dope temperature over the course of the run would make any explanation of the results difficult as intuitively this would move the dope towards displaying more solid like qualities. From comparison of the ambient temperature results to the elevated temperature results solid like behaviour would lead to increased flux and decreased selectivity of all gases rather than the changes being seen here. If heat were building up in the system over time then

it would be expected that bubbles of THF would start to form in the lines and the membrane might be expected to show some sign of this in the form of structural weakness. It is also likely that if the THF was coming out of solution in the pipes then it would be difficult to form an active layer since there would be reduced high volatility solvent present in the extruded solution. These factors suggest that temperature is unlikely to be the leading cause of the trends unless the temperature is increasing but not enough to make THF come out of solution this would lead to a less viscous dope solution being extruded over time and hence greater molecular orientation could be achieved as the molecules have more freedom to move and align with the flow lines.

The most likely explanation for the trends being produced is that a number of factors are combining which could produce higher molecular orientation. Fluctuations in a number of different factors on the membrane rig can enhance molecular orientation such as draw ratio, extrusion rate and the rheological effects already mentioned. Any number of these could all be contributing in some way to the observed changes and are being controlled as tightly as possible making it difficult to justify how the trends are developing.

In conclusion a second coating of Sylgard 184 caused a decrease in PNF and an increase in selectivity. A trend for a reduction in PNF of the fast gases accompanied by a reduction in selectivity was also revealed by the results for the membranes after a second coating. It is not clear what caused this trend although it is postulated that a number of factors have contributed towards a reduction in the mean free volume cavity size resulting in a closing of certain mass transport gates to the fast gases which were already closed to the slow gases and thus did not affect their flux so severely.

In order to achieve a better understanding of the trends which are thought to be occurring in the membrane production process a larger dope reservoir would be required to spin for longer and smaller timeframe categories could be used. It would also be good to test more membranes to improve the standard error and thus lend greater credence to the trends.

The difference which was achieved from double coating was quantified by taking the ratio of the values for PNF and selectivity which were achieved for a single coating and a double coating. The mean values and errors associated with these comparisons are described in Table 6.2-6.

The flux results show clearly that reduction in mass transfer brought about by the second coating affects each gas differently. The slow gases are affected by a greater extent for all the membrane production time frames which creates the improvement which is seen in the selectivity.

The improvement which is seen for each gas at different time frames show a tendency to be in a similar range which suggests that the coating effect is contributing to the improvement equally across all the categories and therefore should not be considered a factor in the trends over time discussed above. It is also interesting to note that the improvement achieved in selectivity between first and second coating is best for the 30-45min category of membranes, this is unexpected since the selectivity decreases over time towards this category and it might therefore be expected to produce the least degree of improvement from one to two coatings. This is further evidence that the coating procedure is not affecting the trends observed to be developing over time.

Table 6.2-6: MB6 membrane results showing the ratio of the once coated result (subscript o) to twice coated result (subscript t)

Membrane Identity	Statistic	PNF				Selectivity	
		$\frac{O_{2o}}{O_{2t}}$	$\frac{N_{2o}}{N_{2t}}$	$\frac{CO_{2o}}{CO_{2t}}$	$\frac{CH_{4o}}{CH_{4t}}$	$\frac{(O_2/N_2)_o}{(O_2/N_2)_t}$	$\frac{(CO_2/CH_4)_o}{(CO_2/CH_4)_t}$
0-15mins	**x**	1.29	2.48	1.1	1.43	0.558	0.761
	σ	0.27	1.20	0.15	0.42	0.115	0.100
	σ_{mean}	0.13	0.60	0.08	0.21	0.057	0.050
15-30mins	**x**	1.35	1.85	1.5	1.72	0.743	0.856
	σ	0.30	0.46	1.07	0.77	0.097	0.220
	σ_{mean}	0.15	0.23	0.53	0.39	0.049	0.110
30-45mins	**x**	1.35	1.99	1.1	1.42	0.729	0.800
	σ	0.34	0.75	0.24	0.40	0.181	0.153
	σ_{mean}	0.17	0.38	0.12	0.20	0.090	0.076

The standard deviations and standard errors reported in Table 6.2-6 are all fairly large in comparison to the mean values. Which is a reflection on how the improvement achieved varied from membrane to membrane however it is interesting that where these errors are large, for instance nitrogen between 0-15mins, is where the mean value is out from by a greater extent

from the other mean values associated with that gas. So the errors, while large, do not detract from the patterns observed in the change going from one coating to two since they do not cause much overlap in the ratios between gases.

From this point onwards all membranes were double coated in order to achieve a better selectivity. It was felt that the trade-off between selectivity and PNF is worth it in this case. It was also felt that although there appears to be a trend for reduction in selectivity over the course of a spin run and this is something which should be borne in mind in future runs the reduction is not serious enough to make comparisons between membrane categories produced at different points in the spin run invalid.

6.3. Optimisation of 28% PVC Dope Over Different Spinning Conditions (MB7)

6.3.1. Factors to be Investigated and Methodology for MB7

The production of gas separation membranes is a highly multivariate process which requires a great deal of optimisation. Ideally this starts in the dope solution and progresses to the spinning conditions which are utilised from there. In this case however since finding a dope composition and spinning condition which produced effective membranes had proven difficult experimentation time was becoming a factor in the decisions it was decided to press ahead with the 28% PVC dope and attempt an optimisation of the spinning conditions under which the membranes were being produced.

Experimental design is an important aspect in the preparation of many new materials which helps to refine the processes involved. The Taguchi method is one experimental design mechanism which appears regularly in literature in a number of membrane fields such as; fuel cells[21-23], filtration[24, 25] and reverse osmosis[26], although, from the literature search carried out for this work it appears to have much less popularity in the field of gas separation membranes

with investigations into individual effects still bearing the weight of investigation rather than designed sweeps of factors. The reverse osmosis paper by *Idris et al*[26] is used as a guide in this case for how to go about carrying out Taguchi analysis on a series of membranes.

The Taguchi method allows investigation into several factors which effect membrane performance, and the degree to which they do so simultaneously. The experimental design method utilises an orthogonal array of experimental conditions to be tested and then analyses these results using standard statistical methods in order to answer one or multiple of the following three questions:

- What is the optimum set of conditions?
- What factors contribute to the results and to what extent?
- What are the expected results at the optimum conditions?

Once the optimisation process has been carried out the experiment at the predicted conditions should also be carried out to test the results unless it is on or very close to the conditions of one of the experiments already carried out. The design method created by Taguchi is useful because the use of standard statistical methods with its orthogonal arrays gives it consistency and reproducibility which it uncommon amongst statistical methods[27].

The aim of MB7 was to create a series of membranes produced under different conditions which could be used to optimise some of the spinning conditions for the 28% dope. It was decided that three different factors known to affect the properties of gas separation membranes should be investigated and the factors selected were extrusion rate, forced convective gas flow rate and residence time of the membrane below the impingement zone in the forced convective gas chamber. Each of the three factors was assigned a high and low level to be used during the spin run making the Taguchi analysis a 3 factor, 2 level design aimed at optimising the selectivity of the membranes.

The extrusion rate was chosen as a factor to be investigated at it is well known to have an influence on gas separating qualities due to its influence on shear rate and hence molecular orientation[11, 17, 28, 29]. Since extrusion rate influences molecular orientation it was also felt that this would be an interesting factor to alter after the discussion of MB6 suggested there could be

a link between increased molecular orientation and a reduction in selectivity for the PVC membranes which is the opposite of what would be expected. The values of extrusion rate chosen were 2 and 3cm^3/min. These values were selected because they are within a normal range used for the production of gas separation membranes yet the increase represents a 50% difference in the value used and hence it was hoped noticeable differences.

There are other factors which can affect the molecular orientation such as jet stretch ratio but it was decided that the relationship between shear rate and molecular orientation was best analysed first in terms of the selectivity produced.

When adjustments to the flow of dope solution are made this affects the relative flow rate between the dope and the bore fluid. The effect of bore fluid flow rate has also been studied previously[30] although not as extensively as the effect of dope compositions[16, 31-33]. It was suggested by *Gordeyev et al*[30] that the effect of bore fluid flow rate was similar to that of bore fluid composition and was related to the rate at which the non-solvent front from the bore encroaches on the membrane active layer. It was suggested that high bore fluid flow rate produced a damaged active layer due to rapid encroachment and erosion of the active layer before it was fully formed. However, the flow does have to be high enough to maintain the hollow nature of the membranes; it has been the practice when using the spinnerets in this research group to maintain the bore fluid flow at around a third that of the dope fluid flow. It was felt the ratio of the flows of bore to dope fluids was more important than the actual rates involved and so when the dope extrusion rate was altered in MB7 the bore fluid flow rate was also altered to maintain an equivalent ratio.

As mentioned above the bore fluid composition is a factor which has been considered before. There are two main considerations with the bore fluid composition which are the species involved and the ratio of the species. It is most common for a two component system to be used as the bore fluid and for polymer membranes this is generally based around water plus an additional component[34]. Different bore fluids can have different effects on the substructure of the membrane, sometimes creating different sized or shaped voids in the porous substructure which can benefit the permeation of gases through it while still providing strength[35-38]. From the collective studies on bore fluid composition one theory which has evolved is that the best bore

fluid for a particular dope solution is solvent neutral and hence interacts very little with the dope. With regard to the phase separation processes this kind of bore fluid will produce the maximum time between contact of the two solutions and phase separation occurring by delayed de-mixing. The delay slows down the encroachment of the non-solvent front into the membrane and prevents the damaging of the active layer in the same way as a lower flow rate of bore fluid does. Within the Strathclyde group this has in the past been achieved by adding potassium acetate to the water in the bore solution at 20% by mass which has the effect of reducing the water activity in the bore fluid[8]. A reduction in water activity means that the bore fluid solution has less energy and hence will interact less strongly with the dope solution forming the membrane. The bore fluid used in this case was also a 20% by mass potassium acetate solution.

The forced convective gas flow rate is also a factor which has been considered before[29, 30] although it does not seem to feature in as many papers as shear rate. This is likely due to the different methods used to produce hollow fiber membranes such as wet spinning and dry gap spinning where the extruded membrane passes through a dry gap but does not get exposed to forced convection. The values selected for forced convective gas flow were 4 and 8L/min. These again represent reasonable levels of gas flow rate for this spinning method while being different enough that it was hoped a trend between the two different values would be visible. It was also borne in mind when selecting these factors that the membranes produced had to work to separate gases so that the data used in the Taguchi model was not flawed and so extreme values of either high or low flow rates were avoided. From this point on this will be known as the gas flow rate factor.

A study of the literature has found many examples of dry gap residence time studies[39-43] unfortunately since a lot of these studies do not involve forced convection they did not present the opportunity to study exactly where the membrane surface was being formed in the gap. Where residence time has been considered for a forced convective hollow fiber spinning set-up[28, 30] the impingement zone (point in the chamber where the gas flow is directed at the membrane) has been in the centre of the chamber. With this set up it is the overall residence time which is studied in the chamber and the residence times above and below the impingement zone change depending upon the size of the chamber and the extrusion rate which is being used.

For this work the forced convection chambers were designed so that for each category of membrane produced the residence time above the impingement zone was the same and only the time below it altered between categories. It was hoped that by isolating the time below the impingement zone it could be shown that the production of the active layer was occurring above the impingement zone because the residence time below it was not affecting the membrane performance. To show this however the residence times below the impingement zone could not be so high as to allow bore fluid non-solvent encroachment from the membrane lumen to erode or damage the active layer[28, 43]. For this reason the residence times below the spinneret were restricted to 0.248 and 0.496s while the total residence times in the chamber were 0.496 and 0.744s. Creating this set up required the four forced convection chamber arrangements shown in Figure 6.3.1-1. From this point onwards this will simply be referred to as the residence time factor.

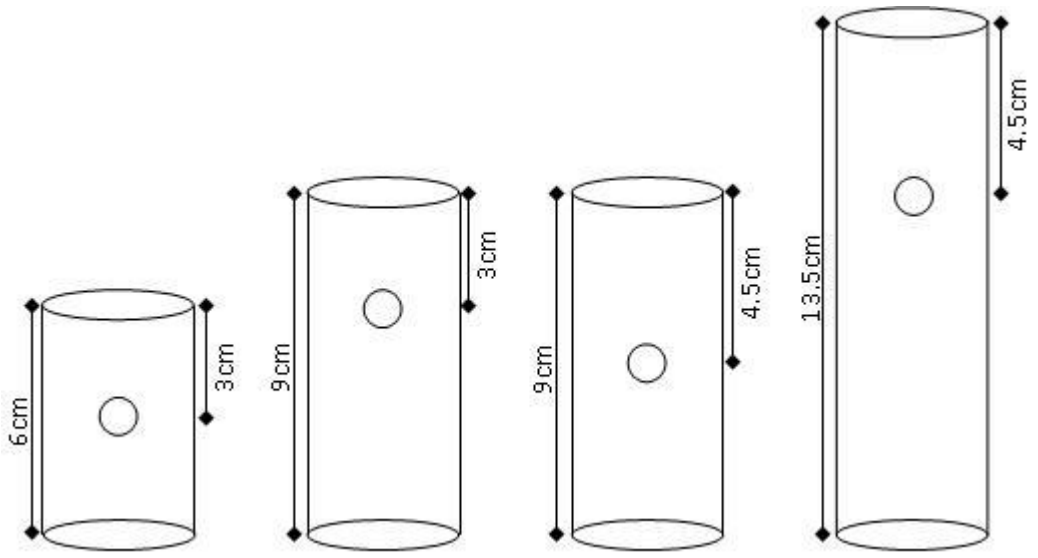

Figure 6.3.1-1: Forced convection chambers used for spinning MB7

The Taguchi analysis requires an orthogonal array to be set up using the conditions and factors. In this case an orthogonal array is a matrix which is generally two dimensional where each entry comes from a set of symbols which define experimental set-ups. The number of these symbols, t, is key as in order to qualify as an orthogonal array if a number of columns is selected equal to

t then they should contain each possible combination of symbols (t-tuples) once i.e. if the symbols are 1 and 2 then t=2, therefore selecting two columns in an array, each would have to contain the combinations (1,2), (2,1), (1,1) and (2,2). Where L and H are used to represent the low and high values for the each of the three factors to be investigated with MB7 setting out the full array of experiments gives the pattern seen in Table 6.3.1-1 and requires eight different categories of membrane.

Table 6.3.1-1: Categories of membrane to be produced in MB7

	Extrusion Rate	Residence Time	Convective Gas Flow Rate
1	L	L	L
2	L	L	H
3	L	H	L
4	L	H	H
5	H	L	L
6	H	L	H
7	H	H	L
8	H	H	H

However, one of the benefits of design of experiments and Taguchi is that it allows the number of experiments to be conducted to be reduced. In this case the eight categories could be reduced to four in order to conduct the analysis as shown in Table 6.3.1-2. This reduction in categories gives a standard orthogonal array for a 3 factor 2 level Taguchi design. However, all eight categories of membrane were produced in order to allow comparisons to be drawn between what the Taguchi analysis shows with what graphical interpretation of the results suggests.

Table 6.3.1-2: Reduced categories in orthogonal matrix for Taguchi Analysis

	Extrusion Rate	Residence Time	Convective Gas Flow Rate
1	L	L	L
4	L	H	H
6	H	L	H
7	H	H	L

The aim was to produce all these membranes within a single spin run so that there were not different dopes being used to produce different categories. Since under the new protocols the dope was to be used immediately after production a larger volume of dope solution had to be prepared in order to undertake the spinning. With the standard spin run of 45mins for 8 categories there would only have been approximately 3mins to produce the membranes for each category once down time for making system changes and allowing equilibrium to re-establish was taken into account, which left the process extremely vulnerable to any failures in the system for example if the membrane thread snapped. The spinning time was increased to 5mins per category by increasing the volume of dope produced so that the spin run lasted for approximately 1hour. The 1hour of spinning time meant that there could be a 2min period between each category where the membranes could be sent to waste while changes were made and equilibrium re-established.

The spinning for MB7 was carried out with the elevated temperature alterations made to the spin rig and at the conditions laid out in Table 6.3.1-3 and the stream compositions shown in

Table 6.3.1-4. After being produced the fibers were coated twice using the standard coating procedure with enough time between coatings for the cure of the first coating to be complete.

Table 6.3.1-3: Compositions of input streams to the spinning process for MB7

Dope Composition	
Chemical	**Concentration (weight %)**
Poly(vinyl chloride)	28%
Dimethylacetamide	50%
Tetrahydrofuran	6%
Ethanol	16%
Bore Fluid Composition	
Chemical	**Concentration (weight %)**
Water	80%
Potassium Acetate	20%
Coagulation Bath Composition	
Chemical	**Concentration (weight %)**
Water	100%

Table 6.3.1-4: Spinning conditions for MB7

Spinning Conditions	
Extrusion rate (cm^3/min)	2.0/3.0
Dope temperature (°C)	50
Jet stretch ratio	1
Bore fluid flow rate (cm^3/s)	0.7/1.0
Bore fluid temperature (°C)	15
Convective gas	Nitrogen
Convective gas flow rate (L/min)	4/8
Convective gas temperature (°C)	17
Convection chamber height (cm)	6.0/9.0/9.0/13.5
Distance to gas jets (cm)	3.0/3.0/4.5/4.5
Bath temperature (°C)	15
Air temperature (°C)	21

6.3.2. Results for MB7

The results of PNF and selectivity for each membrane category are given in Table 6.3.2-1 for uncoated membranes and in Table 6.3.2-2 for the coated membranes.

As expected from the results of previous membrane batches the uncoated membranes did not show a great deal of variation between the categories of membrane produced. All the conditions used produced uncoated membranes with PNF values for the gases in the expected range of low hundreds of magnitude GPU and the selectivity describes the relationship for Knudsen diffusion being the controlling factor in the mass transport through the membranes. While these results are the expected ones the PNF values do suggest the active layer has been produced reasonably well since they are not in the thousands of GPU as in MB1. The results are also very consistent suggesting the spin run has effectively produced consistent membrane material.

Table 6.3.2-1: Uncoated results for MB7

Membrane Identity	Statistic	PNF (GPU)				Selectivity	
		O_2	N_2	CO_2	CH_4	O_2/N_2	CO_2/CH_4
1	x	135	140	129	199	0.964	0.647
	σ	6.11	8.52	5.74	8.10	0.036	0.005
	σ_{mean}	2.73	3.81	2.57	3.62	0.016	0.002
2	x	154	166	147	231	0.932	0.637
	σ	3.24	15.6	3.98	4.73	0.071	0.005
	σ_{mean}	1.45	6.97	1.78	2.12	0.032	0.002
3	x	138	153	130	207	0.900	0.629
	σ	11.0	13.0	9.77	16.9	0.005	0.007
	σ_{mean}	4.91	5.82	4.37	7.55	0.002	0.003
4	x	128	141	121	190	0.908	0.639
	σ	2.46	3.34	2.86	4.81	0.005	0.004
	σ_{mean}	1.10	1.49	1.28	2.15	0.002	0.002
5	x	183	200	174	275	0.915	0.633
	σ	17.4	18.7	16.6	25.4	0.003	0.005
	σ_{mean}	7.78	8.38	7.41	11.3	0.001	0.002
6	x	175	191	166	257	0.915	0.648
	σ	4.78	5.48	4.11	7.14	0.004	0.006
	σ_{mean}	2.14	2.45	1.84	3.19	0.002	0.003
7	x	152	170	144	230	0.894	0.626
	σ	11.1	12.6	12.1	17.7	0.003	0.006
	σ_{mean}	4.98	5.64	5.41	7.89	0.001	0.003
8	x	163	176	152	241	0.925	0.631
	σ	4.85	5.06	5.60	8.20	0.003	0.016
	σ_{mean}	2.17	2.26	2.50	3.67	0.001	0.007

Table 6.3.2-2: Coated results for MB7

Membrane Identity	Statistic	PNF (GPU)				Selectivity	
		O_2	N_2	CO_2	CH_4	O_2/N_2	CO_2/CH_4
1	x	2.96	1.03	11.3	2.87	2.90	3.97
	σ	0.216	0.113	0.793	0.301	0.137	0.234
	σ_{mean}	0.097	0.051	0.355	0.135	0.061	0.105
2	x	2.20	0.497	8.79	1.40	4.50	6.33
	σ	0.182	0.088	0.786	0.213	0.445	0.427
	σ_{mean}	0.081	0.039	0.351	0.095	0.199	0.191
3	x	2.35	0.690	8.52	1.50	3.53	5.76
	σ	0.193	0.157	0.635	0.257	0.720	0.698
	σ_{mean}	0.087	0.070	0.284	0.115	0.322	0.312
4	x	2.13	0.502	8.02	1.10	4.27	7.49
	σ	0.146	0.066	0.685	0.252	0.440	1.07
	σ_{mean}	0.065	0.029	0.307	0.113	0.197	0.477
5	x	2.43	0.653	9.9	1.49	3.72	6.65
	σ	0.160	0.034	1.08	0.207	0.195	0.479
	σ_{mean}	0.072	0.015	0.485	0.093	0.087	0.214
6	x	2.58	0.693	11.0	2.10	3.74	5.25
	σ	0.309	0.061	1.35	0.177	0.452	0.490
	σ_{mean}	0.138	0.027	0.603	0.079	0.202	0.219
7	x	2.80	0.818	10.7	2.05	3.42	5.25
	σ	0.065	0.032	0.384	0.232	0.199	0.479
	σ_{mean}	0.029	0.014	0.172	0.104	0.089	0.214
8	x	2.64	0.662	10.3	1.67	4.02	6.27
	σ	0.269	0.105	0.769	0.251	0.366	0.591
	σ_{mean}	0.121	0.047	0.344	0.112	0.164	0.265

The coated results for MB7 reveal some of the patterns in behaviour changing the conditions which membranes are produced under can bring about. Before returning to the Taguchi method of analysing the fibers it was felt to be useful to check for patterns graphically and report on these.

6.3.3. Graphical Analysis of Twice Coated MB7 Membranes

When comparing the conditions under which fibers were produced there are four direct comparisons available for each of the three factors investigated. These comparisons are made where the only difference between the fiber production conditions is in the factor being looked at, for example if looking at extrusion rate then the only difference between categories 1 and 5 is that 1 is extruded at $2cm^3$/min and 5 at $3cm^3$/min. This allows comparisons to be made as outlined in Table 6.3.3-1.

Table 6.3.3-1: Comparisons which can be made between membrane categories for each spinning parameter

	Factor Being Studied		
	Extrusion Rate	Residence Time	Gas Flow Rate
Comparisons	1_5, 2_6 3_7, 4_8	1_3, 2_4 5_7, 6_8	1_2, 3_4 5_6, 7_8

Figure 6.3.3-1 to Figure 6.3.3-6 show graphs displaying the changes in PNF for each gas and the changes in selectivity for the O_2/N_2 and CO_2/CH_4 gas pairs for each of the three factors investigated. For each factor investigated a set of graphs was produced which show the four relevant comparisons labelled on the chart with the factor being changed on the x-axis and the calculated PNF or selectivity on the y-axis. The error bars shown in the charts are the standard error associated with each value.

The first factor investigated was the extrusion rate of the dope solution. On comparing the graphs showing the PNF for the various gases through the membranes it can be seen that the same pattern establishes itself in all cases. The low extrusion rate membranes produced lower fluxes than the high extrusion rate membranes they were being compared to for all the comparisons except comparison 1_5. Indeed with the exception of nitrogen categories 2, 3 and 4 produced the lowest PNF of all the membrane categories for each gas. The exception to this for nitrogen is also very close and the category three error bars, the category which breaks the trend, has a slightly larger error range at the low end of which overlaps with the category 8 membranes for the third lowest PNF. With the exception of this overlap there is not another occasion when looking at the category 2, 3 and 4 low extrusion rate membranes where the error bars for PNF overlap with the higher extrusion rate category 6, 7 and 8 membranes.

The category 1 membranes contradict this trend giving PNF values higher than any other category. The difference is not enough for any particular gas to call the integrity of the membranes in this category into question but they do buck the trend.

When selectivity is considered the expected trade-off between PNF and selectivity is clear with the low extrusion rate categories 2, 3 and 4 now producing the higher selectivity than the direct comparisons to them. Although when the selectivity is considered the pattern does not appear to be as strong with the category 8 membranes providing better oxygen/nitrogen selectivity than category 3 and better carbon dioxide/methane selectivity than either category 2 or 3. In the case of category 2 the error bars suggest that the category two membranes are consistent while the category 8 membranes can have a lower value at the bottom of the associated error bar than those of category 2. Category 5 also performs well from a selectivity perspective especially when carbon dioxide/methane selectivity is considered.

It does appear that there is a discrepancy in the selectivity performance of the membranes when the two different gas pairs are considered. There are some categories which perform better relative to the other categories on one gas pair than the other. This suggests that there could possibly be some very subtle morphological effects at work in the separations which are better in some membranes than others, possibly as has previously been hinted at in the cavity sizes.

The error bars associated with the extrusion rate effects tend not to overlap with the membranes which are being compared directly i.e. 1 and 5 do not overlap and 2 and 6 do not overlap. There are a couple of exceptions to this but generally this suggests that trends which can be seen in the direct comparisons have a decent chance of being true and would be expected to be reflected in the Taguchi analysis results. The expectation is that the low extrusion rate will be favoured.

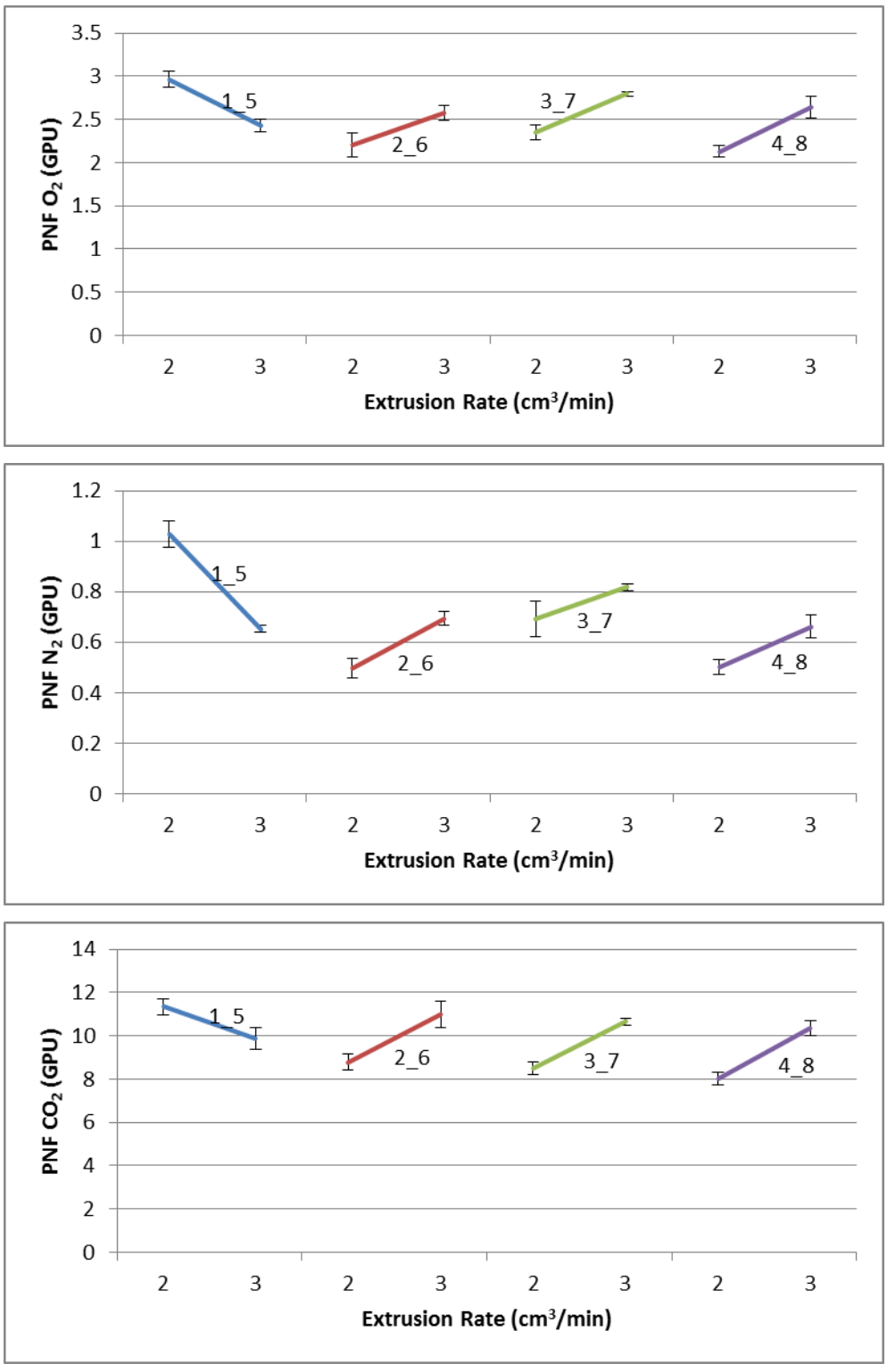

Figure 6.3.3-1: Effects of extrusion rate change on PNF and selectivity values for MB7. Top: O_2 PNF, middle: N_2 PNF, bottom: CO_2 PNF.

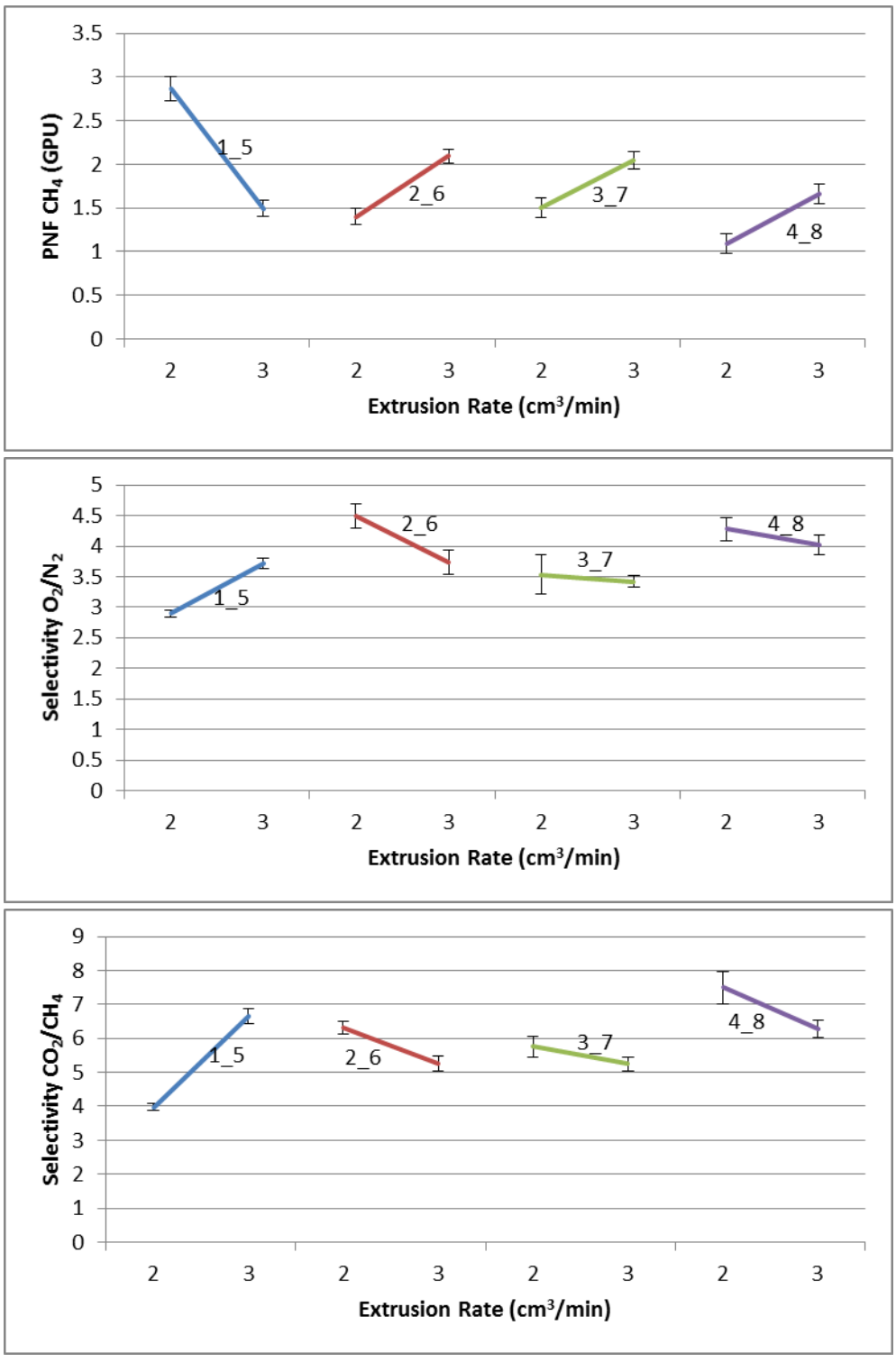

Figure 6.3.3-2: Effects of extrusion rate change on PNF and selectivity values for MB7. Top: CH_4 PNF, middle: selectivity O_2/N_2, bottom: selectivity CO_2/CH_4.

The charts of residence time comparisons are generally less conclusive than those discussed above for the extrusion rate charts. There appears to be more of a trend for the PNF to decrease going from lower to higher residence times, however the 5_7 comparison goes against this trend in all the graphs. Bearing in mind that the category 1 membranes appear to have an elevated PNF and hence depressed selectivity and it is the 1_3 comparison which shows the strongest adherence to the observed trend it is thought that the residence time may not be having a large effect at this point.

Since the category 5 membranes are involved in the apparent exception to the rule shown for the extrusion rate along with category 1 it is possible that the fact that it bucks the trend again is a sign that it varies from the expected results in the opposite manner from category 1, so that where category 1 shows unexpectedly high PNF category 5 shows unexpectedly low values. If this is the case then the trend would become much more definitive but again neither of the categories falls widely outwith expected ranges for the values and therefore they are not excluded from the analysis.

The selectivity shows more of a trend to increase going to higher residence times but again this is only a marginal observation since five of the comparisons show this trend and three the opposite.

The error bars associated with residence time have a larger tendency to be overlapping where comparisons are made between categories than they had when extrusion rate was studied. They are the same error bars as for the extrusion rate and hence the implication that they overlap more suggests that the results tend to be more similar between the directly comparable membranes.

Overall it is expected that the Taguchi analysis will reveal the residence time below the impingement zone to have only a minor effect but that it will lean slightly towards the higher residence times as it will be optimising the selectivity for the highest value possible. It was a concern here that the uncharacteristically high/low levels of some of the results in comparison to similar membranes i.e. category 1 may result in the Taguchi analysis giving too much weight to this production factor.

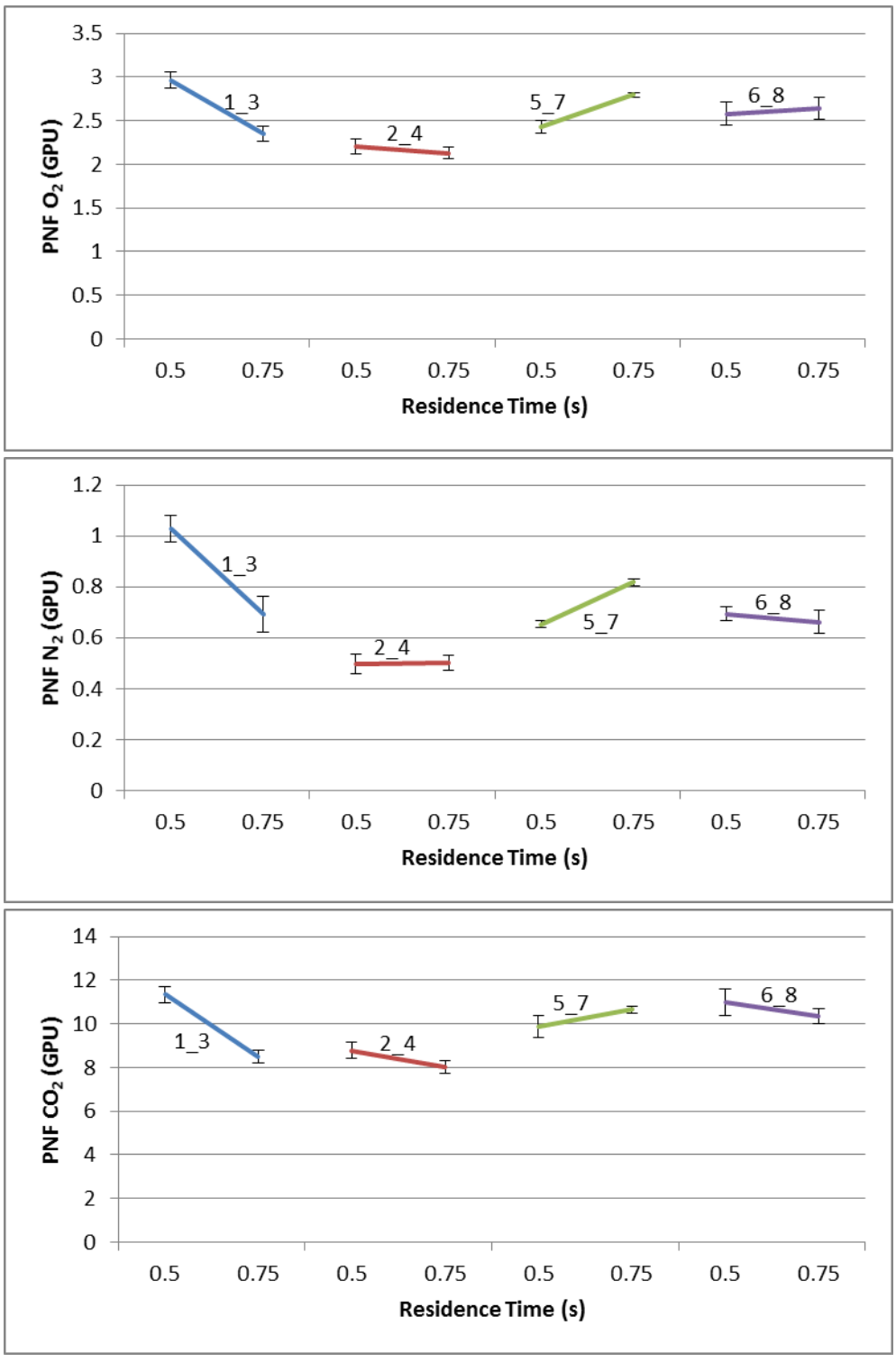

Figure 6.3.3-3: Effects of residence time change on PNF and selectivity values for MB7. Top: O_2 PNF, middle: N_2 PNF, bottom: CO_2 PNF.

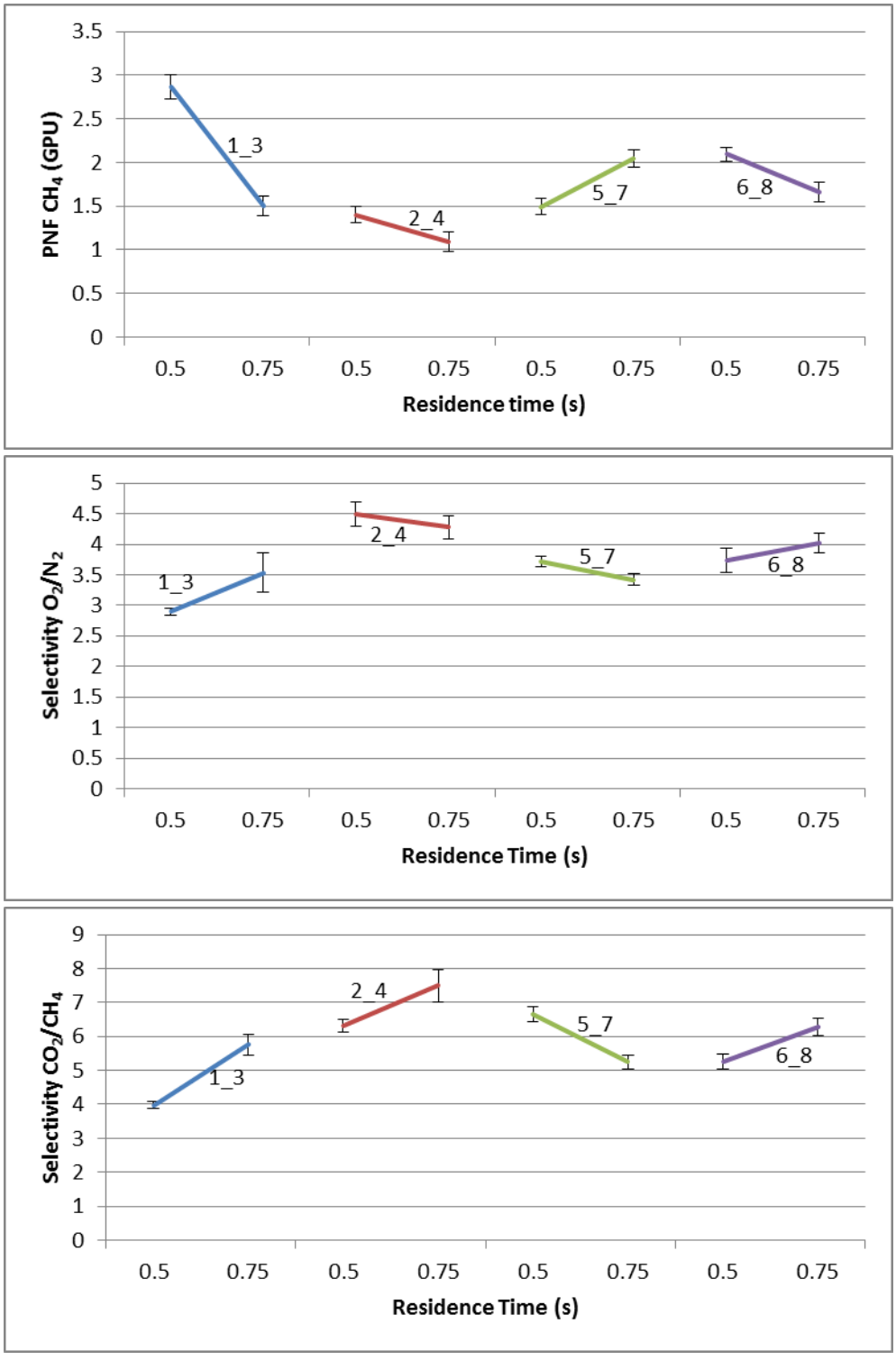

Figure 6.3.3-4: Effects of residence time change on PNF and selectivity values for MB7. Top: CH_4 PNF, middle: selectivity O_2/N_2, bottom: selectivity CO_2/CH_4.

The final factor investigated was the convective gas flow rate. The trends shown in the PNF for as affected by convective gas flow rate are the same for all the test gases. The trend is for the higher convective gas flow rate to give a lower flux. The exception to this is in the comparison for membranes 5 and 6 which show a lower flux at lower gas flow rate. As mentioned in the discussion of the residence time effects it seems that category 5 has produced membranes which are displaying different properties from what they might be predicted to have as it is involved in all the comparisons which seemingly deny the otherwise consistent trends.

When the selectivity of the membranes is considered with respect to changes caused by the gas flow rate the trends are clearer than when the PNF is considered. There is a clear increase in all the selectivity values as the gas flow rate increases in the comparisons which do not contain category 5. This time however the selectivity for the 5_6 comparison shows the same trend as the other categories for the oxygen/nitrogen selectivity so although it still contradicts the other trends in the carbon dioxide/methane chart it is only one of the comparisons which is contradictory. This is reasonable evidence to suggest that the higher of the two gas flow rate settings is the better condition for producing higher selectivity in the membranes.

The error bars for the gas flow rate comparisons display almost no overlaps in the direct comparisons which suggests that they are a good representation of what is occuring.

From the graphs it is expected that the Taguchi analysis will predict that the higher gas flow rate level is better for producing the membranes. It is unclear from the charts how much of an effect the gas flow rate has in comparison to the extrusion rate but it seems likely it will have a stronger influence than the residence time.

The graphs produced and analysed manually suggest that the best set of conditions, of those which were tested, for the production of higher selectivity gas separation membranes are; low extrusion rate, high residence time and high gas flow rate. These conditions correspond to membrane category 4.

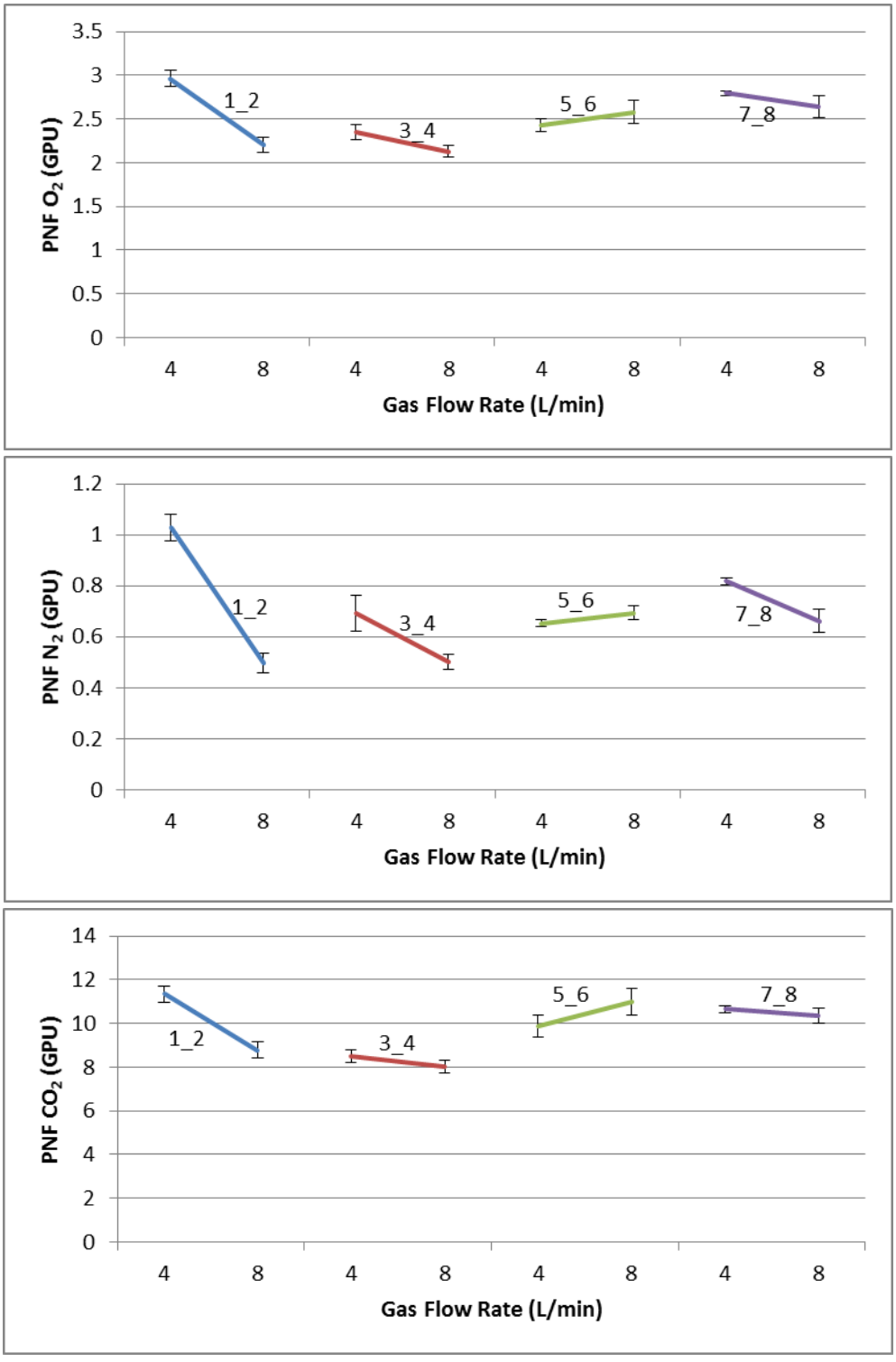

Figure 6.3.3-5: Effects of gas flow rate change on PNF and selectivity values for MB7. Top: O_2 PNF, middle: N_2 PNF, bottom: CO_2 PNF.

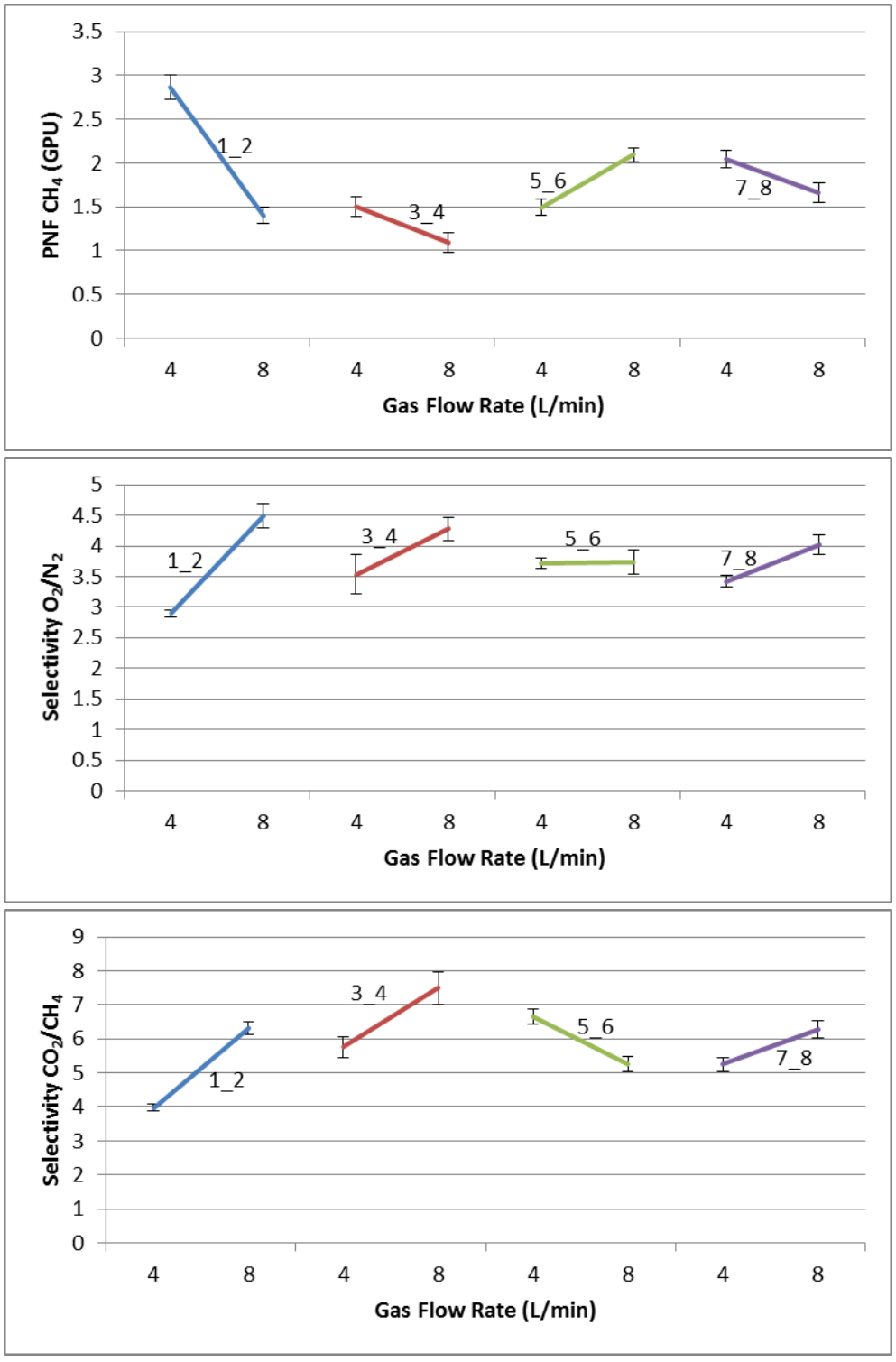

Figure 6.3.3-6: Effects of gas flow rate change on PNF and selectivity values for MB7. Top: CH_4 PNF, middle: selectivity O_2/N_2, bottom: selectivity CO_2/CH_4.

6.3.4. Taguchi Analysis of Twice Coated MB7 Membranes

Returning to the Taguchi method of analysis, it is common practice to utilise signal to noise ratios rather than average values where multiple samples are being used. The signal is the change in the quality characteristic i.e. selectivity, of the experiment in response to factors introduced in the experiment. However, these reults are influenced by other factors or errors which are not necessarily tightly controlled or predictable which are termed the noise factors. The signal to noise ratio (S/N ratio) measures the ratio of the sensitivity of the quality characteristic to the changes produced by the controlled factors to the changes produced by the noise factors. The coefficient of variation has seen extensive use in statistics[44] and the S/N ratio is recognised as the inverse of this as shown in Equation 6.3.4.1.

$$\boldsymbol{S/N = \frac{x}{\sigma}} \qquad \textbf{Equation 6.3.4.1}$$

The higher the value of signal to noise ratio which is found the higher the signal is and the lower the varience in that signal i.e. the noise factors have less effect. This makes the S/N ratio useful as a guide for finding the optimum set of experimental conditions and for comparing two sets of experimental data to determine which provides the best value towards a target value with least variation. The S/N ratio is determined from the mean squared deviation (MSD) as shown in Equation 6.3.4.2 where $Y_1 \ldots Y_N$ are the selectivity values associated with each membrane categories results, N is the number of membranes tested and Y_0 is the target value of selectivity which in this case is set at 5.5 for oxygen and nitrogen (this is the selectivity used in the modeling of the membrane charactersics due to the permeability of PVC films to the gases later in this work). The oxygen and nitrogen results are used for the Taguchi analysis because the final target for the use of these membranes involves oxygen and the literature values for oxygen and nitrogen permeability show less variation than the carbon dioxide and methane values. The signal to noise ratio is then determined from Equation 6.3.4.3.

$$\boldsymbol{MSD = \frac{(Y_1 - Y_0)^2 + (Y_2 - Y_0)^2 + \cdots + (Y_N - Y_0)^2}{N}} \qquad \textbf{Equation 6.3.4.2}$$

$$S/N = -10\log_{10} MSD \qquad \text{Equation 6.3.4.3}$$

The MSD and S/N ratios for the four categories which form part of the Taguchi matrix are shown in Figure 6.3.3-2.

Table 6.3.4-1: Mean squared deviation and S/N ratios for the Taguchi membrane categories

Category	MSD	S/N
1	6.794	-8.321
4	1.656	-2.191
6	3.274	-5.151
7	4.346	-6.381

The signal to noise ratios allow the calculation of the effect which each of the three factors has on the results. This is done by taking the difference of the average S/N ratios for each category of membranes produced at the high and low settings of each factor as shown by Equation 6.3.4.4 for extruion rate.

$$Ext_{eff} = \left(\frac{1}{2}\sum S/N_{i,Ext\uparrow}\right) - \left(\frac{1}{2}\sum S/N_{i,Ext\downarrow}\right)$$

$$Ext_{eff} = \begin{pmatrix} \frac{1}{2} * \left(S/N_6 + S/N_7\right) \\ -\frac{1}{2} * \left(S/N_1 + S/N_4\right) \end{pmatrix} \qquad \text{Equation 6.3.4.4}$$

As these calculations were carried out as high level minus low level S/N ratios a positive value indicated an increase in S/N ratio and a negative value indicated a decrease in S/N ratio going from the lower level to the higher level. Since the aim is to maximise the S/N ratio, as was discussed previously, then a positive value means utilising the factor at its high level is better while a negative value means the low level is better. The average signal to noise ratios for the high and low level of each factor is given in Table 6.3.4-2 along with the difference total. These values indicate that low extrusion rate should be used while residence time and gas flow rate should be kept high which corresponds well with the graphical analysis conclusions that membrane category four is the optimal set-up of those used.

Table 6.3.4-2: Simple factor effects table for high/low level setting determination

Factor	Low Level	High Level	Difference
Extrusion Rate	-5.256	-5.766	-0.510
Residence Time	-6.736	-4.286	2.450
Gas Flow Rate	-7.351	-3.671	3.680

The influence of each of the factors can be quantified more precisely utilising analysis of variance (ANOVA). This analysis attributes a proportion of the varience observed in the experiments to each of the factors which were changed and utilises an error term to take into account any uncontrolled factors which may have changed over the course of the experiments. In the case of this work all the factors during the spinning were rigidly controlled and are not expected to contribute large error terms to the experiments, particularly since all the membrane categories were produced in a single run from the same dope batch. Therefore the error for the spinning conducted is considered to be negligible.

Possible sources of error which were not controlled are the temperature of the water baths and the temperaure during permeation testing. The laboratory for the membrane testing did not have a temperature control facility and it was noted the temperature of the room could vary between 15 and 25°C. Temperature is known to be a factor which influences the results seen when testing gas separation membranes: Duthie *et al*[45] investigated the temperature effects on polyimide membranes and found that temperature affected the diffusivity in the room temperature range significantly. Hwang *et al*[46] studied polysulfone membranes in the operating temperature range of 30°C to 50°C and found that increasing temperature incresed the permeation through the membrane due to increased activation energy of the gases whereas it caused a reduction in selectivity. These works show that the temperature range seen could have an impact and therefore this is included as an error term.

The temperature of the water baths during spinning could also have been affected by the ambient temperature. The volume of water used in the water baths, which was temperature controlled and monitored separately, could only incur small fluctuations which would have minimal influence on the final membrane.

There is a further possible contribution to error during the permeation testing as there were multiple test chambers available but each category was tested separately. Therefore it is possible that in the process of changing the samples being tested the environment within the test chamber could change e.g. humidity however if these changes did occur then they would be small and not expected to have significant impact upon the results obtained.

The percent contribution from each factor to the varience is related to the sums of squares (SS_f) of those factors where; n is the number of categories of membrane tested and S/N_{fj} is the total S/N ratio for the high or low (j) categories of the factor (f) the calculation is for.

$$\boldsymbol{SS_f = \frac{\left(\sum S/N_{f\downarrow} - \sum S/N_{f\uparrow}\right)^2}{n}} \qquad \textbf{Equation 6.4.3.5}$$

The sums of squares for the error term is arrived at differently since its effects have not actually been tested. The equation describing the error sums of squares (SS_E) comes from the S/N ratios but through a more prolonged methodology.

$$\boldsymbol{SS_E = \sum_{i=1}^{n}\left(S/N_i\right)^2 - \frac{1}{n}\left(\sum_{i=1}^{n}\left(S/N_i\right)\right)^2 - \sum SS_f} \qquad \textbf{Equation 6.4.3.6}$$

The varience of each factor including the error term is the sums of squares value divided by its degrees of freedom and this value is used to calculate the F-ratio for each factor. The F-ratio is the ratio of the varience of the factor to the varience of the error term. So where; V is the varience and dof is the degrees of freedom of a factor (f) or error (E) Equation 6.4.3.7 describes the F-ratio for a factor.

$$\boldsymbol{F\text{-}ratio_f = \frac{V_f}{V_E} = \frac{\frac{SS_f}{dof_f}}{\frac{SS_E}{dof_E}}} \qquad \textbf{Equation 6.4.3.7}$$

The pure sum of squares (SS'_f) can also now be calculated for each factor from the varience of that factor and the varience in the error, however since error is not being included in this study then this is not necessary:

$$SS'_f = V_f - V_E \qquad \textbf{Equation 4.3.2.8}$$

This then allows calculation of the percentage effect ($\%_f$) for each factor using the total sums of squares error SS_T, where the use of an error value is required the standard values are used:

$$\%_f = \frac{SS'_f}{SS_T} \qquad \textbf{Equation 4.3.2.9}$$

$$SS_T = \sum SS_f + SS_E \qquad \textbf{Equation 4.3.2.10}$$

Following the ANOVA calculations through with the data collected here gives the results shown in Table 6.3.4-3.

Table 6.3.4-3: ANOVA results for Taguchi analysis

Factor	DOF	Z1	Z2	SS_f	V_f	F-Ratio	SS'_f	%
Extrusion Rate	1	-10.51	-11.53	0.26	0.26	7.32E+12	0.26	1.31%
Residence Time	1	-13.47	-8.57	6.00	6.00	1.69E+14	6.00	30.31%
Gas Flow Rate	1	-14.70	-7.34	13.55	13.55	3.81E+14	13.55	68.38%
Error	1			3.55E-14	3.55E-14			
Total	4							

The ANOVA table suggests that gas flow rate has the biggest influence on the varience seen in the experiments followed by the residence time and finally the extrusion rate. Meanwhile the error term is too small to make a meaningful contribution to the varience in the results observed. The magnitudes of the effects predicted from the analysis are not exactly what was expected

from the graphical analysis really due to the small varience effect which is seen from the extrusion rate in the analysis. It was predicted that gas flow rate would show a greater impact than the residence time but the effect of the extrusion was less sure. The fact that nearly all the low extrusion rate selectivities were better than their high extrusion rate counterparts in the graphs suggested that there was a definitve varience effect from this factor, however the differences seen in the oxygen/nitrogen selectivity in the graphs are small in spite of the consistency and this results in a low impact on the Taguchi analysis.

The final stage of the Taguchi analysis is the prediction of the result which would be seen at the optimal conditions. Since all the possible combinations of parameters were produced in the work, despite not being required by the Taguchi, then the predicted best condition set has been produced and corresponds to category 4. As a result the Taguchi analysis should predict the selectivity achieved with category 4 which over the 5 membranes tested gave a mean value of 4.27.

In order to determine the the optimum condition the grand average of performance, T, must be found across the categories.

$$\boldsymbol{T = \frac{1}{n}\sum_{i=1}^{4} S/N_i} \qquad \textbf{Equation 4.3.2.11}$$

In this case all the factors are considered significant to include in the prediction because the error contribution from other factors is so low and hence the F-ratio large. With this being the case the expected result, E_R, from the factors can be calculated from the factor effects at the optimal condition and the grand mean. Hence, the factor effects used are for the low extrusion rate, $F_{Ext,L}$, the high residence time, $F_{Res,H}$, and the high gas flow rate, $F_{Gas,H}$.

$$\boldsymbol{E_R = T + \left(T - F_{Ext,L}\right) + \left(T - F_{Res,H}\right) + \left(T - F_{Gas,H}\right)} \qquad \textbf{Equation 4.3.2.12}$$

The contribution for each factor, C, is determined from the difference between the optimal signal to noise ratio for that factor and the grand mean such that for the extrusion rate factor Equation

4.3.2.13 gives the contribution. The total contribution to the optimal condition from all the factors is then the total of the individual contributions.

$$\boldsymbol{C_{Ext} = F_{Ext,L} - T} \qquad \textbf{Equation 4.3.2.13}$$

These calculations result in a grand mean of -5.51 and an expected result of -2.19. The contributions to these results is summarised in Table 6.3.4-4.

Table 6.3.4-4: Summary of contributions to the optimal set of factors

Factor	Optimal Condition	Level	Factor Effects	Contribution
Extrusion Rate	2cm^3/s	L	-5.256	0.255
Residence Time	0.74s	H	-4.286	1.225
Gas Flow Rate	8L/min	H	-3.671	1.840
			Total	3.320

The expected result is the signal to noise ratio of the optimal set of conditions and can be related to the MSD by Equation 4.3.2.14.

$$\boldsymbol{S/N = -10\log(MSD) = -2.19}$$
$$\boldsymbol{MSD = 1.66} \qquad \textbf{Equation 4.3.2.14}$$

The MSD is the deviation from the the target result which could be expected and hence where the maximum selectivity expected is 5.5 the predicted selectivity of the optimal set-up using the conditions specified in the matrix result in:

$$\boldsymbol{\Omega_{O_2/N_2} = 5.5 - 1.66 = 4.21} \qquad \textbf{Equation 4.3.2.15}$$

The mean value obtained from the Taguchi analysis compares well with the 4.27 actually found and agrees with what was predicted to be the best option by the graphical methods on the full eight category production run.

The results of comparison by both graphical and Taguchi methods shows validation of the use of Taguchi methods for design applications using polymer gas separation membranes. However, the results are limited by both the number of factors which were investigated and the range of parameters used. The Taguchi analysis results in finding the best set of parameters of those tested with this methodology and hence the more factors and levels investigated the more accurate the results will be although these benefits have to be traded off against the cost and time implications of conducting the experiments. The small scale example here demonstrates the applicability of the system against a full investigation and finds the use justified.

Overall membrane category 4 is seen to have been produced under the best set of conditions for producing the desired selectivity of those tested. This category was hence focused on when producing membranes to determine the ozone separations and also in the characterisation processes.

6.4. Bibliography

1. Zhang, L, He, G, Zhao, W, Nie, F, Li, X, and Tan, M, *Studies on the coating layer in a PTFPMS/PEI composite membrane for gaseous separation.* Journal of Membrane Science, 2011. **371**(1–2): p. 141-147.
2. Pagliero, C, Marchese, J, and Ochoa, N, *Effect of coating procedure on composite gas separation membrane performance.* Gas Separation & Purification, 1993. **7**(3): p. 147-149.
3. Alentiev, AY and Yampolskii, YP, *Free volume model and tradeoff relations of gas permeability and selectivity in glassy polymers.* Journal of Membrane Science, 2000. **165**(2): p. 201-216.
4. Barbari, TA, *Dual-mode free volume model for diffusion of gas molecules in glassy polymers.* Journal of Polymer Science Part B-Polymer Physics, 1997. **35**(11): p. 1737-1746.
5. Paul, DR and Yampol'skii, YP, *Polymeric gas separation membranes,* 1994, Boca Raton: CRC Press. x, 623 p.
6. Thran, A, Kroll, G, and Faupel, F, *Correlation between fractional free volume and diffusivity of gas molecules in classy polymers.* Journal of Polymer Science Part B-Polymer Physics, 1999. **37**(23): p. 3344-3358.
7. Chen, Y, Fouda, AE, Matsuura, T. in *Advances in Reverse Osmosis and Ultrafiltration*. 1989. Vancouver: National Research Council of Canada.
8. Ismail, AF, Dunkin, IR, Gallivan, SL, and Shilton, SJ, *Production of super selective polysulfone hollow fiber membranes for gas separation.* Polymer, 1999. **40**(23): p. 6499-6506.
9. Lo, C-H, Hung, W-S, De Guzman, M, Huang, S-H, Li, C-L, Hu, C-C, Jean, Y-C, Lee, K-R, and Lai, J-Y, *Investigation on CO2-induced plasticization in polycarbonate membrane using positron annihilation lifetime spectroscopy.* Journal of Membrane Science, 2010. **363**(1–2): p. 302-308.
10. Huang, Y-H, Chao, W-C, Hung, W-S, An, Q-F, Chang, K-S, Huang, S-H, Tung, K-L, Lee, K-R, and Lai, J-Y, *Investigation of fine-structure of polyamide thin-film composite membrane*

under swelling effect by positron annihilation lifetime spectroscopy and molecular dynamics simulation. Journal of Membrane Science, 2012. **417–418**(0): p. 201-209.

11. Li, FY, Li, Y, Chung, T-S, Chen, H, Jean, YC, and Kawi, S, *Development and positron annihilation spectroscopy (PAS) characterization of polyamide imide (PAI)–polyethersulfone (PES) based defect-free dual-layer hollow fiber membranes with an ultrathin dense-selective layer for gas separation.* Journal of Membrane Science, 2011. **378**(1–2): p. 541-550.
12. Li, C-L, Huang, S-H, Hung, W-S, Kao, S-T, Wang, D-M, Jean, YC, Lee, K-R, and Lai, J-Y, *Study on the influence of the free volume of hybrid membrane on pervaporation performance by positron annihilation spectroscopy.* Journal of Membrane Science, 2008. **313**(1–2): p. 68-74.
13. Hu, C-C, Lee, K-R, Ruaan, R-C, Jean, YC, and Lai, J-Y, *Gas separation properties in cyclic olefin copolymer membrane studied by positron annihilation, sorption, and gas permeation.* Journal of Membrane Science, 2006. **274**(1–2): p. 192-199.
14. Wate, S, Acharya, NK, Bhahada, KC, Vijay, YK, Tripathi, A, Avasthi, DK, Das, D, and Ghughre, S, *Positron annihilation lifetime and gas permeation studies of energetic ion-irradiated polycarbonate membranes.* Radiation Physics and Chemistry, 2005. **73**(5): p. 296-301.
15. Schrader, DM and Jean, YC, *Positron and positronium chemistry*. Studies in physical and theoretical chemistry1988, Amsterdam The Netherlands ; New York: Elsevier. xiii, 395 p.
16. Qin, J-J and Chung, T-S, *Effects of orientation relaxation and bore fluid chemistry on morphology and performance of polyethersulfone hollow fibers for gas separation.* Journal of Membrane Science, 2004. **229**(1–2): p. 1-9.
17. Cao, C, Chung, T-S, Chen, SB, and Dong, Z, *The study of elongation and shear rates in spinning process and its effect on gas separation performance of Poly(ether sulfone) (PES) hollow fiber membranes.* Chemical Engineering Science, 2004. **59**(5): p. 1053-1062.
18. Chung, T-S, Lin, W-H, and Vora, RH, *The effect of shear rates on gas separation performance of 6FDA-durene polyimide hollow fibers.* Journal of Membrane Science, 2000. **167**(1): p. 55-66.

19. Ismail, AF, Shilton, SJ, Dunkin, IR, and Gallivan, SL, *Direct measurement of rheologically induced molecular orientation in gas separation hollow fibre membranes and effects on selectivity.* Journal of Membrane Science, 1997. **126**(1): p. 133-137.

20. Qin, J-J, Wang, R, and Chung, T-S, *Investigation of shear stress effect within a spinneret on flux, separation and thermomechanical properties of hollow fiber ultrafiltration membranes.* Journal of Membrane Science, 2000. **175**(2): p. 197-213.

21. Wu, S-J, Shiah, S-W, and Yu, W-L, *Parametric analysis of proton exchange membrane fuel cell performance by using the Taguchi method and a neural network.* Renewable Energy, 2009. **34**(1): p. 135-144.

22. Wu, H-W and Gu, H-W, *Analysis of operating parameters considering flow orientation for the performance of a proton exchange membrane fuel cell using the Taguchi method.* Journal of Power Sources, 2010. **195**(11): p. 3621-3630.

23. Chang, K-Y, Lin, H-J, and Chen, P-C, *The optimal performance estimation for an unknown PEMFC based on the Taguchi method and a generic numerical PEMFC model.* International Journal of Hydrogen Energy, 2009. **34**(4): p. 1990-1998.

24. Pourjafar, S, Jahanshahi, M, and Rahimpour, A, *Optimization of TiO2 modified poly(vinyl alcohol) thin film composite nanofiltration membranes using Taguchi method.* Desalination, (0).

25. Gönder, ZB, Kaya, Y, Vergili, I, and Barlas, H, *Optimization of filtration conditions for CIP wastewater treatment by nanofiltration process using Taguchi approach.* Separation and Purification Technology, 2010. **70**(3): p. 265-273.

26. Idris, A, Ismail, AF, Noordin, MY, and Shilton, SJ, *Optimization of cellulose acetate hollow fiber reverse osmosis membrane production using Taguchi method.* Journal of Membrane Science, 2002. **205**(1–2): p. 223-237.

27. Roy, RK, *A primer on the Taguchi method*1990, Dearborn, Mich.: Society of Manufacturing Engineers. xiii, 247 p.

28. Sharpe, ID, Ismail, AF, and Shilton, SJ, *A study of extrusion shear and forced convection residence time in the spinning of polysulfone hollow fiber membranes for gas separation.* Separation and Purification Technology, 1999. **17**(2): p. 101-109.

29. Ismail, AF, Ng, BC, and Abdul Rahman, WAW, *Effects of shear rate and forced convection residence time on asymmetric polysulfone membranes structure and gas separation performance.* Separation and Purification Technology, 2003. **33**(3): p. 255-272.

30. Gordeyev, SA and Shilton, SJ, *Forced convection spinning of gas separation hollow fibre membranes: some underlying factors, mechanisms and effects.* Journal of Membrane Science, 2004. **229**(1-2): p. 225-233.

31. Bakeri, G, Ismail, AF, Rahimnejad, M, Matsuura, T, and Rana, D, *The effect of bore fluid type on the structure and performance of polyetherimide hollow fiber membrane in gas–liquid contacting processes.* Separation and Purification Technology, 2012. **98**(0): p. 262-269.

32. Rahbari-sisakht, M, Ismail, AF, and Matsuura, T, *Effect of bore fluid composition on structure and performance of asymmetric polysulfone hollow fiber membrane contactor for CO2 absorption.* Separation and Purification Technology, 2012. **88**(0): p. 99-106.

33. Tan, X, Liu, N, Meng, B, and Liu, S, *Morphology control of the perovskite hollow fibre membranes for oxygen separation using different bore fluids.* Journal of Membrane Science, 2011. **378**(1–2): p. 308-318.

34. Wallace, DW, Staudt-Bickel, C, and Koros, WJ, *Efficient development of effective hollow fiber membranes for gas separations from novel polymers.* Journal of Membrane Science, 2006. **278**(1–2): p. 92-104.

35. Li, DF, Chung, T-S, Wang, R, and Liu, Y, *Fabrication of fluoropolyimide/polyethersulfone (PES) dual-layer asymmetric hollow fiber membranes for gas separation.* Journal of Membrane Science, 2002. **198**(2): p. 211-223.

36. Pesek, SC and Koros, WJ, *Aqueous quenched asymmetric polysulfone membranes prepared by dry/wet phase separation.* Journal of Membrane Science, 1993. **81**(1–2): p. 71-88.

37. McKelvey, SA, Clausi, DT, and Koros, WJ, *A guide to establishing hollow fiber macroscopic properties for membrane applications.* Journal of Membrane Science, 1997. **124**(2): p. 223-232.

38. Kapantaidakis, GC, Koops, GH, and Wessling, M, *Effect of spinning conditions on the structure and the gas permeation properties of high flux polyethersulfone—polyimide blend hollow fibers.* Desalination, 2002. **144**(1–3): p. 121-125.

39. Hasbullah, H, Kumbharkar, S, Ismail, AF, and Li, K, *Preparation of polyaniline asymmetric hollow fiber membranes and investigation towards gas separation performance.* Journal of Membrane Science, 2011. **366**(1–2): p. 116-124.

40. Khayet, M, *The effects of air gap length on the internal and external morphology of hollow fiber membranes.* Chemical Engineering Science, 2003. **58**(14): p. 3091-3104.

41. Khayet, M, García-Payo, MC, Qusay, FA, and Zubaidy, MA, *Structural and performance studies of poly(vinyl chloride) hollow fiber membranes prepared at different air gap lengths.* Journal of Membrane Science, 2009. **330**(1–2): p. 30-39.

42. Khulbe, KC, Feng, CY, Hamad, F, Matsuura, T, and Khayet, M, *Structural and performance study of micro porous polyetherimide hollow fiber membranes prepared at different air-gap.* Journal of Membrane Science, 2004. **245**(1–2): p. 191-198.

43. Wang, DL, Li, K, and Teo, WK, *Preparation and characterization of polyetherimide asymmetric hollow fiber membranes for gas separation.* Journal of Membrane Science, 1998. **138**(2): p. 193-201.

44. Barker, TB, *Quality Engineering by Design - Taguchis Philosophy - a Look at an Example of Taguchis Ideas Being Put into Action.* Quality Progress, 1986. **19**(12): p. 32-42.

45. Duthie, X, Kentish, S, Powell, C, Nagai, K, Qiao, G, and Stevens, G, *Operating temperature effects on the plasticization of polyimide gas separation membranes.* Journal of Membrane Science, 2007. **294**(1–2): p. 40-49.

46. Hwang, HY, Nam, SY, Koh, HC, Ha, SY, Barbieri, G, and Drioli, E, *The effect of operating conditions on the performance of hollow fiber membrane modules for CO2/N2 separation.* Journal of Industrial and Engineering Chemistry, 2012. **18**(1): p. 205-211.

7. Membrane Characterisation

7.1. Surface Imaging

7.1.1. Importance of Surface Imaging to Membrane Processes

The gas transport through membranes is governed by a combination of the transport mechanisms which have been discussed above. Any of the above methods can provide separation of some sort depending upon the system which is being studied however generally for gas separation processes the separation factor which is achieved is best for solution diffusion and worst for viscous flow. The type of flow which is achieved through the membrane is inextricably linked to the size of the pores which are present. It is therefore very important for understanding the types of flow which will be achieved by a membrane to find characterisation methods which can grant information on the surface morphology of the membranes which are being produced.

It is worth noting that some general information on what might be expected from surface images might be gleaned by comparing the achieved separation characteristics of produced membranes to those achieved in the literature or known values. In order to confirm this however surface imaging techniques may be utilised to look for surface pores. The flow mechanism seen may be influenced not only by the size of the pores but also by the number of them: even although Knudsen diffusion is a much faster transport mechanism it is possible that good separation could still be achieved by a membrane which shows very few pores which are of a size for Knudsen diffusion to occur. This can present a conundrum for imaging techniques since the sample size is generally small and it takes time to map larger areas.

The main imaging technique which has gained popularity in membrane characterisation is scanning electron microscopy (SEM)[1-4]. It is used both to confirm the absence of large pores and also in the case of mixed matrix membranes to study the dispersion of the inclusions and how they appear at the surface of the membrane. An SEM uses a beam of electrons in order to produce images at high magnification with high resolution. The interactions between the electrons and the surface can be detected and it is the results of these interactions which are

used in order to build up the picture. In order to be used with SEM the samples of non-conducting polymer membranes must be gold coated before being put into the imaging chamber as for conventional SEM techniques the sample must be conductive. The gold coating applies only a very thin layer to the sample and thus preserves the contours and shapes on the surface.

7.1.2. SEM Imaging of PVC Membranes

For this work SEM images were obtained for each of the eight categories produced in spin run MB7. It was hoped that by doing this an explanation for some of the patterns observed for MB7 could be found and also to provide an opportunity to look at the pore sizes in the membranes.

In order to produce samples for imaging a membrane was selected and placed into liquid nitrogen. The liquid nitrogen was used because hollow fiber membranes exhibit a tendency to collapse at the point through which they are cut making cross sectional images difficult to achieve of high quality. This collapse can be displayed in two forms either the bore of the fiber closes up or the structure itself becomes compressed due to the force applied in order to cut the membrane. Liquid nitrogen dipping is generally recognised as being a good way to mitigate against these issues. In this work various dipping times into the liquid nitrogen were tried ranging from a 1second soak to a 15min soak unfortunately this did not show the expected effects when it came to cutting the membranes and both collapse effects were seen. For this reason obtaining a good image for a full cross section of the membranes was not possible and only sections of the cross sectional area are shown here.

Following being cut the membranes were mounted on platforms using black carbon tape to support them in place. The membranes on the platforms were then gold coated using a gas flow sputtering technique which coated the membranes in a thin film of gold. The gold coating is necessary as for SEM imaging the material being imaged has to be conductive in order to obtain a clear image. The gold coating is thin enough that it does not have a significant effect on the nature of the surfaces being imaged during the SEM. The gold coated membranes were then transferred into the vacuum chamber where the imaging occurred.

The first images were taken before the coating process was utilised and showed the surfaces and also the ends of the membranes. First the images of the ends of the membrane were studied. There were some difficulties in obtaining a cut through the membranes which would leave the ends undamaged in order to view the structure and this made the use of the SEM images in order to estimate active layer thickness difficult, however a rough estimate of 250nm is made for this from some of the better images. The active layer thickness will vary between membrane categories depending on the conditions under which they were spun but these differences are likely to be small and would require a very clean cut through the membrane in order to give an image which could show these differences effectively. In many works the images produced by SEM show the porous network in the membrane substructure as an open porous structure consisting of many small interlinked open porous areas[3, 5] others show much larger voids running through the substructure of the membrane[6, 7]. Other images including those of the PVC membranes in this work show larger voids towards the outer regions of the membrane but a structure of much smaller pores towards the middle of the membrane wall[8].

This morphology over a cross section of the membranes combined with the gas separation parameters which were found in MB7 suggests that, in general for the categories, the dope solution composition at the outer surface is entering the spinodal decomposition region and instantaneously demixing to produce a very thin layer the surface of which coalesces by capillary pressure. It is thought this layer exists as the separation factors suggest that there is a dense layer present in the membranes even though from the SEM images it is difficult to assess the presence of this layer. It is possible the surface has been close to being able to produce the required dense configuration for gas separation and the coating process has been enough to tip the resistance balance in the favour of solution diffusion. The separation factors achieved are greater than those that would be seen for polydimethylsiloxane alone (2.21 for oxygen/nitrogen pair) and therefore there has to be a contribution from the PVC material.

With a very thin imperfect skin the layers near the outer surface of the membrane would phase separate very quickly on immersion into the coagulation baths. This rapid separation produces the larger pores seen near the edge of the membrane but then as the rate of solvent encroachment decreases then the phase separation occurs more rapidly leading to the porous network of smaller voids in the centre of the wall. At the inner surface the same effect is repeated

as the membrane is immediately exposed to the bore fluid on spinning but with the reduced water activity of the bore fluid due to potassium acetate this only cause macrovoids near the inner surface. Again as the solvent front encroaches from the inner diameter of the membrane it also results in a more closely packed structure with smaller voids than near the edges.

The PVC membranes proved difficult to cut in such a manner as to avoid collapsing the end of the hollow fibers and therefore obscuring the details which could be obtained about the surface layers of the fiber from a cross sectional viewpoint. In particular it made seeing a dense layer at the surface challenging as the ends of the membranes tended to collapse over the region where this would be seen. The best photos obtained for each category are shown in the images below to illustrate the discussion above. For each category the image on the left shows a section across the full wall thickness and the second image shows a closer view on the external wall.

While it does appear from the images that the voids do not extend all the way to the surface of the membrane the outer regions still appear to possess a nodular characteristic rather than a completely dense layer. This indicates that the nodules being produced during the dry phase are too hard to coalesce completely under the capillary pressure which is experienced during the spinning. However as the coated membranes are producing greater than Knudsen diffusion selectivity the active layer must be adequately complete following coating to encourage the dominance of a solution diffusion mechanism and it follows that the nodules in the surface are very closely packed to deny gas transport. This also suggests that the surface nodules were very close to forming a complete active layer.

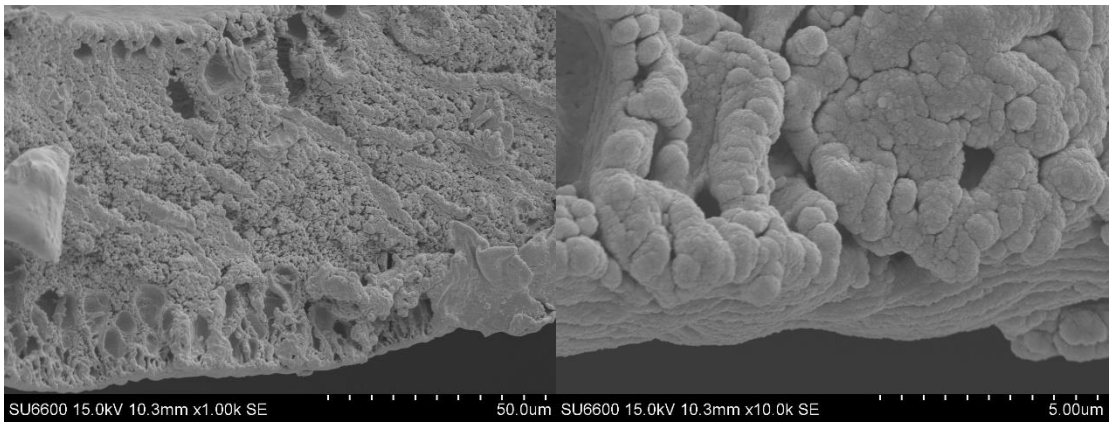

Figure 7.1.2-1: MB7 category 1 fiber end views

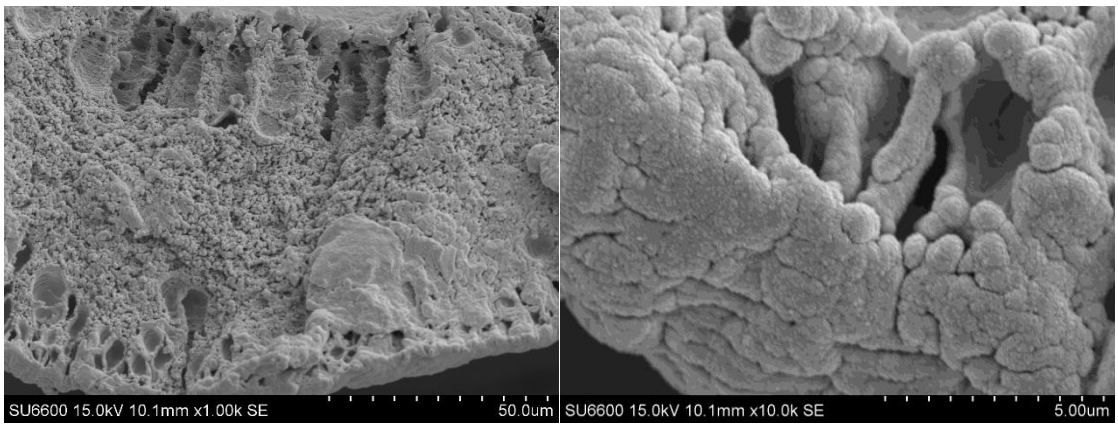

Figure 7.1.2-2: MB7 category 2 fiber end views

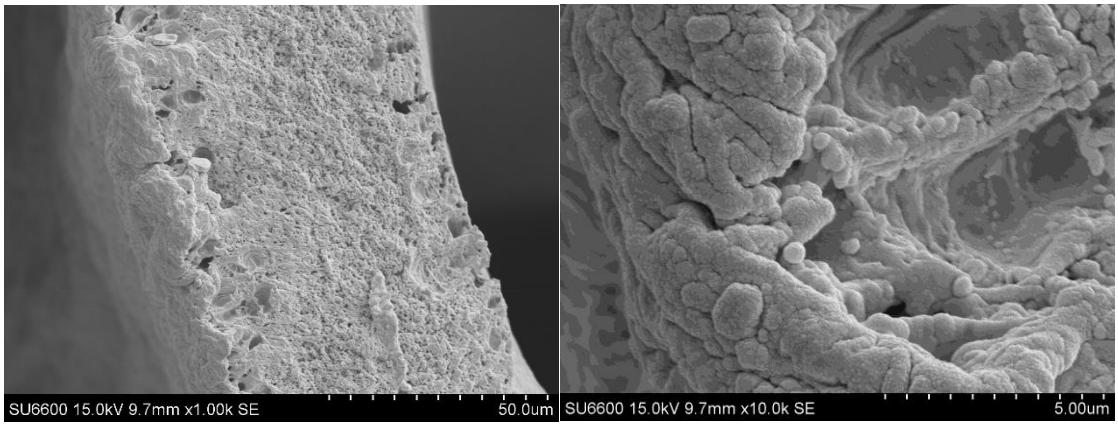

Figure 7.1.2-3: MB7 category 3 fiber end views

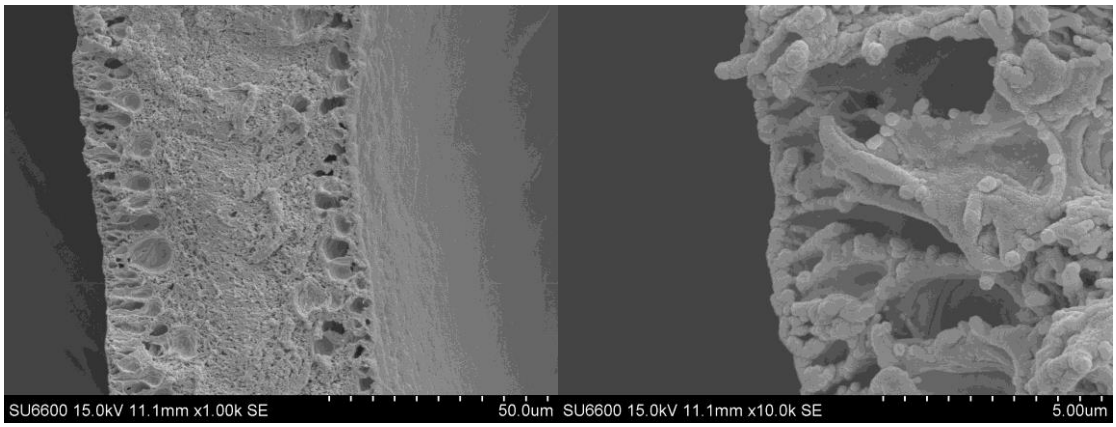

Figure 7.1.2-4: MB7 category 4 fiber end views

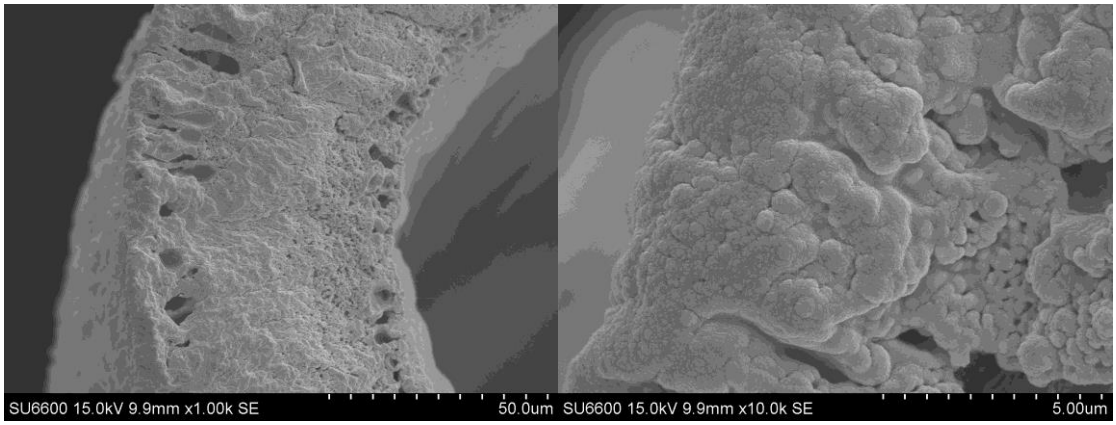

Figure 7.1.2-5: MB7 category 5 fiber end views

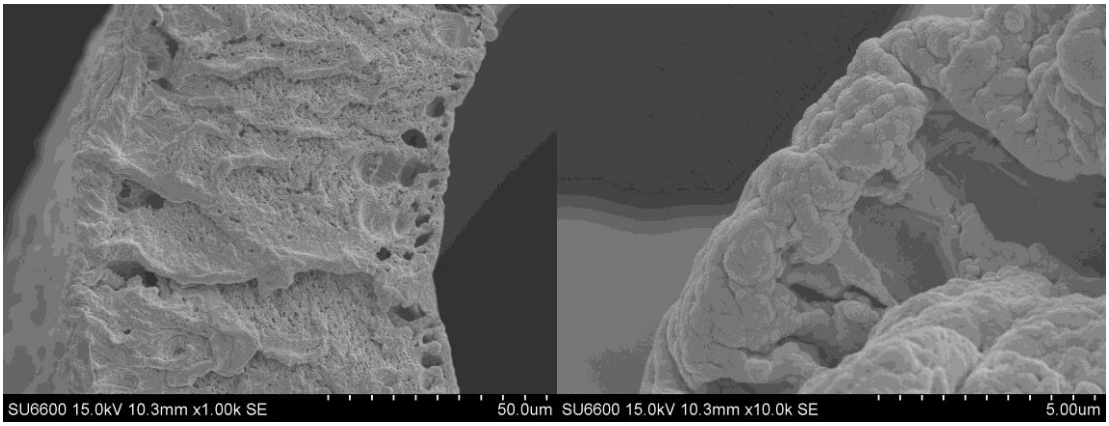

Figure 7.1.2-6: MB7 category 6 fiber end views

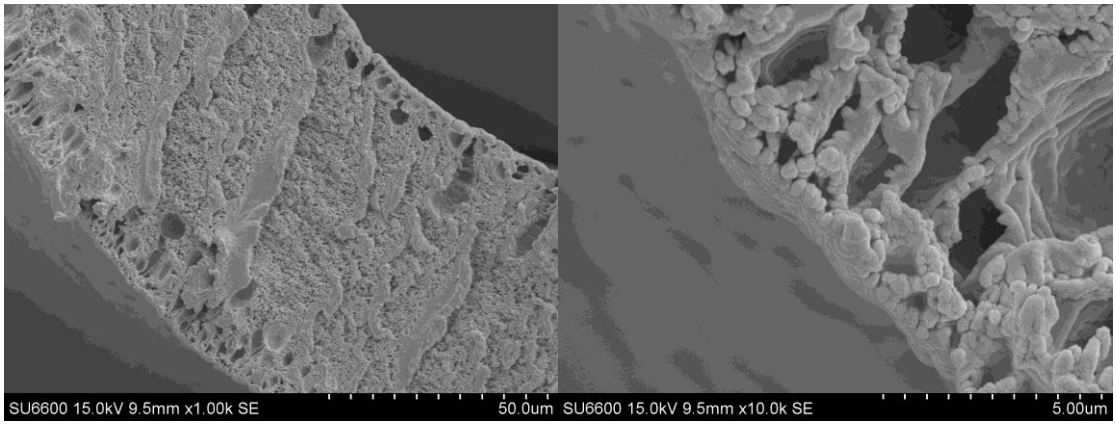

Figure 7.1.2-7: MB7 category 7 fiber end views

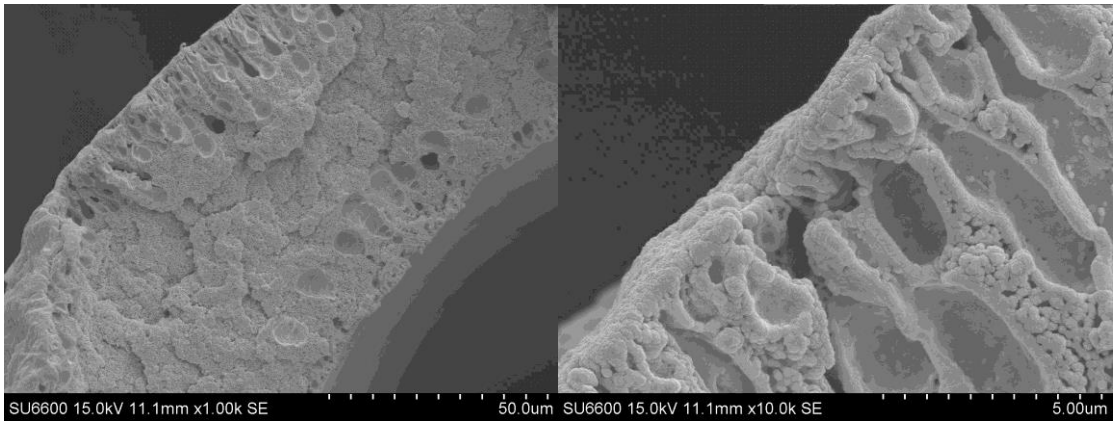

Figure 7.1.2-8: MB7 category 8 fiber end views

In addition to the images of the fiber ends images were also taken of the external surfaces of the membranes. By taking these images it was hoped to be able to identify if there were larger pores present in the surface and to see if there were still nodules present on the membranes as may have been indicated by what is visible of the surfaces in the cross sections. Images were taken as at a magnification of 60k times of all the surfaces. Under this magnification the samples were becoming charged by the electron beam and this was causing blurred images when looking at a largely flat surface. However, what the images show clearly is that there was very little difference between the surfaces of the membranes produced for each category.

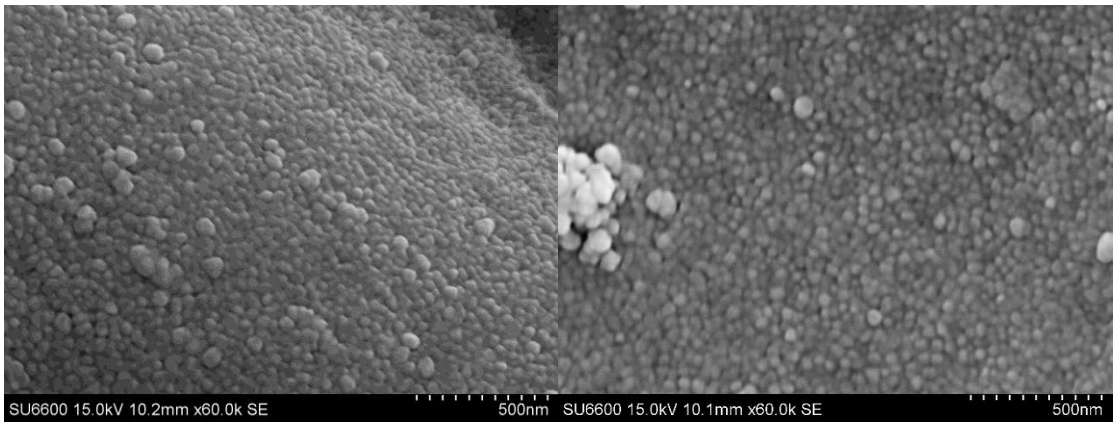

Figure 7.1.2-9: MB7 category 1 60K magnification

Figure 7.1.2-10: MB7 category 2 60K magnification

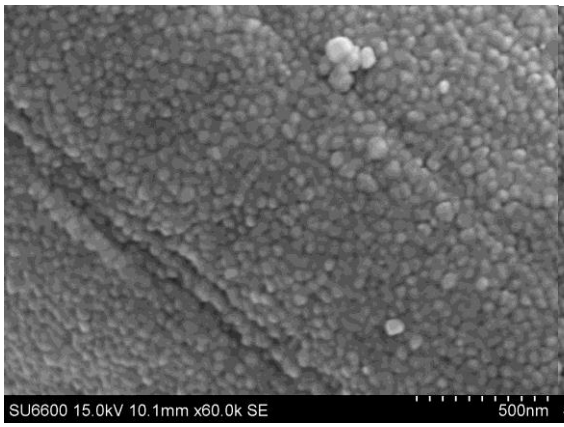

Figure 7.1.2-11: MB7 category 3 60K magnification

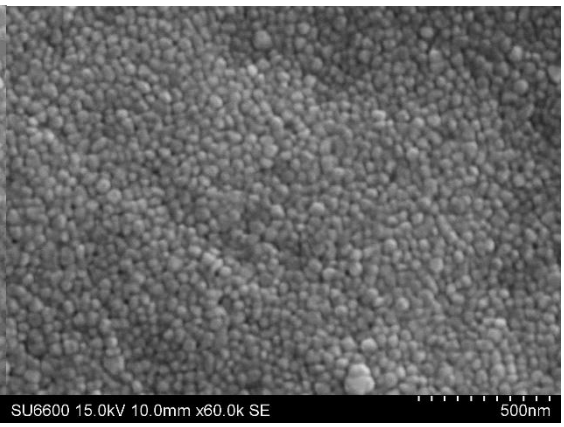

Figure 7.1.2-12: MB7 category 4 60K magnification

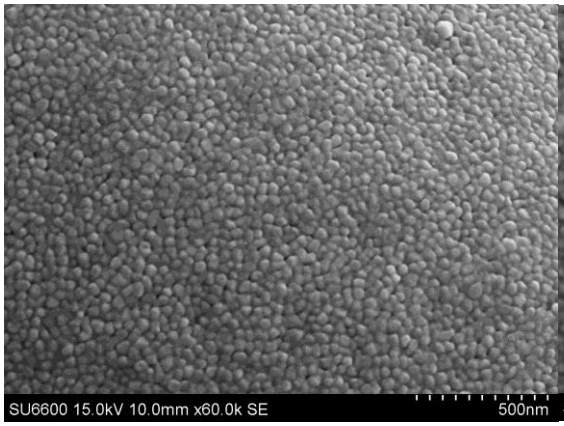

Figure 7.1.2-13: MB7 category 5 60K magnification

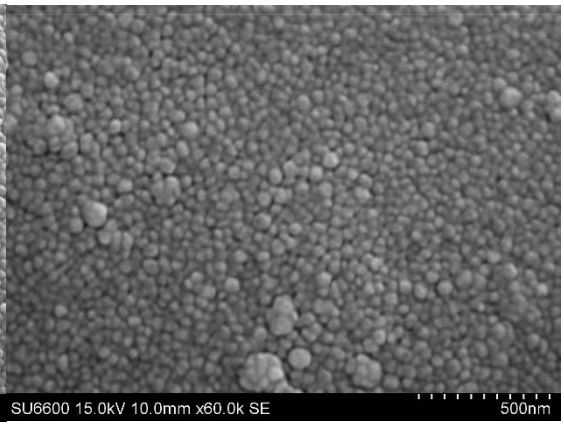

Figure 7.1.2-14: MB7 category 6 60K magnification

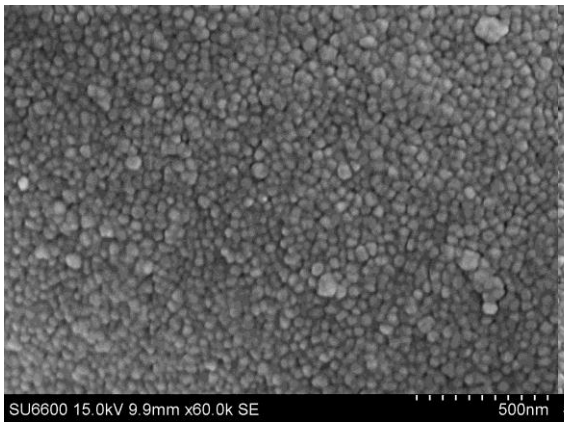

Figure 7.1.2-15: MB7 category 7 60K magnification

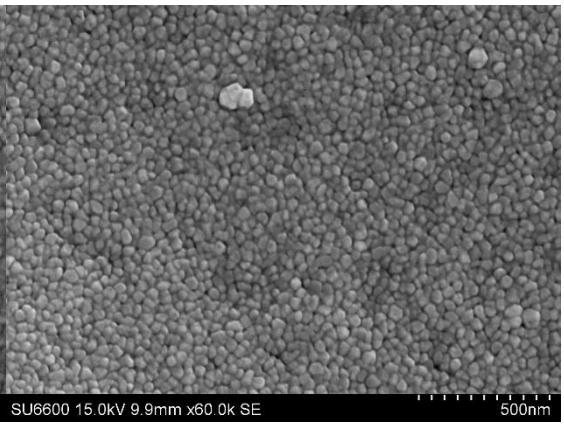

Figure 7.1.2-16: MB7 category 8 60K magnification

The images do show a nodular structure on the surface which confirms the idea that the nodules formed during the dry phase have not been subjected to a high enough pressure in order to coalesce the top surface layer fully. However, the nodules faces do appear to fit quite closely together which suggests that the pressure has been high enough to shape them if not merge the areas of high polymer concentration produced during the phase inversion as suggested above. This may explain why the membranes show no sign of separating qualities before being coated as with the nodular structure there are still small spaces which have not been filled by the deformation of the nodules but the coating process is enough to fill these areas. Indeed there are a few hints of darker areas which may show these pores in the photos particularly in the bottom right of the image for category 8. The size of these pores is approximately 150nm.

Feng *et al 2013*[9, 10] reported on surface imaging utilising atomic force spectroscopy (AFM) on hollow fiber membranes produced from polyetherimide (PEI) while altering the bore fluid flow rate. They found that the membrane outer surface nodules showed elongation which increased when the bore fluid flow rate was lower. The explanation provided in the paper for this was that at lower flow rates the membrane spent a longer time in the dry gap and this led to a stretching of the membrane under gravitational influence and therefore elongated the nodules as they formed. Additionally they noted elsewhere in the paper that the dope solution velocity was increased with the bore fluid velocity and the increased shear this would cause within the spinneret before extrusion could lead to a higher degree of molecular orientation which for long molecules could then lead to elongated nodules. In the images of the PVC membranes above there does not appear to be much elongation of the nodules which suggests that either the polymer solution flow rate was not enough to induce this effect, nodules formed are too hard to be stretched by gravity during the air gap or the air gap time was not long enough to give elongated nodules. The air gap in the work by Feng was 80cm which is much larger than the air gap used for the PVC membranes in this work but had no forced convection. Producing PVC membranes with a less aggressive air gap may lead to results more similar to that seen in the above work however it was also noted that they also saw pores between the nodules approximately sized 40-80nm which is in line with the pore size in the PVC membrane images above. The nodule size in the work by Feng is averaged at 63nm which is also similar sized to the nodules in the images above. The use of a less aggressive air gap may also have benefits for the

ability to coalesce the nodules produced in the gap as it may be expected that a less aggressive gap would lead to lower penetration into the phase diagram and hence softer nodules.

The surface images displayed in Figure 7.1.2-9 to Figure 7.1.2-16 show an outer surface which is similar to those which are seen in other types of membrane. Another feature which the PVC membranes have in common with other membranes is that the surface when considered from a less highly magnified position exhibit a wave like structure on the surface with the ripples running in an axial direction along the membrane. This rippling is thought to occur as a result of reduction in volume as the membrane solidifies and the structure of the outer layer not being strong enough to withstand this reduction in volume without changing shape. The rippling effect is shown in Figure 7.1.2-17 to Figure 7.1.2-24.

However, the PVC membranes also showed some surface features which are different from those normally seen on membranes and are unwelcome for separations purposes. Figure 7.1.2-17 to Figure 7.1.2-24 also show a rip in the surface of the membrane which was present in each category, the features look almost identical on each membrane category and there was no pattern discernible in regularity of the rip so a selection of magnifications are shown for the different categories.

The widths of these rips varied within a single category and even on the same small section, this is demonstrated by the images for category 2 and 5 where it can be seen that the width dimension changes around the circumference of the membrane. The largest rip found during the SEM session is that imaged in Figure 7.1.2-19 and is 20μm across, generally the range seen was between 5 and 20μm. The other feature of the rips which is consistent among all the membranes is that they occur in the surface layer but below this it can be seen that the porous substructure is as would be expected. The fact that the damage is not visible on the porous substructure suggests the membrane is ripping before the substructure is fully formed and the substructure is therefore able to react to the forces acting on the membrane in a manner in which the surface layer is not.

For this to be the case the rip is forming either during the dry step or not long after this. One possible contribution is from the jet stretch ratio between the spinneret extruding the fiber and the wind-up drum collecting it. If a high enough jet stretch ratio was being used then it may be

possible for the surface layer to solidify at a point far enough in advance of the supporting substructure and in a thin enough layer that it could not support the fiber against the effect of gravity and the jet stretch ratio combined. Since the outer layer could not stretch in the solidified form in a manner to match the substructure then the solidifying layer gets pulled apart revealing the sub layers beneath. There is evidence for this kind of stretching motion forming the rips in the images for category 3 and 4 where there appear to be small tendrils from the edge of the strips as would be seen from the ductile failure of a tensile specimen. The exposed sub-layers would then be exposed immediately to the water in the quench baths and this could also explain the large size of the pores seen at these surfaces due to rapid de-mixing of the solution. However, against this point is the fact that the wind-up rates were equal to the extrusion rates for this work i.e. the jet stretch ratio was 1 so the only force acting on the fiber being spun is gravity. In order for gravity to be responsible it could be that the nodule stretching noticed by *Feng et al*[9, 10] is going further and causing the fracture since the nodules are too hard to stretch during the production process.

Another possible mechanism may be that a process similar to the volume reduction which causes the rippling effect is at play. In order for coalescence of nodules to occur there is a force acting to pull nodules together, for a homogeneous surface all the capillary forces responsible for this balance each other out and the surface layer holds together as is coalesces but if this force were to be locally unbalanced the combined effect may result in nodules being pulled in one direction or another. If the effect was large enough then it may lead to the surface pulling itself apart. In the spinning system used it is difficult to identify a possible source to introduce this kind of inbalance to the system but perhaps the high flow convective gas flow rate impingement zone area could result in buffeting the membrane to the extent where this happens.

Of these two mechanisms the first is by far the most likely reason behind the rips and it may be the case that for the active layer forming in the spinning process gravity is enough force by itself over the drop between the spinneret and coagulation bath to cause a tear in these membranes.

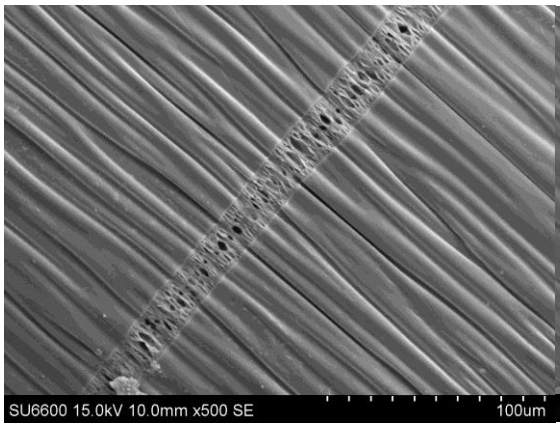

Figure 7.1.2-17: Category 1 surface feature

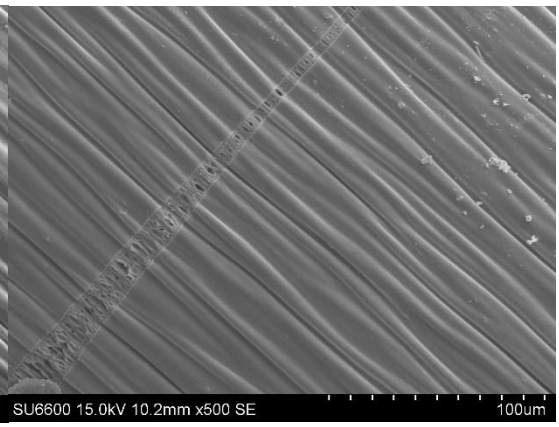

Figure 7.1.2-18: Category 2 surface feature

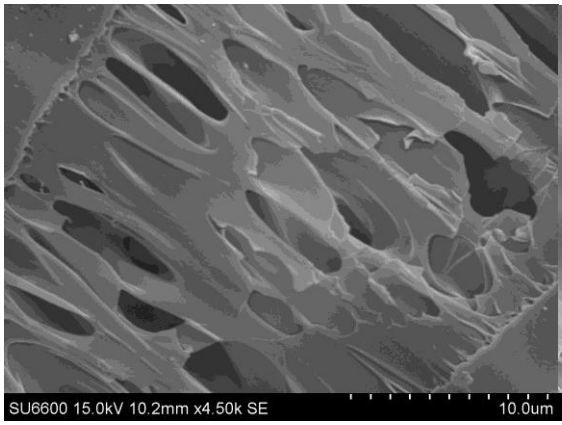

Figure 7.1.2-19: Category 3 surface feature

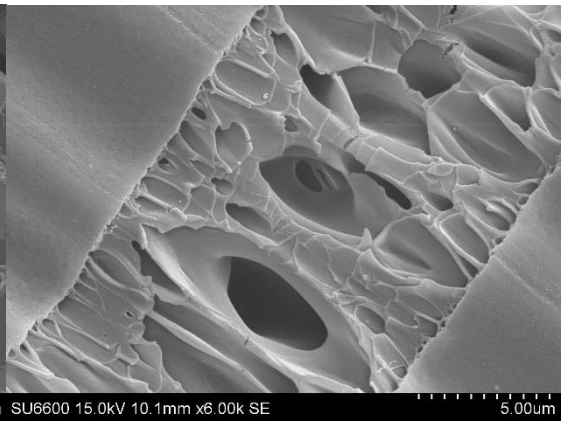

Figure 7.1.2-20: Category 4 surface feature

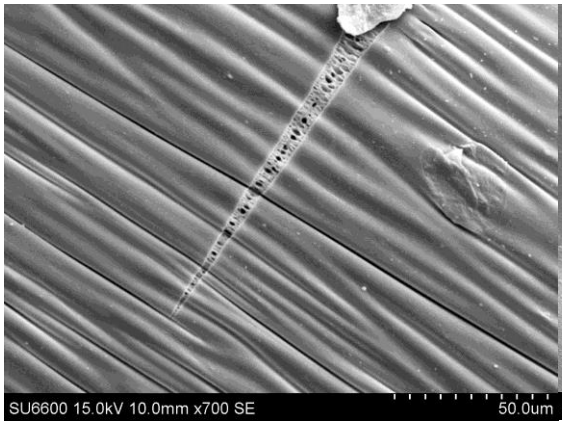

Figure 7.1.2-21: Category 5 surface feature

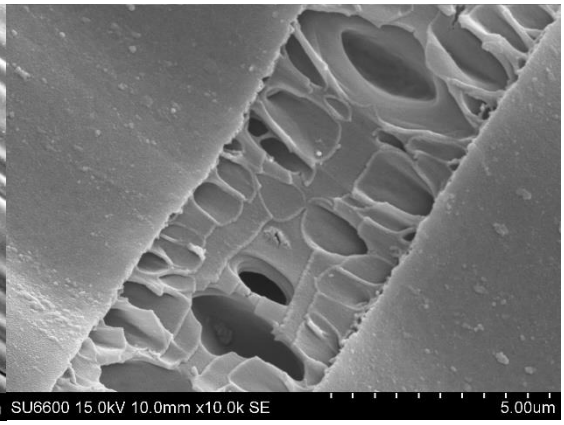

Figure 7.1.2-22: Category 6 surface feature

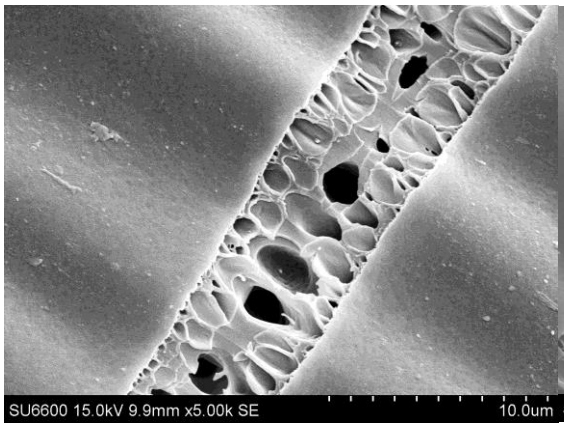

Figure 7.1.2-23: Category 7 surface feature

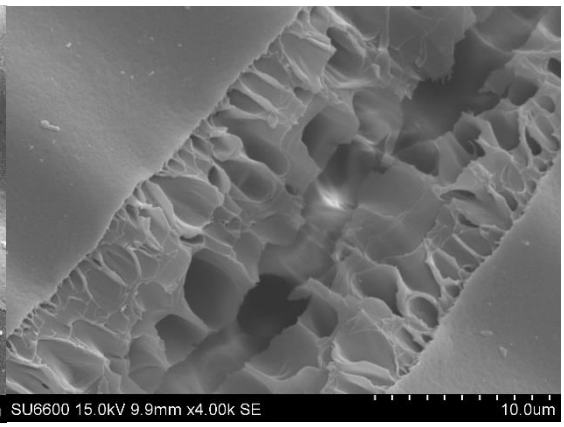

Figure 7.1.2-24: Category 8 surface feature

The SEM images produced displayed a number of interesting characteristics of the membranes. For modelling the separation however it is the thicknesses of active layer and pore sizes at the surface layer which are important. As discussed earlier it is expected that the active layer thickness will lie around 250nm for most membrane categories and the pore radius used in the model will be 75nm based on the more highly magnified surface images. The rips in the surface must have an effect on the separation qualities of the membranes as they contain large pores which would definitely lend themselves towards transport mechanisms associated with higher flow rates i.e. Knudsen flow, however, as the membranes exhibit better separating properties than this when coated the coating must be raising the resistance offered by these pores enough for solution diffusion to dominate the flow regime. Additionally the rips show pores inside which are clearly smaller than the surface effects, hence these smaller pores would be the rate determining factor. In an attempt to look at the effect of the coating process on the pores SEM images were also taken of the membranes post coating. The images shown are for category 1 which was a poorer performing category, and category 4 which was one of the better performing categories.

The images taken after coating took on a ghostly quality particularly in the regions of the tears. First of all the pore density and size within the tear appears to be slightly reduced from those seen in the uncoated photos. Either the membranes used for these photos were better than the

previous membranes imaged or the coating was having the effect of making some of the pores less visible in the images.

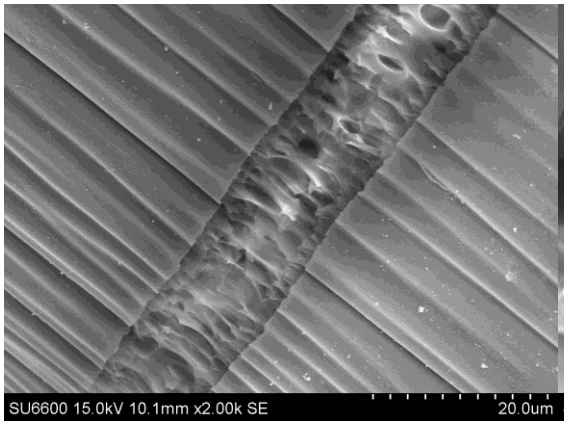

Figure 7.1.2-25: MB7 coated category 1 membrane 2k magnification

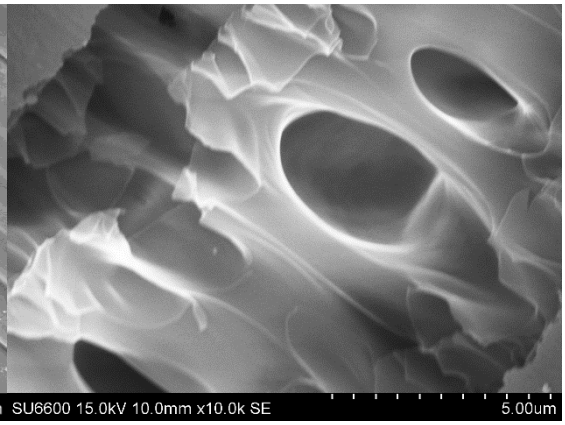

Figure 7.1.2-26: MB7 coated category 1 membrane 20k magnification

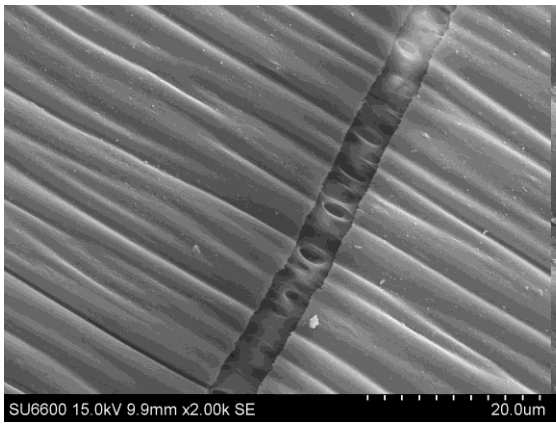

Figure 7.1.2-27: MB7 coated category 4 membrane 2k magnification

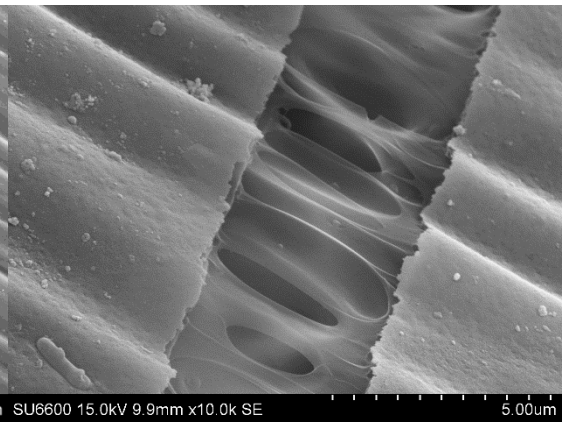

Figure 7.1.2-28: MB7 coated category 4 membrane 10k magnification

The same membranes could not be used for uncoated and coated images as the gold coating required for the uncoated images prevents the Sylgard 184 coating procedure from getting to the membrane surface. The membranes imaged for the coated comparisons were taken from the same membrane strands as the previous images and hence are sampled from within 30-40cm of production of the other images in an attempt to minimise the effects of moving to a different

sample. Hence, although it was not possible to eliminate the sample variation completely between the uncoated and coated images the precautions which could be taken to eliminate or reduce the associated impact have been.

It is therefore concluded that the images are showing an effect induced by the coating which is reasonable since the separation qualities of the membranes improved dramatically after coating. The tears and pores are still visible in the membrane however and the coating does not show up on the membrane surface in any other detectable way. It is thought the ghosting effect is caused by the presence of a very thin layer of the coating polydimethylsiloxane. The coating layer is so thin that the electron beam is able to penetrate through it to generate the surface image of the PVC. However, because the coating layer is causing secondary election scattering which is used to build up the image even if not in large amounts then these electrons produce the ghostly effect to the images.

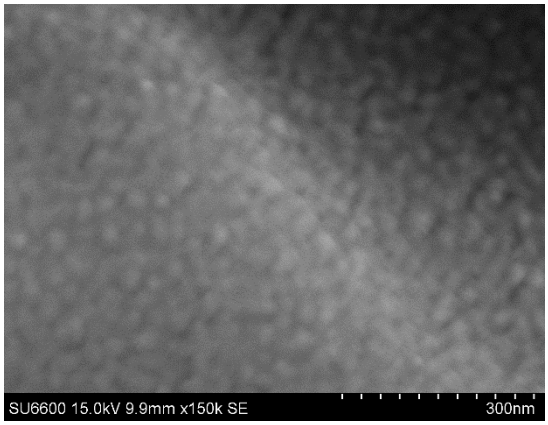

Figure 7.1.2-29: Membrane surface image after coating

The effect made it such that it was almost impossible to get clear images of the surface of the membranes as shown in Figure 7.1.2-29. This was the clearest image which was attained of the surface and shows the nodules as were visible before coating but the coating has the impact of making it more difficult to discern the shapes of the nodules.

Overall while it is not possible to see the coating on the membranes with the SEM imaging undertaken it has had an effect on the clarity of the images which the SEM is capable of taking

and this adds weight to the argument that the coating is having an impact on the final membrane characterisation. It is therefore necessary to take it into account when undertaking modelling.

7.2. Membrane Modelling – Development of Resistance Model

Membrane modelling was discussed in the introduction as a method of analysing the different flow mechanisms through a gas separation membranes. In this work a resistance model has been developed which uses the mass transport relationships through the membranes in combination with the SEM images in a Wheatstone bridge analogous model to determine the active layer thicknesses and surface porosity of the membranes.

The SEM surface images gave a pore radius of 75nm to be used in the membrane model. This pore size does not take into account the rip features seen in the surface as described above which are much larger but the separation properties of the membranes push towards Knudsen diffusion. If the rip size was taken into account then the pore radius to be used would be around 10μm. At these two pore sizes the corresponding Knudsen numbers are calculated and shown in Table 7.2-1. If the pore size indicated by the rips was applied in the model since the Knudsen Number would be below 0.01 for all the gases concerned then viscous flow regimes would apply to the membranes and there would be no separation achieved on the basis of either solution or Knudsen diffusion. However, as has already been intimated the uncoated membranes displayed separation characteristics which were in line with what would be expected to be seen from Knudsen diffusion.

Table 7.2-1: Knudsen numbers calculated for popular gases in membranes with pore radii of 75nm and 10μm

Gas	Molecular Diameter (Å)	Mean Free Path (Å), at p_{mean} and 20°C	Knudsen Number for 75nm	Knudsen Number for 10μm
Oxygen	3.59	235	0.313	0.002
Nitrogen	3.74	216	0.289	0.002

Gas	Molecular Diameter (Å)	Mean Free Path (Å), at p_{mean} and 20°C	Knudsen Number for 75nm	Knudsen Number for 10µm
Carbon Dioxide	4.58	144	0.144	0.001
Methane	4.11	179	0.319	0.002

Using the pore radius of 75nm results in Knudsen numbers which fall into the transition region of flow regimes between Knudsen and viscous flow i.e. between Knudsen Numbers of 10 and 0.01. The Knudsen numbers are below 1 so, according to work by Dushman[11], the flow would be expected to be less than 85% Knudsen. However, the evidence of the membrane separation factors being so close to Knudsen as shown in Table 7.2-2 suggests that the use of this 75nm pore radius is either conservative for the true pore radius in the membranes or that in this case the Knudsen flow dominates for a larger range of Knudsen numbers than was seen in the work of Dushman.

Table 7.2-2: Comparison of the theoretical Knudsen diffusion selectivity with the average selectivity which was achieved from the uncoated membranes produced for MB7

Gas Pair	True Knudsen Selectivity	Average Uncoated Membrane Selectivity Across MB7
Oxygen/Nitrogen	0.94	0.92
Carbon Dioxide/Methane	0.60	0.64

The oxygen/nitrogen gas pair was used in the creation of the model for the membranes since the final aim of the PVC membranes is in the separation of an oxygen/ozone gas pair and hence one of the species would remain the same. Additionally the information available on the permeation of the oxygen and nitrogen in the literature is more prevalent and consistent than that available for carbon dioxide and methane (this topic will be touched on later).

The first part of the model to determine the characteristics of the membranes therefore focuses on the uncoated membranes and assumes that the selectivity is entirely down to Knudsen diffusion. This assumes that, as shown above, the pores are reasonably sized for Knudsen

diffusion to occur and also that the resistance presented by a solution diffusion transport mechanism through the solid has such a high resistance in comparison to the Knudsen transport that it does not have a significant impact on the uncoated membranes. This second assumption is also well supported by the collected data showing very near Knudsen selectivity. Therefore the equation describing Knudsen diffusion (Equation 7.1.2.11) can be used along with the experimental data to determine the ratio of surface porosity (A_p) to active layer thickness (L) by Equation 7.3.1 where the flow becomes the pressure normalised flux of the gases (PNF_i) obtained during the experimental measurements. The resulting ratios for oxygen and nitrogen for each of the membrane categories in MB7 are shown in Table 7.2-3 along with an average of the ratio for the gases. The average is necessary for use in the calculation of the results for the coated membranes as this value should not change during the coating process and the variation displayed in the calculated values for the two different gases will come from the experimental measurements. This is shown by the values obtained through the model calculation being very similar for both gases.

$$\frac{A_p}{L} = PNF_{gas}\frac{3(2\pi R_0 TMW_i)^{0.5}}{8r_{pore}} \qquad \textbf{Equation 7.2.1}$$

Table 7.2-3: Surface porosity to active wall thickness ratio for MB7 membranes for Oxygen, Nitrogen and the average of these gases

Membrane Category	Oxygen A_p/L (1/m)	Nitrogen A_p/L (1/m)	Average A_p/L (1/m)
1	4.626	4.494	4.560
2	5.279	5.326	5.302
3	4.711	4.896	4.804
4	4.389	4.522	4.455
5	6.259	6.394	6.326
6	5.977	6.111	6.044
7	5.194	5.437	5.316
8	5.568	5.630	5.599

In order to determine the properties of the coated membranes the situation is more complicated as there are more resistances to gas transport which have to be taken into account. The increase in selectivity experienced after coating is caused by the gases being forced to proceed through the membrane by a solution diffusion mechanism in the solid PVC. Therefore the first path is completely controlled by solution diffusion mechanisms firstly through the poly(dimethyl siloxane) (PDMS) coating and then through the PVC. The second possible path is transport through the PDMS coating and then through the pore where the PDMS can be expected to have penetrated into the pore to some extent. In the model then the thickness of the PDMS coating above the surface can be ignored as this is the same for both paths through the membrane. Similarly the thickness of the porous substructure below the active layer can also be ignored and is assumed to display separation properties which are Knudsen dependent. The permeation model therefore becomes a combination of solution diffusion mechanisms through the solid polymer with a path length corresponding to the active layer thickness (L), and a second path consisting of Knudsen diffusion through the pores (L_2) followed by solution diffusion through the coating which has penetrated into the pores (L_3).

The permeability coefficients of the species involved come into play when dealing with solution diffusion mechanisms. A literature survey conducted on the permeability of the common test gases reveals variable values for permeability through PVC but particularly in those quoted for carbon dioxide, this is likely due to different levels of swelling being induced in the membrane by carbon dioxide. The conflict in these values results in selectivity between gas pairs being more variable where carbon dioxide is involved. The values in Table 7.2-4 show these figures and demonstrate another reason why the model was focused around the oxygen/nitrogen gas pair which give much more consistent numbers particularly in terms of selectivity.

Table 7.2-4: Literature permeability values for common test gases in PVC

Source	**Permeability coefficient *10^{10} (cm^3.cm/s.cm^2.cmHg)**				**Selectivity for gas pair**	
[ref]	**P_{O_2}**	**P_{N_2}**	**P_{CO_2}**	**P_{CH_4}**	**O_2/N_2**	**CO_2/CH_4**
[12]	0.07	0.01	0.25	-	7.0	-
[13]	0.124	0.022	0.540	0.024	5.6	22.5
[14]	-	-	-	-	5.0	20.0

Source [ref]	Permeability coefficient *10^{10} (cm^3.cm/s.cm^2.cmHg)				Selectivity for gas pair	
	P_{O_2}	P_{N_2}	P_{CO_2}	P_{CH_4}	O_2/N_2	CO_2/CH_4
[15]	-	0.00945	0.243	0.0108	-	22.5
[15]	-	0.00668	0.184	0.00850	-	21.6
[16]	0.12	0.04	1.0	-	3.0	-
[17]	-	0.028	0.32	0.06	-	5.33
[18]	0.05	0.01	0.15	0.025	5.0	6.0
[19]	-	-	0.16	0.0106	-	15.1

The values used in the model for permeability of oxygen and nitrogen in PVC were 0.12barrer and 0.022barrer respectively which results in oxygen/nitrogen selectivity in the model of 5.5. The values for permeability through PDMS were taken from the work of Robb[20] on thin silicone membranes and gave values of 620barrer and 280barrer. It should be reiterated at this point that that this suggests a membrane reliant on the PDMS for selectivity would give a separation factor of 2.21 but that all the membrane categories for MB7 showed better selectivity than this and hence it is not the PDMS alone which is causing the selectivity achieved.

To create the equations for separation achieved through the coated membranes the resistance paths described above were converted into an electrical analogue whereby the pores (R_2) and PDMS (R_3) resistances are connected in series and the resistance through the PVC (R_1) is in parallel to this route. The appropriate equation for either Knudsen or solution diffusion flow is then substituted in place of the resistance term which gives two simultaneous equations for the pressure normalised flux of the gases which can be solved if the ratio of surface porosity to active layer thickness (L) is also added into the equations and made equal to that found for the uncoated membranes for each category. Additional assumptions which have to be made to allow the model to be prepared are:

- A_p is much smaller than 1 and hence the membrane area can be used as the area of solid polymer which can be calculated from the circumference of the spinneret used to produce the membrane and the length of membrane, this also assumes that the die swell

associated with the production of the membranes is minimal (some of this effect may be cancelled out by the shrinking on solidification)

- The resistance offered by the surface coating is negligible with respect to the thickness of the coating above the surface of the membrane across the full membrane surface
- L_3, the penetration depth of PDMS into the pores is much smaller than L, the active layer thickness, and hence the corresponding pore length, L_2, is approximately equal to L

So where the subscript C is for coated membranes and A_{mem} is the surface area of the membrane the derivation follows the path:

$$\frac{\mathbf{1}}{\boldsymbol{R_C}} = \frac{\mathbf{1}}{\boldsymbol{R_1}} + \frac{\mathbf{1}}{\boldsymbol{R_2 + R_3}} \qquad \textbf{Equation 7.2.2}$$

Where:

$$\boldsymbol{R} = \frac{\mathbf{1}}{\boldsymbol{PNF_i A}} \qquad \textbf{Equation 7.2.3}$$

Substitution gives:

$$\boldsymbol{PNF_C A_{mem}} = \boldsymbol{PNF_1 A_{mem}} + \frac{\mathbf{1}}{\frac{\mathbf{1}}{\boldsymbol{PNF_2 A_{mem} A_p}} + \frac{\mathbf{1}}{\boldsymbol{PNF_3 A_{mem} A_p}}} \qquad \textbf{Equation 7.2.4}$$

Dividing throughout by A_{mem} gives:

$$\begin{aligned} \boldsymbol{PNF_C \cancel{A_{mem}} \frac{\mathbf{1}}{\cancel{A_{mem}}}} & \\ &= \boldsymbol{PNF_1 \cancel{A_{mem}} \frac{\mathbf{1}}{\cancel{A_{mem}}}} \\ &+ \frac{\mathbf{1}}{\frac{\mathbf{1}}{\boldsymbol{PNF_2 \cancel{A_{mem}} A_p}} + \frac{\mathbf{1}}{\boldsymbol{PNF_3 \cancel{A_{mem}} A_p}}} \frac{\mathbf{1}}{\cancel{A_{mem}}} \end{aligned} \qquad \textbf{Equation 7.2.5}$$

$$\boldsymbol{PNF_C} = \boldsymbol{PNF_1} + \frac{\mathbf{1}}{\frac{\mathbf{1}}{\boldsymbol{PNF_2 A_p}} + \frac{\mathbf{1}}{\boldsymbol{PNF_3 A_p}}} \qquad \textbf{Equation 7.2.6}$$

Inserting the appropriate relationship for either solution or Knudsen diffusion depending on the flow regime for each location gives:

$$PNF_C = \frac{P_1}{L} + \frac{1}{\frac{1}{\frac{8}{3}\left(\frac{1}{2\pi R_0 TMW_i}\right)^{1/2} \frac{r_{pore}}{L_2} A_p} + \frac{1}{\frac{P_3}{L_3} A_p}}$$

Equation 7.2.7

Rearranging and applying the assumption that $L_2 \approx L$:

$$PNF_C = \frac{P_1}{L} + \frac{1}{\frac{3(2\pi R_0 TMW_i)^{0.5}}{8r} \frac{L}{A_p} + \frac{L_3}{P_3 A_p}}$$

Equation 7.2.8

If the ratio $A_p/L=Z$ and is known from the uncoated equations then this can be substituted into the equation for the coated membrane in order to eliminate the A_p variable:

$$PNF_C = \frac{P_1}{L} + \frac{1}{\frac{3(2\pi R_0 TMW_i)^{0.5}}{8r_{pore}} \frac{1}{Z} + \frac{L_3}{P_3 ZL}}$$

Equation 7.2.9

When experimental values are used to provide data of the actual PNF for a coated membrane then this derived form Equation 7.2.9 contains only two unknown values which are L and L_3. Hence, having an equation for each part of the gas pair allows the solving of the equations simultaneously by iterative processes. Mathcad 15 (Parametric Technology Corporation) was used to find solutions to Equations 7.2.10 and 7.2.11.

$$PNF_{O_2,C} = \frac{P_{O_2 PVC}}{L} + \frac{1}{\frac{3(2\pi R_0 TMW_i)^{0.5}}{8r_{pore}} \frac{1}{Z} + \frac{L_3}{P_{O_2 PDMS} ZL}}$$

Equation 7.2.10

$$PNF_{N_2,C} = \frac{P_{N_2 PVC}}{L} + \frac{1}{\frac{3(2\pi R_0 TMW_i)^{0.5}}{8r_{pore}} \frac{1}{Z} + \frac{L_3}{P_{N_2 PDMS} ZL}}$$

Equation 7.2.11

Additionally, the value of A_p can then be back calculated from the A_p/L ratio and since the pore radius is 75nm this allows the calculation of the mean number of pores per unit area, N_{pore}, and the mean distance between these pores G_{pore}. These values are tabulated alongside the results of the modelling calculations in Table 7.2-5.

$$N_{pore} = \frac{A_p}{\pi r_{pore}^2} \qquad \textbf{Equation 7.2.12}$$

$$G_{pore} = N_{pore}^{-0.5} \qquad \textbf{Equation 7.2.13}$$

Table 7.2-5: Summary of the calculated characteristics of the membrane surface and thicknesses

Membrane Category	Active Layer Thickness, L (Å)	PDMS penetration depth, L_3 (Å)	Surface porosity, A_p	Pores per unit area, N_{pore} (1/cm^2)	Pore separation distance, G_{pore} (cm)
1	1014	11	4.62E-07	2617	0.0195
2	646	56	3.43E-07	1939	0.0227
3	862	20	4.14E-07	2344	0.0207
4	702	46	3.13E-07	1770	0.0238
5	726	25	4.59E-07	2599	0.0196
6	679	24	4.10E-07	2323	0.0207
7	721	17	3.99E-07	2256	0.0211
8	606	29	3.40E-07	1921	0.0228

The model predictions show some interesting comparisons with the properties of the membranes as seen in the membrane fabrication section of this work. Membrane categories 1, 2, 3 and 4 were prepared at a lower extrusion rate than 5, 6, 7 and 8, the lower extrusion rate appears to have resulted in a thicker active layer with a mean thickness for these membranes of 806Å in comparison to 683Å at the higher extrusion rate (the other parameters altering between membranes allow direct comparison of the following membrane category pairs 1 & 5, 2 & 6, 3 & 7 and 4 & 8). This could be explained by the slightly longer time which the membranes produced

at the lower extrusion rate would be exposed to the impingement zone gas velocity allowing the evaporation of the high volatility solvent to occur to a greater extent producing the thicker layer. This increase in thickness does not seem to transfer itself into the model prediction of surface porosity where a trend is more difficult to establish.

In balance to this argument for the increased exposure to the impingement zone producing a thicker skin is the observed pattern for the different flow rates of forced convective gas. If greater time of exposure produces thicker walls then it may be expected that greater gas flow rate would also induce a similar effect, however the opposite appears to be the case from the results. Membrane categories 1, 3, 5 and 7 are produced at a low convective gas flow rate while 2, 4, 6 and 8 are produced with a higher flow rate. This time the direct comparisons which can be made between categories are for the pairs 1 & 2, 3 & 4, 5 & 6 and 7 & 8. These comparisons all show the lower convective gas flow rate predicting a higher skin thickness. The theory for why this might occur is that the high gas flow rate very quickly causes the formation of a thin active layer which prevents the process penetrating deeper into the membrane. On the other hand the slightly slower progress at the lower flow rate allows the boundary of the active layer to proceed deeper into the membrane before the final structure is formed. This time the pattern also appears to be reflected in the porosity of the membrane with the high gas flow rate and possible faster forming active layer reducing the surface porosity.

The final factor focused on in this investigation was the residence time below the impingement zone with direct comparisons possible between category pairs 1 & 3, 2 & 4, 5 & 7 and 6 & 8. However, the model does not show any easily identifiable trends in the active layer or porosity predictions for these pairs suggesting that the membrane structure is formed before this part of the process, this adds some weight to the ideas behind the influence of the convective gas flow rate in that it suggests there is a limit to the depth of the membrane structure which can be affected within the dry zone. This follows on from the need for mass transport to occur through the forming surface membrane structure in order for change to occur deeper into the membrane.

These trends shows the model predicts the gas flow rate to have a large impact on the final membrane performance, with a secondary effect from the extrusion rate and no notable effect

from the residence time. This pattern agrees well with the observations from the Taguchi analysis and the graphical representations described in the membrane fabrication sections for the influences which could be expected from the different parameters.

7.3. Tensile Properties of Membranes

7.3.1. Importance of Tensile Properties for Hollow Fibers

Hollow fiber membranes are viewed as being a greener and cheaper alternative to other separation processes however one of their disadvantages is fragility. This has impacts on both the production and also on the lifetime of membrane units.

During hollow fiber spinning some polymer solutions will exhibit instability in the continuous production because the fiber is not materially strong enough to hold together the weight of the membrane as it forms. This can result in membrane breakage and extensive down time on production runs as the membrane has to be re-threaded, while this might be workable under laboratory conditions in order to assess the suitability of the separating qualities of a polymer it will never lead to that particular solution being used industrially as it is too unpredictable. It is likely that the dope used in this work is treading close to this line with the tear formations seen on the outer surface of the membranes. However, there was never any problem with the membrane snapping under production conditions.

The hollow fibers may have to go through potting-up procedures and coating procedures in order to be commercially useful, this means that the separating qualities of the fibers must be resilient to a certain amount of processing once they are fully formed. When dealing with surface layers which are as thin as in the case of gas separation membranes it does not take much force in order to cause damage which reveals the porous sub-structure beneath and this kind of damage influences the performance which is achieved. A strong material enhances the protection against

this processing damage and provides better assurance that more consistency will be achieved between membranes.

Membrane units are operated under pressure so it is necessary for the structure to be capable of withstanding the conditions it will be exposed to. These conditions tend to be more easily adaptable than other requirements of the process although if the membranes are capable of supporting larger pressure differences across the retentate and permeate sides of the membrane then this will increase the flux through the membrane which has processing benefits in terms of unit scaling.

Once a membrane unit has been assembled and put into service the membranes inside will be expected to have a service lifetime which is consistent. There are a few factors which can affect this service lifetime. The first is physical aging affecting the separation properties of the membrane, this is a well-documented effect on a number of different polymers[12, 21-23] and focuses on the gradual reduction in free volume of the membrane over time causing the flux to decrease and the selectivity to increase. An increase in selectivity can be viewed as a benefit but industrial processes have to hit production targets and significant reduction in flux makes meeting these targets more difficult.

The second in service factor is the process conditions when the membrane is in use. It is very rare in the processing industries that the environment in which a membrane system is operating will only be exposed to binary gas mixtures, it is much more likely that the feed stream will contain a number of species some of which can have detrimental effects on the membrane materials. There are two main detrimental effects on the process which other species may have: chemical attack or fouling. Chemical attack on the membrane will eventually leave it unusable and therefore the unit has to be replaced. Fouling on the other hand is sometimes reversible, hollow fiber module arrangements will often have the capability for back flushing to occur and hence regeneration of the membranes. As with most processes where regeneration can occur such as absorption columns the processes will generally not return the membrane unit to its original operating capacity but will extend the usable lifetime which may offer benefits in comparison to complete decommissioning and recommissioning of the unit.

Regeneration processes can have an impact on the final reason for membrane replacement which is damage incurred to the membrane over time in the process environment. As has been mentioned already strong materials help the membranes to resist damage incurred during preparation but they can also help extend the lifetime of the membranes during practical use. The sources of damage to a membrane under operation can come from the feed stream or time effects but gradually more of the individual membranes in a unit will give a reduced performance due to mechanical failure. The tensile strength of the membrane material is one factor which is considered as a guide for helping to avoid the replacement of membrane modules occurring as a result of mechanical failure of the membranes inside. Some examples of the tensile strengths for various polymeric materials are shown in Table 7.3.1-1 as described in "Physical Properties of Polymers Handbook", J. E. Mark, Springer 2007[24].

The table shows that most of the polymers commonly used for gas separation membranes have tensile strengths which are in the region of 70MPa (although the precise conditions for determination of this factor are not described and factors such as test temperature and pulling rate have a strong effect on these values). It can be seen that un-plasticised (rigid) PVC falls on the low end of this and that plasticised (flexible) PVC has very low strength for consideration as a gas separation membrane. Cellulose acetate also falls down on this front having a lower tensile strength than is commonly seen and this may be one reason why a large amount of research and processes have moved away from the use of this material when it was one of the first to be used successfully in gas separation membranes under both lab and industrial conditions.

Table 7.3.1-1: Physical Properties of Various Polymers used for Gas Separation Membranes[24]

Polymer	Tensile Strength, Solid Plastic, σ (MPa)	Tensile Strength, Membranes, σ (MPa)
Poly(vinyl chloride), rigid	40-75	
Poly(vinyl chloride), flexible	6-25	
Poly carbonate	70-90	45(sheets)[25]
Cellulose acetate	25-45	3.4(sheets)[26], 11.7(sheets)[27]
Poly(methyl methacrylate)	55-75	33.8(sheets)[28]
Polysulfone	70	≈4.5(fibers)[29]
Polyethersulfone	80-90	29.4(fibers)[30], 1.5(fibers)[31]

The expected use also plays a part on strength consideration however and the ozone/oxygen processes which the PVC membranes are being considered for would place a very light load on the membranes. Due to the production processes used the feed streams will often be highly constrained in the impurities which the membranes could be subjected to and the low reactivity is one of the benefits PVC presents. The production processes for ozone also tend to display both low flow and low pressure which mean that the low tensile strength of the PVC may be ok.

The differences in mechanical strength shown by the table are to some extent mitigated because membranes are required to have such high porosity and free volume to work effectively that the strength is greatly compromised with respect to solid plastic material as comparisons between the second and third columns of the table show. The mechanical properties of the membranes can vary greatly from that of the parent material and the membrane production processes can also influence the strength as they affect the orientation, dense layer thickness and porosity of the membrane; this is demonstrated by the polyethersulfone fibers particularly well where one author obtained over 29MPa[30] for their fibers while another obtained less than 2MPa[31].

Another influence on the variation between membranes of the same material is the strain rate of the tensile testing. This value does vary in the literature but it can have an impact on the stresses obtained from the tensile testing with a higher rate bringing a higher tensile stress value and the modulus will also be more accurate at low strain rates it is therefore an important value to report. However because the cross sectional area of membranes is so small it may be expected that the differences which strain rate would bring about are low. The relationship between strain rate and tensile strength is related to the elastic properties of materials in relation to viscous properties i.e. where the rate is fast the load is applied quickly and the material reacts elastically which is a response associated with higher energy, however the viscous long time frame response allows the energy to dissipate more resulting in lower strength.

One factor which may play into the reduction for values seen for membranes is also the calculation of the cross sectional area of the membranes. The basis on which the cross sectional area of the fiber is calculated is the same as the dimensions of the spinneret used to produce that fiber, however there are various factors which affect this:

- Die swell on leaving the spinneret
- Fiber drawing as it is produced
- Shrinkage of the fiber due to solidification (the ripple effect seen in the SEM images)

These factors make it unlikely that the membrane actually has the dimensions associated with the spinneret but using this value means that the basis is consistent between spin runs which are conducted. Measurements on hollow fibers by mechanical means are an alternative but often the diameters are so low and the fibers so easily compressed by the mechanical method that this can prove difficult to achieve accurately also.

Finally as was mentioned in the introduction there are other ways of providing strength to membranes with composite or ceramic substructures being one method of giving additional strength to a weaker polymer material while providing a porosity which enables the separating qualities of the desired material to be utilised. As an additional benefit to this process it may be that the reduction in free volume seen through polymer aging as discussed above is less an issue for these membranes as the ceramic layer is less susceptible to this type of ageing effect.

7.3.2. PVC Hollow Fiber Membrane Tensile Strength

The mechanical properties of PVC membranes were measured using an Instron Tensile Test machine. The tensile properties of two categories were measured and the categories chosen were 2 and 4 as they represented the best membranes as found from the optimisation work carried out in MB7. The samples were tested uncoated and without any further treatment after the drying process following solvent exchange from the spinning production run so as to give values associated with the fiber before any processes were undertaken which could affect the nature of the membrane in any way.

The samples were prepared using a standard template for each test in order to maintain as much reproducibility as possible through the testing. The template consisted of a sheet of card which had windows cut out of it 30mm long. The windows were in rows of five and had a line down the

centre of the card portion of each template. A membrane was placed along the line down the centre of the windows, without stretching it, and secured in place at either end of the row with sticky tape.

Unfortunately tape could not be used to hold the membranes in the test jaws since the strength of the membranes could not withstand the compression which the grips applied, this would have resulted in failure of the membrane occurring where it was crimped in the grips rather than in the middle of the available gauge length. To remedy this a method of holding the membrane onto the template which could withstand the force of the Instron clamping grips had to be found.

A number of glue products were tested for compatibility with the PVC membranes and the ability to stack up in order to produce a gripping platform. It was found that Super Glue did not seem to have any adverse effect on the membranes and by applying a thick layer over the top of the membrane to hold it against the template could protect from the grip while holding the membrane in place and allowing failure to occur in the gauge length (since during the testing failures occurred away from the ends of the sample this suggests that the super glue gripping method was not affecting the results).

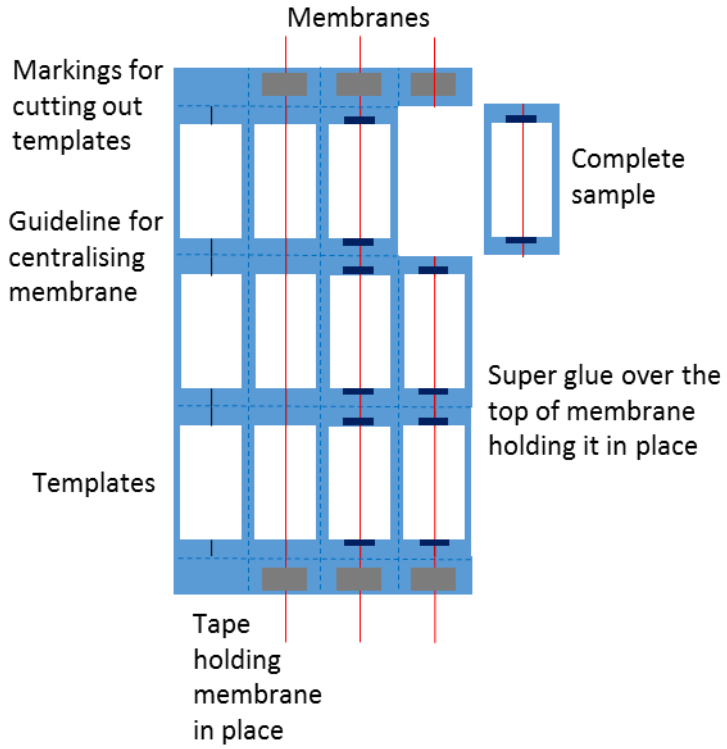

Figure 7.3.2-1: Preparation stages of samples for tensile testing

Figure 7.3.2-1 shows the final arrangement of a length of membrane on the templates. Each individual sample template was then cut out to produce one test sample. For each of the two membrane categories twenty samples were prepared and tested by clamping the ends of a single template in the grips, closing the grips on the lower glue first then onto the top glue in order to minimise the impact of strain being applied during clamping. Once the sample was secured in place and the Instron tensile tester was set-up ready to go the sides of the sample template were cut. Leaving the cutting of the template sides until this point meant that the chances of applying any form of pre-strain onto the membrane was minimised as the sides of the card template supported it, this is very important due to the small cross sectional areas and the influence which even small pre-stresses could have on the strength as a result of this. In order to allow this test method of sample preparation to occur the tensile tester was equipped with an automatic slack correction feature. This feature meant that the small amount of slack in the membranes when the template sides were cut did not affect the elongation readings for the membranes.

The samples were tested at room temperature and at a strain rate of 5mm/min which is a common set of conditions for the testing of hollow fibers. The results of the tensile testing are shown in Table 7.3.2-1 and Table 7.3.2-2 for MB7 membranes category 2 and 4 respectively.

Table 7.3.2-1: Tensile testing results for membrane category 2

Sample Number	Corrected Gauge Length (mm)	Load at Break (N)	Ultimate Stress (MPa)	Strain at Break (mm)	Modulus (MPa)
1	30.25	1.81	6.56	30.45	236.68
2	30.39	2.20	7.98	45.47	249.93
3	30.49	2.05	7.45	29.31	211.59
4	30.22	2.09	7.58	25.30	228.58
5	30.25	2.04	7.40	32.03	226.29
6	29.88	1.71	6.21	40.36	-
7	30.56	2.13	7.74	27.74	257.84
8	30.23	2.01	7.29	18.65	210.36
9	30.18	2.06	7.49	22.81	211.85
10	30.37	2.16	7.86	42.25	199.67
11	30.30	1.82	6.62	33.65	252.76
12	30.40	1.98	7.17	42.75	214.23
13	30.61	1.97	7.13	35.34	243.23
14	30.37	1.89	6.86	21.28	233.65
15	30.46	2.02	7.33	46.86	185.59
16	30.84	1.97	7.14	33.39	237.76
17	30.68	1.90	6.91	25.17	235.38
18	30.78	1.89	6.85	24.76	240.64
19	31.04	1.86	6.76	16.84	239.57
20	30.63	2.04	7.39	36.02	209.87
Mean	30.48	1.99	7.24	31.05	227.66
σ	0.24	0.11	0.41	8.87	19.33
CV	0.01	0.06	0.06	0.29	0.08

Table 7.3.2-2: Tensile testing results for membrane category 4

Sample Number	Corrected Gauge Length (mm)	Load at Break (N)	Ultimate Stress (MPa)	Strain at Break (mm)	Modulus (MPa)
1	30.69	2.01	7.31	31.95	249.22
2	30.74	2.08	7.53	45.42	236.88
3	30.71	2.00	7.25	34.91	249.15
4	31.08	2.02	7.34	39.85	269.88
5	30.64	1.94	7.03	30.65	237.01
6	30.85	1.90	6.91	27.72	258.92
7	30.75	2.05	7.42	38.86	232.73
8	30.75	1.98	7.19	31.61	243.55
9	30.89	2.00	7.25	35.56	241.63
10	30.52	2.00	7.27	37.51	282.90
11	30.74	2.01	7.30	44.52	215.01
12	30.88	1.97	7.16	44.76	251.19
13	30.66	1.79	6.51	44.73	202.25
14	30.81	1.86	6.74	14.13	221.33
15	30.91	1.96	7.13	32.85	257.52
16	30.61	1.92	6.99	27.85	258.16
17	31.02	2.06	7.47	38.83	235.58
18	31.36	2.03	7.36	39.90	238.38
19	30.97	1.91	6.92	19.92	247.36
20	30.74	1.91	6.93	27.40	260.21
Mean	30.81	1.97	7.16	34.80	243.68
σ	0.19	0.07	0.26	8.46	18.82
CV	0.01	0.04	0.04	0.24	0.08

The results for the tensile properties suggest that the membranes within a category do not show a great deal of variation. Neither of the two categories contain results within the sample sets which are outliers to the rest of that categories samples as demonstrated by the coefficients of variance which are less than 10% for all the values except the strain at break. The automatically corrected gauge lengths do not vary greatly which shows that the template was effective in providing a sample which did not have a large amount of pretension applied to it. The values for tensile strength are low as was expected from the values displayed for the different materials

above. While the membranes have enough strength to hold themselves the low strength is a concern for use in an industrial process. The strain at break shows the most variation for both categories with the lower values being generally associated with the weaker membranes with regards to tensile strength. This suggests that these membranes may have a strength reducing imperfection which allows the failure to propagate more readily, in this case perhaps the tears seen in the SEM images are responsible for making it easier for some membranes to fail over others.

The results for the tensile properties suggest that there is very little difference between the two membrane categories. It can be seen that in all categories with the exception of the corrected gauge length both the means for the categories overlap the error bars within one standard deviation from either category. Therefore it was concluded that it was not possible to tell the difference between the membrane production conditions of these PVC membranes through the use of mechanical tensile testing.

Overall the mechanical properties of the PVC membranes show the behaviour expected from them revealing lower mechanical properties than are ideal for gas separation membranes but providing consistent numbers. This means that the losses of membranes due to damage occurred during the separation processes might be expected to be larger than seen with other more traditional gas separation materials such as polysulfone. However, in competition to this are the processes which the PVC membranes are being aimed at being particularly clean, for ozone processing this is a key component to successful operation. The flow rate and pressures associated with ozone production are also factors which can contribute to creating good conditions for membrane survival since they provide a low stress environment. In order to fully assess the impact which the low mechanical strength would have on the process a pilot plant type unit would have to be produced. The membranes can support themselves under the reasonable pressures associated with operating conditions (5bar), as the separation results show, so with other operating conditions being favourable the PVC membranes should be appropriate for use with a suitably designed module which provides the support the PVC requires.

7.4. Bibliography

1. Perez, EV, Balkus Jr, KJ, Ferraris, JP, and Musselman, IH, *Mixed-matrix membranes containing MOF-5 for gas separations.* Journal of Membrane Science, 2009. **328**(1–2): p. 165-173.
2. Kim, K, Choi, W, Jo, H, Kim, J, and Lee, HK, *Hollow fiber membrane process for the pretreatment of methane hydrate from landfill gas.* Fuel Processing Technology, 2014. **121**(0): p. 96-103.
3. Rafiq, S, Man, Z, Maulud, A, Muhammad, N, and Maitra, S, *Effect of varying solvents compositions on morphology and gas permeation properties on membranes blends for CO2 separation from natural gas.* Journal of Membrane Science, 2011. **378**(1–2): p. 444-452.
4. Jiang, L, Chung, T-S, Li, DF, Cao, C, and Kulprathipanja, S, *Fabrication of Matrimid/polyethersulfone dual-layer hollow fiber membranes for gas separation.* Journal of Membrane Science, 2004. **240**(1–2): p. 91-103.
5. Aroon, MA, Ismail, AF, Montazer-Rahmati, MM, and Matsuura, T, *Morphology and permeation properties of polysulfone membranes for gas separation: Effects of non-solvent additives and co-solvent.* Separation and Purification Technology, 2010. **72**(2): p. 194-202.
6. Han, J, Lee, W, Choi, JM, Patel, R, and Min, B-R, *Characterization of polyethersulfone/polyimide blend membranes prepared by a dry/wet phase inversion: Precipitation kinetics, morphology and gas separation.* Journal of Membrane Science, 2010. **351**(1–2): p. 141-148.
7. Saedi, S, Madaeni, SS, and Shamsabadi, AA, *Fabrication of asymmetric polyethersulfone membranes for separation of carbon dioxide from methane using polyetherimide as polymeric additive.* Chemical Engineering Research and Design, (0).
8. Hasbullah, H, Kumbharkar, S, Ismail, AF, and Li, K, *Preparation of polyaniline asymmetric hollow fiber membranes and investigation towards gas separation performance.* Journal of Membrane Science, 2011. **366**(1–2): p. 116-124.

9. Feng, CY, Khulbe, KC, Matsuura, T, and Ismail, AF, *Recent progresses in polymeric hollow fiber membrane preparation, characterization and applications.* Separation and Purification Technology, 2013. **111**(0): p. 43-71.
10. Feng, CY, Khulbe, KC, Chowdhury, G, Matsuura, T, and Sapkal, VC, *Structural and performance study of microporous polyetherimide hollow fiber membranes made by solvent-spinning method.* Journal of Membrane Science, 2001. **189**(2): p. 193-203.
11. Dushman, S, *Scientific foundations of vacuum technique*1962: Wiley.
12. Bierbrauer, K, López-González, M, Riande, E, and Mijangos, C, *Gas transport in fluorothiophenyl modified PVC membranes.* Journal of Membrane Science, 2010. **362**(1–2): p. 164-171.
13. Tiemblo, P, Guzmán, J, Riande, E, Mijangos, C, and Reinecke, H, *The gas transport properties of PVC functionalized with mercapto pyridine groups.* Macromolecules, 2002. **35**(2): p. 420-424.
14. Tiemblo, P, Guzman, J, Riande, E, Mijangos, C, and Reinecke, H, *Erratum: Effect of physical aging on the gas transport properties of PVC and PVC modified with pyridine groups (Polymer (2001) 42 (4817-4823) PII: S0032386101003391).* Polymer, 2001. **42**(19): p. 8321.
15. El-Hibri, MJ and Paul, DR, *Effects of uniaxial drawing and heat-treatment on gas sorption and transport in PVC.* Journal of Applied Polymer Science, 1985. **30**(9): p. 3649-3678.
16. Li, NN, *Recent Developments in Separation Science*1972: CRC Press.
17. Tikhomirov, BP, Hopfenberg, HB, Stannett, V, and Williams, JL, *Permeation, diffusion, and solution of gases and water vapor in unplasticized poly(vinylchloride).* Die Makromolekulare Chemie, 1968. **118**(1): p. 177-188.
18. Baker, R and Blume, I, *Permselective membranes separate gases.* Chemtech, 1986. **16**(4): p. 232-238.
19. Mulder, M, *Basic principles of membrane technology*. 2nd ed1996, Dordrecht ; Boston: Kluwer Academic. 564 p.
20. Robb, WL, *THIN SILICONE MEMBRANES-THEIR PERMEATION PROPERTIES AND SOME APPLICATIONS.* Annals of the New York Academy of Sciences, 1968. **146**(1): p. 119-137.

21. Hu, C-C, Fu, Y-J, Hsiao, S-W, Lee, K-R, and Lai, J-Y, *Effect of physical aging on the gas transport properties of poly(methyl methacrylate) membranes.* Journal of Membrane Science, 2007. **303**(1–2): p. 29-36.

22. Adewole, JK, Ahmad, AL, Ismail, S, and Leo, CP, *Current challenges in membrane separation of CO2 from natural gas: A review.* International Journal of Greenhouse Gas Control, 2013. **17**(0): p. 46-65.

23. Chung, T-S and Khean Teoh, S, *The ageing phenomenon of polyethersulphone hollow fibre membranes for gas separation and their characteristics.* Journal of Membrane Science, 1999. **152**(2): p. 175-188.

24. Mark, JE, *Physical Properties of Polymers Handbook*2007: Springer.

25. Suin, S, Maiti, S, Shrivastava, NK, and Khatua, BB, *Mechanically improved and optically transparent polycarbonate/clay nanocomposites using phosphonium modified organoclay.* Materials & Design, 2014. **54**(0): p. 553-563.

26. Zafar, M, Ali, M, Khan, SM, Jamil, T, and Butt, MTZ, *Effect of additives on the properties and performance of cellulose acetate derivative membranes in the separation of isopropanol/water mixtures.* Desalination, 2012. **285**(0): p. 359-365.

27. Ahmad, AL, Jawad, ZA, Low, SC, and Zein, SHS, *A cellulose acetate/multi-walled carbon nanotube mixed matrix membrane for CO2/N2 separation.* Journal of Membrane Science, 2014. **451**(0): p. 55-66.

28. Kausar, A, Zulfiqar, S, and Sarwar, MI, *Nanoblends of PMMA/aramid: A study on morphological and physical properties.* Solid State Sciences, 2013. **24**(0): p. 36-43.

29. Ohya, H, Shiki, S, and Kawakami, H, *Fabrication study of polysulfone hollow-fiber microfiltration membranes: Optimal dope viscosity for nucleation and growth.* Journal of Membrane Science, 2009. **326**(2): p. 293-302.

30. Ghasem, N, Al-Marzouqi, M, and Zhu, L, *Preparation and properties of polyethersulfone hollow fiber membranes with o-xylene as an additive used in membrane contactors for CO2 absorption.* Separation and Purification Technology, 2012. **92**(0): p. 1-10.

31. Chung, T-S, Qin, J-J, and Gu, J, *Effect of shear rate within the spinneret on morphology, separation performance and mechanical properties of ultrafiltration polyethersulfone hollow fiber membranes.* Chemical Engineering Science, 2000. **55**(6): p. 1077-1091.

8. Oxygen/Ozone Binary Gas Mixture Separations

8.1. Background

As has been mentioned, when working with a material such as PVC for gas separation membrane processes which does not exhibit properties which make it ideal for general use in an existing large membrane market it is important that the niche which offers a practical use for the membrane is investigated. In this case the market identified is gas separation processes where the environment present is likely to promote oxidative interaction with the membranes. In order to establish the membrane resistance to this environment and also show its ability to separate a strong oxidising gas ozone/oxygen separation was identified as a process which represented the harsh environment and also offered an additional niche market on its own. The opportunity which ozone presents for a number of industries and the challenges which its use also poses as described in the introduction section of this thesis present a material such as PVC which is resistant to the chemical attack of ozone with the niche market opening for its use in an otherwise unlikely field.

It is desirable as a result of this not just to show how the PVC membranes perform on common gases for gas separation but also in the target processes for which the membranes are being targeted at. Hence a system whereby the qualities of PVC for separating binary mixtures of ozone and oxygen could be assessed is a key part of the development of the membranes. Working with ozone is not easy due to the high reactivity it possesses which means that material selection, process technology and safety precautions which are put in place are really important. Ozone processing can also be dangerous with high voltage electrical equipment being used in the production and a UK Health and Safety Executive Work Exposure Limit (WEL) of 0.2ppm in air averaged over a 15min period[1]. These practical impediments to experimentation with ozone combined with the expense of ozone equipment meant that in order to carry out ozone separation work some expertise in the area was sought out.

T. Wang and G. Huang in the Strathclyde University Electronic and Electrical Engineering Department have experience in working with ozone production and have all the necessary

production equipment as described in their proceedings paper "Investigation of ozone generation using dielectric barrier discharges at 50Hz, 2.6kHz and 20kHz"[2]. A partnership was formed with them where a small module would be looked at to test the suitability of the equipment which was available for running alongside a membrane unit.

8.2. Experimental Set-up

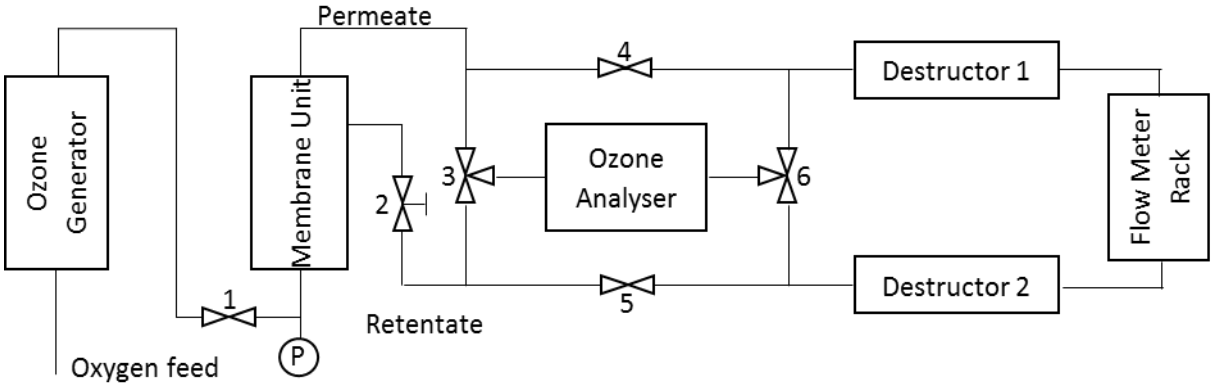

Figure 8.2-1: Schematic of the experimental set-up used to test membrane separation of ozone

A compressed gas cylinder of 99.99% oxygen provided from BOC is used to provide a flow of oxygen to the ozone generator. The use of high purity oxygen gives a higher output concentration of oxygen from the generator than the use of air, it also makes the monitoring of the separation processes easier to manage as the gas mixture produced is binary oxygen/ozone. If an air feed was used not only would this result in the other components of air being present in the separation system and competing for transport through the PVC membrane but also nitrous oxides would be created by the generation process also. While PVC is also resistant to attack of nitrous oxide it is generally better to avoid the production as they should not be released and the process already has to deal with the ozone gas which has to be converted back to oxygen before release.

The generator is a dielectric barrier discharge model developed in the University of Strathclyde's Electric and Electronic Engineering department and the full set up involving the generator has been described by the group[2]. The power supply for the generator in this case was run at 50Hz AC supply. Inside the generator three borosilicate glass tubes act as the dielectric barriers with stainless steel electrodes and a grounding water electrode surrounding the set up. The distance between the high voltage electrode and the glass dielectric barrier was 0.3mm. The water provided the additional benefit of allowing temperature control at a constant 15°C during the production. The generator design was developed to investigate ozone production efficiency under various sets of conditions, however the design utilising glass results in a maximum output pressure of 1bar from the generator. The result of this low production pressure is that the pressure difference driving force across the membrane is significantly lower than that which the gas separation membranes were tested with while utilising the more common test gases. Industrial ozone generators would be expected to provide a higher output pressure than this but it may be necessary to study how to increase the feed pressure to the membrane unit in order to provide the driving force necessary for an efficient separation process.

The oxygen/ozone mix produced by the generator passes to the membrane unit through ball valve 1. This valve allows the membrane and ozone detection systems to be isolated from the generation system which allows unsteady state, no feed tests, to be conducted if the vessel is initially charged with ozone/oxygen mixed gases then isolated and the permeate concentration monitored. However, again due to the low output pressure of the generator the starting pressure and hence permeation flow were low under these conditions making these experiments of limited value with the current generation system.

The membrane unit contains a potted up membrane module consisting of a number of membranes in a tube sheet and end cap which hang suspended in the gas fed into the unit. The module contained thirty individual membrane strands. This was the largest number of membrane strands which had been potted up in a single module over the course of this work and was undertaken in an attempt to compensate for the low feed pressure presented to the unit by increasing the surface of membrane available.

Both permeate and retentate flows from the module lead to ozone destructors through ball valves 4 and 5 respectively. In the destructors the ozone is catalytically converted back to oxygen and the pure oxygen flow passes to the bubble flow meter rack where an appropriately sized bubble flow meter can be selected for measuring the flow. The catalyst for the ozone destruction was carulite® 200 (Manganese dioxide/copper oxide) and is in a granular form used to create a packed bed through which the streams can flow towards the outlet. The bubble flow meters vented to atmosphere in a fume cupboard which was turned off whenever measurements were to be taken. An ozone alarm was also located in the fume cupboard such so that if ozone was coming through the destructors without being destroyed it could be detected.

Ball valves 3 and 6 are three way valves which could allow the flow of either permeate or retentate to be diverted through an IN-USA Mini-HiCon Ozone Analyser or they can be set for neither flow to go through the analyser. Valve 2 is a series of three valves, a ball valve followed by two needle valves. This set up allows control of the retentate flow down to the same level as the permeate flow. A single valve was found to be unable to accomplish this task requiring the pressure drop across multiple valves in order to reduce the flow to the extent required.

The poly(vinyl chloride) (PVC) hollow fibre membranes used for this experiment were produced from a solution via a dry wet spinning process and potted up into modules of thirty membranes before being coated using Sylgard 184. The membranes produced for conducting these experiments were produced under the conditions associated with membrane category 4 in MB7.

The first step in the experiment was to precondition the membranes using oxygen only. To do this the oxygen supply was turned on and allowed to purge the membrane module to pure oxygen. Valve 2 was closed and the membranes were left for 3hrs at 1 bar pressure. This step is conducted to ensure there is no back flow of other air gases into the membrane generator and it also purges these gases from the system such that the system can be considered binary oxygen/ozone. It also reduces the impact of any swelling of the membranes due to the oxygen which could increase the permeation rate.

Once the membranes have been preconditioned the ozone generator was turned on and valve 2 opened. This flushes the system at a flow rate of 100mL/min of the oxygen/ozone mixture. The concentration of ozone throughout the shell side system rose to approximately 22g/m^3. After

flushing the system for 5mins the flow rate of the permeate gas was measured so that the stage cut for the system could be set at an appropriate value.

The retentate flow was then reduced and controlled to the required stage cut using valve 2. After checking the flow rates of the streams again and that the pressure was still at 1 bar in the system readings could be taken for the concentration of ozone in the system.

All flow times recorded for this experiment were averaged over at least 6 measurements and no measurements were taken until the system had been at a steady equilibrium for 2mins after any change.

Finally, the system also had a by-pass from the ozone generator to the ozone analyser. This allowed detection of the concentration and flow rate in the generation stream. These measurements were required in order to allow material balances to be constructed over the system.

8.3. Results and Discussion

The first experiment which was conducted was a straight forward flow experiment where the generator was set to run at 1bar and the flow was controlled but could either pass through the membrane to the permeate stream or leave the module by the retentate stream.

The average permeate flow rate obtained was 1.57ml/min. The retentate flow rate was controlled down to 5.66ml/min which gave a ratio of retentate flow to permeate flow of 3.62. At these settings the ozone concentrations of both permeate and retentate streams were taken with the ozone analyser. The permeate concentration gave a read out of 0.00g/m^3 ozone. The retentate reading exhibited an unsteady state nature and was constantly rising over the period of the test (30mins).

The permeate constantly reading a concentration of 0.00 g/m^3 was a promising sign as if there was no ozone coming through the membranes then they would be providing excellent separation. However, there are a couple of explanations as to why this reading may not be an accurate representation of what was occurring in the experiment.

The first of these was a problem with the ozone analyser being used in conjunction with the system. The manufacturer's specifications suggest that the analyser has a minimal flow rate of 100mL/min for accurate measurement. It is therefore possible that as the flow rate in this case was only 1.57ml/min it is not getting enough gas to sample for a reading.

An attempt was made to address the low flow issue, or at the very least obtain an idea of the system sensitivity. By removing all parts of the membrane system from the experiment and connecting the ozone generator directly to the analyser then controlling the flow to as low a level as possible it was hoped to show that if there was ozone present even at these low flow rates it would be detectable by the analyser.

The lowest flow that could be generated through the system was 3.19 mL/min so approximately twice the flow of permeate during the testing. Under these conditions the ozone analyser proved capable of detecting the presence of ozone. Similarly to the retentate in the main experiment, an unsteady state process was occurring during the period of testing (30mins) whereby the concentration of ozone in g/m^3 was seen to increase steadily throughout.

From this secondary test it was seen that at least the analyser could detect ozone under flow conditions which were similar to those seen in the permeate stream. Although it should also be born in mind that the concentrations being detected here were larger than anything which would have been present in the permeate stream during the main experiment.

The second possible explanation for why the ozone concentration being given as zero in the permeate stream might not be an excellent result would be if ozone is being converted back into oxygen during the solution diffusion through the PVC membranes. If this was occurring then quantitative data would be required in order to conduct calculations to show that there was ozone missing from the outlet streams.

However, the unsteady state nature of some parts of the experiment is a major problem when it comes to gathering quantitative results. Even if it is assumed that the problems outlined above are not occurring i.e. the analyser can be trusted to read accurately at the low flow rate and the ozone is not being destroyed by the separation process, then it is still not possible to do quantitative calculations with the system which is in place. If steady state was reached then it would have been possible to obtain quantitative data from material balances across the membrane system using the by-pass to obtain information on the feed stream contents.

The ozone concentration build up is another problem which is associated with the low flow rates which are involved in the system. Because the flow rate is low, the hold-up which the gas experiences in the ozone generator and even short lengths of pipe is large. The result of this is that a particular volume of gas is reacted for longer in the generator causing the concentration to build up towards the equilibrium value more than would be experienced at higher flow rates. However, the transfer of this high concentration through the system is very slow due to the flow rate and out with the time scale of the experiments. The simplest solution to this would be to run the experiments for an extended period of time to allow the equilibrium concentration to be established throughout the system. However, the power supply used with the system had a tendency to over-heat due to the high load required of it in running the generator and this limited the experimentation duration to 30mins which proved to be too short a time frame for equilibrium to be established.

In an attempt to obtain some quantitative data a dead end test was attempted. For this test the vessel was charged with the oxygen/ozone mix by again flushing gas through it at 100mL/min. Valves 1 and 2 were both shut trapping the gas in the vessel with the exception of the permeate line. The chamber was then left for 15mins while monitoring the flow rate of gas out through the permeate line. After this time valve 2 was opened to allow the rest of the gas in the chamber to flow through the retentate line to the analyser in an attempt to show an increase in the ozone concentration from what was experienced during the flushing stage.

While this test is also unsteady state by monitoring the permeate flow closely it would have been possible to predict the pressure in the chamber at any particular time. Unfortunately the test

failed as the release of the contained gas from the chamber at the end of the experiment did not produce a sustained enough flow for the ozone analyser to provide a reading.

8.4. Oxygen/Ozone Binary Gas Mixture Separation Summary

There is qualitative evidence that separation of ozone and oxygen has been achieved using PVC hollow fibre membranes. However, there were a number of problems associated with the system which mean that quantitative data is difficult to obtain. Most of these problems relate to the low flow rate which is obtained from the small number of membranes (30) which were used in these experiments. The low flow rate causes problems for the ozone analyser, in terms of the manufacturer's specifications; although it has been shown that the analyser is capable of detecting ozone with flow rates close to the minimal observed in the experiment. The low flow also causes issues relating to the establishing of equilibrium in the system with the ozone production method resulting in a building up of ozone concentration throughout the apparatus over time. Eventually the concentration build-up would reach equilibrium in the generator for the energy being provided and the flow rate would carry this through the system but the generator power supply cannot be used for the time scales required in order to achieve this.

There are possible improvements which could be made to the system which would allow for the generation of quantitative data on the ozone/oxygen separation by PVC.

Improvements to the experimental set-up are required before it can be used to generate data on the separation of oxygen/ozone binary gas mixtures. A survey of ozone analysers reveals that nearly all the manufacturer's specifications show a similar level of sensitivity with a minimal flow of 100 mL/min or higher. Unfortunately this means that the flow through the system really has to be increased or an alternative method of setting up the system and testing has to be found. New systems, at least a larger capacity membrane unit, are likely to be required to deal with the restricted flow creating unsteady state situations so aiming to achieve minimal flows in line with

this 100mL/min is a reasonable step. On the basis of the flow rates seen in this experimentation the required number of membranes approximately 25cm long would be approximately 2000.

The numbers of membranes required could be significantly reduced if the pressure difference across the membranes could be increased. The current generator is limited by its construction to operating pressures of 1bar (gauge) so in order to increase the pressure on the shell side of the system a new generator would be required. The pressure on the tube side (permeate side) of the system is open to atmosphere so it is possible that a vacuum could be drawn on this side to increase the driving force although the bubble flow meters make this more difficult so an alternative means of measuring low flow may also be required.

Alternative analysis measures may also provide an ability to work at low flow rates. If gas chromatography could be used as a gas detection method for instance then either the dead end experiment carried out above could be run but allowing the gas at the end to be released to the chromatograph or the continuous process could be sampled and run through the chromatograph. The problem with this is that for chromatography columns to function the gases have to interact differently with the stationary species in the column. While there is a high degree of difference in the strength of ozone and oxygen in the strength of their interactions the ozone is so reactive it would be difficult to identify a stationary species it would not just react with and hence never leave the end of the column.

8.5. Bibliography

1. *Ozone: Health hazards and control measures*, 2014, Health and Safety Executive.
2. Huang, GW, T.; Timoshkin, I.; MacGregor, S.; Given, M.; Wilson, M., *Investigation of ozone generation using dielectric barrier discharges at 50Hz, 2.6kHz and 20kHz.* Proceedings of the XIX International Conference on Gas Discharges and Their Applications, 2012: p. 650-653.

9. Conclusions

9.1. General Conclusions

Membrane processes offer a number of advantages when compared to conventional separation techniques such as distillation. The benefits of the use of membrane processes cover a variety of areas which are important to industry including costs, environment, design, consistency and process/species interactions. However, the processes tend not to offer a completely effective solution to separation issues for a number of reasons including the purity of the separated streams which they achieve, versatility for stage cut creation, fouling and chemical compatibility. In gas separation applications membranes have made a large impact on other methods since there is no need for a phase change in order to separate the species and they avoid the use of expensive catalysts.

The gas separation membranes which have seen success in industry have been made from a variety of models but the preferred confirmation is when a bulk polymer membrane can be used as the separation medium and can be constructed into separation units containing hollow fibers. The key aspect to the production of these hollow fibers is being able to produce a defect free surface layer which forces the gas transport through the membrane to be by a solution diffusion mechanism rather than Knudsen or viscous flow through pores, this affect can also be achieved by coating the membrane to increase the pore resistance. The production of a hollow fiber can be conducted in a number of ways but dry/wet spinning provides a highly optimisable process while avoiding some issues associated with wet only production in terms of coagulation bath contents. The mechanisms proposed by *Pinnau* and *Koros*[1] provide a good explanation of what is occurring during the formation processes involved in the dry/wet phase formation mechanisms.

While gas separation membranes have been adopted across a range of industries the gases which they have been targeted at separating fall into a fairly narrow field: oxygen, nitrogen hydrogen, carbon dioxide and methane being the main protagonists. There are still various different markets which offer potential for the expansion of gas separation membranes into new

areas. One such area is the separation of ozone and oxygen. The use of ozone in process industries has been growing over the last couple of decades but this expansion is limited by a number of factors including the concentration of the gas which can be produced by current generation mechanisms. The use of an oxygen/ozone separating gas separation membrane would open up new markets for both ozone and gas separation membrane technology. Ozone is gaining in popularity largely down to its excellent oxidising potential. However, this high reactivity poses problems when dealing with physical contact processes such as gas separation membranes because the material used in the production has to be resistant to the chemical attack of the ozone. PVC offers one solution to this problem. PVC has not been popular in gas separation processes since it has low permeability and hence low flux increasing the unit size required. In this situation though if the membrane was showing good selectivity in the oxygen/ozone separations then the membranes may offer potential for use in industry in a previously unexplored market.

The dope composition is a crucial aspect of gas separation membrane production. The dopes used for dry/wet production methods can have complicated compositions, in this case the PVC concentration was initially set at 24% as this was similar to the concentrations used for other gas separation membrane work. This was also a little higher than the amount of PVC used in other membrane applications such as ultrafiltration but was selected because it was expected that to produce the dense layer required for gas separation a higher initial concentration would be beneficial. Due to the role of the high volatility solvent in the dry step, where it is rapidly evaporated to move the composition of the surface layers of the dope through the phase diagram, and the desire to produce a very thin active layer for the low permeability PVC the concentration of tetrahydrofuran (THF) was kept low at 7%. The non-solvent composition was set at 16% as it was felt this would allow the concentration to be easily increased or decreased. The balance of the solution was then made up with the low volatility solvent, N,N-dimethylacetamide (DMac).

9.2. Ambient Temperature Spinning Conclusions

The first membranes produced (MB1) involved the use of propan-2-ol as the non-solvent in the dope solution. When used in permeation experiments these membranes gave Knudsen diffusive selectivity when uncoated and very low selectivity once coated. The Knudsen selectivity when uncoated suggested that the surface layer was imperfect with either damage having being caused to the surface layer or failure to produce an active layer in the first place. That the coating did not produce a massive improvement in the properties meant that the active layer was in poor condition with either very large pores or many smaller pores such that the transport of gas by methods other than solution diffusion was too favourable for the membranes to offer good separating properties in terms of gas separation. Propan-2-ol is not a common choice for the non-solvent in the dope solution for gas separation membranes with ethanol being a much more common choice. While the use of propan-2-ol in place of ethanol was justifiable due to the similarity in properties of the species it was concluded that the reduced mobility of the non-solvent in the solution provided by propan-2-ol could have contributed to the problems with the membranes and that ethanol should be used going forward.

The second batch of membranes produced (MB2) was prepared with the same concentrations of the different aspects of the dope but replacing the propan-2-ol with ethanol. Only one set of spinning conditions was maintained throughout the spinning run with various parameters being set at typical values for gas separation membrane production. The sampling of membranes was conducted at various times over the course of the spinning run in order to determine if comparisons could legitimately be made across a run or if the properties varied during the production time. When uncoated the membranes continued to show Knudsen diffusion properties. After coating this time the membranes showed a larger improvement in selectivity although there did appear to be a trend in the membrane properties over time with the membranes at the start giving better selectivity than those at the end. From this run this indicated that comparisons made over a spin run with varying conditions would be invalid.

Having achieved some level of selectivity in MB2 for the next two batches of membranes (MB3 and MB4) it was decided to increase the concentration of the polymer being used to 26% and 28% respectively. This was done in an attempt to increase the linear density of the dope solution

as it was being spun and hence increase the ease of formation of the active layer. This was successful to some extent with the membranes produced showing a high degree of consistency across the spin run for the two different concentrations which was in contrast to the MB2 results suggesting the spinning protocols were conducted to a higher level. The membranes continued to show Knudsen selectivity while uncoated with the coating process bringing about a swing towards solution diffusion, however the results obtained were still far below the intrinsic selectivity of the polymer (5.5). The dope solution itself changed nature rapidly over the increase in concentration becoming noticeably thicker, it was concluded that this could be dope passing through the critical concentration for the polymer as postulated by *Chung et al*[2, 3] and as such that the 28% dope may hold better prospects for gas separation membrane preparation than the 24% dope. It was postulated at this point that the lack in effective separation was due to a lack of coalescence of the nodules due to penetration into the phase diagram during the dry step crossing the solidus tie line and resulting in hard nodules which were able to resist the capillary forces involved in surface layer formation.

For MB5 in order to reduce the penetration into the phase diagram the concentration of high volatility solvent was reduced to 4% and the concentration of high volatility solvent also decreased to 12%. During the spinning process itself it was decided to alter the flow rate of gas at the impingement zone during the dry step with the hope that less aggressive production conditions would also relax the composition change, a range of values of 2, 4 and 6L/min were used for this over the course of a single spin run which seemed to have been validated by the consistency of the membranes which were produced for MB3 and MB4. The uncoated membranes continued to show Knudsen selectivity under all the new conditions. The coated membranes also failed to show improvement on what had previously been achieved.

The MB5 membranes failure to produce effective membranes resulted in a consideration of the spinning conditions and procedures being used in areas which were until that point not being considered. So far membrane spinning had been conducted at ambient temperature in an attempt to produce membranes which worked with the lowest production costs possible. However, preliminary work had indicated that membranes prepared at elevated temperatures may exhibit more success in meeting the aims of the work.

9.3. Rheological Conclusions

It was decided to investigate two factors which were felt could be having an impact on the results which were being achieved. These were the time between dope production and the temperature at which spinning was occurring. A rheological investigation was conducted into the dope composition used in MB5 to assess if these factors had an impact on the nature of the solution. Samples were subjected to flow, oscillatory and creep rheological testing.

Flow rheology tests were conducted where the temperature was varied between 20°C and 60°C and the time of testing was varied by up to a day from the dope production. The dope was noted to exhibit thixotropic behaviour on the up and down flow curves for all samples. It was also noted that there was a degree of slippage associated with some of the samples within the test cell.

The thixotropic effect was much more pronounced in the dope tested at 20°C than the tests conducted at 60°C. Although the storage occurring at the lower temperature before testing at 60°C seemed to have very little effect. This suggested that the thixotropic effect was linked to the temperature being tested at. However, for any set of conditions since this effect is clearly demonstrated the process may see an increase in consistency if an additional pre-shear step were to be included. Indeed after a conditioning period the 20°C tested dope saw enough difference to suggest that if the 60°C dope was successful in producing membranes then inclusion of a pre-shear may move the 20°C dope towards producing more similar results to that observed in the 60°C dope. However, overall the 60°C dope still exhibits a lower viscosity it could be concluded that this viscosity may play an important part in the production process due to the increased mobility of the solution components.

The slippage in the test cell during flow experiments was also worse for the 20°C dope. It was postulated this could be linked to the high viscosity of the solution at the lower temperature such that at the high shear rates the solution was unable to respond quick enough to the forces acting upon it. This slippage appeared at shear rates which would be possible to experience within the spinnerets. If this were occurring in the spinneret then the assumption of a no slip condition which applies to flow conditions may not be accurate and hence the shear of the dope passing through the spinneret would effectively not act on the outer layers of the dope being spun. If this were the case then the shear induced molecular alignment widely accepted to be a

contributory factor in producing separating layers in gas separation membranes could not occur. This may be a contributing factor to the low selectivity achieved during the ambient spinning test program.

The storage time of the solutions did not appear to have a large impact on the results which were obtained in comparison to the temperature. However, there were some signs that the viscosity could be increasing if the spinning of the solution was delayed. It was concluded from this that the solutions should be spun as quickly as possible in order to discount any influences from a storage time effect.

Finally from the flow analysis it was hoped to obtain estimates of relaxation times by determining the critical point for the dope solutions i.e. the transition point between the first Newtonian Region and Power Law behaviour. This is the point where the molecular orientation process can begin to act within the dope solution. Both 20°C and 60°C dopes exhibit critical points at very low shear rates so the spinning process is definitely operating in a region where this would be expected behaviour. The reciprocal of the critical shear rate is often termed the relaxation time and is a measure of how long it takes the solution to lose the conformation which the shearing process imparts to it. Relaxation times of 100s for the 20°C dope and 0.067s for the 60°C dope meant that the freezing in of any orientation achieved should be possible since polysulfone often exhibits relaxation times as low as 0.0025s[4]. These results meant that the use of mass transfer models to determine skin layer thickness were stunted in terms of the use of relaxation time because the governing factor would be more likely to be the rate of transfer of the high volatility component through the system. This links in with the idea that the dope at 60°C may exhibit better molecular mobility through the solution and hence have a greater possibility of producing a thicker active layer.

In order to assess the applicability of the results to the situation being seen in the spinneret it was necessary to model the flow conditions experience by the dope within the spinneret. This work was carried out with software developed by S.J. Shilton[5]. The modelling conducted with this software allowed the velocity, shear stress and shear rate profiles of the dope within the spinneret to be determined. The velocity profiles showed that the 20°C dope travelled slower towards the centre of the annulus than the 60°C dope but faster towards the walls of the

spinneret. This resulted in an almost flat profile in the centre of the annulus for the 20°C dope as opposed to the more common parabolic rate distribution for the 60°C dope. The higher velocities at the wall for the 20°C dope give the expected associated increases in shear rate and shear stress. This might normally be considered a good thing imparting a higher level of molecular alignment. However, it pushes the 20°C dope towards the shear levels which were resulting in slippage during the flow rheology experiments. This gave the main conclusion that the ambient spun membranes may be lacking an orientated surface layer due slippage occurring within the spinneret which has a negative impact on the selectivity which the membranes exhibit.

Creep rheology experiments were conducted in order to investigate the type of properties which the different dope solution exhibit with respect to their viscoelastic properties. It was concluded that if slippage of the dope as it passed through the spinneret was an influencing factor on the performance of the membranes then the slippage occurring would be greater exacerbated by more solid like behaviour as this would be less likely to flow. Creep analysis allowed the assessment of the stresses required in order to move the different dope solutions from gel or solid like behaviour i.e. elastic behaviour into liquid like behaviour i.e. viscous behaviour. The tests conducted found that the 20°C dope contained a much higher degree of elastic characteristics than the 60°C dope, in fact the 60°C did not exhibit any elastic behaviour under the most scrutinising conditions which could be achieved with the experimental set-up.

As an extension to the creep testing conducted the dope solutions were subjected to oscillatory testing. This testing confirmed the results obtained so far with the 60°C dope exhibiting behaviour which was more favourable in terms of behaviour under shear within the spinneret although the readings obtained for the dope were not what was expected.

Overall the rheological experimentation gave clear indications that spinning the dope at elevated temperature provided access to more favourable conditions for the production of gas separation membranes than the ambient conditions.

9.4. Elevated Temperature Spinning Conclusions

The aim of MB6, the first membranes to be produced at elevated temperature, was to show that the protocols put into place to spin immediately after dope production and at an elevated temperature would have an impact on producing greater selectivity from the PVC membranes. It was also part of this to again take samples from various points of the production run in order to assess the validity of comparisons made on membranes produced at various points in the run under the new conditions. Additionally the membranes were subjected to and tested after two coating processes as well as a single coating to assess if the results could be improved any. The uncoated membranes continued to show Knudsen selectivity suggesting that the new protocols were not enough to produce a perfect active layer on the membranes prior to coating. Selectivity results improved greatly after the first coating procedure with a corresponding reduction in the pressure normalised flux through the membranes. They also saw further improvement after a repeat coating procedure. These improvements showed that the elevated temperature spinning process could produce membranes where the primary method of transport was solution diffusion. The selectivity properties of the produced membranes were lower than for isotropic films but still high enough to show more promising separating qualities.

Over the course of the spinning run the membranes produced in MB6 displayed a small decrease in the separation properties associated with them. The reason postulated for this change in properties was that there was a change being induced in the mean free cavity sizes. The evidence for this came from the different effects which were seen between the fast and slow gases in the gas pair where the fast gases saw their flux affected to a greater extent than the slow gases. The observed trends could be explained by the closing of cavity spaces reducing the mass transfer associated with the fast gases while providing no reduction to the transfer of the slow gases as this was already denied by the initial sizing. Overall the impact of the changes over the course of a spin run was not seen to be a large enough difference to affect the comparisons between membranes produced at different points in the spin run.

Having shown that PVC membranes could be manufactured at elevated temperatures which gave selectivity for the test gases which could be attributed to solution diffusion mechanisms the next step was to attempt an optimisation of the production conditions. The factors identified to

be varied for optimisation were the dope extrusion rate, forced convective gas flow rate and residence time in the dry step below the impingement zone. The dope extrusion rate and forced convective gas flow rate are factors known to impact on the properties of membranes. The residence time in other works is not generally separated into times above and below the impingement zone. It was hoped by isolating these positions the important area for formation of the active layer in the dry step could be more accurately identified. The factors were investigated both graphically and by Taguchi statistical analysis in order to look for consensus between the different methods and hence show the validity of the use of the Taguchi methodology with gas separation membrane processes. Each of the three factors was utilised at a high and a low level.

In order to conduct the experimentation eight different membrane categories were produced at elevated temperature. All the uncoated results exhibited the expected Knudsen diffusion results. The coated results however exhibited a range of different separating properties dependent upon the production conditions for each category.

The graphical analysis suggested that the best set of conditions, of those which were tested, for the production of higher selectivity gas separation membranes were; lower extrusion rate, higher residence time and higher gas flow rate. These conditions corresponded to membrane category 4 being the most suitable category of membrane.

The Taguchi analysis agreed with the results of the graphical analysis that category 4 membranes were the best membranes adding to this conclusion that the forced convective gas flow rate had the biggest effect followed by the residence time below the spinneret and finally the dope extrusion rate. This showed that the Taguchi method was a suitable statistical tool for analysing the results associated with gas separation membranes.

9.5. Characterisation and Modeling Conclusions

Having produced membranes which showed solution diffusion mass transfer properties the next stage was to build up some characterisation information on the membranes. Scanning Electron Microscopy (SEM) is one of the key characterisation tools for gas separation membranes allowing detailed imaging of surface features such as pore size and sometimes information on the thickness of the active layer.

Cross sectional cuts through the membranes showed that the membranes tended to have a very thin active layer, with relatively large pores just below the surface, then a region with smaller pores in the middle of the wall before having larger pores towards the inner wall of hollow fiber again. Surface images showed that the membrane was composed of a large number of nodules which were pressed together. Combining this membrane conformation with the results of MB7 gave the conclusion that the membranes were very close to forming a perfect active layer but that the nodules were a little too hard for nodule coalescence to work completely effectively resulting in small pores of approximately 150nm where the spheres could not properly coalesce. The hard nodular structure results in the very thin almost perfect active layer but not enough to replicate isotropic film performance.

The surface SEM images also revealed a number of unexpected rip like features in the surface of the membrane. These rips varied in size, between 5 and 20μm, and regularity. However, it was noted that they only seemed to affect the top layer of material indicating that they were being formed during the dry step most likely. Two reasons for the rip formation were proposed: jet-stretch ratio and solidification volume reduction. The jet-stretch ratio is the most likely cause of the issue with either irregular wind up speed (since this was set to match membrane extrusion rate only variation would give the effects) or the influence of gravity on the membranes in the dry gap providing the force required to rip the forming active layer.

Images of coated samples were also produced since even with the rips features in the surface the membranes were providing respectable selectivity values. It was therefore anticipated that effect of the coating might be visible in the SEM images. The images produced had a ghost like quality to them which was not noticeable in the uncoated membranes. It was reasoned that the

coating is forming such a thin layer over the membrane surface that the SEM penetrates this layer and this ghostly visual effect is the sign that the coating was present.

The SEM images were used to aid in the inputs to create a membrane model which could be used to determine the active layer thickness and surface porosity of the membranes. The model was based on an electrical resistance analogue and found that the active layer thicknesses were generally in the region of 600-800Angstroms and contained a large number of small pores. This fits in well with the SEM images and the conclusions from these. The lower extrusion rate gave higher active layer thicknesses due to increased exposure to the impingement zone flow in the dry step. The lower forced convective gas flow rate also resulted in thicker skins on the membrane thought to be as a result of the high flow rate doing a better job of “searing” the active layer onto the membranes preventing the deeper penetration which the lower flow rate achieved. The model showed no trends in terms of the residence time below the impingement zone during the dry step suggesting that the thickness of the active layer is set before this point. The model variations agreed well with the Taguchi and graphical analysis of the MB7 membranes.

Tensile testing on the membranes was also conducted as strength is an important parameter for industrial applicable membranes. The results showed consistency within a single category in the strength which the membranes displayed and only small variations between categories. However, the strength associated with the membranes is low for an industrial process. This was an expected issue with the PVC in comparison to other materials which have seen effective use in gas separation but the target markets for these membranes involve particularly clean processes, therefore the reduced strength of the membrane is less impactful on the potential of the process.

9.6. Ozone/oxygen Binary Mixture Separation Conclusions

Ozone/oxygen separation experimentation presented a number of problems with respect to the equipment which was available. Experiments were undertaken under flow conditions initially. The results of these experiments showed separation occurring but the flow rates seen were below those which the detection equipment was specified to deal with. The impact of the low flow was assessed and it was believed that the equipment would have detected the low level of ozone in the membranes if it had been present rather than showing no reading as was the case. If this is accurate then either the membrane was working to separate the ozone/oxygen mixture or the ozone was being destroyed on its passage through the membrane. Dead end testing was also conducted but did not change this situation any.

The ozone/oxygen work suggested that there was qualitative evidence that the membranes were working to separate the gases. The experimental methodology which could be conducted using the equipment available meant that obtaining quantitative data on the separations was not possible. New more sensitive equipment or a much larger membrane unit would be required in order to conduct the experiments effectively.

The PVC membranes exhibited resistance to the oxidative effects of one of the strongest oxidising agents which is commonly used industrially in the form of ozone. This chemical resistance combined with the values from the elevated temperature membranes suggests that the membranes produced from PVC show potential for separating some of the more commonly separated gases in industry in oxidative environments. The PVC membranes do not exhibit good enough separation characteristics to compete with current membranes in a benign environment however in an oxidative environment which would destroy membranes produced from polymers such as polysulfone there is a possible market.

Considering all the results throughout the work the PVC membranes have shown that they have some viability but there are a number of issues which require better understanding and resolving before they could see progress towards use in an industrial environment.

9.7. Bibliography

1. Pinnau, I and Koros, WJ, *A qualitative skin layer formation mechanism for membranes made by dry/wet phase inversion.* Journal of Polymer Science Part B: Polymer Physics, 1993. **31**(4): p. 419-427.
2. Chung, TS, Teoh, SK, and Hu, XD, *Formation of ultrathin high-performance polyethersulfone hollow-fiber membranes.* Journal of Membrane Science, 1997. **133**(2): p. 161-175.
3. Chung, TS, Kafchinski, ER, and Vora, R, *Development of a Defect-Free 6fda-Durene Asymmetric Hollow-Fiber and Its Composite Hollow Fibers.* Journal of Membrane Science, 1994. **88**(1): p. 21-36.
4. Gordeyev, SA and Shilton, SJ, *Forced convection spinning of gas separation hollow fibre membranes: some underlying factors, mechanisms and effects.* Journal of Membrane Science, 2004. **229**(1-2): p. 225-233.
5. Shilton, SJ, *Flow profile induced in spinneret during hollow fiber membrane spinning.* Journal of Applied Polymer Science, 1997. **65**(7): p. 1359-1362.

10. Future Work

When this section of work completed there were a number of areas which offered opportunities for the continuation of the research in order to refine or better understand the PVC membranes and progress the development process.

The first area which could be investigated further is the dope solution. During the research some features of the polymer solution were identified which affected the results obtained from the membranes and having a better idea of the behaviour of the PVC solutions may provide a better understanding of the overall conditions being seen during the processing. The work conducted indicated clearly that the dopes required elevated temperature in order to produce membranes with good separating qualities. There were a few differences identified between the dope solutions tested at low and high temperature: thixotropic behaviour, slippage effects during testing and the relationship between viscous and elastic behaviour.

The thixotropic effect seen during the research was much larger for the low temperature dope than for the high temperature dope. On the downward sweep of the rotational flow rheology curves the behaviours of the high and low temperature dopes were much more similar than on the upward sweep. Experimentation into the effect which pre-shearing the dope could have on the process would be of interest since the viscosity is reduced so much after a period of shear at the low temperature. This experimentation could be conducted first of all on a rheometer then moved into the lab and used to produce membranes which perhaps utilise different production conditions or dope compositions than those generated in this work. Shear in the spinneret is also known to contribute to molecular alignment which can improve the performance of gas separation membranes. With a suitable pre-shear method the molecular alignment could be influenced prior to the spinneret perhaps obtaining some of the same benefits in addition to changing the behaviour of the dope[1]. Additionally this may help on the second point of slippage as perhaps a lower shear spinneret could be designed and utilised under these circumstances.

The slippage effect was particularly noticeable in the dope at low temperature and was incurred where high shear rates were present. The modelling of the flow within the spinneret showed

that the conditions within the spinneret could result in shear rates which were in the region which was inducing slippage during the rheology. Hence spinneret design could be considered which would control the shear rates seen during production[2-4] in order to keep under any established threshold value for the dope being spun where slippage sets in. Again this effect could be studied on different dope compositions at different temperatures in order to establish the boundary conditions which could be operated within. The main method of investigation would have to be by use of a rheometer in this case.

The final difference which was established between the dope at low and elevated temperature was in the viscoelastic nature of the solution with the low temperature dope exhibiting highly elastic behaviour while the low temperature dope exhibited highly viscous behaviour. The change in nature of the solution was felt to have strongly contributed to the change in the selectivity of the dope between the ambient and elevated temperature conditions. This is partially through contribution to points mentioned above in the shape of the slippage. The nature of the solution could also be critical to the mobility of the molecules within the solution hence the ability of the molecules to align in the active layer. One key to the ability of the PVC membranes to separate gases could therefore lie in achieving a solution displaying more viscous behaviour like the elevated temperature dope. Establishing whether this change in nature is sudden or gradual and under what conditions it exists could help establish a set of boundary conditions for the production of gas separating PVC membranes.

All the factors mentioned so far could allow the use of a different dope composition for the production of the PVC membranes and perhaps allow the relaxation of some of the production conditions such as temperature. This being the case an understanding of the phase diagram of the PVC solutions and how it varies with temperature and different compositions could be very useful in understanding the production process. The development of a phase diagram for use in understanding the position of the dope during the spinning process has become a tool used by a few authors[5-8] where generally it is the binodal curve which is the focus of the work and is determined by cloud point experimentation. Although phase separation and boundary locations are influenced by shear conditions these phase diagrams could be combined with a mass transfer model of what is occurring in the dry step to predict the composition of the dope and the kind of phase separation which may be induced through the membrane. This would also require

development of a suitable mass transfer model to describe the behaviour of the dope as it passes through the dry step.

The development of a model to describe this aspect of the process is not something which has seen extensive attention. A model has been created by *Shilton*[9] which was used to predict active layer thicknesses by studying solvent evaporation during the dry step and this was suggested as a "framework" for further development. By extending this model and further developing it then it may be possible to determine the positions within the phase diagram of the spun membranes at the end of the dry step of production.

Moving on from the dope solution to the membranes and the membrane production techniques. The work carried out in MB7 displayed that the conditions under which the membranes were produced would have an influence on the results achieved. The optimisation of these production conditions can therefore be continued to include other aspects of the production, particularly if a new dope were to be established for use. In tandem with this alternative ways of producing the membranes which make the process more controllable could also be developed. It was noted during the experimentation that there appeared to be small variation in the results which would be achieved from a single batch of membrane production over time. It is likely these variations are in response to the conditions under which the membranes are produced and hence improvements in control should allow for more consistent and reliable results. This work should also address the ripping which was seen in the membrane surface during SEM imaging. It was concluded that these rips were likely an artefact of the production techniques used and hence refinements which prevented these phenomenon from forming could see a dramatic improvement in the selectivity properties displayed by the membranes.

The modelling and of the process to calculate active layer thickness could see some improvement if a more definitive determination of the separating qualities of isotropic PVC could be determined. The production of thin films of PVC for use in determination of the separating qualities which it has would allow a more accurate representation of the model to be developed and would also give a better idea of where the membranes were situated in relation to Robeson's Upper Bound. This would be useful as a performance characterisation tool.

There are a number of opportunities to develop the work further in the use of ozone. The experimentation carried out for the creation of this thesis gave qualitative evidence that the membranes were being successfully separating ozone and oxygen binary gas mixtures. In order to provide quantitative evidence however the flow through the equipment must fall within the specified operating range and allow mass balances to be carried out over the system to determine the separations achieved. This requires the development of a pilot scale module or the acquirement of equipment suitable for dealing with the low flow rates associated with the process.

Furthermore from any positive results found in working with ozone and oxygen the best way to set up and industrial unit would have to be considered in order to achieve concentrated streams while obtaining high productivity.

One of the issues with directing work at the ozone oxygen separation activity is the reactivity of the ozone with many polymer materials. Another polymer material which has seen use for membranes and provides good ozone resistance is polycarbonate[10-12]. Polycarbonate exhibits some of the same problems as PVC for use in gas separation membranes having low permeability towards gases[10] but additionally to these is not commonly seen in hollow fiber membranes even for other types of processing. This means that polycarbonate may be worth considering as an alternative to PVC but the development of a suitable spinning solution would require a great deal of work.

Another alternative membrane type to attempt to boost the membrane properties may be the preparation of mixed matrix type membranes. It may be worth investigating the effect of including ozone compatible particulates into the membrane in an attempt to maintain the selectivity of the membranes but increase the permeability seen.

Overall, there are a number of opportunities for the development and refinement of PVC membranes in order to make them into a suitable and attractive industrial option.

10.1. Bibliography

1. Peterson, EC and Breedveld, V, *Shear-induced demixing in polymeric membrane dopes.* Journal of Membrane Science, 2013. **431**(0): p. 131-138.
2. Widjojo, N, Chung, T-S, Arifin, DY, Weber, M, and Warzelhan, V, *Elimination of die swell and instability in hollow fiber spinning process of hyperbranched polyethersulfone (HPES) via novel spinneret designs and precise spinning conditions.* Chemical Engineering Journal, 2010. **163**(1–2): p. 143-153.
3. Peng, N and Chung, TS, *The effects of spinneret dimension and hollow fiber dimension on gas separation performance of ultra-thin defect-free Torlon® hollow fiber membranes.* Journal of Membrane Science, 2008. **310**(1–2): p. 455-465.
4. Chung, T-S, Qin, J-J, and Gu, J, *Effect of shear rate within the spinneret on morphology, separation performance and mechanical properties of ultrafiltration polyethersulfone hollow fiber membranes.* Chemical Engineering Science, 2000. **55**(6): p. 1077-1091.
5. Wallace, DW, Staudt-Bickel, C, and Koros, WJ, *Efficient development of effective hollow fiber membranes for gas separations from novel polymers.* Journal of Membrane Science, 2006. **278**(1–2): p. 92-104.
6. Barzin, J and Sadatnia, B, *Theoretical phase diagram calculation and membrane morphology evaluation for water/solvent/polyethersulfone systems.* Polymer, 2007. **48**(6): p. 1620-1631.
7. Neelakandan, C and Kyu, T, *Membrane morphology and phase diagrams of mangiferin modified poly(amide)/poly(vinyl pyrrolidone) blends.* Journal of Membrane Science, 2011. **367**(1–2): p. 240-248.
8. Song, Z, Xing, M, Zhang, J, Li, B, and Wang, S, *Determination of phase diagram of a ternary PVDF/γ-BL/DOP system in TIPS process and its application in preparing hollow fiber membranes for membrane distillation.* Separation and Purification Technology, 2012. **90**(0): p. 221-230.
9. Shilton, SJ, *Forced convection spinning of hollow fibre membranes: Modelling of mass transfer in the dry gap, and prediction of active layer thickness and depth of orientation.* Separation and Purification Technology, 2013. **118**(0): p. 620-626.

10. Lai, J-Y, Liu, M-J, and Lee, K-R, *Polycarbonate membrane prepared via a wet phase inversion method for oxygen enrichment from air.* Journal of Membrane Science, 1994. **86**(1–2): p. 103-118.
11. Chen, S-H, Ruaan, R-C, and Lai, J-Y, *Sorption and transport mechanism of gases in polycarbonate membranes.* Journal of Membrane Science, 1997. **134**(2): p. 143-150.
12. Iqbal, M, Man, Z, Mukhtar, H, and Dutta, BK, *Solvent effect on morphology and CO2/CH4 separation performance of asymmetric polycarbonate membranes.* Journal of Membrane Science, 2008. **318**(1–2): p. 167-175.